REGULATION OF MAP KINASE ACTIVATION STUDIED BY HX-MS

By

Kevin Murphy Sours

B.S. Bucknell University, 1998

A thesis submitted to the faculty of the Graduate

School of the University of Colorado in partial

fulfillment of the requirement for the degree of

Doctor of Philosophy

Department of Chemistry & Biochemistry

2011

This thesis entitled:

Regulation of MAP Kinase Activation Studied by HX-MS

written by Kevin Murphy Sours

has been approved for the Department of Chemistry and Biochemistry

_____

Natalie G. Ahn

_____

Marcelo C. Sousa

Date_____

The final copy of this thesis has been examined by the

signatories, and we find that both the content and the form

meet acceptable presentation standards of scholarly work in

the above mentioned discipline.

ABSTRACT

Sours, Kevin Murphy (Ph.D., Department of Chemistry & Biochemistry)

Regulation of MAP Kinase Activation Studied by HX-MS

Thesis directed by Professor Natalie G. Ahn

Hydrogen exchange mass spectrometry (HX-MS) is an experimental technique that can be used to examine solvent accessibility and conformational mobility in biological macromolecules. HX-MS is well suited to probe protein solvent accessibility and conformational mobility, which can directly relate to cellular behavior and regulation. This thesis summarizes studies using HX-MS as the primary experimental technique to examine the regulated motions of MAP kinase and their role in protein activation.

MAP kinases are a conserved family of proteins that are important for cellular regulation and proliferation that share a conserved secondary and tertiary structure and are activated by dual phosphorylation. The first study examines p38α MAPK to see how changes in regulated motions upon activation compare between closely related family members. Structural analysis such as proteolysis, solvent accessibility, crystal structure details and dimerization are investigated and compared to earlier work examining ERK2 MAPK. The results reveal that even closely related proteins show vastly different changes in regulated motions upon activation. This work also touches on experimental strategies and methods for optimizing data recovery and resolution which have become possible due to the improvement of instrumentation and increased popularity of HX-MS.

A second study built on past research and investigated changes in the hinge region of ERK2, previously identified as a region of interest. These studies examine the role the

hinge plays in domain closure, substrate binding, catalysis and the changes that take place upon activation. Hinge mutants were created to increase flexibility to help determine the role the hinge plays in domain closure which is known to be important in the formation of a competent active site. The results suggest that enhanced hinge flexibility upon phosphorylation is needed for domain closure. In addition there is preliminary evidence that some residues in the hinge are important for ATP binding affinity. Lastly, the flexibility in the hinge leads to minimal increase in catalytic activity, indicating more than hinge flexibility is crucial for the increase in activity.

DEDICATION

I would like to dedicate this work to Dr. Katheryn A. H. Resing, our beloved friend and mentor. Katheryn's love of science, teaching, and life were evident from our first encounter, and I could not help but to be inspired by her passion. From teaching me how to take apart a mass spectrometer to light-hearted discussions about current events, she was always willing to listen and help. Unfortunately, she passed away January 8, 2009 and is not here to see the completion of this work. Thank you for the opportunity and thank you for always believing in me. You are remembered fondly!

ACKNOWLEDGEMENTS

I would like to start by thanking my advisor, Natalie Ahn, for all of her guidance and assistance over the years. I would not have made it this far without you, thank you! I would also like to thank Thomas Lee for his help throughout the years, from both near and far you were an excellent mentor and friend. I also thank Adam Ring for his curiosity and persistence, you were fun to mentor. I also thank the members of mass spec for insight, software, and coffee breaks. In particular I would like to thank Stephane Houel for all of his assistance with running and analyzing samples, and his help troubleshooting and caring for the instruments. For their knowledge I would like to thank Will Old, Shuji Kato, Eric Witze, Brian Eichelberger, Petia Gatzeva-Topalova, and Johnny & Carrie Croy. A long distance thanks goes to John Fitzpatrick for maintaining the Pulsar in excellent condition, and Michelle Kremp for my early mass spectrometry education. I thank the Caruthers lab for their assistance and flexibility, and the Batey Lab for all of their help, but you haven't seen the last of me. I also thank the Pardi Lab and my committee, Marcelo Sousa, Debbie Wuttke, Charles McHenry, and Debra Goldberg for your insight and direction. A special thanks to all of the past and present members of the Ahn Lab who have made this enjoyable as well as educational. Finally, I would like to thank all of my enormous family for their encouragement and laughs, you have always been there when I needed help or needed to escape, especially Drew, Derek & Rescue. In particular I would like to thank my parents, Richard & Charlotte, for all of your support, guidance, and understanding throughout my education and my life. Above all I would like to thank my wife, Kelly, for her weekend trips to the lab as well as her support, encouragement, and infinite patience. I love you all!!

CONTENTS

TABLES

TABLE

FIGURES

FIGURE

CHAPTER 1

Introduction: HX-MS as a method for studying regulated motions in proteins.

HX theory, mechanism, and measurements in proteins

Studies measuring the exchange rates for amino acid amide hydrogens were pioneered by Kaj Linderstrom-Lang in the 1950's, and by Walter Englander in the 1970's. Intrinsic amide hydrogen exchange rates were measured by NMR for each residue within oligopeptides under numerous experimental conditions (Bai et al. 1993). The exchange rate was measured with varied salinity, pH, temperature and even the physical and chemical properties of neighboring residues were considered to ensure the rate was determined accurately in many different experimental conditions. These intrinsic exchange rates are still the foundation of modern protein hydrogen exchange, but subsequent work has yet to define a theory that accurately combines these rates with protein secondary or tertiary structure. The lack of an all encompassing theory leads to results that are sometimes difficult to interpret. Nonetheless protein hydrogen exchange continues to provide valuable insight into protein behavior and is growing in popularity.

The chemical exchange reaction can be described as a two part mechanism that first involves the abstraction of a proton followed by the addition of a deuteron. This

reaction is acid catalyzed at low pH and base catalyzed at high pH (pH >2.5-3). Figure 1 details this reaction and models how this exchange occurs in proteins. In unfolded proteins, or EX1 exchange, the intrinsic exchange rate, k_{ch} is much faster than k_{cl}, because amide hydrogens are not protected by protein secondary or tertiary structure and as a result the measured k_{obs} is approximately equal to k_{op}. Protein folding studies often utilize EX1 conditions at high or low pH or in the presence of a denaturant. In contrast, exchange can be measured in native folded proteins, by what is known as EX2 exchange. Measurements under EX2 conditions maintain the functionality and biological characteristics of the protein. For proteins in their native conformation and at neutral pH, the reaction is often described by a two state mechanism where exchange occurs through protein fluctuations that transiently expose protons to solvent, followed by exchange with deuterium. In other words, as the protein samples an ensemble of conformations, backbone amide hydrogens become exposed and exchange with deuterons from D_2O solvent. In EX2 exchange the observed rate (k_{obs}) is a function of the open (k_{op}) / close (k_{cl}) equilibrium times the intrinsic exchange rate (k_{ch}). There is a general consensus that secondary and tertiary structural features, such as hydrogen bonds, packing interactions, and distance to surface (ex: probability of solvent exposure) of native folded proteins affect the exchange rate, but this is poorly understood and impossible to predict. Even without an all encompassing theory both exchange regimes have been used to study protein structure and function.

At its most basic application, hydrogen exchange has the ability to report on protein conformation and conformational mobility, but it also has the ability to report on protein dynamics under certain experimental conditions. By measuring k_{obs} under both

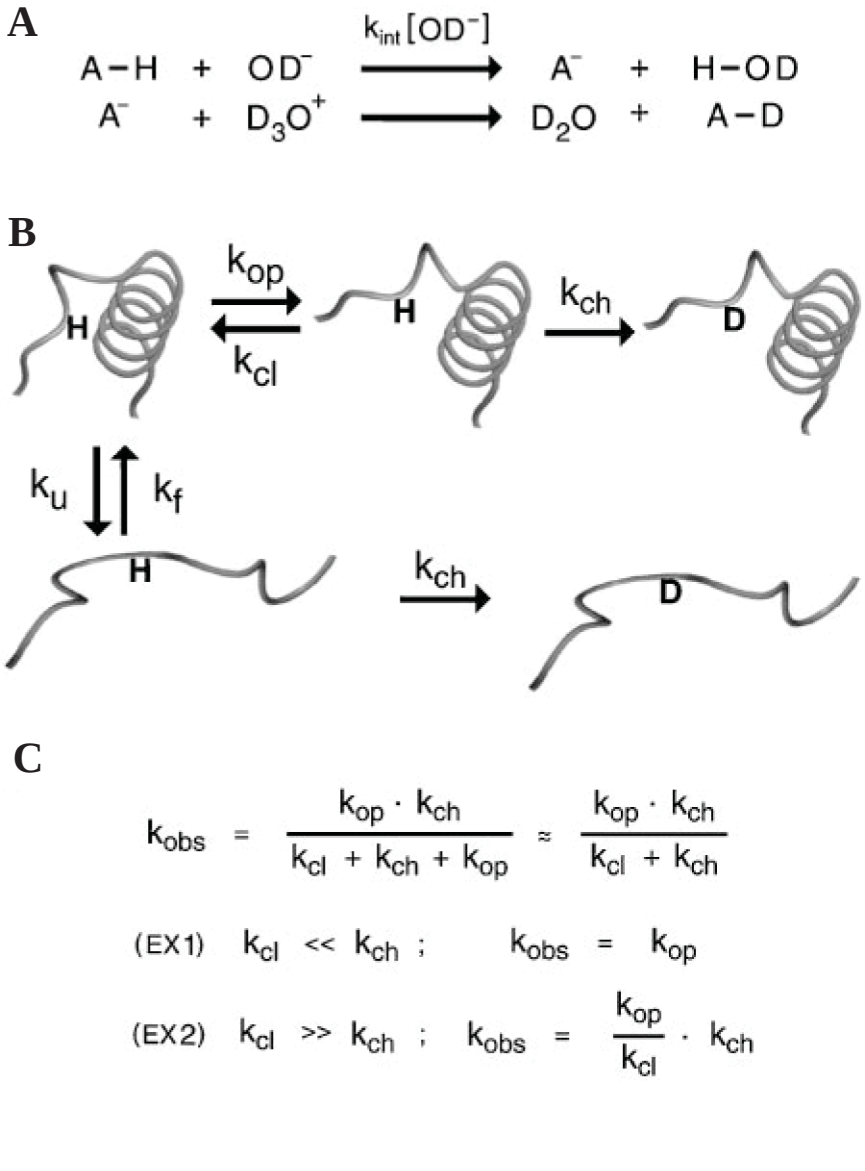

Figure 1: Mechanism of HX in proteins. A. The two part exchange reaction where the top reaction details the base catalyzed proton abstraction and the bottom reaction details the acid catalyzed deuteron addition. **B.** This scheme shows the exchange as it occurs in proteins with the top reaction occuring in native folded protein with small fluctuations and the bottom reaction occuring in unfolded protein. **C.** Kinetic parameters for exchange in proteins. The EX1 parameters apply for unfolded protein, the bottom scheme of B, while the EX2 parameters apply for native folded protein, the top scheme in B. Figure adapted from Hoofnagle et al. 2003.

EX1 and EX2 regimes and applying Englander's intrinsic rate measurements, the values for k_{op} and k_{cl} as well as the Gibbs free energy (ΔG) can be determined. The Robertson lab utilized hydrogen exchange coupled to mass spectrometry and NMR under EX1 and EX2 conditions to determine the k_{op} and k_{cl} rate constants and ΔG for specific backbone amides in turkey ovomucoid third domain (OMTKY3) and ubiquitin (Arrington et al. 1999, Arrington & Robertson, 2000a, Arrington & Robertson, 2000b, Sivaraman et al. 2001, Ferraro et al. 2004). While it was not surprising that k_{cl} values were significantly faster than k_{op} for native proteins, it was interesting that the rate constants spanned four orders of magnitude in OMTKY3 ($30 – 40 \times 10^4$ s^{-1}) and five orders of magnitude in ubiquitin ($0.8 \times 10^{-3} – 57$ s^{-1}). It is noteworthy that all of the rate measurements in ubiquitin were significantly slower than those in OMTKY3, suggesting differences in conformational mobility and rigidity at least under these experimental conditions. Despite the differences in rate, the ΔG values for specific backbone amides for each protein remained similar, between 1 – 8 kcal/mol, suggesting little difference in the energy requirement for backbone mobility. These results eloquently illustrate how amide HX can be applied to improve our understanding of backbone conformational mobility and protein behavior. While all of the experiments discussed here were performed under EX2 conditions so the specific k_{op} and k_{cl} rates could not be determined, much was learned about the role conformational mobility plays in MAP kinase activation.

Recent evolution of hydrogen exchange

Hydrogen-deuterium exchange (HX) methods have provided useful approaches for exploring conformational and dynamic properties of biomolecules. Although often

performed by nuclear magnetic resonance (NMR), HX coupled with mass spectrometry has increased in popularity over the last fifteen years (Hoofnagle et al., 2003; Englander, 2006). Advances in the resolution and speed of mass spectrometry instrumentation allow experiments to be performed readily on macromolecules. Early publications provided the basic strategy for HX-MS of proteins, which are still prevalent among current studies of protein folding, macromolecular interactions, ligand binding, enzyme activation, and conformational mobility (Zhang & Smith, 1993; Johnson & Walsh, 1994).

Measurements of HX by NMR has advantages but also has drawbacks that can be difficult to overcome. An advantage of NMR is its ability to examine individual residues and directly measure HX rates at specific backbone amides in a folded protein. HX experiments by NMR have been applied to well characterized proteins such as cytochrome c and ubiquitin to correlate HX rates and corresponding changes in protein behavior. For example, HX has been used to monitor protein-protein interactions between cytochrome c and monoclonal antibody, protein folding including rates of folding and properties of intermediates, and the relationship between protection factors and secondary and tertiary structural motifs (Mayne et al., 1992; Paterson et al., 1990; Roder et al., 1988; Englander & Mayne, 1992; Marmorino et al., 1993; Briggs & Roder, 1992; Milne et al., 1998).

HX measurements by NMR also have drawbacks. First, NMR peaks need to be assigned to residues which can be incomplete and time consuming. This becomes increasingly difficult as the protein size increases and peaks in spectra become more complicated and less well resolved. In addition, NMR often requires protein concentrations in the millimolar range for good signal to noise which can be problematic

for proteins that are insoluble or tend to aggregate at high concentrations. HX measurements by NMR also require dissolution of lyophilized proteins or dilution of concentrated proteins into D_2O, followed by insertion of the sample into the instrument. This introduces a dead time of several minutes, which limits the ability to measure fast-exchanging amides (Smith et al., 1997).

Many of these limitations can be overcome by HX-MS. An examination of the benefits of HX-MS illustrates why the technique has grown so rapidly in popularity in recent years and why researchers are constantly developing new applications. This is in part because of improved technologies for mass spectrometry over the last two decades, and the growth in the field of proteomics, which continue to drive the technology forward. Mass spectrometers have highly sensitive, down to sub-picomole amounts, allowing an entire HX-MS experiment to be performed with protein levels in the microgram to nanogram range. This allows working with proteins that are hard to express or insoluble, and at concentrations closer to cellular levels. HX-MS reactions can also be quenched after seconds (or milliseconds with the help of quench-flow instrumentation) so that fast-exchange rates can be measured (Dharmasiri & Smith 1996). HX-MS also has the ability to analyze large proteins or protein complexes, with the current record held by HX studies on a 250 kDa protein complex (Wales et al., 2008).

Two significant drawbacks of HX-MS are its limited resolution in determining the site(s) of HX and the lengthy time needed for data analysis and interpretation. HX-MS resolution is currently limited by the length of peptides generated by proteolysis, which are usually 5-20 residues long. However, this limitation is starting to be solved by new advances in instrumentation. For example, each generation of mass spectrometers allows

faster scanning, and combined with higher resolution in HPLC or UPLC, allows high sequence coverage and increased number of peptides that overlap in sequence. Combined with improvements in proteolysis, which utilize alternative proteases, overlapping peptides can specify resolution down to 2 – 4 residues (Cravello et al., 2003). In addition, advances in nebulization and fragmentation strategies have allowed fragmentation of deuterated peptides. Previous attempts using collision induced dissociation led to deuteron scrambling, but new methods using electron transfer dissociation with controlled gas phase temperatures enable fragmentation without scrambling (Ferguson & Konermann, 2008; Rand et al., 2009; Zehl et al., 2008). The reliability of sequencing can be validated by the degree of N-terminal deammoniation and lack of integral deuteration at specific positions (Rand et al., 2010). With these advances HX-MS is rapidly advancing towards single amide resolution. However, since HX-MS provides no structural information, it is still beneficial to have atomic resolution X-ray or NMR structures to aid in interpretation of results.

A second limitation of HX-MS is that mass spectrometers produce large amounts of data, and with high sequence coverage, many peptides to analyze. Data analysis is usually the most time consuming part of the experiment, and often data analysis takes anywhere from a few days to several months, depending on the size of the experiment. However, new software allows semi-automated to fully-automated data analysis, enabling reductions in analysis time (Sours & Ahn, 2010). Custom HX-MS liquid chromatography instrumentation is now being commercially produced with software for rapid data analysis (Wales et al., 2008). All of this has led to fewer obstacles in the HX-MS experiment and increased popularity for protein studies.

A common question regarding HX studies is its interpretation with respect to protein backbone mobility and what these changes actually tell us about protein motions. The OMTKY3 study by the Robertson lab discussed above used HX-NMR and HX-MS in a complementary manner to measure backbone folding and unfolding behavior in solution. This study revealed that local unfolding was predominant and showed rate measurements spanning four orders of magnitude. Using HX-MS and modeling to complement the HX-NMR data, these investigators showed that multiple unfolding reactions occur in the native protein and these may or may not correlate with exchange at backbone amides. This led to the idea that the unfolding reactions can proceed through correlated or uncorrelated backbone motions, depending on the local region of the protein in question, leading to an ensemble of states the protein can adopt before global unfolding occurs (Arrington et al., 1999; Arrington & Robertson, 2000). These studies together produced a more complete picture of OMTKY3 folding, illuminating how useful HX can be.

HX-MS applied to protein kinases

HX-MS has proven to be a powerful method for obtaining new insight into protein kinase regulation, specifically involving interactions with other proteins, changes upon substrate binding, and identification of intramolecular allosteric networks. An excellent example is recent work from John Engen's lab on the oncogenic protein kinase Bcr-Abl, whose dysregulated activity is responsible for the onset of chronic myelogenous leukemia (CML). Engen and coworkers utilized many approaches to define the biochemical properties of Bcr-Abl, but HX-MS has been their primary tool for analyzing

kinase conformational mobility. The Bcr-Abl fusion protein consists of an NCap domain, SH2 and SH3 domains, and a linker to the kinase domain (Chen et al., 2007). HX-MS has revealed multiple allosteric networks between the domains of Bcr-Abl and throughout the kinase domain (Iacob et al., 2008; Chen et al., 2008a; Chen et al., 2008b; Zhang et al., 2010). They have documented existing interconnecting networks between the activation lip phosphorylation site, phosphorylation sites in the SH3 and linker regions (Y89 & Y245), the myristate-binding pocket, and the "gatekeeper" residue (T315). Phosphorylation at Y89 has been shown to disrupt the interactions between the SH2, SH3, and linker domain, leading to decreased affinity for substrate peptide. Disruption of the SH3 domain with the linker is predicted to lead to dynamic changes and kinase activation (Chen et al., 2008a; Chen et al., 2008b). The myristoylated Bcr-Abl has lower activity which has been shown to be dependent on dynamic and conformational changes throughout the entire protein (Chen et al., 2008a; Chen et al., 2008b; Iacob et al., 2008). When myristic acid is bound, the NCap stabilizes the SH3 domain, but only in the presence of the SH2 domain. The addition of the myristic acid also leads to a conformation where the SH2 domain is on top of the small lobe of the kinase, leading to down-regulated kinase activity. This conformation has been observed by X-ray crystallography while the allosteric networks can be observed by HX-MS (Chen et al., 2008a; Chen et al., 2008b; Iacob et al., 2008). Lastly, it has recently been shown that the myristate binding pocket communicates with the T315 "gatekeeper" residue and substrate binding pocket. While this network is not completely understood it was found that binding of kinase inhibitor binding to both sites might provide a promising method for inhibition of Bcr-Abl activity and treatment of CML patients (Zhang et al., 2010). The

interconnecting allosteric networks of Bcr-Abl that have been illuminated through HX-MS analysis prove the power of this technique for investigating biochemical properties and kinase regulation.

Another use for HX-MS is its ability to map binding sites of protein-protein interactions, substrate binding, or small molecule ligands. Hamuro et al. (2002) investigated the binding of AMP-PNP and ADP to Csk, the tyrosine kinase, by HX-MS. Both ligands protected regions surrounding the active site; however, the smaller ADP molecule protected the Gly-rich loop in the N-terminal lobe to a greater extent than AMP-PNP whereas AMP-PNP led to allosteric changes in regions of the protein far from the binding site. Although the basis of these differences are not entirely understood, the authors speculate that some are due to changes in protein mobility, while others are due to larger conformational rearrangements. It is interesting to see differences in protein behavior introduced by the γ-phosphate as detected by HX-MS, an insight not obvious from X-ray crystallography.

HX-MS has also been used to understand binding interactions between ERK2 and substrate as well as with MAP kinase phosphatases (MKP) (Lee et al., 2004; Zhou et al., 2006). One study used HX-MS to identify binding sites for docking motifs, sequences within substrates and scaffolds, which confer high affinity binding to MAP kinases (Lee et al., 2004). Binding of a DEJL docking motif (consensus sequence Arg/Lys-X_{2-4}-Φ-X-Φ) interacted with a hydrophobic groove previously identified in X-ray co-crystal structures, while a DEF docking motif (consensus Phe-X-Phe) interacted with a novel binding pocket formed upon rearrangement of the activation lip following phosphorylation. In studies of the binding interface between ERK2 and MKP3 (Zhou et

al., 2006), HX-MS was used to map regions within kinase and phosphatase that were protected from exchange in the heterodimeric complex. Site-directed mutagenesis confirmed that binding of MKP3 involved the DEJL and DEF docking motif binding sites and the activation lip of ERK2, while binding of ERK2 involved corresponding docking motif sequences in MKP3, revealing that two distinct domains in the MKP3 interact with distally spaced regions in ERK2. These studies highlighted the importance of structural changes in ERK2 following activation and how they direct binding of substrates and phosphatase regulators.

These studies illustrate how HX-MS can be effective for understanding the regulation of protein mobility and its importance for kinase activation, as well as protein interactions involved in kinase enzymatic function and regulation. Additional studies showed that activation of p38 MAPK and MKK1 also caused changes in HX that were consistent with regulated conformational mobility (Resing et al., 1999; Sours et al., 2008). Such changes occur within distinctive regions of each enzyme, suggesting that regulated motions vary significantly across related MAP kinases.

In these studies we expand on previous work examining the activation of MAP kinase by using HX-MS to address two outstanding questions regarding the regulation of MAP kinase activation. One, how do closely related members of the MAP kinase family compare in their control of regulated mobility upon activation as detected by HX-MS? Here we compare proteins in the MAP kinase family, namely p38α and ERK2. While solvent accessibility throughout the family remains similar, interestingly, the regulation of activation appears to have evolved differently even between close family members. Two, is enhanced backbone flexibility in the ERK2 hinge after activation needed for

domain closure? Hinge mutants were studied to determine how hinge flexibility controls domain closure, which is known to be important for catalysis. The results suggest that enhanced backbone flexibility in the hinge region upon phosphorylation is needed to promote domain closure and formation of a competent catalytic site. In addition, the results suggest that some residues in the hinge are important for ATP binding affinity. While interactions between the hinge and the adenine ring are well documented, how these interactions contribute to binding affinity has not been examined. Lastly, the flexibility in the hinge leads to minimal increase in catalytic activity, indicating more than hinge flexibility is crucial for the increase in activity. Further investigations are needed to understand how changes in protein mobility control kinase activation and how backbone flexibility is controlled by phosphorylation.

CHAPTER II

Analysis of regulated motions in the MAP kinase p38α measured by HX-MS.

INTRODUCTION

MAP kinase (MAPK) family members, including various forms of ERK, JNK and p38 MAPK, control diverse aspects of cellular regulation. p38 MAPKs and JNKs regulate responses to stress and inflammation while ERKs regulate events required for cell proliferation, motility and differentiation. Many family members are under exploration as drug targets, and inhibitors of p38 show therapeutic effects towards diseases of inflammation (Lee et al., 2000). MAPKs are closely related by sequence, with p38α MAPK sharing 48% sequence identity with ERK2 and 60% identity with p38β and p38γ MAPK forms.

Mechanisms for activating MAP kinases are conserved. Like other protein kinases, they display a conserved bilobal kinase structure, consisting of an active site located between an N-terminal ATP binding domain and a C-terminal substrate binding domain (Johnson et al., 2001). Each MAP kinase is activated by dual phosphorylation at a pThr-Xxx-pTyr sequence motif located within the activation lip. This leads to conformational changes around the active site, which are best understood for ERK2, the only MAP kinase for which X-ray structures of both inactive and active forms have been determined (Zhang et al., 1994; Canagarajah et al., 1997).

Three major changes occur as a result of dual phosphorylation. First, ion-pair interactions between the phosphorylated residues and basic side chain amino acids cause a dramatic reorganization of the activation lip, into a conformation which enables substrate binding and recognition of a Ser/Thr-Pro sequence motif for phosphorylation. Second, ion pair interactions lead to connectivity between the lip and N-terminal helix αC as well as repositioning of active site residues for catalysis. Third, a docking motif binding site forms upon reorganization of the activation lip, enabling high affinity substrate binding (Lee et al., 2004). Thus, dual phosphorylation and activation lip remodeling lead to conformational changes which facilitate substrate binding and formation of a competent catalytic site.

In addition to conformational changes, protein kinase activation causes changes in internal protein motions as determined by hydrogen exchange-coupled mass spectrometry (HX-MS) (Resing & Ahn, 1998; Hoofnagle et al., 2001). By examining hydrogen exchange with D_2O on peptides formed by proteolysis, localized effects within a molecule can be detected (Hoofnagle et al., 2003, Hoofnagle et al., 2004b; Busenlehner & Armstrong, 2005). Several studies have now shown that hydrogen exchange measurements on kinases detect localized changes in protein fluctuations which are low energy and not always observable by X-ray crystallography (Hoofnagle et al., 2001; Hamuro et al., 2003; Wong et al., 2004; Alverdi et al., 2007). These can include motional changes, in which a protein adopts conformers which differ by free energies on the order of 1 kcal/mol. Regulation of protein fluctuations and flexibility could lead to changes in protein function, even when structural changes are not apparent.

HX-MS measurements reveal that in ERK2, kinase activation leads to changes in hydrogen-deuterium exchange at backbone amides within the hinge region separating N- and C-terminal domains (Hoofnagle et al., 2001). Because X-ray structures show that atoms within the

hinge region are superimposable between active and inactive forms, the corresponding changes in HX have been ascribed to regulated conformational mobility. In agreement, site-directed spin labeling EPR measurements show activation-induced changes in correlation times of side chains at hinge residues (Hoofnagle et al., 2004). Furthermore, evidence from HX-MS suggests that regulated protein motions are important for activation. In the active form of ERK2, the nonhydrolysable ATP analog, AMP-PNP, sterically protects amides from hydrogen-deuterium exchange in both the N and C-terminal domains of the ATP binding pocket (Lee et al., 2005). In contrast, only the N-terminal domain is protected from exchange by AMP-PNP in the inactive form of ERK2. This indicates that in solution, the N- and C-terminal lobes in active ERK2 adopt a closed conformation around nucleotide, whereas inactive ERK2 is somehow constrained from interdomain closure and instead adopts an open conformation. Together, the evidence suggests that increased backbone flexibility at the hinge following ERK2 phosphorylation enables induced fit interdomain closure, a necessary event for catalytic function.

X-ray structures of p38α MAPK and JNK1 in their inactive forms show large diversity in activation lip conformation (Wang et al., 1997; Wilson et al., 1996; Xie et al., 1998; ter Haar et al., 2007; White et al., 2007). Although structures of corresponding active forms are not available, an X-ray structure of diphosphorylated active p38γ MAPK reveals that the activation lip adopts a conformation similar to that of diphosphorylated active ERK2 and the cAMP dependent kinase catalytic subunit (Bellon et al., 1999). Thus, the diverse activation lip conformations in various inactive forms of MAPKs converge towards a uniform active state conformation that confers catalytic rate enhancement. This is expected, because only a limited range of structures should produce catalytic function (Nolen et al., 2004). In addition, active p38γ MAPK shows greater closure between N- and C- terminal domains due to a rigid body

rotation of >15 º compared to inactive p38α MAPK, where the domains are held in an open conformation (Bellon et al., 1999). In contrast, structures of ERK2 show a smaller difference in domain rotation (5 º) between active and inactive forms (Canagarajah et al., 1997).

To date there is no information available as to whether phosphorylation-dependent changes in conformational mobility are also similar between different MAPKs. On one hand, MAPK family members share similarities in primary sequences, activation mechanisms, and structural motifs. On the other hand, small differences in sequence may yield large differences in control of regional flexibility. Conceivably, the role that protein internal motions play in activation may differ significantly between these closely related enzymes.

Here, we investigate the effect of kinase activation on conformational mobility of p38α. By monitoring peptide sequences over the entire protein we present a global picture of amide hydrogen exchange behavior, and how this differs between active and inactive forms of the kinase. Overall, the patterns of in-exchange are similar between p38α and ERK2, reflecting their similarities in sequence and structure. Upon p38α activation, regional changes in hydrogen exchange are observed, some of which can be ascribed to changes in structure and others to conformational mobility. This suggests that kinase activation regulates mobility within localized regions. Importantly, the patterns of regulated mobility differ significantly between p38α and ERK2. Thus, closely related MAP kinase family members show divergent behavior with respect to effects of phosphorylation and activation on protein motions.

MATERIALS AND METHODS

Proteins.

Doubly phosphorylated active kinase (2P-p38α) was produced in BL21(DE3)-pLysS using the plasmid pET(His)-MKK6DD/p38α, which expresses wild-type mouse His6-p38α and constitutively active MKK6, as previously described (Wilsbacher & Cobb 2001). Unphosphorylated, inactive kinase (0P-p38α) was produced in pET(His)-MKK6DD/p38α modified by deleting the MKK6 open reading frame. Monophosphorylated, inactive kinase (1P-p38α) was produced in pET(His)-MKK6DD/p38α modified by inserting a stop codon at residue Tyr64 of MKK6. Each kinase was purified using Ni-NTA agarose (Qiagen) chromatography and MonoQ FPLC (14), dialyzed overnight into 50 mM KPO_4 (pH 7.4), 100 mM KCl, and 5 mM dithiothreitol (DTT), and stored in aliquots at -80°C. Mass spectrometry confirmed phosphorylation stoichiometry at the activation lip, where 0P-p38α was >99% unphosphorylated, 2P-p38α was >99% diphosphorylated at Thr180 and Tyr182, and 1P-p38α was 85% monophosphorylated at Tyr182 and 5.5% at Thr180 (data not shown).

Hydrogen-exchange mass spectrometry (HX-MS) measurements

Data collection and analysis of weighted average mass, in-exchange, and back exchange was performed as described (Resing et al., 1999; Hoofnagle et al., 2004; Lee et al., 2006). Data were collected on a QStar Pulsar QqTOF MS interfaced with an Agilent Cap1100 HPLC (500 μm i.d. x 10 cm column, packed with POROS R1 20 resin). Proteins (4 μg) were incubated in 90% D_2O at 10°C allowing the in-exchange reaction to take place from 8 s to 4 h. Reactions were quenched with 90 μL 25 mM succinic acid, 25 mM citric acid (pH 2.4), and cooled rapidly to 0°C. Proteins were digested by adding 10 μL pepsin (4 μg), and analyzed by LC-MS. Time-

zero measurements were performed by quenching the reaction before adding D_2O. Samples were randomized to control for systematic variations, and replicate runs were performed at 0 s, 60 s, and 1800 s. Across all time points, the average standard deviation of weighted average mass was 0.05 Da, with maximum standard deviation 0.13 Da. Deuteration time courses were corrected for artifactual in-exchange and back-exchange, then fit to a sum of exponentials.

Weighted average mass calculations were carried out using HX-Analyzer, an interactive tool for increasing accuracy and speed of analysis of HX-MS data, developed in-house and implemented in Visual Basic using ABI Analyzer QS, MS Office XP, and MS XP software library modules. HX-Analyzer inputs a list of LC-MS/MS files (.wiff) and a spreadsheet summarizing information about peptide ion mass and approximate elution time, presents isotopic peaks for examination across several datasets for manual inspection, and then outputs isotopic masses and weighted average mass for each peptide ion. HX time courses were fit by nonlinear least squares (NLSQ) to the equation $Y = N - Ae^{-k1t} - Be^{-k2t} - Ce^{-k3t}$, where Y is the number of deuterons exchanged at time t, A, B, and C are the number of backbone amides exchanging at rates k_1, k_2, and k_3, N is the maximal deuteration over the experimental time period ($N = A + B + C$). Subtracting N from the total number of exchangeable backbone amides yields NE, the number of amides that are non-exchanging over the experimental time period (Hoofnagle et al., 2004; Lee et al., 2006). NLSQ curve fitting was performed and results plotted using DataFit 7.1 (Oakdale Engineering).

For LC-MS/MS, proteins incubated in water were treated and proteolyzed as above. Samples (4 μg) were analyzed on the Pulsar mass spectrometer with m/z window = 400-1600 Da, duty cycle 15.5 s, and 3 MS/MS per cycle. Samples (60 ng) were analyzed on the LTQ-Orbitrap mass spectrometer interfaced with an Eksigent 2DLC HPLC (75 μm i.d. x 150 mm

column, Zorbax C18 resin), with m/z window = 300-2000 Da, duty cycle 4-6 s (~10-14 cycles/min), and 5 MS/MS per cycle. MS/MS were converted to .mgf files and searched against the p38α sequence using the Mascot search program (v.1.9), with no enzyme specified. Mass tolerances used for Pulsar datasets were 2.5 Da for parent ions and 1.2 Da for fragment ions. Mass tolerances for LTQ-Orbitrap datasets were 1.2 Da for parent ions and 0.8 Da for fragment ions. The Manual Analysis Emulator was used to generate theoretical spectra for the top two sequence assignments made by Mascot, and Similarity scores evaluating overlap between theoretical and observed spectra were calculated as described (Sun et al., 2006). High confidence thresholds used were Mowse = 30 and Similarity = 0.5, which yielded false discovery rate (FDR) = 0.3%.

Analytical ultracentrifugation equilibrium experiments

Sedimentation equilibrium analyses were performed on a Beckman Proteomelab XLI analytical ultracentrifuge with absorbance optics at 280 nm for the detection of aromatic residues. Samples were loaded into 12 mm Epon cells at concentrations ranging from 0.32 to 0.44 mg/ml. The samples were then centrifuged at 20 °C at 20,000, 24,000, and 28,000 x *g* for 24 h to achieve equilibrium, and successive radial absorbance scans were recorded. Protein molecular weights and oligomerization behavior were determined by fitting the sedimentation equilibrium data from different initial loading concentrations and rotor speeds to various monomer-oligomer equilibrium schemes using WIN NonLIN (v.1.035, University of Connecticut) fitted to theoretical partial specific volumes based on compositions (Johnson et al., 1981). The partial specific volume of the sample and density of the buffer were calculated using SednTerp (v.1.06, University of New Hampshire) using the weighted average of the amino acid

content. To obtain observed molecular weight, dissociation constants, oligomerization states, absorbance results were converted to linear plots of ln(*AU*) *versus* r^2 (radius) to the theoretical monomer and dimer (single-species models) using the equation:

$$C_r = C_o \exp [M ((1-\nu_{bar})\rho) \omega^2 (r^2+r_o^2) / 2 RT]$$

where C_r is the concentration at radius r(*A*), C_o is the concentration at the meniscus, *M* is the monomer molecular weight, ν_{bar} is the partial specific volume calculated by SednTerp, ρ is the buffer density, and ω is the angular velocity.

RESULTS

Achieving high coverage of exchangeable amide hydrogens

HX measurements were made by incubating protein in D_2O for varying periods of in-exchange. After quenching the in-exchange reaction, proteins were proteolyzed, and extent of deuteration was quantified by LC-MS mass measurements of peptides in the digest. High coverage of exchangeable amides over the protein sequence is needed in order to obtain a global view of amide hydrogen exchange behavior. In addition, because resolution is limited in peptides with large numbers of residues, greater recovery of peptides with overlapping sequences allows exchange behavior to be localized within narrower protein regions. Thus, techniques that maximize identification of peptides from proteolytic digests are needed to optimize HX measurements.

In an effort to maximize peptide identifications, we examined the influence of sampling, instrument, and peptide search algorithm on peptides observed in LC-MS/MS datasets of p38α. Peptides present within protein digests are often missed because they fail to be identified with high confidence. Sampling statistics often limit the number of peptides that are sequenced in any

MS/MS run, when digests are complex. Low instrument sensitivity may limit the ability to sequence low abundance ions. Finally, automated search programs may yield scores that are too low to confidently match peptide sequences to MS/MS spectra.

Three experiments were carried out to examine how each of these factors affects coverage and resolution (Figure 1A). p38α incubated in water was proteolyzed and peptides were sequenced by LC-MS/MS, identifying peptides using the Mascot search program. Two instrument platforms were used for LC-MS/MS. The QStar Pulsar is a quadrupole time-of-flight (TOF) mass spectrometer which is used to perform HX mass measurements by LC-MS, as well as LC-MS/MS sequencing. The LTQ-Orbitrap is an ion trap mass spectrometer which provides fast MS/MS scan rates, high sensitivity, and high mass accuracy. Peptides were then matched to those routinely observed in HX-MS datasets of p38α incubated in D_2O to allow in-exchange. In each experiment, effects on sequence coverage and number of exchangeable amides were quantified.

The first experiment tested the effect of sampling on sequence coverage. Peptide identifications may be enhanced by repeating LC-MS/MS runs on the same digest, which increases sampling depth and the probability that an ion will be selected for MS/MS. LC-MS/MS performed on the Pulsar identified 39 peptides in a single run, yielding 77% sequence coverage. Combining results from 3 or 9 runs respectively yielded 77 peptides (88% sequence coverage), or 98 peptides (99% coverage) (Table 1, Table 2). Of these, respectively 30, 45, and 67 peptides could be routinely identified in HX-MS datasets under conditions of p38α deuteration identifying peptides using the Mascot search program. Therefore, increasing the depth of sampling by performing 3 or 9 LC-MS/MS runs respectively improved peptide recovery by 1.5-fold or 2-fold over a single run, and increased the percentage of peptide identifications may also

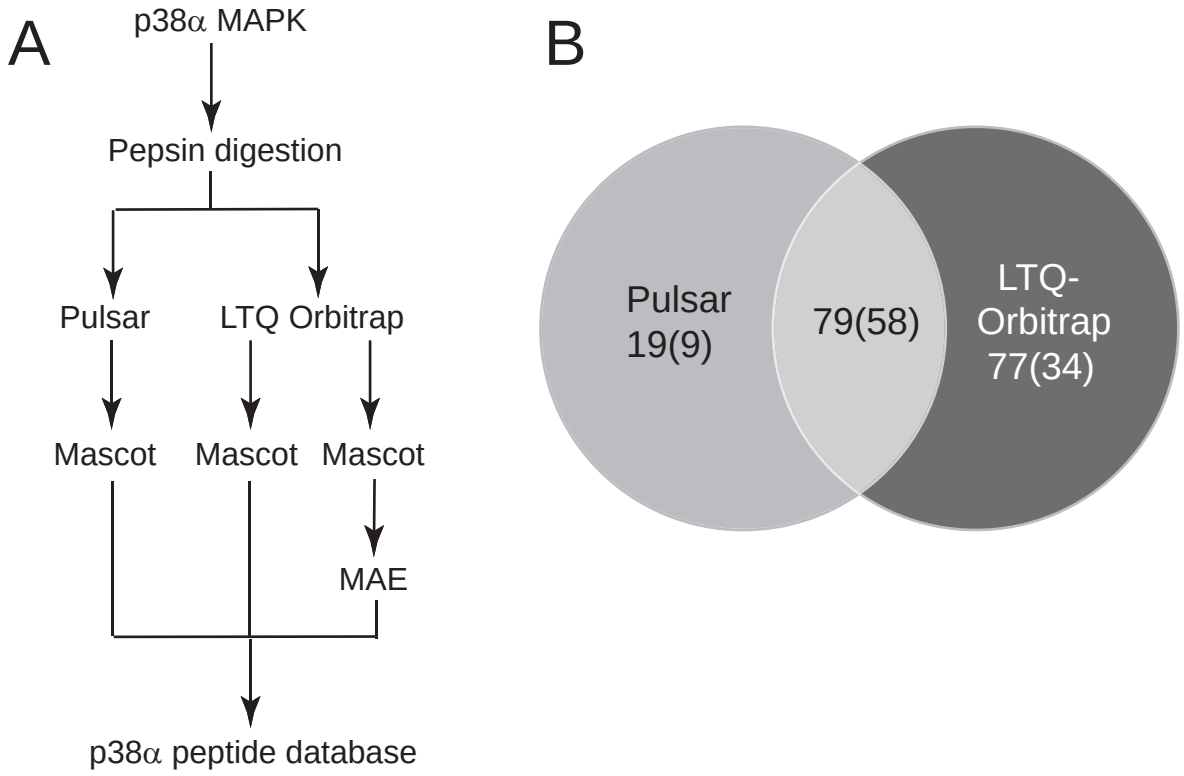

Figure 1. Methods for LC-MS/MS data collection and analysis. (A) Experiments used to identify peptides created by pepsin digestion. Purified p38α was proteolyzed and peptides sequenced by LC-MS/MS on Pulsar QqTOF and LTQ-Orbitrap mass spectrometers. Data were analyzed using the Mascot search program and post-processed using Manual Analysis Emulator (MAE) in-house software, then compiled into a database of observed peptides (Table 1). **(B)** Peptides identified from 9 replicate LC-MS/MS runs collected on the Pulsar mass spectrometer and 3 replicate runs collected on LTQ-Orbitrap mass spectrometer. Numbers indicate total unique peptides, and parentheses indicate unique peptides matched to ions observable in HX-MS datasets.

Table 1: Peptides recovered from LC-MS/MS experiments and sequence coverage.
Summary of results for unique peptide sequences, with full dataset in Table 2.

		Total peptide IDs		Peptides matching HX-MS dataset			
Instrument and analysis method	**# runs**	**Unique peptides**	**Full sequence coverage (%)**	**Unique peptides**	**Coverage of exchangeable amides (%)**	**Minimum peptides covering sequence**	**Peptides with overlapping sequence**
Pulsar QqTOF Mascot	1	39	77	30	64	21	9
	3	77	88	45	81	23	21
	9	100	99	67	95	28	39
LTQ-Orbitrap Mascot	1	95	86	61	72	22	39
	3	110	86	68	81	23	45
LTQ-Orbitrap Mascot + MAE	1	129	90	78	75	24	54
	3	151	93	87	90	27	60
LTQ-Orbitrap Total IDs	1	132	96	81	80	26	55
	3	156	99	92	95	29	63
Pulsar + LTQ-Orbitrap IDs	12	177	100	101	98	29	72

Table 2: Unique peptides observed by LC-MS/MS (Pulsar + LTQ-Orbitrap)

			Calculated m/z, with observed peptide ions indicated in bold						
Residues #	Sequence	Mass	MH+	2.00	3.00	4.00	5.00	6.00	Elution Time
-7.8	AHHHHHHAMAQERPTF	1942.89	1943.89	**972.45**	**648.63**	**486.72**			6
9.13	YRQEL	707.37	**708.37**						4.4
9.39	YRQELNKTIWEVPERYQNLAPVGSGAYGSVC	3526.74	3527.74	1764.37	**1176.58**	**882.69**	706.35	588.79	11.5
14.39	NKTIWEVPERYQNLAPVGSGAYGSVC	2837.39	2838.39	1419.70	**946.80**	**710.35**	568.48	473.90	11.3
40.71	AAFDTKTGHRVAVKKLSRPFQSIIHAKRTYRE	3711.07	3712.07	1856.54	**1238.02**	**928.77**	**743.21**	619.51	7.7
42.71	FDTKTGHRVAVKKLSRPFQSIIHAKRTYRE	3568.99	3569.99	1785.50	**1190.66**	**893.25**	**714.80**	595.83	9.5
72.86	LRLLKHMKHENVIGL	1800.06	1801.06	**901.03**	**601.02**	**451.02**			7.7
72.87	LRLLKHMKHENVIGLL	1913.15	1914.15	**957.58**	**638.72**	479.29			10.3
75.86	LKHMKHENVIGL	1417.79	1418.79	**709.90**	**473.60**				6.4
75.87	LKHMKHENVIGLL	1530.87	1531.87	**766.44**	**511.29**				7.15
75.88	LKHMKHENVIGLLD	1645.90	1646.90	823.95	**549.63**	412.47			9
87.95	LDVFTPARS	1004.53	1005.53	**503.26**					5.6
87.98	LDVFTPARSLEE	1375.71	1376.71	**688.86**	459.57				8
87.99	LDVFTPARSLEEF	1522.77	1523.77	**762.39**	508.59				9.8
87.101	LDVFTPARSLEEFND	1751.84	1752.84	**876.92**	584.95	438.96			9.4
87.103	LDVFTPARSLEEFNDVY	2013.98	2014.98	**1007.99**	**672.33**	504.50	403.80		11.5
88.98	DVFTPARSLEE	1262.61	1263.61	**632.31**	421.87				7.3
88.103	DVFTPARSLEEFNDVY	1900.88	1901.88	**951.44**	634.63	476.22			9.7
89.98	VFTPARSLEE	1147.59	1148.59	**574.79**					6.35
99.103	FNDVY	656.29	**657.29**						5.9
99.104	FNDVYL	769.36	**770.36**						7.6
104.108	LVTHL	581.36	**582.36**						4.5
104.129	LVTHLMGADLNNIVKCQKLTDDHVQF	2951.51	2952.51	1476.76	**984.84**	**738.88**	**591.30**	492.92	9.5
105.115	VTHLMGADLNN	1183.57	1184.57	**592.78**					6
107.115	HLMGADLNN	983.46	**984.46**	**492.73**					4.7
116.129	IVKCQLTDDHVQF	1672.87	1673.87	**837.44**	**558.62**	419.22			6.4
130.135	LIYQIL	761.48	**762.48**						8
130.145	LIYQILRGLKYIHSAD	1902.08	1903.08	**952.04**	**635.03**	**476.52**			9.7
130.156	LIYQILRGLKYIHSADIIHRDLKPSNL	3188.83	3189.83	1595.42	**1063.94**	**798.21**	**638.77**	**532.47**	10.5
131.156	IYQILRGLKYIHSADIIHRDLKPSNL	3075.73	3076.73	1538.87	**1026.24**	**769.93**	**616.15**	513.62	9.25
133.145	QILRGLKYIHSAD	1512.84	1513.84	**757.42**	**505.28**				6.8
133.156	QILRGLKYIHSADIIHRDLKPSNL	2799.59	2800.59	1400.79	**934.20**	**700.90**	**560.92**	467.60	8.5
134.156	ILRGLKYIHSADIIHRDLKPSNL	2671.53	2672.53	1336.76	**891.51**	**668.88**	535.31	446.25	8.5
136.145	RGLKYIHSAD	1158.61	1159.61	**580.31**					5.1

Residues #	Sequence	Mass	MH+	2.00	3.00	4.00	5.00	6.00	Elution Time
136.156	RGLKYIHSADIIHRDLKPSNL	2445.37	2446.37	1223.69	**816.12**	**612.34**	**490.07**	408.56	8
146.156	IIHRDLKPSNL	1304.76	1305.76	**653.38**	**435.92**				5.6
157.164	AVNEDCEL	891.37	**892.37**	**446.69**					8.1
164.178	LKILDFGLARHTDDE	1741.90	1742.90	871.95	**581.63**	436.47			8.4
164.181	LKILDFGLARHTDDEMTG	2031.01	2032.01	**1016.50**	**678.00**	508.75			8.8
164.182	LKILDFGLARHTDDEMTGY	2194.07	2195.07	**1098.04**	**732.36**	549.52	439.81		9.3
165.179	KILDFGLARHTDDEM	1759.86	1760.86	880.93	**587.62**	440.96			8.1
165.181	KILDFGLARHTDDEMTG	1917.91	1918.91	**959.96**	**640.30**	480.48			7.8
165.182	KILDFGLARHTDDEMTGY	2080.98	2081.98	**1041.49**	**694.66**	521.25	417.20		8.4
165.187	KILDFGLARHTDDEMTGYVATRW	2694.32	2695.32	1348.16	**899.11**	**674.58**	539.86	450.05	9.9
165.187	KILDFGLARHTDDEM**T**G**Y**VATRW	2854.26	2855.26	1428.13	**952.42**	**714.57**	571.85	476.71	9.1
169.182	FGLARHTDDEMTGY	1611.70	1612.70	**806.85**	538.23	403.92			7.5
183.187	VATRW	631.33	**632.33**						8
183.194	VATRWYRAPEIM	1491.49	1492.49	**746.74**	**498.16**				8.5
188.195	YRAPEIML	991.52	992.52	**496.76**					8
195.202	LNWMHYNQ	1104.48	1105.48	**553.24**					8
195.205	LNWMHYNQTVD	1419.62	1420.62	**710.81**	474.21				8.4
195.206	LNWMHYNQTVDI	1532.72	1533.72	**767.36**	**511.91**				9.1
195.207	LNWMHYNQTVDIW	1718.79	1719.79	**860.39**	573.93	430.70			10.4
195.210	LNWMHYNQTVDIWSVG	1961.91	1962.91	**981.95**	**654.97**	491.48			10.35
196.210	NWMHYNQTVDIWSVG	1848.83	1849.83	**925.41**	617.28	463.21			10.4
206-210	IWSVG	560.30	**561.30**						6.15
211-215	CIMAE	565.23	**566.23**						6.3
214.231	AELLTGRTLFPGTDHIDQ	1983.01	1984.01	**992.50**	**662.00**	496.75			8.25
214.234	AELLTGRTLFPGTDHIDQLKL	2337.27	2338.27	**1169.63**	**780.09**	**585.32**	468.45		9.4
216.234	LLTGRTLFPGTDHIDQLKL	2137.13	2138.13	**1069.57**	**713.38**	**535.28**	428.43		11.1
216.236	LLTGRTLFPGTDHIDQLKLIL	2363.36	2364.36	1182.68	**788.79**	**591.84**	473.67		10
217.234	LTGRTLFPGTDHIDQLKL	2024.11	2025.11	**1013.06**	**675.70**	**507.03**	405.82		10.5
217.236	LTGRTLFPGTDHIDQLKLIL	2250.28	2251.28	**1126.14**	**751.09**	**563.57**	451.06		10.1
235.238	ILRL	513.37	**514.37**						5.5
235.245	ILRLVGTPGAE	1124.66	1125.66	**563.33**					6.7
235.246	ILRLVGTPGAEL	1237.74	1238.74	**619.87**					7.8
235.257	ILRLVGTPGAELLKKISSESARN	2451.42	2452.42	1226.71	**818.14**	**613.85**	491.28	409.57	8.9
237.246	RLVGTPGAEL	1011.57	1012.57	**506.79**					6.35
237.257	RLVGTPGAELLKKISSESARN	2225.25	2226.25	1113.62	**742.75**	**557.31**	446.05		8.5
239.246	VGTPGAEL	742.39	**743.39**						4.8

Residues #	Sequence	Mass	MH+	2.00	3.00	4.00	5.00	6.00	Elution Time
239.257	VGTPGAELLKKISSESARN	1956.06	1957.06	979.03	**653.02**	490.02			8
239.262	VGTPGAELLKKISSESARNYIQSL	2560.39	2561.39	**1281.19**	**854.46**	**641.10**	513.08	427.73	10.2
246.262	LLKKISSESARNYIQSL	1949.09	1950.09	**975.55**	650.70	488.27			8.3
247.257	LKKISSESARN	1231.68	1232.68	**616.84**	411.56				3.6
247.262	LKKISSESARNYIQSL	1836.02	1837.02	**919.01**	**613.01**	460.01			8
258.262	YIQSL	622.34	**623.34**						5.2
263.270	AQMPKMNF	965.45	**966.45**	**483.72**					7.5
263.273	AQMPKMNFANV	1249.59	1250.59	**625.80**	417.53				7.95
263.274	AQMPKMNFANVF	1396.66	1397.66	**699.33**	466.55				9.7
263.284	AQMPKMNFANVFIGANPLAVDL	2360.19	2361.19	**1181.10**	**787.73**	591.05	473.04		11.35
271.274	ANVF	449.23	**450.23**						4.6
275.284	IGANPLAVDL	981.56	**982.56**	**491.78**					8.5
275.288	IGANPLAVDLLEKM	1482.81	1483.81	**742.41**	495.27				10.3
285.307	LEKMLVLDSDKRITAAQALAHAY	2556.37	2557.37	1279.19	**853.12**	**640.09**	512.27	427.06	9.1
289.307	LVLDSDKRITAAQALAHAY	2055.12	2056.12	**1028.56**	**686.04**	**514.78**	412.02		10.2
289.308	LVLDSDKRITAAQALAHAYF	2202.19	2203.19	**1102.10**	**735.06**	**551.55**	441.44		11.6
292.307	DSDKRITAAQALAHAY	1729.87	1730.87	**865.94**	**577.62**	433.47			7.1
308.327	FAQYHDPDDEPVADPYDQSF	2354.97	2355.97	**1178.49**	**785.99**	589.74	471.99		8.8
309.327	AQYHDPDDEPVADPYDQSF	2207.90	2208.90	**1104.95**	**736.97**	552.98	442.58		8.4
327.333	FESRDLL	878.45	**879.45**	**440.22**					6.75
328.333	ESRDLL	731.39	**732.39**						7.3
328.336	ESRDLLIDE	1088.54	1089.54	**545.27**					6.4
332.336	LLIDE	601.33	**602.33**						5.2
334.341	IDEWKSLT	990.50	991.50	**496.25**					7.2
334.345	IDEWKSLTYDEV	1496.70	1497.70	**749.35**	499.90				8.7
337.343	WKSLTYD	911.45	**912.45**	**456.73**					6.8
337.344	WKSLTYDE	1040.48	1041.48	**521.24**					7
337.345	WKSLTYDEV	1139.55	1140.55	**570.77**					7.8
344.348	EVISF	593.31	**594.31**						7
344.357	EVISFVPPPLDQEE	1597.80	1598.80	**799.90**	533.60	400.45			8.5
346.360	ISFVPPPLDQEEMES	1716.79	1717.79	**859.40**	**573.26**				8.7
349.360	VPPPLDQEEMES	1369.61	1370.61	**685.80**	457.54				5.9

be enhanced by fast scanning mass spectrometers which increase the number of MS/MS attempts in a single LC-MS/MS run. In a second experiment, we addressed the effects of instrument sensitivity and scan rate, by analyzing p38α digests on an LTQ-Orbitrap mass spectrometer, which is sensitive to low femtomoles and collects MS/MS ~4-5 times faster than the Pulsar. A single LC-MS/MS run identified 95 peptides, of which 61 were observable in HX-MS datasets, covering 72% of exchangeable amides (Table 1, Table 2). Three LC-MS/MS runs yielded 110 peptides, of which 68 were observable in HX-MS datasets, representing 81% amide coverage. Thus, replicate runs on the LTQ-Orbitrap yielded greater numbers of peptides, consistent with the higher sensitivity and faster scan rate of this instrument. However, most of the additional peptides yielded overlapping sequence information, and surprisingly, the amide coverage from peptides sequenced by the LTQ-Orbitrap was not significantly higher than that of the Pulsar. This suggested that another factor limits peptide identification.

A third experiment asked whether peptide identifications could be impacted using improved methods for matching MS/MS spectra to peptide sequences. Conventional search programs match m/z values between fragment ions observed in MS/MS spectra and those calculated from peptide sequences. This is the case for Mascot, which calculates a MOWSE score using a probabilistic model to evaluate the likelihood of observing fragments from a given sequence (Perkins et al., 1999). Recent studies have shown that correct matches which fall below high confidence MOWSE thresholds can be successfully captured using Similarity scores which evaluate relative intensities of fragment ions as well as m/z (Zhang, 2004; Zhang, 2005; Sun et al., 2006). We incorporated this principle into in-house software named the Manual Analysis Emulator (MAE) (Sun et al., 2006), which uses the MassAnalyzer algorithm of Zhang (Zhang 2004; Zhang 2005) to simulate relative intensities of fragment ions in theoretical MS/MS

spectra and then rescores assignments made by Mascot using Similarity scoring. This has the effect of capturing peptides which are correct sequence assignments, but are rejected because MOWSE scores are low.

The datasets from 3 LC-MS/MS runs on the LTQ-Orbitrap (Experiment 2) were rescored using MAE. By accepting assignments with either MOWSE or Similarity scores above high confidence thresholds, 156 peptides were identified, covering 99% of the p38α sequence (Table 1, Table 2). Of these, 92 were observable in HX-MS datasets, representing 95% of exchangeable amides. Thus, improved scoring methods yielded higher data capture, so that the 3 LC-MS/MS runs on the LTQ-Orbitrap provided equivalent amide coverage and 60% more peptides with overlapping sequences, compared to 9 LC-MS/MS runs on the Pulsar. As expected, the LTQ-Orbitrap experiments identified more ions with low intensity compared to the Pulsar experiments (data not shown), although very weak ions were often filtered out because they were not observed in HX-MS datasets. Importantly, our results suggest that MS/MS fragmentation differs between the LTQ and Pulsar instruments in a way which differentially affects the resulting MOWSE scores. The fact that sequence coverage was similar between the LTQ-Orbitrap and Pulsar in Experiments 1 and 2 implies that certain peptide sequences are less readily identified from MS/MS collected on the ion trap instrument, and that rescoring algorithms like MAE are needed to capture these sequences.

Peptide yields are summarized in Figure 1B and Figure 2, showing unique peptide sequences observed with each instrument, ignoring redundancies due to multiple ion forms with different charge states. A total of 175 peptides and 101 HX-MS-observable peptides were identified between the two instruments (Table 1). Of these, 45% of total peptides and 57% of HX-MS-observable peptides were observed by both instruments (Figure 1B). Our combined

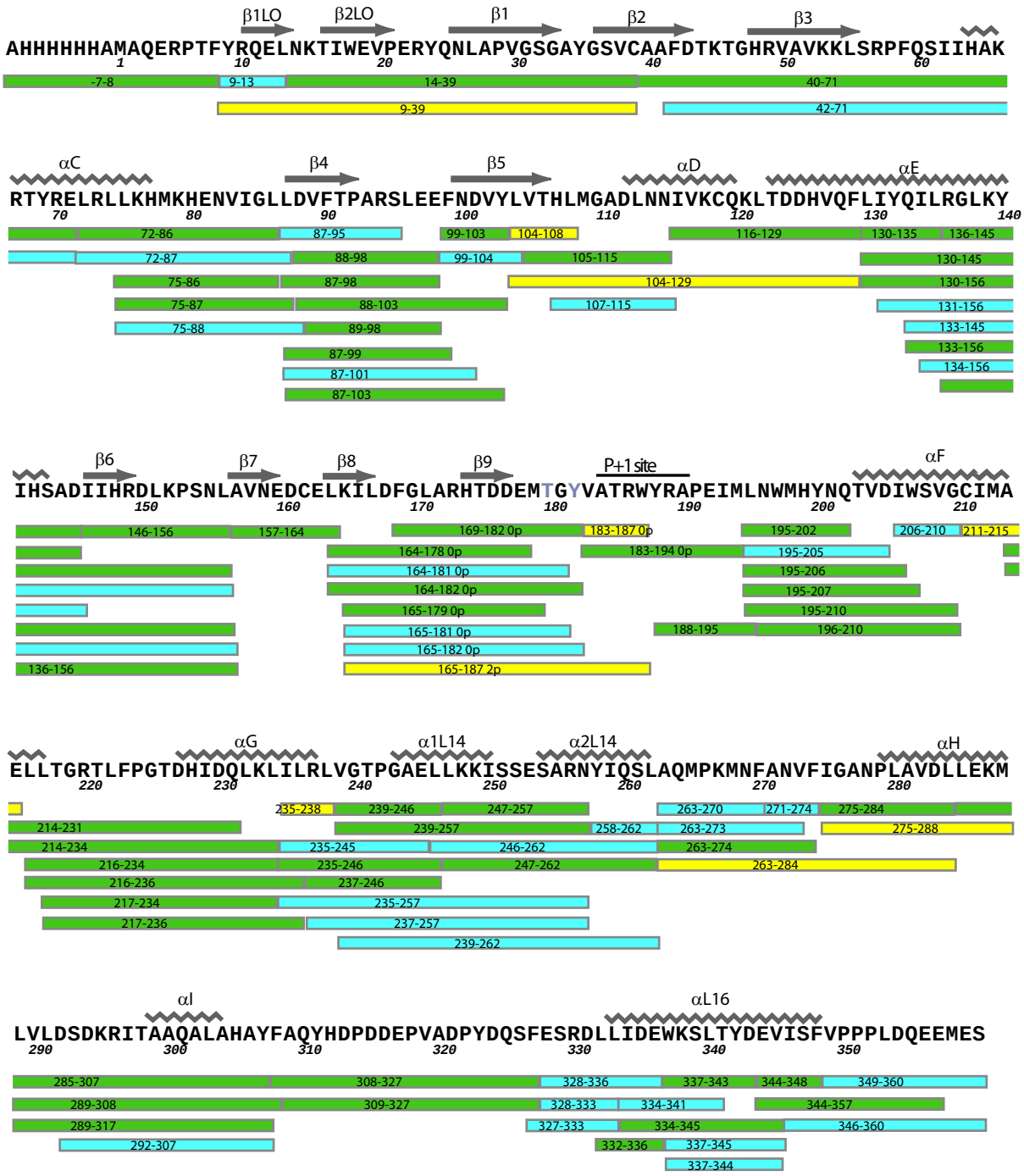

Figure 2. Peptides recovered by LC-MS/MS. Green indicates peptides observed in both Pulsar and LTQ-Orbitrap datasets. Cyan indicates peptides observed only in LTQ-Orbitrap datasets. Yellow indicates peptides observed only in Pulsar datasets. Sequence coverage map of p38α, indicating residue numbering and secondary structures as reported (Wang et al., 1997; Wilson et al., 1996).

datasets from 12 LC-MS/MS experiments yielded 98% coverage of exchangeable amides (Table 1), with greater resolution due to overlapping peptides (Figure 2). High sequence coverage can be difficult to achieve in HX-MS studies, and coverage is often 50% or less, limiting the ability to survey events the entire protein. Our analysis shows that sampling depth and search strategies are important factors to consider for maximizing sequence coverage.

Amide hydrogen exchange in p38α

p38α was incubated in D_2O between 0-4 h and HX measurements were made on 101 peptides (Figure 3). Deuteration at 4 h was then measured for 29 peptides selected to provide highest coverage of residues without overlapping sequences which allowed us to evaluate the extent of hydrogen exchange in localized regions of the protein. These were mapped against the backbone structure of p38α (Figure 4A)

Two regions of low hydrogen exchange (0-40%) were observed in p38α. One was found in the C-terminal lobe, and included the active site β6 strand and helices αE and αF, which form helix interactions with each other and connect to the active site. The second region included N-terminal strands β3, β4, and intervening helix αC. In contrast, high levels of exchange were observed in regions with high solvent accessibility, including the activation lip, the MAP kinase insert, and various loops including the Gly rich loop, which modulates ATP binding. Thus, the HX measurements revealed slow exchanging core regions within both N- and C-terminal domains of the bilobed structure and faster exchange within peripheral regions and loops. Regions within the active site containing the conserved catalytic base (Asp^{150}-Leu-Lys) and Asp^{168}-Phe-Gly motifs exchanged more slowly than the activation lip and P+1 substrate

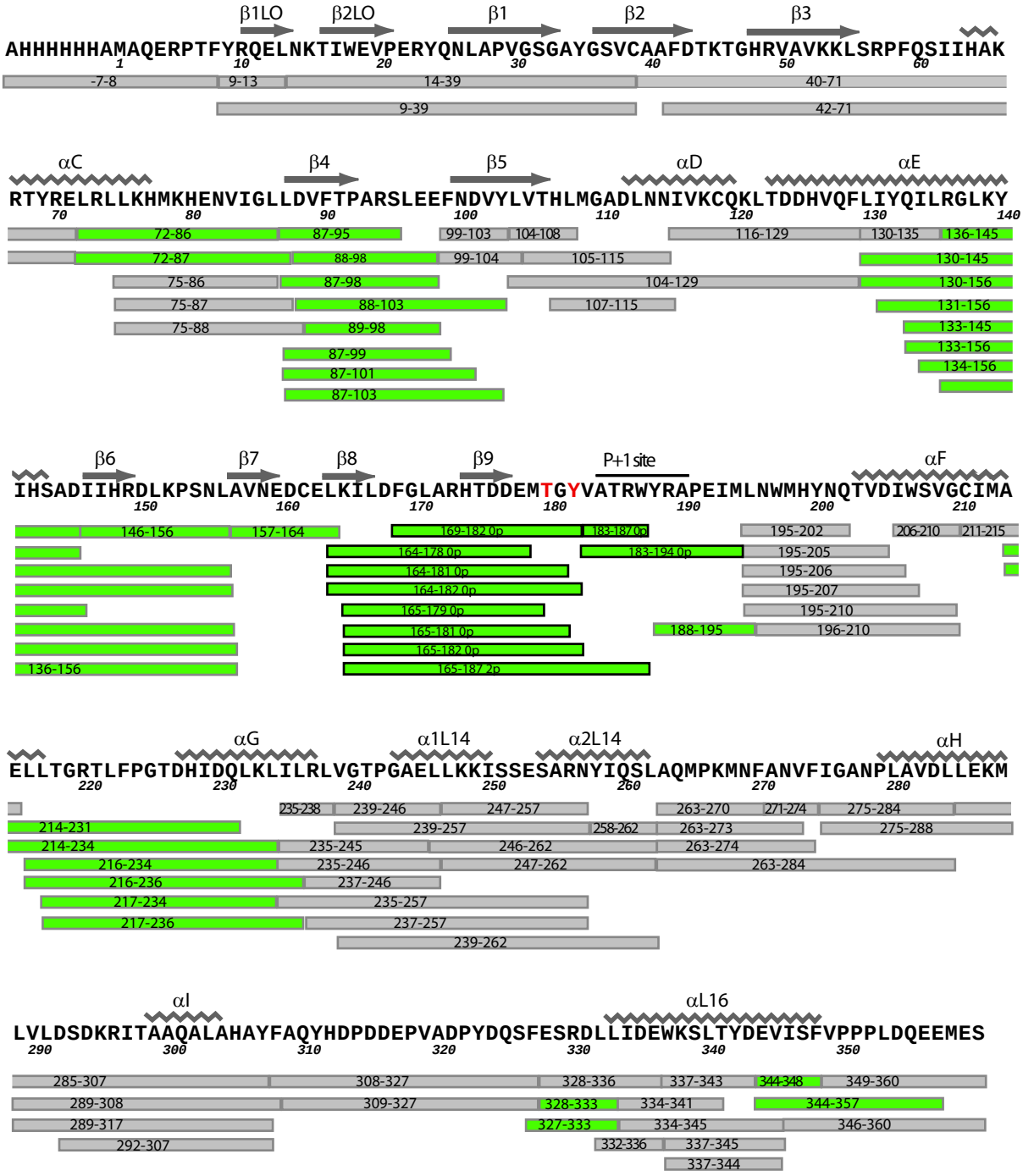

Figure 3. Summary of HX-MS analyses of p38α. Sequence coverage map of p38α, indicating residue numbering and secondary structures as reported (Wang et al., 1997; Wilson et al., 1996). Observed peptides are shown as bars below the sequence, and are named according to residue number. Peptides colored white show cases where hydrogen exchange rates were unaffected by phosphorylation and activation. Peptides in green show cases where hydrogen exchange rates decreased significantly upon activation. All peptides were observed in both 0P and 2P forms of p38α, except those outlined in bold, which indicate those unique to 0P-p38α or 2P-p38α as indicated.

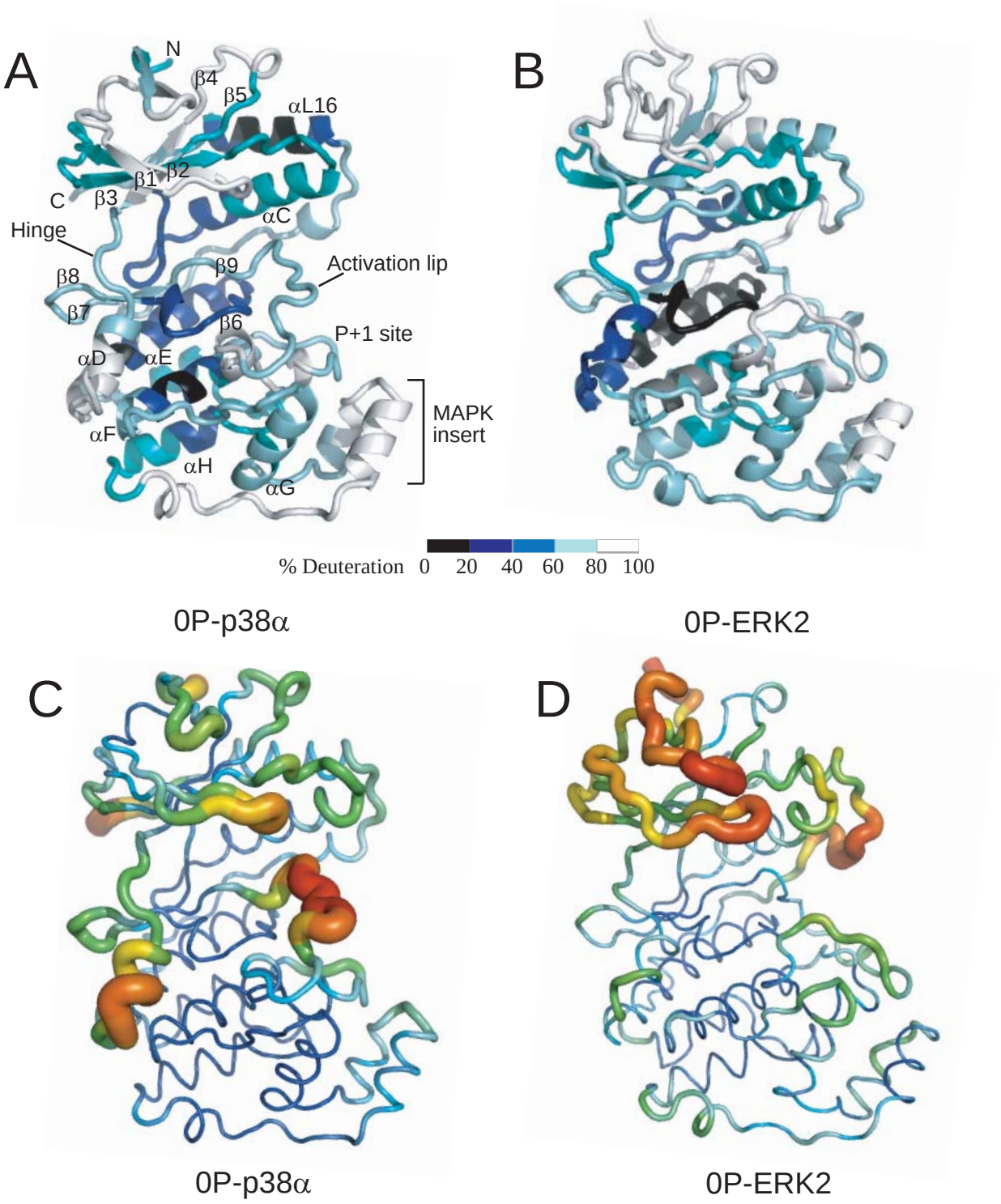

Figure 4. Regional hydrogen/deuterium in-exchange *vs* crystallographic B-factors. **(A)** Hydrogen exchange into 0P-p38α shows extent of deuteration after 4 h, normalized for each region by the number of exchangeable amides. Colors distinguish regions deuterated to 0-20% (black), 21-40% (blue), 41-60% (teal), 61-80% (cyan), and 81-100% (white) of exchangeable amides. **(B)** Normalized deuteration into 0P-ERK2 at 4 h, data from Hoofnagle et al. (2001). (C,D) Crystallographic B-factors in p38α (1P38, Wang et al., 1997) and ERK2 (1ERK, Canagarajah et al., 1997). Images were generated using PyMol 0.99

recognition site, the latter which underwent almost complete exchange in 4 h. Overall, the pattern of regional hydrogen exchange was consistent with that expected from tertiary structure.

Comparison of HX in p38α and ERK2

HX measurements of p38α were compared to previous measurements of ERK2 (Hoofnagle et al., 2001). The extent of protein deuteration at 4 h was similar, respectively measured at 62% and 60% for p38α and ERK2. In most regions, patterns of regional hydrogen exchange were similar between the two kinases. Thus, in both p38α and ERK2, slower exchange was observed within the C-terminal core encompassing the catalytic site, αE, and αF, as well as the N-terminal core containing β3-αC-β4, while faster exchange occurred within peripheral regions and loops as well as the MAP kinase insert (Figure 4A,B).

Two exceptions were helix αD and C-terminal helix αL16, where in each case the percentage deuteration in p38α and ERK2 differed by more than 40%. In helix αD, 84% of exchangeable amides were deuterated after 4 h in p38α, in contrast to 39% in ERK2. This correlated well with regional differences in main chain B-factors within helix αD, which were higher in p38α (37-76 $Å^2$) than ERK2 (15-38 $Å^2$) (Figure 4C,D). Calculating the distance of each amide to the solvent accessible surface (distance-to-surface) as well as the length and orientation of amide hydrogen bonds showed similar structures and solvent accessibility of amide hydrogens within helix αD, between the two kinases. This suggests that side chain interactions in p38α confer greater mobility within αD, whereas the same region is less dynamic in ERK2.

Helix αL16 represents the C-terminal extension in MAP kinases, interacting with the N-terminal lobe in a pocket formed between the β3-β4-β5 sheet and helix αC. In p38α, helix αL16

exchanges slowly, with 10% deuteration after 4 h, whereas in ERK2, >58% of amides in the same region undergo deuteration. This difference was not reflected by B-factors (Figure 4C,D), nor was it predicted from structure, where distance-to-surface and hydrogen bonding of amide hydrogens within αL16 showed very similar patterns between the two kinases. We infer that the conformational mobility of αL16 in solution is significantly lower in p38α than in ERK2.

Taken together, the hydrogen exchange measurements reveal that regional conformational mobility is conserved between p38α and ERK2 MAP kinases, reflecting conservation of sequence and tertiary structure. Differences were noted in helix αD, where p38α showed higher mobility compared to ERK2, an effect recapitulated in B-factor measurements. It was noteworthy that B-factors also predicted the high degree of hydrogen exchange observed within the activation lip of p38α, as well as the Gly-rich loop and other β-sheet loops within the N-terminus of both enzymes. However, B-factors in αL16 were unable to predict differences in conformational mobility between p38α and ERK2, and were also inconsistent with high levels of hydrogen exchange observed within the activation lip and P+1 loop of ERK2, or the MAP kinase insert in either enzyme. Overall, whereas the patterns of hydrogen exchange showed strong similarities between p38α and ERK2, the B-factor patterns appeared more divergent.

Regional hydrogen exchange is altered by phosphorylation and activation of p38α.

Hydrogen exchange measurements were compared between unphosphorylated (0P) and diphosphorylated (2P) forms of p38α, in order to define regions responsive to kinase activation. Sites of proteolytic cleavage were nearly identical between the two forms. The sole exception was the activation lip, where several cleavage sites surrounding the Thr-Xxx-Tyr region in 0P-p38α were masked from proteolysis in 2P-p38α (Figure 3). This may be explained by altered

proteolytic specificity by phosphorylation, or conformational changes that convert a proteolytically accessible activation lip in 0P-p38α to a more protected conformation in 2P-p38α.

Of the 101 peptides, 32 showed significant differences in deuteration between active vs inactive p38α, where in all cases, HX decreased upon enzyme activation (Figure 3, indicated in green). Many of these peptides overlapped in sequence, and in all, ten peptides were sufficient to summarize the changes in HX (Figure 5).

Differences in HX either reflect changes in conformation upon p38α activation, or alternatively, report changes in conformational mobility and internal motions of the folded state. In order to evaluate contributions from structural changes, X-ray coordinates of unphosphorylated p38α (1P38, Wang et al., 1997) were compared to that of diphosphorylated p38γ (1CM8, Bellon et al, 1999) in regions where HX decreased upon p38α activation. The lip and catalytic site structures in p38γ overlay well with those in diphosphorylated ERK2 and cAPK (Bellon et al., 1999), providing a reasonable prediction of how p38α would undergo conformational remodeling upon phosphorylation. Outside the lip and catalytic site, backbone conformations of active p38γ and inactive p38α resemble each other closely, with rms deviations of 1.2 Å and 0.62 Å when N- and C-terminal domains are respectively superimposed between each enzyme (Bellon et al., 1999). Thus, the difference in domain angle between these kinases reflects rigid body movements of the N- and C-terminal lobes.

Peptides displaying the greatest changes in HX were located within five regions (Figs. 6-10) For kinetic fits and error analysis of HX-MS data discussed see Tables 3 and 4:

(1) Activation lip and P+1 specificity site. Peptide residues (pr) 165-187 (KILDFGLARHTDDEMTGYVATRW) contains the activation lip, with residues comprising

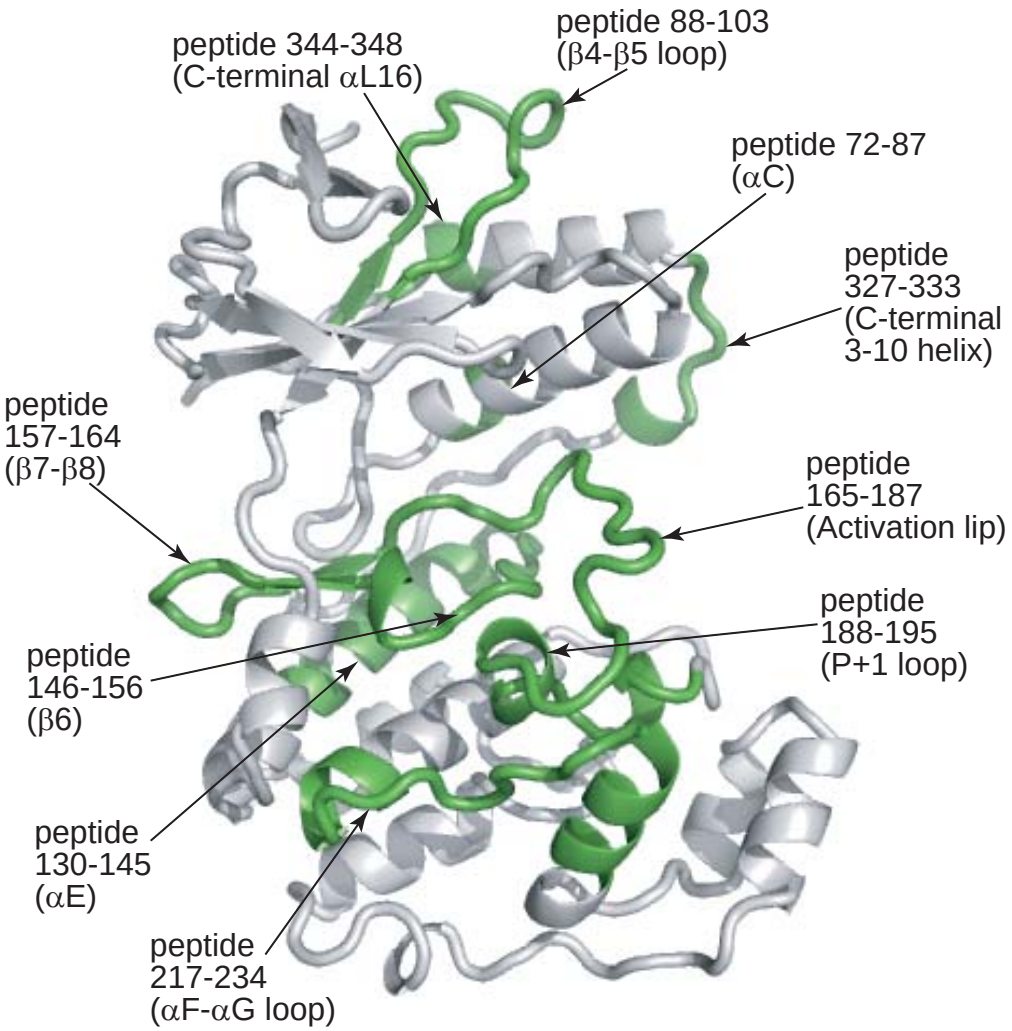

Figure 5. Summary of HX changes induced by p38α activation. Representative peptides show regions significantly decreased in HX upon diphosphorylation of p38α, which are indicated in green on the main chain ribbon structure.

Table 3: Kinetic parameters for p38α in-exchange, fit by non-linear least squares.

Sequence [1]		Residues	Calc Mass	Obs. m/z	#EA	% BE	RSS	A [2]	B	C	N	k_1	k_2	k_3
AHHHHHHAMAQERPTF	0P	-7.8	1942.89	972.45	14	25.90	0.52	6.74(.42)	0.66(.38)		7.41(.067)	30.05(19.39)	1.73(1.34)	
	2P						0.61	7.07(.16)	0.46(.13)		7.53(.11)	15.10(1.38)	0.035(.032)	
YRQEL	0P	9.13	707.37	708.37	4	21.20	0.44	1.58(.22)	1.35(.15)		2.93(.12)	22.20(18.88)	.11(.04)	
	2P						1.07	1.47(.25)	1.41(.21)		2.90(.16)	7.18(2.98)	0.085(.047)	
YRQELNKTIWEVPERYQNLAPVGSGAYGSVC	0P	9.39	3526.74	1176.58	28	30.30	4.57	13.19(.81)	4.62(1.28)	5.36(1.35)	23.17(.40)	28.44(19.04)	0.40(.22)	0.030(.017)
	2P						4.06	12.73(.66)	3.93(.68)	7.40(.62)	24.06(.40)	19.16(4.99)	0.51(.23)	0.022(.0050)
NKTIWEVPERYQNLAPVGSGAYGSVC	0P	14.39	2837.39	946.8	23	31.80	2.44	10.60(.70)	1.88(.60)	6.76(.50)	19.22(.57)	14.23(2.69)	0.52(.44)	0.015(.0051)
	2P						5.63	10.20(.85)	2.44(.77)	6.65(.68)	19.28(.74)	12.80(3.10)	0.50(.44)	0.014(.0051)
AAFDTKTGHRVAVKKLSRPFQSIIHAKRTYRE	0P	40.71	3711.07	928.77	30	30.10	1.92	6.62(.74)	3.07(.70)	2.83(.66)	12.52(.25)	11.40(2.84)	0.62(.35)	0.032(.019)
	2P						2.64	4.11(.71)	5.71(.64)	3.81(.99)	13.62(1.12)	18.50(13.31)	0.92(.20)	0.0079(.0052)
FDTKTGHRVAVKKLSRPFQSIIHAKRTYRE [7]	0P	42.71	3568.99	714.8	28	31.60	3.42	7.17(.83)	3.20(.79)	2.32(.73)	12.70(.33)	13.62(4.29)	0.56(.35)	0.030(.023)
	2P						5.19	5.17(.50)	4.72(.54)	2.52(.51)	12.41(.28)	13.60	0.60	0.03
LRLLKHMKHENVIGL	0P	72.86	1800.06	601.02	14	31.90	5.29		3.53(.37)		3.53(.22)		0.56(.18)	
	2P						1.00		1.49(.26)	2.27(.25)	3.76(.16)		1.20(.43)	0.031(.0098)
LRLLKHMKHENVIGLL	0P	72.87	1913.15	638.72	15	47.00	2.27		1.34(.46)	4.28(.29)	5.62(.24)	9.42(6.83)	0.066(.015)	
	2P						1.16		1.88(.28)	3.33(.28)	5.14(.22)		0.56(.18)	0.019(.0049)
LKHMKHENVIGL	0P	75.86	1417.79	473.6	11	29.40	1.48	1.83(.21)	2.20(.19)		4.03(.22)	2.00(.54)	0.011(.0036)	
	2P						0.67	1.29(.18)	2.31(.17)		3.60(.13)	1.87(.63)	0.033(.0074)	
LKHMKHENVIGLL [3]	0P	75.87	1530.87	511.29	12	26.60	0.41	1.25(.23)	1.66(.31)	1.59(.82)	4.5	13.99(7.41)	0.23(.10)	0.0066(.0091)
	2P						0.83	1.71(.19)	2.04(.18)		3.75(.16)	2.02(.52)	0.023(.0063)	
LKHMKHENVIGLLD	0P	75.88	1645.90	549.63	13	16.50	0.92	1.65(.23)		2.53(.75)	4.19(.78)	1.50(.48)		0.0078(.0049)
	2P						5.52		3.08(.32)		3.08(.39)		0.33(.16)	
LDVFTPARS	0P	87.95	1004.53	503.26	7	25.70	6.14		3.31(.34)		3.31(.24)		0.32(.12)	
	2P						1.51	2.06(.37)	1.65(.22)		3.71(.19)	14.89(8.01)	0.032(.015)	
LDVFTPARSLEE	0P	87.98	1375.71	688.86	10	13.90	0.59	3.68(.26)	2.48(.54)	1.52(.45)	7.68(.28)	18.20(5.40)	0.21(.082)	0.016(.016)
	2P						0.84	3.26(.37)	1.56(.33)	3.18(.24)	8.00(.24)	18.19(8.64)	0.76(.37)	0.016(.0040)
LDVFTPARSLEEF	0P	87.99	1522.77	762.39	11	29.00	0.46	4.74(.25)	2.23(.27)	2.27(.24)	9.24(.23)	24.57(9.76)	0.38(.17)	0.016(.0075)
	2P						1.44	4.37(.55)	1.68(.50)	3.14(.32)	9.18(.24)	13.38(4.53)	0.75(.49)	0.021(.0063)
LDVFTPARSLEEFND [7]	0P	87.101	1751.84	876.92	13	34.90	5.18	6.45(.71)	5.24(.43)		11.67(.34)	13.63(4.20)	0.10(.026)	
	2P						6.73	4.34(.81)	3.65(.63)	5.26(.67)	13.25(.50)	13.60	1.00	0.01
LDVFTPARSLEEFNDVY	0P	87.103	2013.98	1007.99	15	28.90	1.39	6.86(.40)	3.01(.64)	2.65(.62)	12.52(.82)	17.13(3.76)	0.19(.083)	0.010(.010)
	2P						2.14	5.68(.75)	2.31(.68)	4.42(.39)	12.41(.41)	16.99(7.62)	1.10(.57)	0.014(.0042)
DVFTPARSLEE	0P	88.98	1262.61	632.31	9	27.50	0.85	3.91(.27)	3.60(.16)		7.51(.14)	25.86(15.01)	0.078(.011)	
	2P						3.08	4.17(.35)	3.25(.28)		7.44(.24)	10.49(2.55)	0.042(.011)	
DVFTPARSLEEFNDVY	0P	88.103	1900.88	951.44	14	30.20	2.23	6.85(.44)	5.20(.26)		12.05(.21)	18.57(4.96)	0.11(.017)	
	2P						2.84	5.48(.98)	2.42(.90)	4.60(.42)	12.50(.41)	14.70(7.01)	1.16(.72)	0.016(.0049)
VFTPARSLEE [7]	0P	89.98	1147.59	574.79	8	23.40	2.75	3.75(.49)	3.14(.28)		6.90(.24)	14.8	0.11(.032)	
	2P						3.85	3.37(.40)	3.76(.33)		7.13(.29)	14.80(7.04)	0.043(.011)	
FNDVY	0P	99.103	656.29	657.29	4	27.60	1.50	0.83(.11)			0.83(.22)	1.24(.75)		
	2P						0.51	0.77(.14)		0.83(.33)	1.60(.35)	6.18(2.56)		0.0088(.0081)
FNDVYL	0P	99.104	769.36	770.36	5	25.80	0.52	0.61(.15)			0.61(.058)	2.54(1.29)		
	2P						0.46	0.75(0.00)	0.76(.13)		0.76(.059)	2.16(.85)		
LVTHL	0P	104.108	581.36	582.36	4	46.10	7.70	2.31(.59)	1.75(.30)		4.07(.26)	18.69(15.18)	0.082(.047)	
	2P						4.72	2.12(.48)	1.71(.35)		3.77(.22)	8.26(4.67)	0.14(.092)	
LVTHLMGADLNNIVKCQKLTDDHVQF	0P	104.129	2951.51	984.84	25	29.40	1.22	13.13(.76)	6.03(.67)	1.84(.32)	20.99(.24)	14.98(2.25)	1.18(.23)	0.022(.015)
	2P						5.09	9.66(1.38)	8.80(1.27)	3.28(.62)	21.72(.67)	12.53(3.98)	1.06(.25)	0.014(.0087)
VTHLMGADLNN	0P	105.115	1183.57	592.78	10	25.80	0.47	4.68(.41)	2.87(.37)		7.55(.064)	18.38(5.60)	1.34(.24)	
	2P						1.80	4.22(.64)	3.33(.60)		7.55(.11)	9.78(2.98)	.72(.23)	
HLMGADLNN [3]	0P	107.115	983.46	492.73	8	22.60	0.46	3.84(.37)	1.66(.33)		5.5	17.03(5.28)	1.10(.33)	
	2P						0.74	3.03(.32)	2.18(.28)		5.21(.073)	11.32(2.99)	0.55(.16)	

Sequence [1]		Residues	Calc Mass	Obs. m/z	#EA	% BE	RSS	A [2]	B	C	N	k_1	k_2	k_3
IVKCQLTDDHVQF	0P	116.129	1672.87	558.62	12	29.70	0.90	6.95(.27)	1.77(.17)		8.74(.15)	12.47(1.27)	0.053(.016)	
	2P						2.32	6.62(.30)	2.12(.27)		8.76(.25)	8.55(1.00)	0.025(.0092)	
LIYQIL [4]	0P	130.135	761.48	762.48	5	21.30	No Fit	0	0	0				
	2P						No Fit	0	0	0				
LIYQILRGLKYIHSAD	0P	130.145	1902.08	635.03	15	31.20	0.00	0.34(0.0)		3.21(.0001)	3.55(.0001)	1.21(.0002)		0.0036(0.0)
	2P						0.06			2.69(.81)	2.72(.82)			.0025(.0010)
LIYQILRGLKYIHSADIIHRDLKPSNL [3]	0P	130.156	3188.83	798.21	25	31.30	1.76		0.84(.24)	3.04(.19)	4.5	0.72(.47)	0.016(.0036)	
	2P						2.08	1.37(.29)	3.54(.45)		4.93(.48)	3.26(1.65)	0.016(.0056)	
IYQILRGLKYIHSADIIHRDLKPSNL [3]	0P	131.156	3075.73	769.93	24	29.80	7.45		2.67(.42)		2.67(.27)		0.45(.23)	
	2P						1.23	1.16(.27)	3.34(.77)		4.5	1.91(1.08)	0.015(.0088)	
QILRGLKYIHSAD	0P	133.145	1512.84	757.42	12	25.70	2.12		1.39(.18)		1.39(.21)		0.19(.099)	
	2P						1.06		1.29(.15)		1.29(.15)		0.014(.0056)	
QILRGLKYIHSADIIHRDLKPSNL [3]	0P	133.156	2799.59	934.2	22	30.20	0.62	1.17(.24)	3.29(.26)		4.47(.26)	14.31(8.80)	0.033(.0065)	
	2P						1.07	1.31(.23)	2.69(.53)		4	1.90(.77)	0.018(.0085)	
ILRGLKYIHSADIIHRDLKPSNL	0P	134.156	2671.53	891.51	21	28.60	0.52	1.34(.21)	3.46(.18)		4.80(.18)	13.15(5.65)	0.017(.0032)	
	2P						0.95	0.98(.20)	3.38(.24)		4.36(.24)	7.57(3.94)	0.016(.0034)	
RGLKYIHSAD	0P	136.145	1158.61	580.31	9	28.20	4.12	1.58(.42)			1.58(.13)	3.23(1.57)		
	2P						1.37			3.57(2.41)	3.73(2.43)			0.0034(.0034)
RGLKYIHSADIIHRDLKPSNL	0P	136.156	2445.37	816.12	19	29.50	7.23		3.15(.54)		3.15(.35)		0.75(.34)	
	2P						0.68	1.35(.18)		4.36(2.20)	5.70(2.29)	1.39(.42)		0.0072(.0059)
IIHRDLKPSNL [3]	0P	146.156	1304.76	435.92	9	31.20	2.51	1.30(.29)		1.38(.17)	3.5	1.94(.90)		0.0063(.0029)
	2P						0.85	1.38(.16)		1.59(.077)	3.0	4.97(1.37)		0.0054(.0012)
AVNEDCEL [3]	0P	157.164	891.37	892.37	7	30.10	0.13	1.18(.11)	1.57(.084)	4.25(.082)	7.0	27.39(26.44)	0.27(.046)	0.0033(.00018)
	2P						0.34	1.16(.12)	1.39(.099)	2.45(.081)	5.0	24.42(23.91)	0.30(.071)	0.0048(.00039)
LKILDFGLARHTDDE [5]	0P	164.178	1741.90	581.63	14	30.80	1.54	5.69(.40)	1.50(.24)		7.19(.17)	22.98(10.50)	0.25(.13)	
LKILDFGLARHTDDEMTG [5]	0P	164.181	2031.01	1016.5	17	28.40	1.29	9.39(.43)	1.09(.31)		10.47(.12)	23.87(7.64)	0.55(.40)	
LKILDFGLARHTDDEMTGY [3,5]	0P	164.182	2194.07	732.36	18	29.30	2.26	11.52(.40)		0.96(.12)	12.5	17.07(2.16)		0.0033(.0025)
KILDFGLARHTDDEM [5]	0P	173.179	1759.86	587.62	14	26.70	0.45	7.39(.22)	0.40(.13)		7.78(.092)	32.14(15.45)	0.21(.19)	
KILDFGLARHTDDEMTG [5]	0P	173.181	1917.91	959.96	16	28.20	0.77	9.26(.31)	0.84(.20)		10.09(.094)	23.83(5.48)	0.44(.31)	
KILDFGLARHTDDEMTGY [5]	0P	173.182	2080.98	1041.49	17	28.20	0.80	10.04(.39)	0.79(.31)		10.84(.094)	28.85(11.86)	0.94(.69)	
KILDFGLARHTDDEMTGYVATRW [6]	0P	173.187	2694.32				1.73	15.11(.39)	0.86(.23)		15.97(.18)	25.02(5.06)	0.14(.12)	
KILDFGLARHTDDEMTGYVATRW [6]	2P	173.187	2854.26	952.42	22	28.70	3.74	13.86(.37)	1.58(.35)		15.44(.33)	12.74(1.18)	0.023(.015)	
FGLARHTDDEMTGY [5]	0P	169.182	1611.70	806.85	13	26.60	1.09	7.74(.27)			7.74(.065)	25.45(7.01)		
VATRW [5]	0P	183.187	1494.64	632.33	4	36.30	0.74	4.88(.21)			4.88(.049)	24.75(7.81)		
VATRWYRAPEIM [5]	0P	183.194	631.33	498.16	10	30.30	1.37	4.41(.35)	6.13(.22)		10.55(.18)	14.39(3.31)	0.066(.0068)	
YRAPEIML [3]	0P	188.195	1491.49	496.76	6	29.60	0.61	1.97(.25)	2.36(.47)	1.61(.51)	6.0	5.74(1.46)	0.14(.052)	0.012(.0051)
	2P						1.27	2.22(.21)		2.60(.16)	5.0	1.11(.24)		0.011(.002)
LNWMHYNQ [3]	0P	195.202	991.52	553.24	7	27.10	1.85	6.50(3.51)		1.34(.11)	7.0	24.35(11.77)		0.0021(.0014)
	2P						1.68	5.74(.26)		1.26(.11)	7.0	13.84(2.33)		0.0027(.0015)
LNWMHYNQTVD [3]	0P	195.205	1104.48	710.81	10	31.00	0.49	5.16(.25)	1.61(.17)	1.22(.14)	8.0	22.25(6.42)	0.38(.13)	0.0050(.0016)
	2P						0.66	5.07(.22)	1.41(.19)	1.69(.14)	8.0	15.33(2.59)	0.35(.15)	0.0060(.0014)
LNWMHYNQTVDI [3]	0P	195.206	1419.62	767.36	11	30.20	0.71	5.76(.35)	1.35(.29)	1.29(.29)	8.39(.35)	26.21(13.54)	0.58(.32)	0.013(.013)
	2P						1.06	5.35(.35)	1.46(.31)	1.89(.71)	8.7	14.89(3.49)	0.49(.30)	0.0074(.0071)
LNWMHYNQTVDIW	0P	195.207	1532.72	860.39	12	33.10	2.80	6.63(.50)	1.93(.35)		8.57(.31)	14.82(3.49)	0.068(.035)	
	2P						4.68	6.59(.47)	2.32(.37)		8.92(.31)	11.19(2.43)	0.046(.023)	
LNWMHYNQTVDIWSVG [3]	0P	195.210	1718.79	981.95	15	30.10	4.83	6.52(.59)		3.48(.18)	10.0	13.90(3.52)		0.0051(.0014)
	2P						4.51	6.14(.41)	2.21(.38)		8.36(.36)	9.20(1.67)	0.023(.012)	
NWMHYNQTVDIWSVG [3]	0P	196.210	1961.91	925.41	14	30.10	1.34	4.13(.60)	1.04(.49)	1.84(.19)	7.0	17.99(9.49)	0.92(.83)	0.0077(.0025)
	2P						0.81	3.76(.41)	1.20(.36)	1.84(.74)	6.79(.82)	20.97(11.88)	0.77(.49)	0.0069(.0064)
IWSVG	0P	206.210	1848.83	561.30	4	21.30	No Fit	0	0	0				
	2P						No Fit	0	0	0				
CIMAE	0P	211.215	560.30	566.23	4	25.10	No Fit	0	0	0				
	2P						No Fit	0	0	0				

Sequence [1]		Residues	Calc Mass	Obs. m/z	#EA	% BE	RSS	A [2]	B	C	N	k_1	k_2	k_3
AELLTGRTLFPGTDHIDQ	0P	214.231	565.23	662.00	16	33.40	3.12	3.09(.51)	5.31(.32)		8.41(.26)	16.24(9.38)	0.077(.014)	
	2P						2.10	2.39(.37)	2.39(.47)	5.40(1.39)	10.16(1.71)	11.03(4.94)	0.22(.12)	0.0065(.0044)
AELLTGRTLFPGTDHIDQLKL [3]	0P	214.234	1983.01	585.32	19	28.30	1.41	2.49(.43)	3.45(.62)	5.06(.54)	11	20.96(19.39)	0.29(.12)	0.017(.0070)
	2P						3.80	3.63(.38)		6.83(.53)	10.47(.55)	2.98(.77)		0.014(.0033)
LLTGRTLFPGTDHIDQLKL [3]	0P	216.234	2337.27	713.38	17	30.20	3.27	2.65(.54)	4.56(.76)	3.79(.72)	11.0	19.21(17.71)	0.20(.073)	0.010(.0073)
	2P						4.74	3.49(.41)	7.38(.60)		10.87(.65)	2.72(.79)	0.013(.0030)	
LLTGRTLFPGTDHIDQLKLIL	0P	216.236	2137.13	788.79	19	28.10	4.47	3.32(.61)	7.13(.39)		10.45(.33)	10.08(4.03)	0.049(.0081)	
	2P						2.87	3.12(.33)	7.00(.39)		10.13(.39)	4.20(1.08)	0.016(.0029)	
LTGRTLFPGTDHIDQLKL	0P	217.234	2363.36	675.70	16	30.70	1.30	2.49(.45)	2.82(.67)	4.66(.70)	9.97(.23)	16.96(11.32)	0.38(.20)	0.027(.010)
	2P						0.88	1.84(.33)	2.38(.29)	6.25(.49)	10.47(.57)	18.96(16.35)	0.62(.19)	0.0086(.0019)
LTGRTLFPGTDHIDQLKLIL	0P	217.236	2024.11	751.09	18	28.40	2.89	3.02(.49)	6.25(.31)		9.30(.26)	10.76(4.06)	0.061(.0091)	
	2P						3.61	2.89(.36)	6.00(.39)		9.05(.38)	4.39(1.32)	0.018(.0035)	
ILRL [4]	0P	235.238	2250.28	514.37	3	31.20	No Fit	0	0	0				
	2P						No Fit	0	0	0				
ILRLVGTPGAE	0P	235.245	513.37	563.33	9	24.80	0.25	3.61(.19)	0.73(.15)	1.62(.65)	5.96(.72)	23.03(7.82)	0.44(.26)	0.0063(.0055)
	2P						1.29	3.74(.21)		2.55(1.10)	6.30(1.13)	15.70(3.91)		.0058(.0044)
ILRLVGTPGAEL [3]	0P	235.246	1124.66	619.87	10	27.40	0.20	4.43(.17)	1.37(.15)	1.13(.21)	6.93(.26)	20.67(4.04)	0.40(.12)	0.011(.0079)
	2P						0.67	4.29(.19)	1.25(.20)	1.47(.20)	7.0	14.47(2.40)	0.17(.078)	0.0060(.0018)
ILRLVGTPGAELLKKISSESARN	0P	235.257	1237.74	818.14	21	27.10	4.04	13.71(.76)	5.36(.54)		19.06(.21)	24.86(10.02)	0.58(.15)	
	2P						7.68	14.90(.77)	4.55(.61)		19.46(.26)	15.62(3.14)	0.39(.15)	
RLVGTPGAEL	0P	237.246	2451.42	506.79	8	24.40	0.41	4.85(.19)	1.67(.11)		6.51(.10)	17.79(2.68)	0.063(.013)	
	2P						0.77	4.68(.17)	1.65(.14)		6.33(.12)	14.90(2.22)	0.045(.011)	
RLVGTPGAELLKKISSESARN	0P	237.257	1011.57	742.75	19	27.60	4.04	13.70(.76)	5.36(.54)		19.06(.21)	24.90(10.42)	0.59(.15)	
	2P						3.93	13.96(.90)	4.38(.82)	2.00(.52)	20.33(.47)	19.13(5.41)	0.93(.36)	0.018(.018)
VGTPGAEL	0P	239.246	2225.25	743.39	6	24.40	0.58	4.19(.22)	0.59(.13)		4.77(.11)	20.65(5.70)	0.12(.086)	
	2P						1.03	4.11(.20)	0.59(.15)		4.69(.12)	16.55(3.84)	0.080(.065)	
VGTPGAELLKKISSESARN	0P	239.257	742.39	653.02	17	27.00	0.85	13.97(.67)	3.20(.63)	1.05(.62)	18.21(.14)	21.69(4.49)	1.47(.64)	0.12(.11)
	2P						2.25	13.78(.86)	3.30(.78)	1.30(.41)	18.37(.23)	17.99(3.90)	1.31(.56)	0.037(.029)
VGTPGAELLKKISSESARNYIQSL [7]	0P	239.262	1956.06	854.46	22	32.20	8.52	7.31(.84)	8.41(.53)		15.71(.45)	16.15(6.23)	0.045(.0087)	
	2P						6.99	8.12(.17)	7.81(.044)		15.93(.048)	16.20(0.00)	0.011(.0002)	
LLKKISSESARNYIQSL	0P	246.262	2560.39	975.55	16	22.10	9.80	15.86(.83)			15.98(.22)	12.00(1.51)		
	2P						5.86	14.46(.78)	2.41(.63)		16.86(.31)	11.59(1.74)	0.33(.25)	
LKKISSESARN [3]	0P	247.257	1949.09	616.84	10	23.10	1.82	7.77(.43)	1.22(.14)		9.0	16.12(4.70)	0.013(.0095)	
	2P						2.19	6.92(.76)	1.77(.70)		8.69(.15)	19.31(9.84)	0.96(.59)	
LKKISSESARNYIQSL	0P	247.262	1231.68	919.01	15	26.90	0.89	12.96(.57)	2.56(.50)		15.52(.088)	18.85(2.97)	1.35(.37)	
	2P						3.47	12.80(.78)	2.92(.70)		15.71(.15)	13.18(2.18)	0.73(.34)	
YIQSL [3]	0P	258.262	622.34	623.34	4	22.90	0.24	2.27(.14)	0.36(.089)		2.63(.076)	15.71(3.21)	0.046(.034)	
	2P						0.63	2.24(.14)		0.77(.058)	3.0	8.68(1.44)		0.0032(.0015)
AQMPKMNF	0P	263.270	965.45	483.72	6	33.10	0.63	4.87(.32)	1.41(.25)		6.28(.072)	20.29(6.37)	0.71(.26)	
	2P						1.03	5.11(.30)	1.26(.24)		6.35(.089)	10.50(1.57)	0.38(.20)	
AQMPKMNFANV	0P	263.273	1249.59	625.80	9	28.90	0.66	7.02(.30)	2.24(.21)		9.35(.088)	14.92(1.95)	0.42(.11)	
	2P						1.36	7.02(.31)	2.42(.24)		9.43(.12)	10.95(1.36)	0.30(.092)	
AQMPKMNFANVF	0P	263.274	1396.66	699.33	10	31.00	0.47	6.85(.27)	3.75(.19)		10.60(.070)	21.56(4.58)	0.60(.074)	
	2P						1.70	6.36(.62)	3.34(.59)	1.35(.46)	11.05(.20)	14.28(3.95)	0.82(.32)	0.041(.029)
AQMPKMNFANVFIGANPLAVDL	0P	263.284	2360.19	1181.10	19	29.80	1.33	9.54(1.01)	6.45(.93)		15.98(.14)	18.66(7.49)	0.66(.19)	
	2P						8.31	7.81(1.52)	7.96(1.35)		15.76(.41)	16.52(11.72)	0.67(.25)	
ANVF	0P	271.274	449.23	450.23	3	20.60	1.32		2.33(.11)		2.33(.20)		0.65(.15)	
	2P						0.58	1.56(.35)	0.75(.31)		2.37(.09)	0.94(.33)	0.074(.060)	
IGANPLAVDL	0P	275.284	981.56	982.56	8	26.00	0.23	1.36(.19)	1.56(.13)		2.93(.05)	14.07(5.55)	0.47(.11)	
	2P						0.57	1.07(.27)	1.93(.24)		2.99(.06)	10.39(6.23)	0.53(.15)	
IGANPLAVDLLEKM	0P	275.288	1482.81	742.41	12	31.00	0.75		2.15(.15)		2.15(.078)		0.87(.15)	
	2P						1.02		2.54(.14)		2.54(.082)		0.80(.12)	

Sequence [1]		Residues	Calc Mass	Obs. m/z	#EA	% BE	RSS	A [2]	B	C	N	k_1	k_2	k_3
LEKMLVLDSDKRITAAQALAHAY	0P	285.307	2556.37	853.12	22	26.10	0.42	3.60(.26)	3.69(.50)	3.45(.54)	10.73(.11)	18.67(5.71)	0.40(.098)	0.041(.011)
	2P						5.53	4.53(.50)	6.27(.39)		10.84(.30)	7.21(1.95)	0.067(.013)	
LVLDSDKRITAAQALAHAY [3]	0P	289.307	2055.12	1028.56	18	27.30	0.47	3.38(.26)	3.60(.76)	3.11(.81)	10.09(.12)	19.66(6.94)	0.33(.10)	0.044(.016)
	2P						1.47	2.86(.42)	3.84(.39)	4.30(.35)	11.0	21.10(17.79)	0.56(.15)	0.017(.0047)
LVLDSDKRITAAQALAHAYF	0P	289.308	2202.19	735.06	19	28.80	2.46	3.68(.46)	6.18(.28)		9.87(.22)	16.74(7.67)	0.11(.015)	
	2P						1.42	2.85(.42)	3.41(.36)	4.57(.31)	10.83(.21)	21.46(18.71)	0.71(.21)	0.025(.0051)
DSDKRITAAQALAHAY	0P	292.307	1729.87	865.94	15	21.80	0.76	2.09(.27)	4.36(.16)		6.46(.12)	9.30(2.47)	0.10(.011)	
	2P						2.93	3.09(.37)	3.62(.39)		7.09(.34)	1.11(.29)	0.019(.0063)	
FAQYHDPDDEPVADPYDQSF	0P	308.327	2354.97	1178.49	16	30.00	2.15	6.73(.46)	3.81(.27)		10.54(.18)	19.44(6.14)	0.23(.054)	
	2P						6.16	7.24(.51)	3.82(.38)		11.06(.29)	10.14(2.03)	0.079(.025)	
AQYHDPDDEPVADPYDQSF [3]	0P	309.327	2207.90	1104.95	15	30.80	1.58	6.14(.38)	3.50(.22)		9.64(.14)	16.89(3.91)	0.23(.048)	
	2P						2.62	3.36(.59)	2.28(.52)		10.5	0.83(.34)	0.026(.012)	
FESRDLL [3]	0P	327.333	878.45	879.45	6	27.60	0.57	0.73(.27)	2.61(.21)	2.18(.20)	5.5	7.80(5.78)	0.26(.070)	0.0052(.0011)
	2P						0.80		1.45(.17)	3.67(1.55)	5.13(1.63)		0.78(.22)	0.0045(.0033)
ESRDLL	0P	328.333	731.39	732.39	5	29.80	0.65	2.45(.25)	1.30(.16)		3.77(.12)	9.70(2.20)	0.082(.030)	
	2P						1.19	1.97(.25)	1.50(.19)		3.47(.12)	8.46(2.71)	0.16(.064)	
ESRDLLIDE	0P	328.336	1088.54	545.27	8	26.10	0.63	3.18(.26)	1.66(.16)		4.84(.098)	9.81(1.75)	0.23(.071)	
	2P						2.28	3.25(.34)	1.82(.30)		5.06(.18)	4.31(1.07)	0.090(.040)	
LLIDE [3]	0P	332.336	601.33	602.33	4	23.90	1.08	1.48(.26)		0.64(.086)	2.25	5.66(1.89)		0.0032(.0025)
	2P						1.94	1.67(.22)		1.07(.12)	2.75	2.72(.85)		0.0042(.0017)
IDEWKSLT [3]	0P	334.341	990.50	496.25	7	25.60	0.30	0.26(.13)	0.92(.22)		1.19(.25)	1.98(2.11)	0.011(.0078)	
	2P						0.24	0.30(.085)		1.28(.065)	1.5	0.97(.66)		0.0052(.00068)
IDEWKSLTYDEV	0P	334.345	1496.70	749.35	11	28.30	0.393		1.55(.11)		1.28(.11)		0.025(.0066)	
	2P						0.83		1.29(.26)		.98(.26)		0.013(.0072)	
WKSLTYD [4]	0P	337.343	911.45	456.73	6	25.00	No Fit	0	0	0				
	2P						No Fit	0	0	0				
WKSLTYDE [4]	0P	337.344	1040.48	521.24	7	24.50	No Fit	0	0	0				
	2P						No Fit	0	0	0				
WKSLTYDEV [4]	0P	337.345	1139.55	570.77	8	27.20	No Fit	0	0	0				
	2P						No Fit	0	0	0				
EVISF	0P	344.348	593.31	594.31	4	20.40	0.27	0.53(.20)	1.14(.20)		1.68(.07)	2.33(1.87)	0.13(.045)	
	2P						0.62	0.54(.24)	1.15(.23)		1.59(.12)	0.95(.80)	0.036(.019)	
EVISFVPPPLDQEE	0P	344.357	1597.80	799.90	10	29.00	0.69	5.40(.23)	2.76(.125)		8.16(.10)	25.08(8.35)	0.11(.016)	
	2P						3.58	5.69(.34)	2.52(.23)		8.24(.17)	14.20(3.30)	0.051(.015)	
ISFVPPPLDQEEMES	0P	346.360	1716.79	859.40	11	29.90	0.67	8.00(.30)	2.60(.21)		10.60(.085)	24.35(6.64)	0.54(.11)	
	2P						2.11	8.26(.36)	2.60(.26)		10.87(.15)	14.80(2.45)	0.27(.086)	
VPPPLDQEEMES	0P	349.360	1369.61	685.80	8	27.20	2.12	8.56(.36)			8.57(.087)	15.76(2.13)		
	2P						1.86	8.29(.25)			8.29(.085)	15.96(2.12)		

Footnotes:

(1) Information for each peptide includes Amino acid sequence, Residue numbers, Calculated mass, Observed mass/charge, Number of exchangable amides (#EA), Percent back-exchange (%BE), and Residual sum of squares for best NLSQ fit (RSS)

(2) A, B, and C equal the number of amides exchanging with rates k_1, k_2, and k_3 respectively. N equals A+B+C. Values are corrected for artifactual in-exchange, back-exchange, and percentage D2O during the incubation.

(3) Fitting constrained N to equal deuteration at 4hrs.

(4) Peptides with "No Fit" -- Fitting failed to converge because no measurable hydrogen exchange could be observed over the 4 h time course.

(5) In nine peptides around the activation lip, differential proteolysis was observed between 0P-p38 and 2P-p38 (See Figure 2). For these peptides, only one activation state is listed. Peptide 173-187 is the only peptide observed in 2P-p38.

(6) Peptide 173-187 was not observed in 0P-p38. Instead the fit represents deuteration vs time summed over peptides 173-182 and 183-187 in 0p-p38.

(7) Rates were fixed to predicted values to better allow model convergence.

Table 4: Hydrogen exchange error measurements.

Standard deviations of weighted average mass (WAM) and number of deuterons incorporated (#DI) were quantified at the 1 min time point in three replicate runs, performed for 0P-p38 and 2P-p38.

	0p-p38α	2p-p38α
Avg Std Dev of the WAM	0.0400	0.0482
Lowest value	0.0075	0.0004
Highest value	0.0985	0.1329
Avg Std Dev of the #DI	0.1611	0.1856
Lowest value	0.0292	0.0025
Highest value	0.3318	0.4175

Peptide Name (Starting Residue. Final Residue)	0p-p38α WAM	#DI	WAM Avg	WAM Stdev	#DI Avg	#DI StDev	2p-p38α WAM	#DI	WAM Avg	WAM Stdev	#DI Avg	#DI StDev
-7.8	975.5114	6.8661	975.5517	0.0701	6.9928	0.2199	975.6623	7.2881	975.6567	0.0226	7.2705	0.0713
	975.6326	7.2467					975.6760	7.3313				
	975.5112	6.8656					975.6319	7.1921				
9.39	1181.6976	19.9505	1181.7338	0.0513	20.0816	0.1970	1181.9660	21.2151	1181.9647	0.0018	21.1509	0.1004
	1181.7701	20.3082					1181.9635	21.2024				
	1181.7048	19.9861					1181.9297	21.0352				
40.71	931.0292	7.9017	931.0240	0.0241	7.8662	0.1652	930.9845	7.5647	930.9618	0.0213	7.4093	0.1460
	931.0452	8.0108					930.9587	7.3881				
	930.9977	7.6861					930.9422	7.2750				
72.86	601.9295	0.7850	601.9925	0.0575	1.1241	0.3093	601.9860	1.0103	601.9696	0.0267	0.9219	0.1444
	602.0059	1.1965					601.9841	1.0001				
	602.0420	1.3907					601.9388	0.7552				
72.87	639.6334	1.1305	639.6780	0.0433	1.4332	0.2943	639.6694	0.8936	639.6530	0.0467	0.7799	0.3232
	639.6806	1.4510					639.6004	0.4153				
	639.7200	1.7182					639.6893	1.0308				
75.87	512.0194	1.1601	512.0570	0.0359	1.3375	0.1693	512.0706	1.3252	512.0768	0.0524	1.3547	0.2487
	512.0908	1.4972					512.0278	1.1221				
	512.0607	1.3551					512.1320	1.6168				
83.94	474.4170	1.3315	474.4254	0.0389	1.3743	0.1988	474.3857	1.1712	474.4126	0.0233	1.3089	0.1194
	474.3914	1.2004					474.4271	1.3828				
	474.4678	1.5911					474.4251	1.3728				
83.96			550.4163	0.0430	0.9317	0.2191	550.4448	1.2778	550.4308	0.0259	1.2071	0.1305
	550.3859	0.7768					550.4008	1.0565				
	550.4467	1.0866					550.4467	1.2871				
87.103	1011.2675	7.5772	1011.2019	0.0647	7.4255	0.1497	1011.2070	7.4775	1011.1836	0.1202	7.4231	0.2795
	1011.1381	7.2779					1011.2904	7.6714				
	1011.2002	7.4214					1011.0533	7.1204				

Peptide Name (Starting Residue. Final Residue)	0p-p38α WAM	#DI	WAM Avg	WAM Stdev	#DI Avg	#DI StDev	2p-p38α WAM	#DI	WAM Avg	WAM Stdev	#DI Avg	#DI StDev
87.98	690.7697	4.1878	690.7432	0.0278	4.1045	0.0876	690.7092	4.0439	690.6666	0.0376	3.9108	0.1176
	690.7142	4.0133					690.6380	3.8210				
	690.7457	4.1124					690.6528	3.8674				
88.98	634.2042	4.2581	634.1481	0.0780	4.0778	0.2507	634.1769	4.0884	634.1518	0.0373	4.0070	0.1213
	634.1811	4.1838					634.1089	3.8676				
	634.0589	3.7916					634.1697	4.0651				
88.103	954.6470	7.6866	954.6292	0.0382	7.6269	0.1279	954.4921	7.1638	954.4708	0.0186	7.0925	0.0622
	954.5853	7.4800					954.4579	7.0495				
	954.6552	7.7141					954.4623	7.0642				
87.99	764.7014	5.3980	764.6906	0.0183	5.3629	0.0593	764.6694	5.2931	764.6464	0.0397	5.2185	0.1287
	764.6695	5.2944					764.6692	5.2924				
	764.7009	5.3963					764.6006	5.0699				
87.101	879.8378	6.7894	879.8822	0.0599	6.9585	0.2285	879.8668	6.9483	879.8407	0.0884	6.8493	0.3356
	879.8584	6.8677					879.9132	7.1243				
	879.9503	7.2184					879.7422	6.4753				
89.98	576.3927	3.5194	576.4166	0.0214	3.5901	0.0632	576.3813	3.2258	576.4677	0.0810	3.4925	0.2502
	576.4233	3.6099					576.5421	3.7222				
	576.4338	3.6410					576.4797	3.5295				
99.104	771.2564	0.5270	771.2529	0.0320	0.5217	0.0492	771.3169	0.7048	771.2673	0.0495	0.6299	0.0748
	771.2193	0.4701					771.2671	0.6296				
	771.2831	0.5679					771.2180	0.5553				
104.129	989.3288	17.0222	989.3628	0.0426	17.1898	0.2101	989.1552	16.2054	989.0896	0.0849	15.8829	0.4175
	989.3490	17.1216					989.1199	16.0319				
	989.4106	17.4255					988.9937	15.4113				
130.156	799.2060	1.1222	799.1963	0.0205	1.0560	0.1402	799.3311	1.8397	799.2803	0.0443	1.4902	0.3041
	799.1729	0.8954					799.2590	1.3440				
	799.1755	0.9134					799.2507	1.2868				
	799.2131	1.1706										
	799.2143	1.1785										
130.145	635.6696	0.1323	635.6768	0.0075	0.1678	0.0371	635.6646	0.0411	635.6703	0.0127	0.0692	0.0628
	635.6762	0.1649					635.6615	0.0255				
	635.6846	0.2062					635.6848	0.1412				

Peptide Name (Starting Residue. Final Residue)	0p-p38α WAM	#DI	WAM Avg	WAM Stdev	#DI Avg	#DI StDev	2p-p38α WAM	#DI	WAM Avg	WAM Stdev	#DI Avg	#DI StDev
131.156	770.8719	1.0027	770.8583	0.0163	0.9115	0.1087	770.8980	1.1977	770.8953	0.0274	1.1795	0.1825
	770.8402	0.7913					770.9212	1.3522				
	770.8626	0.9406					770.8667	0.9886				
133.145	758.1533	0.1180	758.2295	0.0709	0.3533	0.2189	758.2012	0.0331	758.2021	0.0117	0.0356	0.0366
	758.2417	0.3910					758.1908	0.0004				
	758.2935	0.5509					758.2141	0.0734				
133.156	935.3501	0.8247	935.3775	0.0238	0.9645	0.1217	935.4232	1.0149	935.4122	0.0097	0.9585	0.0496
	935.3937	1.0473					935.4050	0.9216				
	935.3887	1.0215					935.4084	0.9389				
134.156	892.5834	0.9077	892.6113	0.0328	1.0445	0.1606	892.6682	1.1426	892.6325	0.0509	0.9666	0.2507
	892.6032	1.0045					892.5742	0.6795				
	892.6475	1.2213					892.6551	1.0777				
136.156	817.2136	1.0455	817.2576	0.0385	1.2670	0.1938	817.2413	0.8967	817.2217	0.0272	0.7972	0.1384
	817.2742	1.3505					817.1907	0.6391				
	817.2850	1.4051					817.2332	0.8559				
157.164	894.2474	1.4788	894.2604	0.0288	1.5011	0.0491	894.2446	1.5211	894.2735	0.0262	1.5700	0.0445
	894.2404	1.4670					894.2800	1.5811				
	894.2935	1.5574					894.2958	1.6079				
164.182	735.2982	10.7872	735.3689	0.0654	11.1392	0.3253						
	735.3815	11.2016										
	735.4271	11.4288										
165.187							956.2982	14.4662	956.2548	0.0467	14.2601	0.2219
							956.2609	14.2890				
							956.2054	14.0252				
183.194	499.5577	4.7043	499.5853	0.0390	4.8453	0.1995						
	499.6129	4.9864										
188.195	497.8511	2.2556	497.8848	0.0476	2.3688	0.1601	497.6174	1.5020	497.6259	0.0120	1.5304	0.0403
	497.9184	2.4821					497.6345	1.5589				
195.210	984.9019	6.6966	984.8080	0.0883	6.3853	0.2928	985.0036	6.9274	985.0646	0.0863	7.1316	0.2887
	984.7267	6.1154					985.1256	7.3357				
	984.7955	6.3439										
211.215	566.7938	0.1558	566.7833	0.0190	0.1398	0.0292	567.0162	0.5454	566.8747	0.1329	0.3310	0.2013
	566.7948	0.1574					566.8553	0.3017				
	566.7613	0.1061					566.7526	0.1461				

Peptide Name (Starting Residue. Final Residue)	0p-p38α WAM	#DI	WAM Avg	WAM Stdev	#DI Avg	#DI StDev	2p-p38α WAM	#DI	WAM Avg	WAM Stdev	#DI Avg	#DI StDev
214.231	663.3316	3.2657	663.3517	0.0259	3.3620	0.1244	663.2650	2.8968	663.2087	0.0493	2.6257	0.2373
	663.3425	3.3177					663.1732	2.4551				
	663.3810	3.5024					663.1878	2.5253				
214.234	586.3834	3.2904	586.3924	0.0103	3.3486	0.0662	586.3583	3.1453	586.3580	0.0004	3.1435	0.0025
	586.3903	3.3346					586.3578	3.1418				
	586.4037	3.4207										
216.234	714.7342	3.4077	714.7760	0.0391	3.6141	0.1935	714.6492	2.8975	714.6394	0.0352	2.8488	0.1749
	714.7819	3.6434					714.6686	2.9942				
	714.8118	3.7913					714.6004	2.6547				
216.236	790.2317	3.5639	790.2200	0.0103	3.5083	0.0490	790.1954	3.2952	790.1735	0.0559	3.1903	0.2676
	790.2123	3.4716					790.2151	3.3895				
	790.2160	3.4893					790.1099	2.8861				
217.234	677.0511	3.3576	677.0785	0.0298	3.4957	0.1505	676.9801	2.9418	676.9779	0.0122	2.9308	0.0616
	677.0740	3.4733					676.9648	2.8644				
	677.1102	3.6560					676.9888	2.9861				
217.236	752.4612	3.3664	752.4476	0.0354	3.3016	0.1689	752.3919	2.8869	752.3671	0.0554	2.7676	0.2664
	752.4075	3.1099					752.4057	2.9535				
	752.4742	3.4285					752.3036	2.4624				
235.257	822.3861	16.3017	822.3929	0.0291	16.3336	0.1363	822.4691	16.6695	822.4268	0.0520	16.4705	0.2440
	822.3678	16.2161					822.4424	16.5438				
	822.4248	16.4831					822.3688	16.1982				
275.288	743.4816	0.9562	743.5069	0.0220	1.0425	0.0748	743.6893	1.7526	743.5843	0.1204	1.3976	0.4069
	743.5205	1.0886					743.6106	1.4865				
	743.5187	1.0826					743.4529	0.9536				
285.307	854.9129	4.8517	854.9181	0.0183	4.8752	0.0832	854.9824	5.1637	854.9263	0.0542	4.9078	0.2475
	854.9030	4.8062					854.9224	4.8899				
	854.9384	4.9676					854.8742	4.6697				
289.308	736.5762	4.1568	736.5969	0.0462	4.2549	0.2191	736.7041	4.7846	736.6670	0.0670	4.6092	0.3172
	736.6498	4.5059					736.7073	4.8000				
	736.5646	4.1019					736.5897	4.2430				
308.327	1181.7384	7.2754	1181.7690	0.0985	7.3782	0.3318	1181.9674	8.0605	1181.9095	0.0666	7.8657	0.2241
	1181.6894	7.1101					1181.9244	7.9157				
	1181.8791	7.7492					1181.8367	7.6207				
327.333	881.0849	1.3532	881.0361	0.0423	1.2742	0.0685	880.8066	0.9476	880.6988	0.1076	0.7740	0.1732
	881.0103	1.2323					880.5914	0.6011				
	881.0132	1.2370					880.6983	0.7732				
346.360	862.7988	8.9223	862.8112	0.0670	8.9639	0.2256	862.9902	9.5628	862.8950	0.0826	9.2420	0.2782
	862.7512	8.7619					862.8515	9.0953				
	862.8835	9.2073					862.8433	9.0678				

the conserved Asp-Phe-Gly motif and Thr-Xxx-Tyr phosphorylation sites. Here, the pepsin cleavage sites differed between 0P- and 2P-p38α (Figure 3). Therefore, we compared the deuteration time course of pr165-187 observed as a single intact peptide in 2P-p38α to a corresponding time course calculated by summing deuteration of two peptides in 0P-p38α (Figure 6A). The time course of pr165-182 + pr183-187 in 0P-p38α showed higher deuteration than peptide pr165-187 from 2P-p38α, despite the fact that the time course represented by composite sequences contained one less exchangeable amide. This confirms that HX decreases significantly within the activation lip in 2P-p38α. Adjacent to this region is pr188-195 (YRAPEIML) which forms the P+1 substrate recognition site. Direct comparison of the same peptide between 0P- and 2P-p38α revealed significantly decreased HX in active p38α (Figure 6B). The X-ray structures of p38α and phosphorylated p38γ predict substantial conformational remodeling of this region upon kinase phosphorylation (Figure 6C). In the 0P-p38α structure, residues 171-179 are highly exposed to solvent with large main chain B-factors (80 $Å^2$), whereas in 2P-p38γ, the activation lip is more constrained with lower B-factors (45-70 $Å^2$). Residues within pr188-195, which are accessible to solvent in 0P-p38α, are buried in 2P-p38γ due to movement of the activation lip. Such changes in conformation readily account for the significant decrease in HX observed in this region upon p38α activation. Domain closure between N- and C-terminal lobes observed in 2P-p38γ may also reduce solvent accessibility of residues in the lip (Bellon et al., 1999). Thus, the effect of p38α phosphorylation on hydrogen exchange occurring within the lip and P+1 loop can be attributed to structural remodeling of the activation lip as well as interdomain interactions which accompany dual phosphorylation.

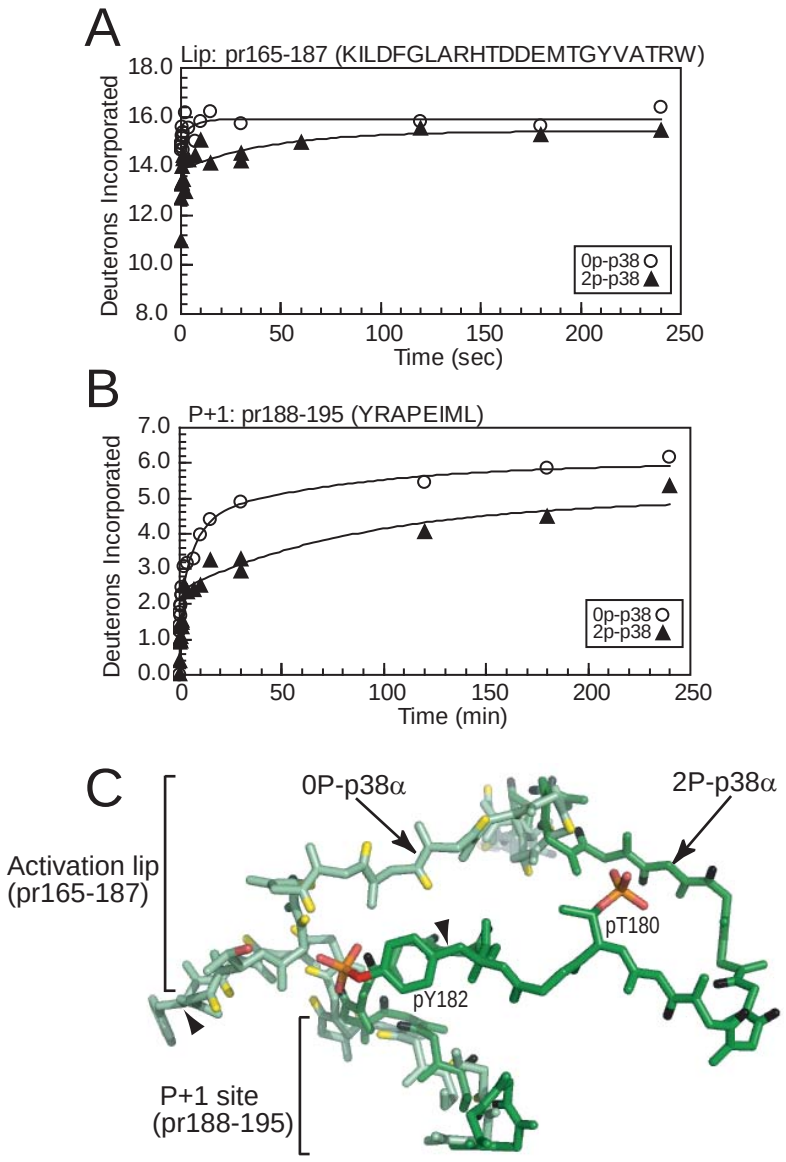

Figure 6. Comparison of peptide HX kinetics between 0P-p38a (○) and 2P-p38a (▲) and associated X-ray structural differences in the activation lip and P+1 substrate recognition site. Time courses of deuteration are shown for **(A)** peptide region (pr) 165-187 in the activation lip and **(B)** pr188-195 in the P+1 site. In 2P-p38α, the deuteration time course for pr165-187 is represented by a single intact peptide, whereas in 0P-p38α, the time course represents the sum of pr165-182 + pr183-187, which contains one less exchangeable amide than pr165-187 in 2P-p38α. Nevertheless, the extent of deuteration decreases in 2P-p38α, reflecting a significant reduction in HX. **(C)** Cα conformation from X-ray structures of 0P-p38α (light green, 1P38) and 2P-p38γ (dark green, 1CM8), overlaying regions in the activation lip and P+1 site. Amide hydrogens from p38α and p38γ are represented by yellow and black sticks, respectively. Arrowheads indicate peptide cleavage sites.

(2) C-terminal helix αE and catalytic site β6. Decreased HX was observed in pr130-145 (LIYQILRGLKYIHSAD) which includes most of helix αE, and pr146-156 (IIHRDLKPSNL) containing the β6-strand and catalytic base, Asp150 (Figure 7A,B). Helix αE forms core α-helix interactions that stabilize the C-terminal domain, and residues in helix αE are deeply buried in p38α, with amide hydrogens typically removed from the surface by 4-7 Å. 2P-p38γ shows no obvious changes in distance to surface or hydrogen bonding patterns in this region (Figure 7C). Thus, the significant decrease in HX upon phosphorylation suggests lower conformational mobility in active p38α, enhancing stability of the C-terminal core. Strand β6 forms interactions with the activation lip upon p38α phosphorylation, through ion pair interactions between Arg149 and lip residue pThr180, which may constrain mobility within β6 (Figure 7C). Side chain interactions between helix αE and strand β6 (Figure 7D) suggests connections between these regions that may explain their correlated decreases in HX.

(3) C-terminal extension and the L16 loop. pr327-333 (FESRDLL) in the p38α structure contains a single 3-10 helical turn at the end of the C-terminal extension, terminating in helix αL16, where HX decreases upon kinase activation (Figure 8A). This region is disordered in 2P-p38γ, thus structural comparisons cannot be made. Nevertheless, much is known about this region, which has been implicated in p38α activation via a cluster of hydrophobic residues involving interactions between Phe327 located within this region and Tyr323 located upstream, Trp337 in helix αL16 , and Tyr69 in helix αC (Figure 8B) (Diskin et al., 2004; Diskin et al., 2007; Avitzour et al., 2007). Studies by Diskin et al., (2007) have shown that mutating Phe327 to Leu or Ser causes p38α autoactivation by promoting

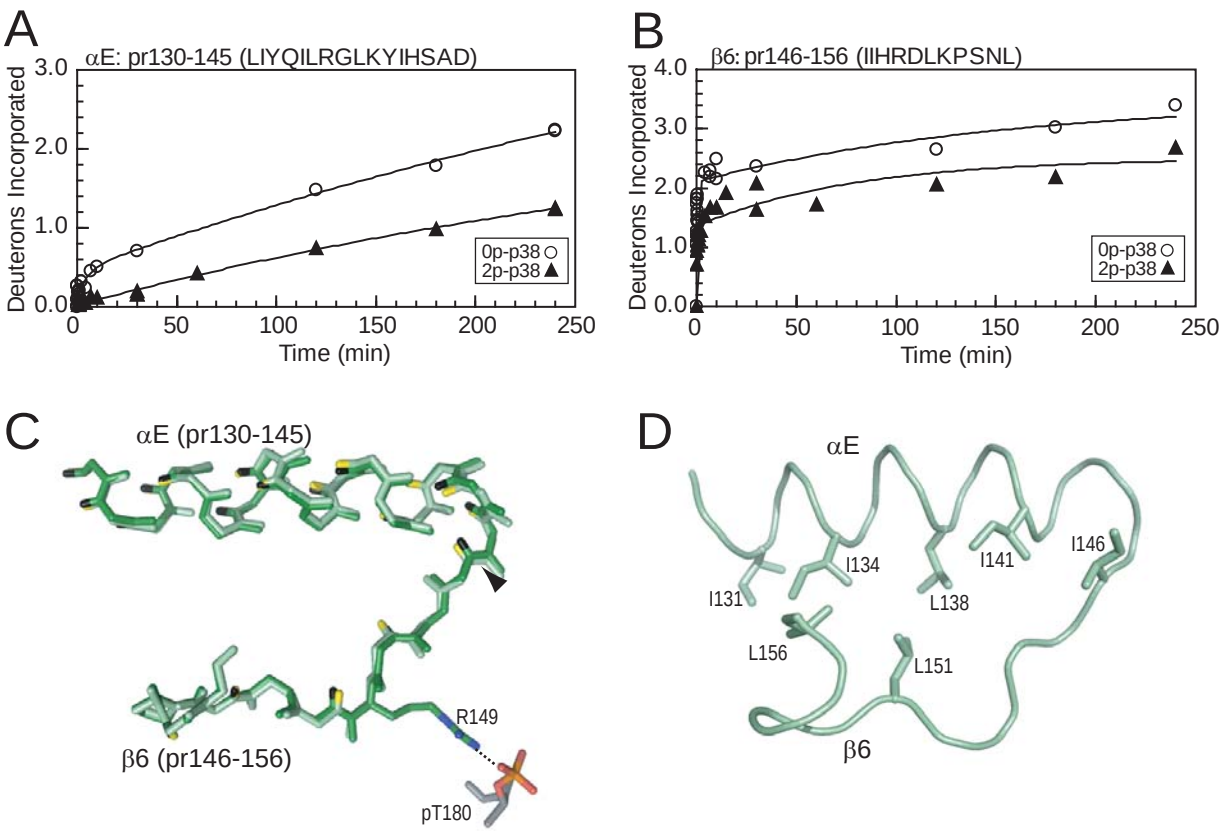

Figure 7. HX-MS behavior and structural comparison in the C-terminal core region. Deuteration of **(A)** pr130-145, containing helix αE, and **(B)** pr146-156 containing β6 and the catalytic base, Asp150. **(C)** Cα structures show similar conformation within αE between p38α (green) and p38δ (dark green). Residue Arg149 in β6 forms ion pair interactions with pThr180 in the activation lip of 2P-p38δ. Arrowheads indicate peptide cleavage sites. **(D)** Residue side chains between αE and β6 suggest potential interactions for coupling between these regions.

autophosphorylation at Thr180, and X-ray evidence shows that these mutations disrupt residue interactions within the hydrophobic cluster (Figure 8C, Diskin et al., 2007). This in turn disrupts ion pair interactions of the adjacent residue Glu328 with Arg70 in helix αC, which in 0P-p38α are separated by 2.9 Å. We speculate that release of Arg70 would enable rotation of helix αC, allowing formation of ion pair interactions with pThr180, as seen in the Arg70-pThr180 distance of 2.9 Å in 2P-p38γ (Figure 8C). This model suggests that the hydrophobic cluster constrains interactions between helix αC and the activation lip by sequestering Arg70. Therefore, it is reasonable to expect that phosphorylation of Thr180 at the activation lip would favor Arg70-pThr180 interactions, disrupting interactions between the hydrophobic cluster residues, and promoting interdomain closure. We hypothesize that the observed decrease in HX in the 3-10 helix reflects conformational changes induced by remodeling of the hydrophobic cluster.

The 3-10 helix in p38α resembles an analogous turn in the X-ray structure of phosphorylated ERK2 (Canagarajah et al., 1997). In ERK2, the 3-10 turn is found uniquely in the phosphorylated kinase, and forms a surface for dimerization, where hydrophobic side chains in this region interdigitate with corresponding residues from a second subunit. It has in fact been suggested that activating mutations facilitate p38α dimerization, given that autoactivation involves transphosphorylation between kinase subunits (Diskin et al., 2007), although no evidence for dimerization was apparent in the X-ray structure of 2P-p38γ or by size exclusion chromatography of 2P-p38α (Doza et al., 1995; Bellon et al., 1999). We therefore examined the possibility that p38α dimerizes following phosphorylation, and that the decrease in HX in pr327-333 might report steric protection from solvent in the dimer. Unphosphorylated and diphosphorylated forms of p38α were examined by sedimentation

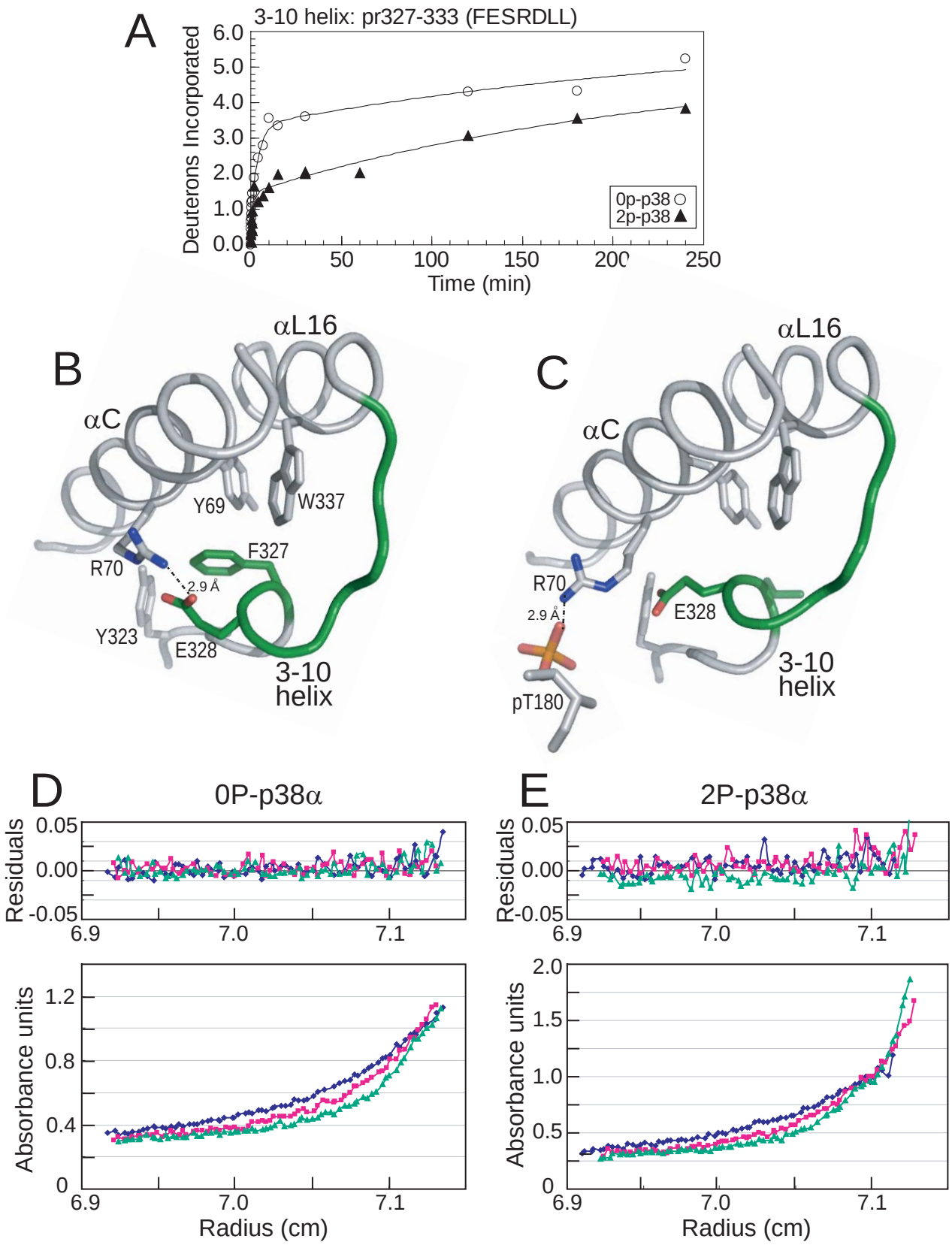
A
3-10 helix: pr327-333 (FESRDLL)
Deuterons Incorporated
Time (min)
0p-p38
2p-p38
B
αL16
αC
Y69
W337
F327
R70
2.9 Å
Y323
E328
3-10
helix
C
αL16
αC
R70
2.9 Å
E328
3-10
helix
pT180
D
0P-p38α
Residuals
Absorbance units
Radius (cm)
E
2P-p38α
Residuals
Absorbance units
Radius (cm)

Figure 8. HX-MS behavior and structural comparison in the C-terminal extension 3-10 helix. (A) Deuteration of pr327-333, containing the 3-10 helical turn indicates a significant reduction in HX upon p38α activation. **(B)** Structure of p38α shows side chain interactions comprising a hydrophobic core region with side chain connectivities between helices αC, αL16 and the 3-10 helix. Ion pair interactions with Glu328 sequester Arg70 from interacting with activation lip residues. Pr327-333 is shown in green. **(C)** X-ray structure of p38α-Phe327Leu mutation (2FST, Diskin et al., 2004) revealing disrupted side chain interactions in the hydrophobic cluster and disruption of ion pair interactions between Arg70 and Glu328 (5.3 Å). Rotation of Arg70 would enable new ion pair interactions between Arg70 and pThr180 (2.9 Å), which are observed in 2P-p38γ. **(D,E)** Sedimentation equilibrium experiments carried out by analytical ultracentrifugation show that **(D)** 0P-p38α and **(E)** 2P-p38α are both monomeric. The bottom panel shows absorbance units *vs* radius at 20,000 rpm (blue), 24,000 rpm (red) and 28,000 rpm (green). The top panel shows residuals after fitting absorbance data to a single component model. Weighted average masses 0P-p38α and 2P-p38α are 40,567 Da and 42,784 Da, respectively (4-7% error).

equilibrium (Figure 8D,E). Both forms of p38α were monomeric under all conditions. Thus, wild-type p38α does not dimerize upon phosphorylation, and the decrease in HX in this region can instead be attributed to conformational changes in monomer.

(4) N-terminal β4-β5 strands and helices αL16 and αC. pr88-103 (DVFTPARSLEEFNDVY) contains strands β4-β5 and the intervening loop which is largely exposed to solvent. Kinase activation leads to decreased HX in this region (Figure 9A). Decreased HX is also observed in pr344-348 (EVISF) (Figure 9B), which represents the C-terminal helix αL16, a structural motif common to MAP kinase family members. Peptide pr72-86 (LRLLKHMKHENVIGL), containing the αC-β4 loop, shows decreased HX whereas overlapping peptide pr75-86 does not (Figure 9C,D), indicating that the decreased HX can be narrowed to amide residues 72-75 within helix αC (LRLL). These regions form side chain interactions with each other within the N-terminal lobe, involving connections between Leu72 in helix αC, Val89, Leu96, and Phe99 in β4-β5, and Tyr342, Val345, Ile346, and Phe348 within αL16 (Figure 9E). Therefore, correlated decreases in HX in both regions may reflect coupling between these regions through hydrophobic side chain interactions Cα structures within this region show high overlap between 0P-p38α and 2P-p38γ (Figure 9F), suggesting that decreased HX may be accounted for by flexibility changes following phosphorylation, although perturbations in this region might also result from helix αC movements accompanying domain closure.

(5) Substrate binding sites: strands β7-β8 and helices αF-αG. pr217-234 (LTGRTLFPGTDHIDQLKL) contains part of conserved helices αF and αG and the intervening loop, and forms an extended surface for interactions with the activation lip of the p38α substrate, MAPKAP kinase 2 (MK2) (ter Haar et al., 2007; White et al., 2007). pr157-

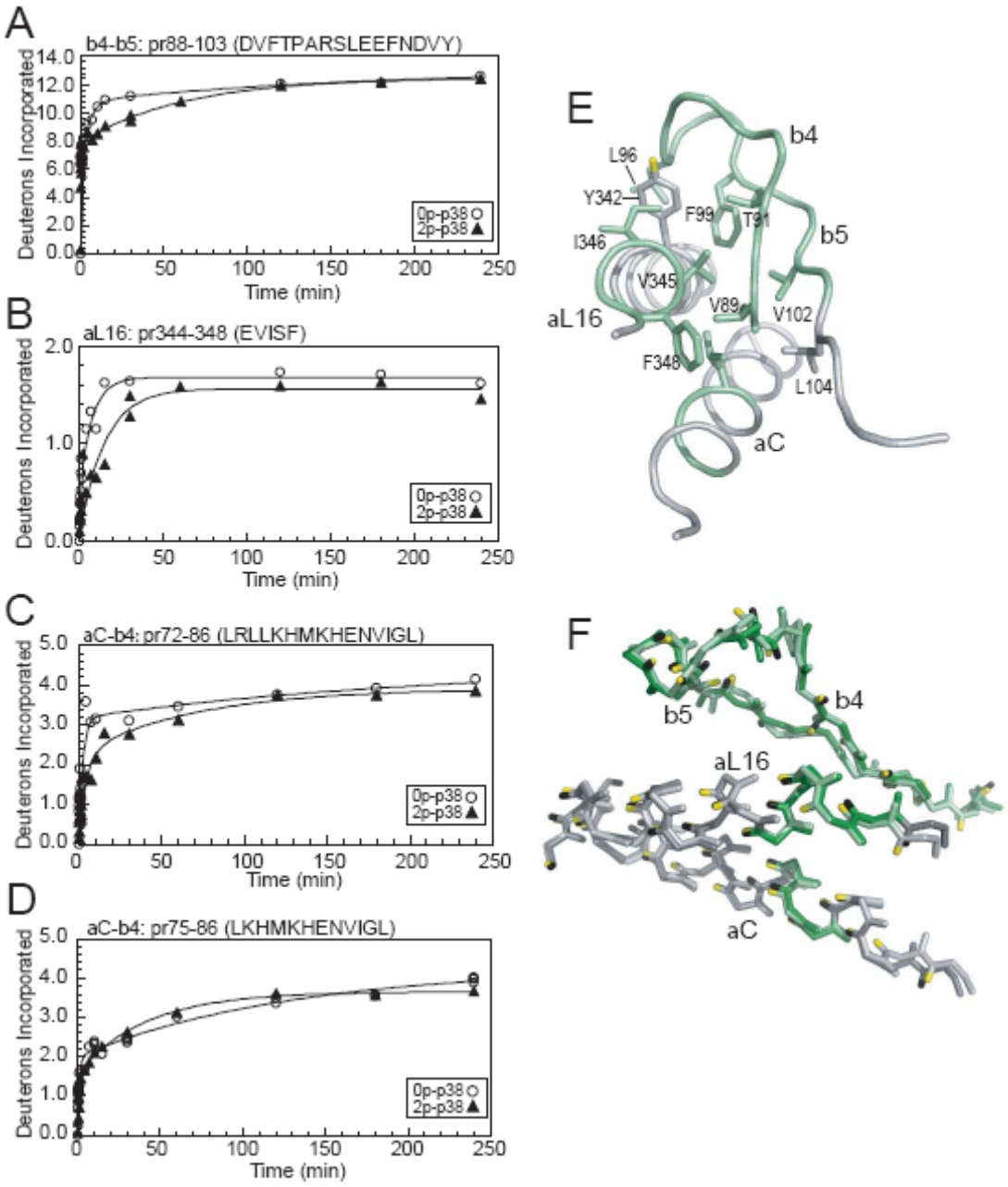

Figure 9. HX-MS behavior and structural comparison in the N-terminal core region of p38. Deuteration of **(A)** pr88-103, containing β4-β5 and intervening loop, and **(B)** pr344-348 containing the C-terminal helix αL16. Within the αC-β4 loop, **(C)** pr72-86 shows decreased HX and **(D)** pr75-86 shows no change, indicating that decreased HX can be localized to residues 72-75 (LRLL). **(E)** Side chain connectivities between β4-β5, αL16, and αC, where regions with decreased HX are shown in green. **(F)** Cα structures closely overlap between 0P-p38α (light green, light grey) and 2P-p38γ (dark green, dark grey), suggesting that the changes in HX reflect alterations in protein mobility rather than structure.

164 (AVNEDCEL) forms part of the binding site for a docking motif ("DEJL" motif) composed of a cluster of basic residues followed by L/I-X-L/I sequence, found in substrates and regulatory proteins, such as scaffold and adaptor proteins, MAP kinase kinases, and MAP kinase phosphatases (Tanoue et al., 2000; Chang et al., 20002). Both the αF-αG loop and the DEJL binding site form major contacts for binding p38α to MK2 (ter Haar et al., 2007; White et al., 2007). The interactions stabilize a high affinity inactive p38α-MK2 complex, localized to the nucleus, which upon phosphorylation of p38α becomes disrupted, enabling phosphorylation and nuclear export of MK2 (ter Haar et al., 2007; Engel et al., 1998). αF-αG loop residue Thr218 also forms a partial interaction surface for the allosteric effector, TAB1, which selectively binds p38α through a modified docking interaction extending from this region to the nearby DEJL-motif binding site (Ge et al., 2002; Zhou et al., 2006a).

In both regions, HX decreased upon p38α phosphorylation (Figure 10A,B). Inspection of 0P-p38α and 2P-p38γ showed little differences in structure within the αF-αG and β7-β8 loop regions (Figure 10C,D). However in 0P-p38α, the activation lip residue Tyr182 makes close contacts with αF-αG loop residues Gly225-Thr226, burying the amide hydrogen at residue Thr226 (Figure 10C). Remodeling of the activation lip in 2P-p38γ disrupts this interaction, exposing the amide to solvent. Interestingly, HX decreased significantly in 2P-p38α, despite the predicted increase in solvent accessibility in this region upon kinase phosphorylation. The lack of concurrence between HX behavior and expected structural changes suggests that protein mobility in these regions decreases upon p38α activation, although structural differences between 2P-p38γ and 2P-p38α cannot be ruled out. Conceivably, decreased

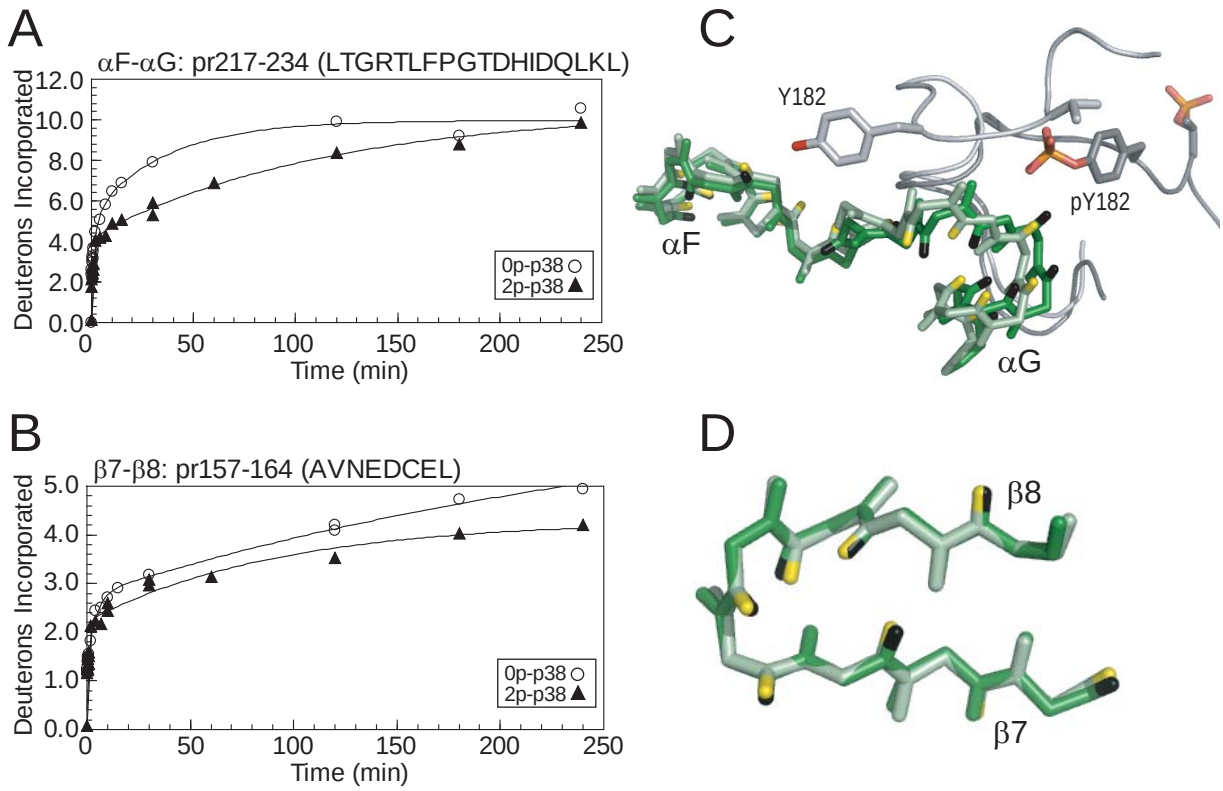

Figure 10. HX-MS behavior and structural comparisons within substrate binding regions. Time courses of deuteration for **(A)** pr217-234 in the αF-aG loop which comprises an extended substrate binding groove, and **(B)** pr157-164 in the β7-β8 loop which comprises part of the DEJL docking motif binding site. **(C,D)** Cα structures of 0P-p38α (light green) and 2P-p38δ (dark green), overlaying regions in the **(C)** αF-αG loop and **(D)** β7-β8 loop.

flexibility within these binding sites might affect binding of substrate or TAB1 by reducing their interactions with the active form of p38α.

Hydrogen exchange in monophosphorylated p38α.

Phosphorylation of p38α occurs preferentially at Tyr182, and p38α-pTyr182 is the predominant monophosphorylated form in stress-treated cells and *in vitro* reactions with MKK3/6 (Doza et al., 1995; Raingeaud et al., 1995). Therefore we examined HX behavior on p38α monophosphorylated at Tyr182 (0.85 mol/mol). Figure 11 shows results for seven peptides where the largest change in HX was observed in active p38α, decreasing deuteration either by >50% or >2 Da over the time course. In each case, time courses of deuteration in monophosphorylated p38α resembled those in unphosphorylated p38α more than diphosphorylated enzyme. This occurred in the activation lip and P+1 site, as well as the substrate binding sites, the N- and C-terminal core regions, and the C-terminal 3-10 helix. This indicates that the conformational and dynamic responses underlying the changes in HX result from phosphorylation at both Thr180 and Tyr182.

DISCUSSION

Hydrogen exchange measurements reveal information about conformational mobility of proteins in solution, and are complementary to structural analysis of low energy conformers by X-ray crystallography. Analysis of p38α reveals slow exchanging core regions composed of β6, αE, and αF in the C-terminal domain and β3, β4 and αC in the N-terminal domain. In contrast, greater levels of exchange were observed in the activation lip, the MAP kinase insert, and peripheral loops where the structure would predict higher solvent accessibility. Thus, an

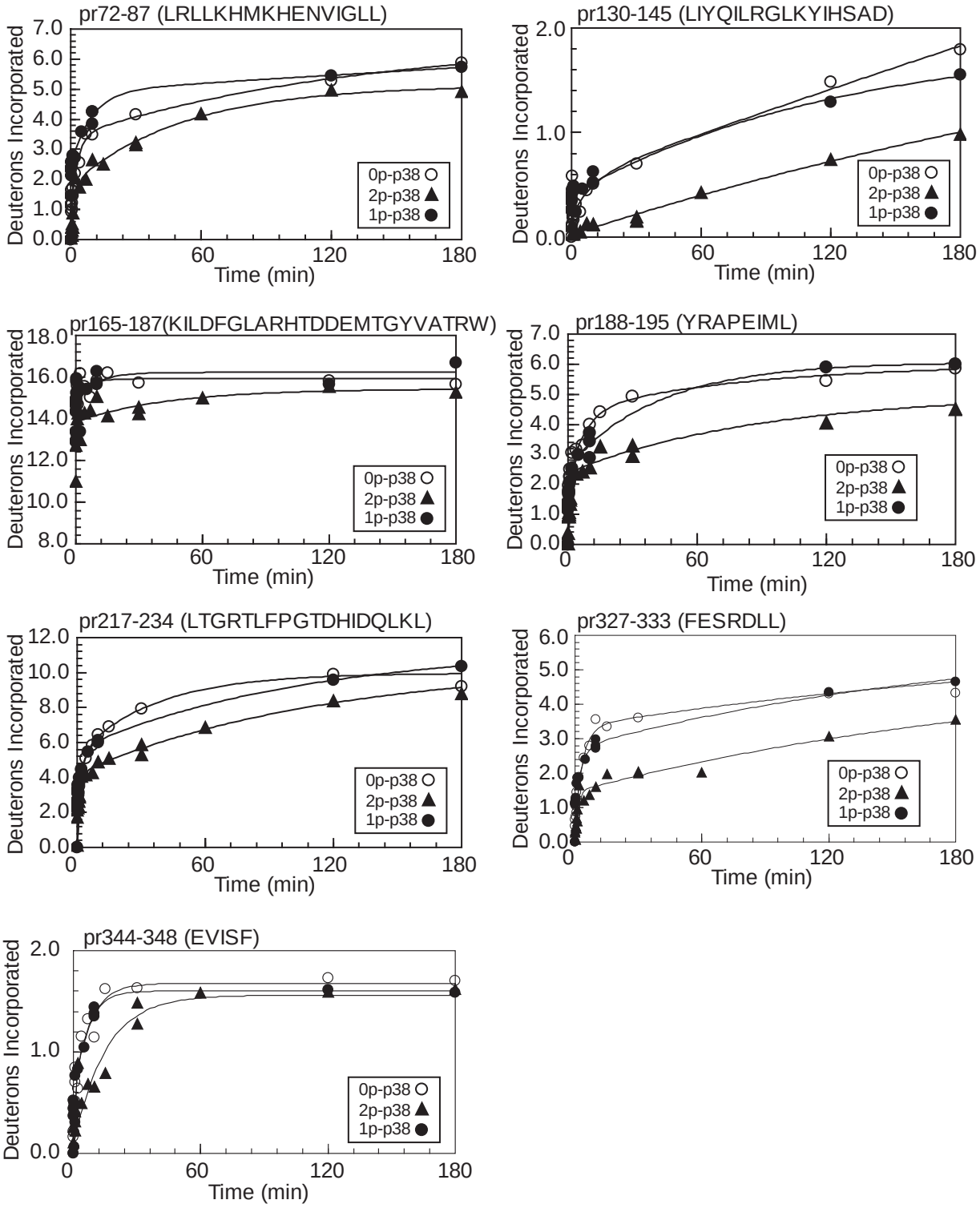

Figure 11. HX-MS behavior of monophosphorylated p38α. Deuteration time courses of peptides from p38α monophosphorylated at Tyr182 (●) are superimposed on time courses of 0P-p38α (o) and 2P-p38α (▲). In 1P-p38α, deuteration time courses of those peptides which significantly decreased in 2P-p38α, more closely resemble those of 0P-p38α.

important finding from this study is that patterns of regional hydrogen exchange in p38α are consistent with tertiary structure. With only a few exceptions, the HX patterns in p38α closely resemble those in ERK2, demonstrating that regional conformational mobility is conserved between these two MAP kinases, as one might expect based on their conserved sequences and tertiary structures.

A key finding is that hydrogen exchange rates are altered in response to phosphorylation, reflecting changes in structure as well as conformational mobility upon kinase activation. These can be interpreted by comparing X-ray structures of 0P-p38α and 2P-p38γ, and incorporating information from prior enzymatic studies. Altered HX within the activation lip, P+1 loop, and active site (β6) are consistent with expected conformational remodeling of the activation lip following phosphorylation. Likewise, changes in HX within the 3-10 helix most likely reflect conformational changes within an N-terminal hydrophobic cluster described by the Livnah group (Diskin et al., 2004; Diskin et al., 2007), which might undergo residue displacement upon activation lip phosphorylation. In contrast, other regions show changes in HX that cannot be readily explained by structural rearrangements, and may instead reflect changes in protein internal motions or flexibility responsive to phosphorylation. These are found in binding sites for substrates and allosteric regulators, N-terminal regions that link the core β4-β5 strand to helices αL16 and αC, and the C-terminal core helix αE. Modulation of protein motions in these regions could contribute to kinase regulation, where decreased protein flexibility in localized regions might somehow facilitate substrate binding and turnover.

HX behavior of 1P-p38α suggests a mechanism paralleling models of lip reorganization in ERK2. X-ray structures of unphosphorylated and diphosphorylated ERK2 show stable activation lip structures (Zhang et al., 1994; Canagarajah et al., 1997), and enzymatic

measurements show that phosphorylation at Tyr185 is kinetically preferred (Haystead et al., 1992). In contrast, in X-ray structures of ERK2 mutants replacing the Thr-Glu-Tyr sequence at the activation lip with acidic residues, the activation lip becomes highly disordered (Zhang et al., 1995). Main chain B-factors increase by >35 $Å^2$ and 55 $Å^2$ in the structures of ERK2-Tyr185Glu and Thr183Glu/Tyr185Glu, respectively. The results suggest that ERK2 undergoes phosphorylation at one residue (preferentially at Tyr) which increases mobility within the activation lip. The lip then remodels into a stable active configuration following phosphorylation at the second residue. Thus, both phosphorylation events are needed for the dramatic change in lip conformation during kinase activation. In p38α, the activation lip is already disordered and highly exposed to solvent in the unphosphorylated form (Wang et al., 1997; Wilson et al., 1996). By analogy with ERK2, incorporation of one phosphate would produce little change in lip stability, until incorporation of the second phosphate tethers the lip into an active conformation. This would explain why HX of monophosphorylated p38α more closely resembles that of the unphosphorylated enzyme. Our data suggests that hydrogen exchange in p38α is mainly regulated by conformational changes following dual phosphorylation, which anchor the lip into the active conformation.

Importantly, patterns of hydrogen exchange regulated by activation show significant differences between p38α and ERK2. As expected, both enzymes show perturbations within the activation lip, corresponding to lip remodeling. In addition, both enzymes share patterns of decreased HX in the αF-αG loop region. Regulated motions in this region may be important to modulate interactions between MAP kinase substrates as well as allosteric regulators, such as TAB1. However, in contrast to p38α, ERK2 activation leads to increased HX within the hinge, Gly-rich loop, and MAP kinase insert (Figure 12). Differences in HX regulation in

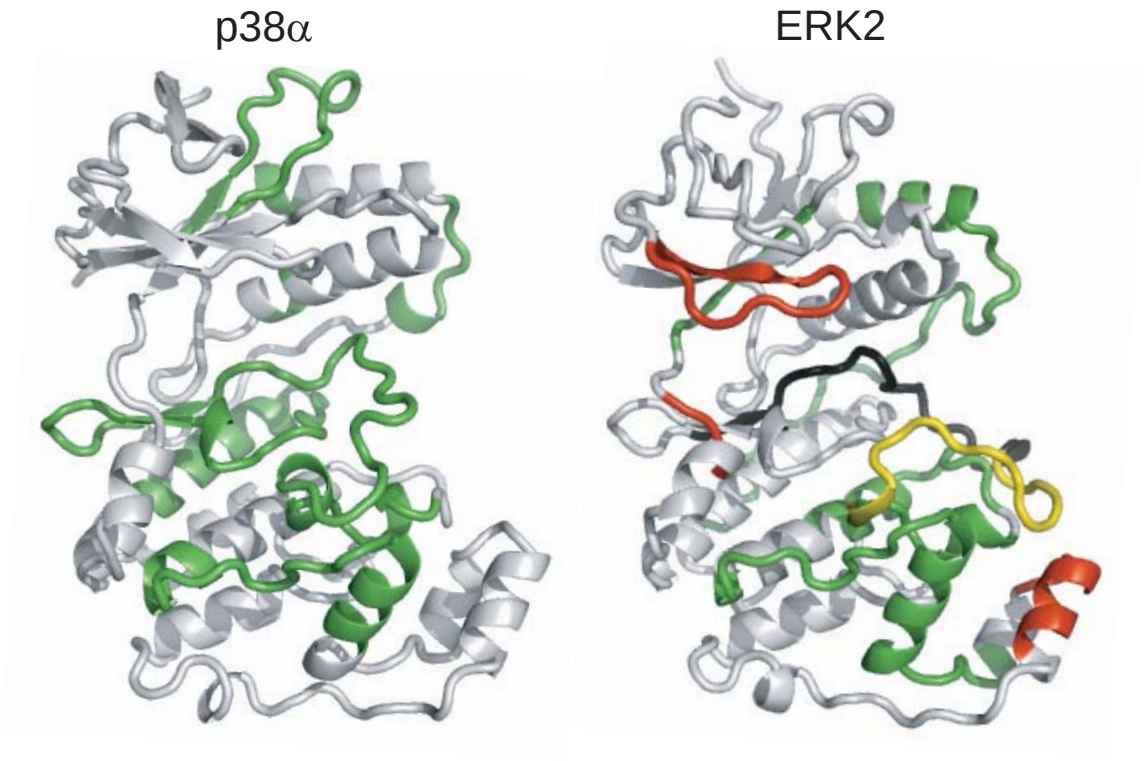

Figure 12. Comparison of activation-induced changes in HX-MS in MAP kinases. Regulated HX in p38α from this study are compared to that of ERK2 from Hoofnagle et al. (2001). Green indicates regions where HX decreases, red indicates regions where HX increases upon kinase activation, and black indicates missing sequence that could not be analyzed. Yellow indicates the activation lip, where both increases and decreases in HX rates could be observed, ascribed to conformational remodeling upon activation. The result shows that conservation of sequence and tertiary structure does not lead to conservation of regulated conformational mobility.

corresponding regions of p38α may reflect differences between these enzymes in mechanisms underlying enzyme activation. For example, the ERK2 hinge represents a region of regulated flexibility which can be linked to interdomain interactions responsive to activity state (Lee et al., 2005). X-ray structures of inactive p38α show wider domain separation than ERK2, as well as hinge rotation allowing hinge residues to interfere with adenine ring interactions (Wang et al., 1997; Wilson et al., 1996). Thus, p38α retains an open conformation, even when bound to ATP-competitive inhibitors or upon MK2 substrate binding (ter Haar et al., 2007; White et al., 2007; Wang et al 1998). Such constraints prevent domain closure, and probably preclude regulation of HX upon activation lip phosphorylation. As a result, ATP binding affinity increases substantially upon activation of p38α (also seen in p38γ), whereas ERK2 shows little change in ATP binding upon activation (Zhang et al, 1994; Lee et al., 2005; Frantz et al., 1998; Fox et al., 1999).

The ability to monitor protein flexibility and mobility by HX adds a new dimension towards understanding how kinases are controlled. The regulated motions revealed by HX alterations upon kinase activation are dissimilar between ERK2 and p38α, which are closely related in sequence, tertiary structure, and dual phosphorylation mechanism. We conclude that while patterns of solvent accessibility may be conserved between related enzymes, patterns of activation-induced motional changes are not conserved. Our findings provide evidence that MAP kinases diverge with respect to regulation of internal protein motions and their potential contribution to function.

CHAPTER III

Hinge Flexibility Controls Interdomain Closure in ERK2

INTRODUCTION

HX-MS has been used to examine properties of enzyme activation, regulated conformational mobility, and substrate binding in the MAP kinase, ERK2, where distinct differences in regional hydrogen exchange rates can be observed between inactive (unphosphorylated) and active (diphosphorylated) states of the enzyme (Hoofnagle et al., 2001). Altered HX was observed in the activation lip, as expected from the conformational reorganization which follows phosphorylation. Increased HX also occurs within the conserved glycine-rich ATP binding loop, and within the hinge region between N- and C-terminal domains. These could not readily be accounted for by differences in X-ray structure between active and inactive ERK2, suggesting that phosphorylation and activation of this enzyme regulates backbone conformational mobility in key regions of this enzyme. For example, increased conformational mobility at the hinge might enable domain closure needed for catalysis.

Follow up experiments were conducted to test this hypothesis. First, site directed spin label-electron paramagnetic resonance spectroscopy (SDSL-EPR) was carried out on

ERK2, in which cysteine residues were individually engineered at different regions of the hinge onto which nitroxide spin label groups were added (Hoofnagle et al., 2004). Residues at the hinge showed significant changes in correlation rate without evidence for conformational perturbations, consistent with altered side chain dynamics at the hinge upon ERK2 activation. Second, HX-MS was used to monitor binding of a nonhydrolyzable nucleotide analog, AMP-PNP, to active and inactive forms of ERK2 (Lee et al., 2005). In inactive ERK2, Mg^{2+}-AMP-PNP binding caused steric protection from deuteration in regions within the N-terminal domain that were known to interact with nucleotide, including the glycine-rich loop, sheet β3/helix αC, and the hinge region, but little protection within the C-terminal domain. In contrast, nucleotide binding to active ERK2 led to comparable protection in N-terminal regions and the hinge, but increased protection around the Asp-Phe-Gly (DFG) motif in the C-terminal domain. Both forms of ERK2 bound Mg^{2+}-AMP-PNP with similar affinity as measured by isothermal titration calorimetry. The findings led to novel insight into the solution conformation of ERK2, by demonstrating that the inactive enzyme is constrained from forming a closed domain solution conformation needed for catalysis, which the active state is able to adopt.

The results are consistent with a model in which the increased flexibility at the hinge induced by phosphorylation allows ERK2 to overcome a barrier to interdomain closure, which is needed in order to form a competent catalytic site. In this way, the mechanism of activation may in part involve regulation of hinge flexibility, reflecting dynamical control of ERK2 activity. However, the results so far only demonstrate correlations, and stop short of proving causality. An alternative interpretation is that the

changes in conformational mobility at the hinge observed in HX-MS studies are not coupled to domain closure. In fact, one could imagine instead that phosphorylation drives domain closure, which then leads to enhanced hydrogen exchange within the hinge, not the other way around.

The goal of this study is to test the hypothesis that interdomain closure can be regulated by hinge flexibility, by introducing glycine substitutions at various hinge residues which would be expected to increase flexibility, and asking whether these lead to domain closure. We focused on a region containing residues ^{105}LMETD^{109}, which in ERK2 increases conformational mobility following kinase activation, and corresponds to the region which serves as the pivot point for hinge bending during domain closure in cAMP-dependent protein kinase. Here we show that replacing residues within the hinge region of the unphosphorylated form of ERK2 with Gly-Gly promotes domain closure, as measured by HX protection by AMP-PNP binding within the conserved DFG region of the C-terminal domain. The results demonstrate that increasing hinge flexibility can promote domain closure, and provide new evidence supporting my hypothesis that hinge mobility regulated by activation lip phosphorylation may be crucial for the mechanism of kinase activation.

MATERIALS & METHODS

Protein expression and purification

ERK2 mutants introducing Gly-Gly substitutions at hinge residues, ^{105}LM^{106}, ^{106}ME^{107}, ^{107}ET^{108}, and ^{108}TD^{109}, were made as described (Emrick et al., 2006). Inactive wild-type ERK2 (0P-ERK2) and mutants were prepared as described with the following changes (Robbins et al., 1993). Cells expressing 0P-ERK2, ^{106}ME/GG, and ^{107}ET/GG were grown at 30 °C to O.D.(600 nm) 0.5-0.6, at which point they were rapidly chilled by placing into an ice-water slurry for 15 minutes. IPTG (isopropyl β-D-1-thiogalactopyranoside, 0.4 mM) was then added and proteins were induced for 6 hours at 23 °C. Active ERK2 (2P-ERK2) was expressed using the dual expression plasmid, NpT7-5 MEK1R4F-His$_6$-ratERK2 (Wilsbacher & Cobb, 2001; Goldsmith et al., 2004), in *E. coli* BL21 (DE3)-pLysS (Invitrogen, Carlsbad, CA) grown in 1 L Terrific Broth at 37 °C, reaching O.D.(600 nm) 0.3-0.4 before induction with 0.4 mM IPTG for 6 hours.

Additional mutants of ERK2 were prepared by combining hinge mutations (substituting ^{105}LM^{106}, ^{106}ME^{107}, ^{107}ET^{108}, and ^{108}TD^{109} with Gly-Gly) and activation lip mutations (Thr^{183} and/or Tyr^{185} to Glu, Asp, or Phe) generated in NpT7-5 His$_6$-ratERK2 (primers listed in Appendix A). Plasmids were transformed into *E. coli* BL21 (DE3) pLysS and the proteins were purified from 200 mL of bacterial culture as described above.

For HX-MS experiments, proteins were produced in 1 L bacterial culture and purified first with Ni^{2+}-NTA agarose (1 mL, Qiagen, Valencia, CA), followed by Mono Q FPLC as described (Emrick et al., 2006; Lee et al., 2005). After Mono Q elution, proteins were dialyzed into 10 mM potassium phosphate pH 7.5, 50 mM KCl, 1 mM

DTT and stored in 65 μL aliquots at -80 °C. Mass spectrometry confirmed phosphorylation stoichiometry at the activation lip as ≥ 95% diphosphorylated for 2P-ERK2 preparations, and ≤ 5% diphosphorylated + monophosphorylated for the 0P-ERK2 and mutant ERK2 preparations (Table 1).

For kinase activity assays, ERK2 proteins were induced in 200 mL of bacterial culture as described (Emrick et al., 2006). Purified protein was eluted from Ni^{2+}-NTA agarose (200 μL) in 50 mM potassium phosphate (pH 8.0), 0.3 M NaCl, 1 mM DTT, 0.3 M imidazole. Fractions containing protein were pooled, dialyzed into 10 mM Hepes, pH 7.5, 0.1 M NaCl, 1 mM DTT, and frozen in aliquots at -80 °C.

Hydrogen-exchange mass spectrometry (HX-MS) measurements

ERK2 was incubated in 85% (v/v) D_2O between 0 - 4 hours, and HX data collection was performed as described (Lee et al., 2005) using a QStar Pulsar QqTOF mass spectrometer interfaced with an Agilent Cap1100 HPLC (500 μm i.d. x 10 cm column, packed with POROS R1 20 resin). Time-zero measurements were performed to measure background in-exchange during proteolysis, by acidifying the reaction before adding D_2O. Time points were randomized to control for systematic variations. Three replicate runs of each ERK2 form were performed at 1 min, in order to determine average standard deviation of deuteration for all peptides (0.12 Da) (Table 2).

Weighted average mass (WAM) calculations were carried out using in-house software for semi-automated analysis (HX-Analyzer, Sours et al., 2008). Deuteration measurements were corrected for artifactual in-exchange, back-exchange, and fit by nonlinear least squares (NLSQ) to the equation $Y = N - Ae^{-k_1 t} - Be^{-k_2 t} - Ce^{-k_3 t}$, where

Table 1: Phosphorylation stoichiometry for the activation lip TEY residues for proteins analyzed by HX-MS

	% diphosphorylate	% monophosphorylated	% unphosphorylated
2P	95	2	3
0P	0	3	97
LM	0	0	100
ME	0	1	99
ET	0	1	99
TD	2	0	98

Notes

2P is ≥ 95% phosphoylated on both TEY residues

0P and the mutants are ≥ 95% unphosphorylated on both TEY residues

Table 2: Kinetic parameters for ERK2 in-exchange, fit by non-linear least squares.

Sequence [1]	Protein	% BE	Condition	Avg. St. Dev. at 1'	RSS	A [2]	B	C	N	k_1	k_2	k_3
AAAGPEMVRGQVFDVGPRYTNL	2P	20.5%	Control	0.0987	2.499	7.290(0.768)	4.471(0.568)		11.761(0.215)	8.800(5.072)	0.345(0.104)	
			AMP-PNP	0.2301	1.790	10.598(0.637)	1.858(0.551)		12.456(0.213)	1.805(0.218)	0.048(0.036)	
	0P	19.4%	Control	0.1955	0.743	6.247(0.938)	5.384(0.895)		11.632(0.136)	4.705(1.272)	0.456(0.148)	
			AMP-PNP	0.1538	2.758	10.074(0.567)	2.500(0.509)		12.573(0.356)	3.146(0.557)	0.029(0.018)	
	LM	20.8%	Control	0.1001	2.001	9.518(0.475)	3.457(0.435)		12.975(0.194)	4.552(0.815)	0.153(0.053)	
			AMP-PNP	0.2488	1.132	9.590(0.458)	3.416(0.330)		13.006(0.113)	8.598(2.242)	0.244(0.070)	
	ME	20.5%	Control	0.3247	2.410	9.077(0.888)	3.187(0.678)		12.263(0.289)	5.816(1.804)	0.245(0.148)	
			AMP-PNP	0.3453	3.128	9.202(0.871)	3.441(0.750)		12.643(0.305)	2.598(0.643)	0.066(0.037)	
	ET	20.5%	Control	0.1233	2.929	7.854(0.860)	4.472(0.699)		12.325(0.181)	4.709(1.076)	0.298(0.114)	
			AMP-PNP	0.1927	2.838	8.146(0.709)	4.367(0.498)		12.512(0.218)	6.288(1.610)	0.178(0.060)	
	TD	20.1%	Control	0.0853	1.038	7.696(0.487)	4.840(0.376)		12.536(0.152)	5.250(0.185)	0.185(0.033)	
			AMP-PNP	0.2761	1.145	7.188(0.417)	5.395(0.266)		12.583(0.153)	8.201(2.564)	0.172(0.026	
DVGPRYTNL	2P	37.3%	Control	0.1300	0.066	1.511(0.094)			1.511(0.035)	0.716(.103)		
			AMP-PNP	0.0682	0.117	1.224(0.151)	0.948(0.110)		2.172(0.065)	3.800(1.360)		
	0P	30.9%	Control	0.2465	0.451	0.997(0.301)	1.195(0.273)		2.192(0.078)	4.058(3.324)	0.270(0.122)	
			AMP-PNP	0.1068	0.264	1.360(0.236)	0.978(0.200)		2.338(0.064)	7.958(6.992)	0.293(0.162)	
	LM	21.7%	Control	0.0500	0.108	2.382(0.252)	0.236(0.228)		2.618(0.080)	1.657(0.349)	0.059(0.128)	
			AMP-PNP	0.1006	0.171	1.857(0.174)	0.879(0.114)		2.736(0.057)	8.441(4.583)	0.105(0.043)	
	ME		Control									
			AMP-PNP									
	ET	..3686	Control	0.0475	0.523	0.984(0.473)	0.990(0.462)		1.974(0.099)	1.513(1.307)	0.073(0.062)	
			AMP-PNP	0.0680	0.073	0.792(0.101)	1.085(0.063)		1.877(0.037)	10.263(9.044)	0.089(0.018)	
	TD	38.3%	Control	0.1245	0.214	1.835(0.120)			1.835(0.057)	0.458(0.087)		
			AMP-PNP	0.1239	0.552	2.306(.217)			2.306(0.086)	0.945(0.165)		
SYIGEGAYGMVCSA	2P	25.0%	Control	0.1388	0.558	2.826(0.312)	2.992(0.207)		5.818(0.109)	7.677(4.214)	0.089(0.019)	
			AMP-PNP	0.2795	0.247	2.910(0.192)	2.427(0.128)		5.337(0.087)	4.051(0.761)	0.042(0.007)	
	0P	20.0%	Control	0.3011	0.707	3.354(0.245)	2.450(0.295)		5.804(0.101)	6.465(2.303)	0.135(0.031)	
			AMP-PNP	0.0717	0.606	2.853(.204)	2.257(0.163)		5.110(0.117)	4.822(1.372)	0.033(0.008)	
	LM	20.1%	Control	0.0051	0.542	3.757(0.196)	2.645(0.175)		5.402(0.112)	5.387(1.305)	0.074(0.017)	
			AMP-PNP	0.0072	0.108	3.489(0.154)	1.997(0.183)	1.248(0.199)	6.735(0.300)	6.664(1.115)	0.202(0.047)	0.008(0.006)
	ME	19.8%	Control	0.0709	0.989	3.777(0.354)	2.444(0.233)		6.220(0.184)	5.082(1.225)	0.038(0.013)	
			AMP-PNP	0.0065	0.064	2.858(0.124)	1.194(0.240)	1.780(0.200)	5.831(0.299)	5.708(0.838)	0.149(0.057)	0.009(0.004)
	ET	19.9%	Control	0.0961	0.225	3.673(0.257)	1.161(0.243)	1.662(0.263)	6.496(0.148)	5.521(0.853)	0.273(0.213)	0.016(0.007)
			AMP-PNP	0.0668	0.171	2.772(0.193)	1.397(0.322)	1.682(0.324)	5.851(0.457)	6.626(1.439)	0.156(0.074)	0.008(0.006)
	TD	19.8%	Control	0.2459	0.788	4.033(0.295)	2.141(0.178)		6.174(0.115)	6.476(1.479)	0.073(0.019)	
			AMP-PNP	0.0281	0.242	3.060(0.176)	2.248(0.115)		5.308(0.089)	5.078(0.970)	0.040(0.007)	
SAYDNL	2P	21.2%	Control	0.1470	0.104	0.316(0.150)	0.720(0.118)		1.035(0.054)	1.749(1.648)	0.040(0.020)	
			AMP-PNP	0.0323	0.010	0.409(0.045)		0.752(0.106)	1.161(0.117)	3.868(2.201)		0.007(0.002)
	0P	21.1%	Control	0.1428	0.110	0.486(0.168)	0.757(0.158)		1.243(0.099)	1.477(1.114)	0.021(0.011)	
			AMP-PNP	0.1232	0.102	0.469(0.120)	0.559(0.103)		1.028(0.080)	2.496(1.859)	0.017(0.010)	
	LM	20.5%	Control	0.0261	0.006	0.405(.0.036)	0.772(0.024)		1.177(0.021)	7.171(2.640)	0.021(0.002)	
			AMP-PNP	0.1400	0.058	0.584(0.108)		0.881(0.222)	1.462(0.251)	1.165)0.375)		0.007(0.004)
	ME	20.7%	Control	0.0569	0.056	0.522(0.095)	0.811(0.077)		1.333(0.073)	6.987(4.400)	0.018(0.005)	
			AMP-PNP	0.1650	0.025	0.530(0.085)	0.528(0.086)		1.057(0.085)	5.457(2.976)	0.015(.007)	
	ET	21.9%	Control	0.0430	0.116	0.574(0.161)		0.815(0.206)	1.389(0.226)	2.659(1.070)		0.009(0.005)
			AMP-PNP	0.0447	0.010	0.433(0.058)	0.578(0.043)		1.010(0.025)	4.019(3.073)	0.034(0.007)	
	TD	21.8%	Control	0.0189	0.045	0.476(0.080)		1.577(0.965)	2.052(0.994)	2.076(0.752)		0.003(0.003)
			AMP-PNP	0.0158	0.063	0.525(0.100)	0.695(0.105)		1.220(0.108)	4.321(2.462)	0.013(0.006)	

Sequence [1]	Protein	% BE	Condition	Avg. St. Dev. at 1'	RSS	A [2]	B	C	N	k_1	k_2	k_3
NKVRVAIKKISPFEHQTYCQRTLRE	2P	21.4%	Control	0.1898	2.422	4.054(0.655)	2.574(0.445)		6.628(0.237)	5.172(2.727)	0.067(0.036)	
			AMP-PNP	0.2548	1.955	5.036(0.646)	1.409(0.546)		6.445(0.284)	0.846(0.208)	0.035(0.033)	
	0P	21.0%	Control	0.3271	0.697	5.481(0.260)	1.729(0.255)		7.210(0.228)	1.865(0.194)	0.017(0.008)	
			AMP-PNP	0.1989	1.743	5.228(0.366)		2.437(0.728)	7.664(0.822)	1.357(0.186)		0.008(0.007)
	LM	21.4%	Control	0.0573	0.833	4.525(0.283)	3.129(0.261)		7.654(0.144)	3.670(0.788)	0.061(0.016)	
			AMP-PNP	0.1926	3.519	5.782(0.856)	1.831(0.707)		7.612(0.295)	1.396(0.387)	0.027(0.027)	
	ME	21.2%	Control	0.0533	0.043	3.178(0.151)	3.373(0.137)	1.749(0.454)	8.299(0.548)	5.162(0.643)	0.268(0.036)	0.006(0.004)
			AMP-PNP	0.1004	0.219	5.261(0.214)	2.180(0.292)		7.441(0.315)	1.843(0.156)	0.011(0.004)	
	ET	20.4%	Control	0.0466	0.727	3.790(0.360)	3.203(0.262)		6.993(0.104)	5.237(1.235)	0.212(0.045)	
			AMP-PNP	0.0767	1.137	3.874(0.505)	2.822(0.415)		6.696(0.278)	2.596(0.781)	0.021(0.009)	
	TD	21.1%	Control	0.1030	0.948	4.052(0.355)	3.114(0.227)		7.166(0.126)	6.805(1.980)	0.102(0.021)	
			AMP-PNP	0.2186	1.359	3.925(0.558)	3.230(0.480)		7.155(0.170)	3.105(1.183)	0.138(0.040)	
IKILLRFRHENIIGIND	2P	20.6%	Control	0.1039	0.324	1.588(0.190)	1.884(0.150)		3.443(0.142)	1.203(0.272)	0.015(0.004)	
			AMP-PNP	0.1087	0.305	1.359(0.203)	1.400(0.154)		2.759(0.111)	1.124(0.304)	0.027(0.009)	
	0P	20.8%	Control	0.1471	0.262	1.844(0.135)		3.289(1.043)	5.133(1.094)	0.674(0.119)		0.004(0.002)
			AMP-PNP	0.1224	0.242	1.322(0.142)	2.146(0.194)		3.468(0.225)	0.638(0.154)	0.010(0.003)	
	LM	20.9%	Control	0.1001	0.261	1.723(0.167)	2.420(0.172)		4.143(0.162)	1.171(0.218)	0.015(0.004)	
			AMP-PNP	0.0608	0.133	1.928(0.123)		2.227(0.161)	4.154(0.194)	0.621(0.091)		0.009(0.002)
	ME	21.1%	Control	0.1262	0.110	1.637(0.121)	2.427(0.175)		4.064(0.197)	1.359(0.192)	0.010(0.002)	
			AMP-PNP	0.1173	0.139	1.498(0.148)		2.826(0.396)	4.324(0.444)	0.741(0.146)		0.007(0.002)
	ET	20.6%	Control	0.0362	0.222	1.720(0.145)	2.307(0.145)		4.037(0.160)	0.917(0.148)	0.013(0.003)	
			AMP-PNP	0.0962	0.189	1.517(0.156)		2.587(0.320)	4.104(0.361)	0.739(0.166)		0.008(0.003)
	TD	20.3%	Control	0.0921	0.392	1.661(0.207)	2.281(0.173)		3.942(0.172)	1.353(0.316)	0.015(0.004)	
			AMP-PNP	0.0889	0.156	1.720(0.145)	2.379(0.170)		4.098(0.192)	0.742(0.124)	0.011(0.003)	
IIRAPTIEQMKD	2P	19.9%	Control	0.2996	0.902	4.380(0.510)	2.452(0.460)		6.832(0.148)	0.773(0.154)	0.047(0.021)	
			AMP-PNP	0.0129	0.138	4.494(0.209)	2.469(0.183)		6.963(0.081)	0.669(0.061)	0.034(0.006)	
	0P	20.9%	Control	0.1636	0.650	5.342(0.251)	1.856(0.239)		7.198(0.208)	0.673(0.070)	0.018(0.008)	
			AMP-PNP	0.1804	0.621	5.033(0.256)	2.189(0.221)		7.222(0.157)	0.788(0.077)	0.019(0.006)	
IIRAPTIEQMKDVY	2P	18.7%	Control	0.2807	0.893	4.687(0.407)	2.316(0.345)		7.003(0.143)	0.833(0.132)	0.043(0.017)	
			AMP-PNP	0.0959	0.508	4.629(0.272)	2.565(0.224)		7.194(0.137)	0.805(0.093)	0.029(0.007)	
	0P	20.2%	Control	0.2679	0.064	1.879(0.362)	4.267(0.340)	2.699(1.439)	8.844(1.516)	2.355(0.668)	0.320(0.036)	0.003(0.003)
			AMP-PNP	0.1551	0.722	5.018(0.282)	2.285(0.243)		7.304(0.159)	0.816(0.086)	0.021(0.007)	
	LM	20.2%	Control	0.1575	0.231	1.889(0.572)	3.747(0.439)	2.252(0.282)	7.888(0.167)	3.707(1.692)	0.402(0.144)	0.016(0.005)
			AMP-PNP	0.0596	0.142	1.978(0.421)	4.042(0.377)	1.998(0.235)	8.018(0.331)	2.757(0.955)	0.326(0.063)	0.008(0.004)
	ME	20.1%	Control	0.1254	0.151	1.537(0.367)	4.330(0.280)	2.327(0.653)	8.194(0.771)	4.538(1.734)	0.379(0.080)	0.006(0.004)
			AMP-PNP	0.1212	0.207	2.049(0.627)	3.612(0.527)	2.296(0.581)	7.966(0.726)	2.897(1.312)	0.364(0.124)	0.007(0.005)
	ET	20.0%	Control	0.0314	0.095	1.509(0.221)	4.304(0.159)	1.933(0.176)	7.746(0.222)	4.506(1.113)	0.346(0.048)	0.009(0.003)
			AMP-PNP	0.1156	0.167	1.409(0.368)	4.091(0.275)	2.094(0.279)	7.593(0.345)	6.285(3.614)	0.391(0.093)	0.009(0.004)
	TD	19.5%	Control	0.0704	0.884	5.365(0.323)	1.947(0.259)		7.312(0.217)	0.826(0.095)	0.018(0.009)	
			AMP-PNP	0.0851	0.634	5.213(0.325)	2.051(0.265)		7.264(0.193)	0.758(0.088)	0.021(0.009)	
IVQDL	2P	14.2%	Control	0.0739	0.102		1.086(0.057)		1.086(0.046)		0.037(0.007)	
			AMP-PNP	0.0263	0.126		1.032(0.071)		1.032(0.065)		0.018(0.004)	
	0P	13.9%	Control	0.0530	0.009	0.306(0.063)	0.774(0.066)		1.080(0.028)	0.580(0.235)	0.034(0.007)	
			AMP-PNP	0.0671	0.062			1.263(0.240)	1.263(0.247)			0.007(0.003)

Sequence [1]	Protein	% BE	Condition	Avg. St. Dev. at 1'	RSS	A [2]	B	C	N	k_1	k_2	k_3
IVQDG	LM		Control									
			AMP-PNP									
	ME		Control									
			AMP-PNP									
	ET		Control									
			AMP-PNP									
	TD	19.6%	Control	0.0330	0.026	0.141(0.017)			1.122(0.028)	1.122(0.038)		
			AMP-PNP	0.0054	0.005	0.187(0.045)	0.947(0.076)		1.134(0.089)	1.191(0.512)	0.183(0.005)	
METDL	2P	19.3%	Control	0.0951	0.038		0.895(0.041)		0.895(0.029)		0.097(0.015)	
			AMP-PNP	0.0312	0.021	0.524(0.046)			0.524(0.024)		0.564(0.145)	
	0P	14.2%	Control	0.0521	0.034	0.412(0.069)	0.523(0.062)		0.935(0.038)	2.353(0.955)	0.033(0.012)	
			AMP-PNP	0.0319	0.050	0.532(0.044)			0.532(0.02)	0.837(0.160)		
	LM		Control									
			AMP-PNP									
GGTDL [4]	ME	24.7%	Control	0.0586	0.048	1.355(0.077)	0.318(0.093)		1.673(0.099)	2.794(0.362)	0.012(0.010)	
			AMP-PNP	0.0895	0.046	1.121(0.082)	0.324(0.098)		1.445(0.106)	1.810(0.269)	0.011(0.010)	
	ET		Control									
			AMP-PNP									
LMEGGL [4]	TD	23.5%	Control	0.1615	0.165	1.332(0.139)	0.557(0.085)		1.888(0.060)	5.253(1.854)	0.043(0.022)	
			AMP-PNP	0.0757	0.071	0.951(0.095)	0.903(0.059)		1.854(0.045)	7.070(3.198)	0.054(0.012)	
IVQDLMETDL	2P	20.5%	Control	0.2001	0.187	2.041(0.171)	1.703(0.131)		3.744(0.076)	1.211(0.182)	0.028(0.008)	
			AMP-PNP	0.1333	0.526	1.090(0.230)		3.214(1.259)	4.304(1.345)	0.627(0.365)		0.005(0.004)
	0P	20.5%	Control	0.1881	0.424	2.150(0.261)	1.547(0.239)		3.698(0.120)	0.781(0.170)	0.034(0.014)	
			AMP-PNP	0.1285	0.540	1.058(0.225)	1.898(0.204)		2.955(0.191)	0.738(0.319)	0.015(0.006)	
IVQDGGETDL	LM	21.0%	Control	0.0358	0.319	2.196(0.220)	1.133(0.200)		3.329(0.145)	1.824(0.391)	0.021(0.011)	
			AMP-PNP	0.0998	0.115	1.360(0.306)	1.136(0.235)	0.727(0.157)	3.222(0.116)	4.631(1.988)	0.372(0.259)	0.014(0.010)
IVQDLGGTDL	ME	20.1%	Control	0.0273	0.115	1.322(0.142)	1.848(0.090)		3.170(0.059)	10.155(9.329)	0.081(0.014)	
			AMP-PNP	0.0371	0.222	1.054(0.183)	2.026(0.132)		3.080(0.094)	3.603(1.812)	0.035(0.007)	
IVQDLMGGDL	ET	18.7%	Control	0.1108	0.247	1.842(0.165)	1.238(0.102)		3.081(0.066)	5.202(1.219)	0.059(0.016)	
			AMP-PNP	0.0779	0.103	1.594(0.114)	1.392(0.096)		2.986(0.093)	3.733(0.618)	0.017(0.004)	
IVQDLMEGGL	TD	16.7%	Control	0.2113	0.356	2.417(0.210)	1.435(0.154)		3.853(0.079)	3.390(0.704)	0.063(0.019)	
			AMP-PNP	0.0788	0.261	1.676(0.200)	2.341(0.160)		4.016(0.138)	1.363(0.294)	0.019(0.004)	
YKLLKTQHLSNDHICY	2P	23.3%	Control	0.3159	0.817	1.747(0.333)	1.160(0.215)		2.907(0.116)	7.246(6.296)	0.105(0.055)	
			AMP-PNP	0.3110	1.222	1.896(0.371)	0.973(0.227)		2.869(0.160)	5.387(3.596)	0.054(0.038)	
	0P	23.4%	Control	0.0605	0.119	2.412(0.111)		1.280(0.461)	3.691(0.493)	2.109(0.226)		0.006(0.004)
			AMP-PNP	0.2519	0.824	1.877(0.270)	1.158(0.254)		3.035(0.238)	3.092(1.342)	0.015(0.011)	
	LM	22.9%	Control	0.2031	0.213	2.298(0.122)	1.736(0.172)		4.036(0.176)	4.070(0.833)	0.013(0.004)	
			AMP-PNP	0.1522	0.397	2.505(0.209)		1.334(0.409)	3.840(0.463)	2.332(0.443)		0.007(0.006)
	ME	23.3%	Control	0.1107	0.046	2.301(0.112)		2.625(1.624)	4.926(1.673)	1.829(0.190)		0.003(0.003)
			AMP-PNP	0.0735	0.184	1.940(0.`56)		2.679(1.393)	4.619(1.423)	3.851(0.884)		0.004(0.003)
	ET	23.7%	Control	0.1036	0.088	2.406(0.105)		1.922(0.309)	4.328(0.334)	1.878(0.181)		0.007(0.002)
			AMP-PNP	0.2231	0.329	2.267(0.200)		1.866(0.650)	4.133(0.682)	3.428(0.678)		0.006(0.004)
	TD	23.7%	Control	0.0985	0.916	2.714(0.317)	3.375(0.226)		6.089(0.210)	5.779(1.875)	0.022(0.005)	
			AMP-PNP	0.2716	1.014	2.828(0.382)	3.177(0.318)		6.005(0.289)	3.561(1.358)	0.024(0.007)	

Sequence [1]	Protein	% BE	Condition	Avg. St. Dev. at 1'	RSS	A [2]	B	C	N	k_1	k_2	k_3
ILRGLKYIHSANVL	2P	20.8%	Control	0.1343	0.356	1.541(0.203)	0.994(0.149)		2.525(0.123)	1.188(0.289)	0.019(0.010)	
			AMP-PNP	0.1029	0.419	1.317(0.254)	0.881(0.197)		2.198(0.116)	1.632(0.604)	0.037(0.022)	
	0P	20.8%	Control	0.1961	0.129	1.700(0.099)		1.198(0.197)	2.898(0.219)	0.776(0.099)		0.009(0.004)
			AMP-PNP	0.0993	0.212	1.168(0.136)	1.459(0.148)		2.627(0.162)	0.711(0.175)	0.012(0.004)	
	LM	21.1%	Control	0.1159	0.216	1.500(0.156)	1.812(0.170)		3.312(0.172)	0.755(0.153)	0.014(0.004)	
			AMP-PNP	0.0380	0.091	1.570(0.112)	1.400(0.099)		2.970(0.115)	0.677(0.104)	0.011(0.003)	
	ME	20.8%	Control	0.1219	0.118	1.553(0.124)		1.837(0.310)	3.390(0.345)	1.145(0.171)		0.007(0.003)
			AMP-PNP	0.0427	0.060	1.269(0.094)		1.738(0.131)	3.007(0.155)	0.600(0.098)		0.009(0.002)
	ET	20.9%	Control	0.1316	0.279	1.589(0.160)		1.733(0.289)	3.322(0.328)	0.607(0.144)		0.009(0.004)
			AMP-PNP	0.0968	0.145	1.380(0.142)		1.596(0.216)	2.977(0.252)	0.482(0.133)		0.009(0.004)
	TD	21.0%	Control	0.1309	0.239	1.426(0.157)	1.362(0.178)		2.788(0.203)	1.093(0.223)	0.012(0.005)	
			AMP-PNP	0.1113	0.096	1.574(0.109)		1.473(0.228)	3.046(0.258)	0.657(0.098)		0.008(0.003)
HRDLKPSNL	2P	22.2%	Control	0.1473	0.152	0.507(0.123)			0.507(0.040)	1.164(0.485)		
			AMP-PNP	0.0329	0.056	0.585(0.071)			0.585(0.020)	5.771(2.452)		
	0P	22.0%	Control	0.1243	0.073	0.544(0.057)			0.544(0.026)	1.692(0.366)		
			AMP-PNP	0.0461	0.153	0.535(0.080)			0.535(0.034)	2.056(0.664)		
	LM	21.0%	Control	0.0339	0.112	0.755(0.083)			0.755(0.038)	3.066(1.010)		
			AMP-PNP	0.0460	0.135	0.838(0.113)			0.838(0.038)	2.573(0.722)		
	ME	21.4%	Control	0.1808	0.067	0.835(0.097)			0.835(0.035)	1.452(0.319)		
			AMP-PNP	0.0086	0.013	0.735(0.044)			0.735(0.018)	1.682(0.223)		
	ET	22.2%	Control	0.0402	0.096	0.509(0.087)			0.509(0.027)	2.678(0.862)		
			AMP-PNP	0.0396	0.081	0.525(0.083)			0.525(0.032)	1.494(0.433)		
	TD	23.6%	Control	0.0930	0.429	0.619(.186)			0.619(0.063)	1.426(0.764)		
			AMP-PNP	0.0473	0.283	0.641(0.157)			0.641(0.051)	2.915(1.565)		
LLNTTCD [5]	2P	17.6%	Control	0.0874	0.077	1.874(0.110)	0.532(0.070)		2.405(0.042)	5.776(1.225)	0.065(0.030)	
			AMP-PNP	0.1253	0.127	1.338(0.157)	0.707(0.109)		2.046(0.046)	10.172(9.595)	0.158(0.095)	
	0P	19.4%	Control	0.1506	0.099	1.913(0.179)	0.492(0.147)		2.405(0.077)	2.468(0.512)	0.056(0.054)	
			AMP-PNP	0.1464	0.104	1.638(0.197))	0.618(0.160)		2.255(0.057)	1.645(0.387)	0.043(0.027)	
	LM	19.2%	Control	0.0075								
			AMP-PNP	0.1212	0.486	1.861(0.264)	0.938(0.199)		2.798(0.103)	2.571(0.915)	0.028(0.015)	
	ME	19.1%	Control	0.0059	0.112	1.795(0.234)	1.018(0.183)		2.813(0.074)	9.946(9.638)	0.238(0.111)	
			AMP-PNP		0.120	1.792(0.206)	0.953(0.157)		2.745(0.089)	5.579(2.219)	0.054(0.025)	
	ET	19.7%	Control	0.0871	0.047	1.870(0.076)	0.974(0.054)		2.844(0.050)	5.627(0.811)	0.019(0.004)	
			AMP-PNP		0.146	1.596(0.170)	0.679(0.120)		2.275(0.080)	4.362(1.108)	0.029(0.016)	
	TD	19.3%	Control	0.1400	0.218	1.989(0.260)	0.805(0.197)		2.794(0.091)	4.296(3.721)	0.035(0.022)	
			AMP-PNP	0.2012	0.337	1.690(0.232)	0.806(0.197)		2.495(0.184)	4.156(1.716)	0.025(0.019)	
LNTTCDL	2P	20.6%	Control	0.0617	0.058	1.906(0.090)	0.537(0.058)		2.444(0.048)	5.113(0.794)	0.023(0.011)	
			AMP-PNP	0.0815	0.082	1.511(0.099)	0.684(0.063)		2.195(0.048)	5.613(1.295)	0.046(0.013)	
	0P	22.3%	Control	0.1263	0.200	1.849(0.112)	0.804(0.180)		2.652(0.191)	3.547(0.690)	0.011(0.007)	
			AMP-PNP	0.0335	0.117	1.704(0.112)	0.636(0.093)		2.340(0.076)	1.711(0.239)	0.017(0.009)	
LKICDFGL	2P	22.3%	Control	0.1150	0.1280	0.376(0.122)	1.739(0.091)		2.115(0.073)	1.057(0.647)	0.019(0.004	
			AMP-PNP	0.1006	0.285	0.899(0.103)			0.899(0.094)	0.028(0.010)		
	0P	23.0%	Control	0.0944	0.214	0.894(0.142)	1.376(0.143)		2.270(0.135)	0.632(0.231)	0.016(0.006)	
			AMP-PNP	0.0388	0.084	0.362(0.078)	1.438(0.180)		1.800(0.201)	1.937(0.933)	0.008(0.003)	
	LM	22.4%	Control	0.0626	0.571	1.020(0.288)	1.519(0.272)		2.536(0.187)	0.684(0.361)	0.020(0.010)	
			AMP-PNP	0.0416	0.108	0.880(0.119)	1.531(0.088)		2.412(0.058)	1.152(0.275)	0.018(0.003)	
	ME	22.4%	Control	0.1133	0.12	0.676(0.132)	1.865(0.110)		2.540(0.077)	2.128(0.930)	0.024(0.004)	
			AMP-PNP	0.0122	0.764	1.573(0.199)			1.573(0.179)	0.027(0.012)		
	ET	23.2%	Control	0.1511	0.247	0.861(0.141)	1.480(0.115)		2.341(0.110)	0.676(0.239)	0.013(0.004)	
			AMP-PNP	0.0725	0.056	0.374(0.088)	1.415(0.072)		1.788(0.070)	5.962(4.027)	0.017(0.003)	
	TD	23.1%	Control	0.1517	0.09	0.911(0.124)	1.582(0.103)		2.493(0.049)	1.120(0.275)	0.031(0.006)	
			AMP-PNP	0.0286	0.071	0.633(0.099)	1.587(0.077)		2.219(0.064)	2.584(1.005)	0.021(0.003)	

Sequence [1]	Protein	% BE	Condition	Avg. St. Dev. at 1'	RSS	A [2]	B	C	N	k_1	k_2	k_3
KICDFGL	2P	24.4%	Control	0.0467	0.055		1.203 (.050)		1.203 (.048)		0.023(.003)	
			AMP-PNP	0.0415	0.146		0.534 (.061)		0.534 (.061)		0.033 (.013)	
	0P	20.5%	Control	0.1171	0.093	0.689 (.086)	0.774 (.118)		1.463 (.129)	0.903 (.228)	0.012 (.005)	
			AMP-PNP	0.0993	0.057	0.404 (.065)	0.083 (.082)		1.239 (.091)	2.317 (.916)	0.011 (.004)	
	LM	25.9%	Control	0.0223	0.02	0748 (.080)	0.498 (.070)		1.246 (.072)	0.261 (.058)	0.012 (.006)	
			AMP-PNP	0.0432	0.151	0.551 (.135)	0.787 (.105)		1.338 (.075)	0.971 (.443)	0.017 (.007)	
	ME	23.8%	Control	0.0880	0.07	0.488 (.113)	0.897 (.097)		1.385 (.055)	1.408 (.623)	0.028 (.008)	
			AMP-PNP	0.0390	0.035		0.886 (.067)		0.886 (.068)		0.013 (.003)	
	ET	21.8%	Control	0.1087	0.137	0.428 (.120)	1.009 (.080)		1.436 (.046)	3.556 (2.363)	0.044 (.011)	
			AMP-PNP	0.0211	0.032	0.254 (.064)	0.841 (.056)		1.095 (.056)	4.631 (2.828)	0.016 (.003)	
	TD	21.2%	Control	0.0622	0.08	0.840 (.106)	0.763 (.087)		1.603 (.060)	1.475 (.356)	0.025 (.009)	
			AMP-PNP	0.0668	0.031	0.477 (.076)	0.833 (.064)		1.310 (.055)	1.353 (.394)	0,017 (.004)	
KICDFGLARVADPDHDHTGF [3]	2P		Control									
			AMP-PNP									
	0P	20.0%	Control	0.0334	1.628	4.107(0.560)	2.662(0.536)		6.770(0.202)	0.586(0.153)	0.036(0.017)	
			AMP-PNP	0.0864	1.429	2.239(0.485)	3.584(0.430)		5.822(0.223)	1.237(0.470)	0.033(0.011)	
	LM	20.1%	Control	0.0863	0.177	1.342(0.272)	3.744(0.276)	2.476(0.336)	7.452(0.113)	7.775(6.311)	0.345(0.096)	0.022(0.006)
			AMP-PNP	0.0737	0.1	1.202(0.166)	4.716(0.154)	2.850(1.609)	8.768(1.718)	6.904(3.640)	0.235(0.023)	0.004(0.003)
	ME	20.1%	Control	0.0753	1.113	3.613(0.493)	3.600(0.441)		7.213(0.221)	0.766(0.189)	0.028(0.009)	
			AMP-PNP	0.0731	0.885	2.017(0.418)	4.163(0.343)		6.180(0.234)	1.478(0.581)	0.022(0.005)	
	ET	19.8%	Control	0.1476	0.95	4.228(0.375)	2.879(0.316)		7.107(0.146)	0.699(0.116)	0.028(0.008)	
			AMP-PNP	0.1139	1.297	2.680(0.506)	3.715(0.423)		6.395(0.233)	1.025(0.353)	0.028(0.009)	
	TD	19.9%	Control	0.1023	1.482	4.479(0.683)	2.602(0.634)		7.080(0.172)	0.803(0.188)	0.049(0.025)	
			AMP-PNP	0.1861	0.981	3.106(0.490)	3.666(0.415)		6.772(0.191)	0.859(0.223)	0.035(0.010)	
ARVADPDHDTGFLpTEpYVATRW [3]	2P	20.5%	Control	0.1376	1.323	6.313(0.457)	1.498(0.298)		7.811(0.185)	3.342(0.973)	0.026(0.021)	
			AMP-PNP	0.0234	1.903	6.088(0.473)	1.814(0.297)		7.902(0.229)	6.597(0.473)	1.814(0.297)	
YVATRW [3]	2P		Control									
			AMP-PNP									
	0P	26.5%	Control	0.2188	0.356	3.513(0.121)			3.513(0.044)	7.662(1.810)		
			AMP-PNP	0.2393	1.426	3.720(0.243)			3.720(0.092)	5.189(1.421)		
	LM	21.1%	Control	0.0394	0.593	3.814(0.147)			3.814(0.072)	5.755(1.211)		
			AMP-PNP	0.0557	1.186	3.941(0.311)			3.941(0.088)	4.029(0.841)		
	ME	20.1%	Control	0.0587	0.226	3.400(0.150)			3.400(0.043)	10.792(3.551)		
			AMP-PNP	0.1558	0.698	3.551(0.262)			3.551(0.077)	5.616(1.433)		
	ET	19.6%	Control	0.2528	1.185	3.494(0.313)			3.494(0.088)	5.358(1.193)		
			AMP-PNP	0.0173	0.291	3.556(0.190)			3.556(0.060)	8.340(1.902)		
	TD	19.8%	Control	0.1760	0.945	3.432(0.269)			3.432(0.073)	5.430(1.063)		
			AMP-PNP	0.1664	0.856	3.264(0.277)			3.264(0.079)	4.923(1.285)		
VATRW [3]	2P		Control									
			AMP-PNP									
	0P	29.0%	Control	0.1272	0.094	3.021(0.101)			3.021(0.030)	7.130(1.084)		
			AMP-PNP	0.1794	0.213	3.062(0.133)			3.062(0.035)	7.838(1.774)		

Sequence [1]	Protein	% BE	Condition	Avg. St. Dev. at 1'	RSS	A [2]	B	C	N	k_1	k_2	k_3
YRAPEIM	2P	22.2%	Control	0.0791	0.051	0.296(0.088)	1.413(0.067)		1.710(0.042)	1.165(0.631)	0.024(0.004)	
			AMP-PNP	0.0651	0.061	0.269(0.089)	1.545(0.063)		1.814(0.055)	3.890(3.551)	0.023(0.003)	
	0P	24.8%	Control	0.2004	0.095	0.646(0.116)	1.807(0.109)		2.453(0.070)	0.674(0.267)	0.024(0.004)	
			AMP-PNP	0.1182	0.148	0.685(0.132)	1.842(0.113)		2.528(0.067)	0.954(0.329)	0.023(0.004)	
	LM	21.2%	Control	0.0532	0.061	0.520(0.080)	1.734(0.069)		2.254(0.054)	7.058(6.187)	0.031(0.004)	
			AMP-PNP	0.0869	0.084	0.815(0.122)	1.557(0.094)		2.372(0.063)	0.955(0.262)	0.017(0.003)	
	ME	24.8%	Control	0.1804	0.204	0.578(0.185)	1.766(0.159)		2.344(0.110)	1.123(0.657)	0.021(0.006)	
			AMP-PNP	0.0872	0.183	0.738(0.191)	1.594(0.162)		2.332(0.124)	0.826(0.389)	0.018(0.006)	
	ET	25.7%	Control	0.0855	0.15	0.691(0.127)	1.737(0.104)		2.428(0.085)	0.612(0.246)	0.018(0.004)	
			AMP-PNP	0.0613	0.063	0.728(0.125)	1.748(0.120)		2.476(0.959)	0.384(0.169)	0.015(0.003)	
	TD	25.6%	Control	0.0792	0.258	0.704(0.186)	1.725(0.152)		2.428(0.095)	0.760(0.382)	0.023(0.006)	
			AMP-PNP	0.0794	0.069	0.796(0.119)	1.797(0.107)		2.593(0.079)	0.616(0.184)	0.024(0.004)	
NSKGYTKSIDIWSVG	2P	21.1%	Control	0.1536	0.368	2.906(0.306)	1.308(0.251)		4.214(0.088)	3.504(0.977)	0.096(0.043)	
			AMP-PNP	0.3429	0.754	3.352(0.344)	0.981(0.251)		4.334(0.203)	2.684(0.651)	0.024(0.021)	
	0P	24.2%	Control	0.0832	0.784	3.958(0.331)	2.289(0.419)		6.247(0.447)	3.685(0.801)	0.011(0.006)	
			AMP-PNP	0.1908	0.346	3.636(0.217)	2.188(0.162)		5.823(0.154)	7.719(2.364)	0.020(0.005)	
	LM	24.5%	Control	0.1397	0.238	3.967(0.130)	2.231(0.128)		6.198(0.109)	5.792(0.977)	0.027(0.007)	
			AMP-PNP	0.1631	0.473	3.874(0.232)	2.291(0.176)		6.165(0175)	4.719(0.887)	0.014(0.004)	
	ME	24.0%	Control	0.1398	0.45	3.845(0.230)		2.790(0.520)	6.635(0.541)	5.922(1.002)		0.008(0.003)
			AMP-PNP	0.1042	0.208	3.840(0.165)		3.238(0.510)	7.079(0.530)	4.890(0.677)		0.007(0.002)
	ET	24.7%	Control	0.0363	0.576	3.868(0.306)	2.648(0.233)		6.516(0.225)	4.391(1.050)	0.019(0.007)	
			AMP-PNP	0.0954	0.275	3.726(0.196)		3.593(0.520)	7.318(0.545)	5.987(0.904)		0.007(0.002)
	TD	24.3%	Control	0.1055	0.349	3.928(0.254)	1.840(0.183)		5.768(0.161)	11.358(8.529)	0.023(0.007)	
			AMP-PNP	0.1503	0.581	4.527(0.370)		1.847(0.559)	6.374(0.615)	1.968(0.349)		0.009(0.008)
LSNRPIFPGKHYLDQLNHILGILGSPSQE	2P	24.5%	Control	0.2266	1.816	5.647(0.692)	3.512(0.534)		9.159(0.324)	2.907(0.931)	0.053(0.025)	
			AMP-PNP	0.1988	1.593	5.989(0.628)	2.836(0.470)		8.825(0.241)	1.359(0.260)	0.042(0.017)	
	0P	24.4%	Control	0.1827	2.839	5.008(0.643)	4.523(0.450)		9.531(0.218)	4.689(1.877)	0.103(0.029)	
			AMP-PNP	0.1789	2.378	6.636(0.456)	4.520(0.523)		11.156(0.552)	1.840(0.274)	0.012(0.005)	
	LM	24.0%	Control	0.0689	0.215	4.635(0.312)	3.216(0.255)	4.749(0.354)	12.601(0.462)	7.592(1.977)	0.355(0.111)	0.009(0.002)
			AMP-PNP	0.1336	0.408	5.163(0.336)	3.261(0.552)	3.100(0.357)	11.524(0.403)	4.865(0.906)	0.189(0.067)	0.012(0.007)
	ME	24.0%	Control	0.1169	0.078	4.864(0.153)	3.838(0.194)	6.867(4.892)	15.568(5.050)	6.106(0.684)	0.164(0.020)	0.002(0.002)
			AMP-PNP	0.0543	2.625	5.774(0.603)	5.818(0.423)		11.592(0.360)	4.888(1.654)	0.026(0.006)	
	ET	24.6%	Control	0.0546	1.279	4.541(0.484)	2.833(1.153)	2.948(1.210)	10.322(0.256)	9.361(5.142)	0.205(0.169)	0.022(0.014)
			AMP-PNP	0.3628	0.658	4.591(0.519)	2.459(1.027)	3.246(1.119)	10.296(0.257)	5.510(1.446)	0.232(0.216)	0.022(0.012)
	TD	25.2%	Control	0.0893	1.46	5.338(0.490)	5.212(0.349)		10.550(0.211)	3.834(1.038)	0.061(0.013)	
			AMP-PNP	0.2293	2.366	5.646(0.570)	5.406(0.370)		11.051(0.243)	5.295(1.813)	0.075(0.015)	
IINLKARNYL	2P	19.8%	Control	0.1557	0.719	3.826(0.390)	2.532(0.325)		6.358(0.106)	3.609(0.981)	0.158(0.038)	
			AMP-PNP	0.2149	0.849	4.728(0.384)	1.654(0.297)		6.382(0.174)	1.847(0.305)	0.047(0.023)	
	0P	20.9%	Control	0.2754	1.42	5.120(0.404)	1.443(0.343)		6.563(0.198)	1.288(0.185)	0.031(0.023)	
			AMP-PNP	0.2744	0.871	3.582(0.384)	2.801(0.357)		6.382(0.115)	3.043(0.893)	0.108(0.027)	
	LM	20.8%	Control	0.1273	0.172	2.683(0.281)	2.853(0.258)	1.299(0.299)	6.835(0.122)	6.810(2.308)	0.349(0.124)	0.019(0.010)
			AMP-PNP	0.0496	1.482	4.810(0.576)	1.729(0.495)		6.539(0.164)	1.426(0.317)	0.042(0.024)	
	ME	21.1%	Control	0.0520	0.037	2.271(0.189)	3.235(0.142)	1.328(0.105)	6.834(0.120)	12.482(9.357)	0.449(0.067)	0.011(0.003)
			AMP-PNP	0.0959	0.122	2.857(0.271)	2.508(0.254)	1.389(0.282)	6.755(0.139)	5.614(1.331)	0.307(0.114)	0.017(0.008)
	ET	21.1%	Control	0.0200	0.118	2.549(0.191)	3.140(0.135)	1.132(0.254)	6.821(0.319)	7.710(1.882)	0.315(0.058)	0.008(0.005)
			AMP-PNP	0.2337	0.208	2.654(0.332)	2.833(0.255)	1.474(0.410)	6.961(0.516)	7.206(2.579)	0.341(0.116)	0.008(0.006)
	TD	20.3%	Control	0.1018	0.105	2.438(0.277)	2.939(0.202)	1.249(0.161)	6.626(0.080)	11.882(11.814)	0.420(0.108)	0.020(0.007)
			AMP-PNP	0.1659	0.206	2.595(0.420)	2.868(0.307)	1.171(0.316)	6.634(0.197)	7.976(4.842)	0.329(0.147)	0.016(0.012)

Sequence [1]	Protein	% BE	Condition	Avg. St. Dev. at 1'	RSS	A [2]	B	C	N	k_1	k_2	k_3
LSLPHKNKVPWNRLFPNADSKALDL	2P	23.2%	Control	0.0590	2.34	5.628(0.514)	3.398(0.324)		9.025(0.261)	4.439(1.212)	0.026(0.009)	
			AMP-PNP	0.4213	1.699	5.901(0.464)	3.455(0.337)		9.357(0.283)	4.208(0.970)	0.023(0.007)	
	0P	22.9%	Control	0.2494	0.688	5.209(0.391)	1.487(0.564)	4.281(1.495)	10.977(1.846)	5.557(1.507)	0.225(0.181)	0.006(0.005)
			AMP-PNP	0.2633	2.229	5.927(0.390)	3.944(0.423)		9.871(0.432)	4.572(1.167)	0.013(0.005)	
	LM	24.3%	Control	0.1344	0.808	5.862(0.219)	4.667(0.268)		10.528(0.260)	4.113(0.611)	0.016(0.003)	
			AMP-PNP	0.0311	0.406	5.244(0.313)	1.948(0.317)	4.179(1.509)	11.371(1.726)	5.131(0.906)	0.212(0.088)	0.005(0.003)
	ME	24.3%	Control	0.1214	1.744	5.326(0.456)	4.743(0.592)		10.069(0.616)	5.109(1.115)	0.011(0.004)	
			AMP-PNP	0.1956	0.927	5.675(0.351)		5.433(0.976)	11.108(1.020)	4.530(0.862)		0.007(0.003)
	ET	24.4%	Control	0.2261	0.974	5.717(0.299)	3.907(0.233)		9.623(0.235)	4.331(0.536)	0.016(0.003)	
			AMP-PNP	0.2244	1.607	5.352(0.447)	4.471(0.430)		9.822(0.436)	4.702(0.962)	0.014(0.004)	
	TD	23.9%	Control	0.0822	2.312	5.585(0.512)	3.897(0.330)		9.482(0.268)	4.437(1.249)	0.025(0.008)	
			AMP-PNP	0.1988	2.215	5.524(0.531)	3.795(0.334)		9.319(0.257)	6.449(2.509)	0.047(0.014)	
LTFNPHKRIEVEQA	2P	30.5%	Control	0.1828	0.929	2.506(0.607)	1.881(0.538)		4.386(0.194)	0.948(0.403)	0.033(0.024)	
			AMP-PNP	0.0703	1.828	2.051(0.465)	3.457(0.310)		5.508(0.241)	4.489(3.093)	0.035(0.009)	
	0P	27.5%	Control	0.0617	1.648	2.643(0.528)	2.213(0.475)		4.856(0.180)	1.828(0.733)	0.053(0.030)	
			AMP-PNP	0.1710	3.755	2.454(0.820)	2.759(0.743)		5.214(0.280)	1.512(0.938)	0.042(0.028)	
	LM	23.4%	Control	0.2700	0.887	2.150(0.359)	2.979(0.326)		5.129(0.160)	7.649(7.566)	0.096(0.030)	
			AMP-PNP	0.1435	0.325	2.722(0.336)	2.767(0.276)		5.490(0.101)	1.013(0.211)	0.036(0.007)	
	ME	26.1%	Control	0.2625	1.357	2.328(0.455)	2.649(0.293)		4.976(0.203)	6.635(4.192)	0.060(0.024)	
			AMP-PNP	0.1328	0.513	1.993(0.293)	2.824(0.185)		4.817(0.134)	9.007(8.822)	0.058(0.014)	
	ET	30.2%	Control	0.2974	1.096	2.356(0.424)	2.526(0.341)		4.872(0.187)	1.267(0.421)	0.030(0.012)	
			AMP-PNP	0.1659	0.977	2.920(0.382)	2.326(0.331)		5.247(0.302)	1.313(0.330)	0.016(0.008)	
	TD	31.5%	Control	0.2489	3.237	1.876(0.689)	3.105(0.502)		4.981(0.315)	3.541(3.048)	0.046(0.022)	
			AMP-PNP	0.0668	0.718	1.733(0.310)	3.332(0.198)		5.065(0.136)	5.708(3.669)	0.068(0.013)	
YYDPSDEPIAEAPFKFDMEL	2P	22.4%	Control	0.0875	2.247	6.948(0.54)	2.561(0.361)		9.509(0.165)	9.048(4.619)	0.177(0.061)	
			AMP-PNP	0.4553	0.523	7.144(0.401)	2.533(0.195)		9.677(0.151)	6.754(1.530)	0.152(0.050)	
	0P	22.0%	Control	0.0434	0.901	7.089(0.331)	2.769(0.276)		9.858(0.117)	7.701(1.986)	0.246(0.066	
			AMP-PNP	0.0707	0.757	8.948(0.382)	1.134(0.341)		10.083(0.255)	2.111(0.242)	0.027(0.025)	
	LM	22.2%	Control	0.2549	0.42	7.402(0.261)	2.992(0.233)		10.394(0.095)	13.013(8.691)	0.246(0.056)	
			AMP-PNP	0.2381	0.479	7.052(0.350)	3.100(0.277)		10.152(0.077)	8.542(2.145)	0.282(0.073)	
	ME	21.4%	Control	0.1089	0.114	7.460(0.150)	2.230(0.099)		9.689(0.055)	7.215(0.636)	0.147(0.028)	
			AMP-PNP	0.0983	0.35	7.317(0.236)	2.397(0.150)		9.714(0.092)	7.730(1.242)	0.118(0.026)	
	ET	21.3%	Control	0.0915	0.644	7.374(0.295)	2.555(0.186)		9.929(0.088)	8.780(1.648)	0.185(0.049)	
			AMP-PNP	0.3386	0.824	7.082(0.395)	2.608(0.273)		9.690(0.126)	11.350(5.526)	0.144(0.061)	
	TD	21.0%	Control	0.1269	0.196	7.538(0.204)	2.356(0.134)		9.894(0.088)	9.265(1.701)	0.132(0.032)	
			AMP-PNP	0.3056	0.46	7.203(0.297)	2.816(0.192)		10.019(0.110)	12.328(7.092)	0.149(0.044)	
DDLPKEKLKELIF	2P	19.1%	Control	0.2048	0.223	1.978(0.175)	1.697(0.127)		3.675(0.075)	1.801(0.313)	0.033(0.008)	
			AMP-PNP	0.0402	0.187	1.925(0.147)	1.607(0.101)		3.531(0.072)	3.215(0.648)	0.036(0.007)	
	0P	19.2%	Control	0.1240	0.315	2.607(0.169)	1.334(0.147)		3.941(0.119)	1.483(0.189)	0.021(0.008)	
			AMP-PNP	0.0222	0.43	1.650(0.173)	1.894(0132)		3.544(0.085)	7.176(4.418)	0.073(0.016)	
	LM	19.5%	Control	0.0367	0.034	1.637(0.063)	1.36(0.126)	1.313(0.127)	4.309(0.182)	11.390(6.046)	0.198(0.043)	0.009(0.004)
			AMP-PNP	0.0339	0.316	2.475(0.254)	1.592(0.181)		4.067(0.156)	2.066(0.523)	0.015(0.006)	
	ME	19.2%	Control	0.0347	0.064	1.619(0.126)	1.380(0.140)	2.246(1.280)	5.245(1.393)	6.715(1.569)	0.212(0.062)	0.004(0.004)
			AMP-PNP	0.0294	0.289	2.195(0.211)	1.627(0.172)		3.822(0.133)	2.362(0.552)	0.021(0.007)	
	ET	19.4%	Control	0.1242	0.135	1.496(0.201)	1.371(0.150)	1.426(0.198)	4.293(0.255)	5.900(1.841)	0.293(0.134)	0.009(0.005)
			AMP-PNP	0.0491	0.033	1.696(0.082)	1.306(0.130)	1.189(0.330)	4.191(0.419)	8.374(1.785)	0.143(0.030)	0.006(0.004)
	TD	19.0%	Control	0.0380	0.721	2.496(0.287)	1.545(0.221)		4.041(0.168)	1.854(0.441)	0.021(0.010)	
			AMP-PNP	0.0459	0.386	2.554(0.238)	1.495(0.195)		4.050(0.179)	1.623(0.291)	0.017(0.008)	

Sequence [1]	Protein	% BE	Condition	Avg. St. Dev. at 1'	RSS	A [2]	B	C	N	k_1	k_2	k_3
EETARFQPGYRS	2P	19.5%	Control	0.1002	0.631	4.011(0.299)	2.396(0.185)		6.408(0.110)	8.669(3.955)	0.085(0.022)	
			AMP-PNP	0.2146	0.705	4.038(0.297)	2.190(0.188)		6.228(0.100)	6.182(1.723)	0.107(0.025)	
	0P	19.0%	Control	0.0345	0.761	3.931(0.257)	2.479(0.207)		6.410(0.111)	5.662(1.604)	0.082(0.019)	
			AMP-PNP	0.0854	0.241	3.949(0.152)	2.634(0.120)		6.583(0.069)	13.189(11.349)	0.078(0.010)	
	LM	19.2%	Control	0.0472	0.313	3.904(0.133)	2.727(0.118)		6.631(0.087)	9.233(3.210)	0.064(0.010)	
			AMP-PNP	0.1468	0.315	3.794(0.215)	2.650(0.133)		6.444(0.072)	9.142(3.540)	0.074(0.012)	
	ME	19.2%	Control	0.1274	0.161	3.895(0.147)	2.542(0.091)		6.436(0.062)	9.322(1.930)	0.087(0.012)	
			AMP-PNP	0.1934	0.238	4.138(0.183)	2.358(0.115)		6.497(0.089)	6.680(1.246)	0.048(0.009)	
	ET	19.7%	Control	0.1160	0.181	3.715(0.135)	2.744(0.078)		6.460(0.048)	9.731(2.133)	0.825(0.008)	
			AMP-PNP	0.2473	0.317	4.108(0.204)	2.425(0.124)		6.533(0.087)	7.925(1.622)	0.048(0.009)	
	TD	19.8%	Control	0.0841	0.361	3.999(0.227)	2.449(0.142)		6.449(0.083)	7.486(2.046)	0.088(0.015)	
			AMP-PNP	0.1592	0.338	3.955(0.232)	2.604(0.148)		6.559(0.091)	11.702(8.467)	0.111(0.018)	
		0P-ERK2 Ctl Avg. St		0.1539								
		2P-ERK2 Ctl Avg. St		0.1447								
		Avg. across samples		0.1220								

Footnotes:

(1) Information for each peptide includes Amino acid sequence, protein designation, % back exchange (BE), experimental condition (± AMP-PNP), the standard deviation of the # of deuterons incorporated at 1 min. and the residual sum of squares (RSS).

(2) A, B, and C equal the number of amides exchanging with rates k_1, k_2, and k_3 respectively. N equals A+B+C. Values are corrected for artifactual in-exchange, back-exchange, and percentage D2O during the incubation.

(3) In four peptides around the activation lip, differential proteolysis was observed between 0P-ERK2 and the hinge mutants compared to 2P-ERK2 (See Figure 13). For three peptides the 2P corresponding peptide was not observed. ARVADPDHDTGFLpTEpYVATRW was the only peptide observed in 2P-ERK2.

(4) Peptides were not sequenced in LC-MS/MS experiments but were identified through peptide mass fingerprinting. Peptides are within a tolerance of 0.1 Da from the theoretical mass and are only observed in the hinge mutant TOF-MS experiment for which they would be expected and are not observed in any other TOF-MS experiment.

(5) The LLNTTCD peptide had individual anomalies. The LM mutant late time point intensity was low and could not be fit, but and error at 1 min could be calculated. The ME & ET mutants had only one measurable time point for the AMP-PNP condition so an error could not measured but the kinetics could still be fit.

(6) General Note: Missing fits are because the peptide was not observed or unanalyzable.

Y is the number of deuterons exchanged at time t, A, B, and C are the number of backbone amides exchanging with rate constants k_1, k_2, and k_3, and N is the maximal deuteration over the experimental time period (N = A + B + C). Subtracting N from the total number of exchangeable backbone amides yields NE, the number of amides that are non-exchanging over the experimental time period (Hoofnagle et al., 2003; Hoofnagle et al., 2004b; Lee et al., 2006). Non-linear least squares curve fitting was performed and results plotted using SigmaPlot 9.0 software (Systat Software, Inc.).

For LC-MS/MS, proteins incubated in water were treated and proteolyzed as above. Samples (5 μg) were analyzed on the QStar mass spectrometer with m/z window = 400-1600 Da, duty cycle 15.5 seconds, and 3 MS/MS per cycle. Samples (60 ng) were analyzed in parallel by LC-MS/MS on a LTQ-Orbitrap mass spectrometer interfaced with an Eksigent 2DLC HPLC (75 μm i.d. x 150 mm column, Zorbax C18 resin), with m/z window = 300-2000 Da, duty cycle 4-6 seconds (~10-14 cycles/minute), and 5 MS/MS per cycle. Peptides were identified by converting MS/MS spectra to .mgf files and searching against wild-type or mutant rat ERK2 sequences using the Mascot search program (v.1.9), with "no enzyme" specificity. Mass tolerances used for Pulsar datasets were 2.5 Da for parent ions and 1.2 Da for fragment ions. Mass tolerances for LTQ-Orbitrap datasets were 1.2 Da for parent ions and 0.8 Da for fragment ions. The score threshold used for high confidence identifications was Mowse ≥ 30.

Protein kinase assays

Activities of 0P-ERK2, hinge mutants and combination mutants (2 μg) were measured by phosphorylation of bovine myelin basic protein (MBP, 2 μg, Sigma, St.

Louis, MO) for 1 hour (combination mutants) or 2 hours (0P, hinge mutants) at 30 °C, and activity of 2P-ERK2 (1 ng) was measured using 5 μg rabbit MBP for 5 minutes at 30 °C. Kinase assay reactions were initiated by addition of 5x reaction buffer [125 mM Hepes, 50 mM $MgCl_2$, 10 mM DTT, 1 mM ATP, and 50 μL [γ-^{32}P] ATP (10 mCi/mL)] to a final volume of 25 μL. IC_{50} measurements were made performed in the presence of AMP-PNP varying between 0-20 mM. Reactions were quenched by spotting 20 μL onto P81 paper strips (Whatman), which were washed in 1% (v/v) phosphoric acid and quantified by scintillation counting. Curves were fit using SigmaPlot 9.0 software (Systat Software, Inc.) and IC_{50} concentrations were determined according to the following equation with log scale on the X axis

$$Y = \text{min} + (\text{max}-\text{min}) / (1 + (x / IC_{50}) \text{ ^ Hillslope}) \quad (1)$$

Isothermal titration calorimetry (ITC)

AMP-PNP was dissolved to 5 mM in the same buffer used for purification of ERK2 (50 mM Tris pH 7.5, 150 mM NaCl, 5 mM $MgSO_4$, 2% (v/v) glycerol, 0.1% (w/v) EDTA). An ITC 200 (Microcal) calorimeter was used to titrate AMP-PNP (28 injections, each 1.37 μL) into 0P-ERK2 (50 μM) at 10 °C. Blank runs were performed without ERK2, subtracted from experimental runs, the thermogram was integrated, and K_d values were estimated using Origin 7.0 software.

RESULTS

HX-MS peptide coverage

HX-MS was used to analyze six forms of ERK2, including unphosphorylated (0P) and diphosphorylated (2P) wild type ERK2, and mutants incorporating Gly-Gly substitutions in the hinge region (^{105}LMETD^{109}), including ^{105}LM^{106}/GG, ^{106}ME^{107}/GG, ^{107}ET^{108}/GG, and ^{108}TD^{109}/GG (Figure 1). Thirty-one peptides were identified from wild-type 0P-ERK2 after pepsin digestion, covering 91% of residues in ERK2 and 87% of exchangeable amides (Figure 2, Table 2 & 3). Differential cleavage was observed in the phosphorylated activation lip of 2P-ERK2, as previously noted (Hoofnagle et al., 2001; Lee et al., 2005). In each of the four hinge mutants, the peptides produced from the activation lip were identical to those in 0P-ERK2. Pepsin cleavages in the hinge region varied between mutants (Tables 2 & 3), but all mutants generated longer peptides containing residues 101 to 110, corresponding to the hinge region of wild type ERK2, ^{101}IVQDLMETDL^{110}. Wild-type ERK2 and mutant TD/GG each generated a peptide containing the N-terminal hinge residues, ^{101}IVQDL^{105}, whereas wild-type and mutants ME/GG and TD/GG generated a peptide containing the C-terminal hinge residues, ^{106}METDL^{110}.

Evidence for native folding of the ERK2 hinge mutants

In order to compare folding in solution between wild-type ERK2 and hinge mutants, the extent of deuteration at the longest time point was measured in different regions of each enzyme. Figure 3 shows the deuteration at 4 hours for each protein form, normalized by the number of exchangeable amides and mapped against the X-ray

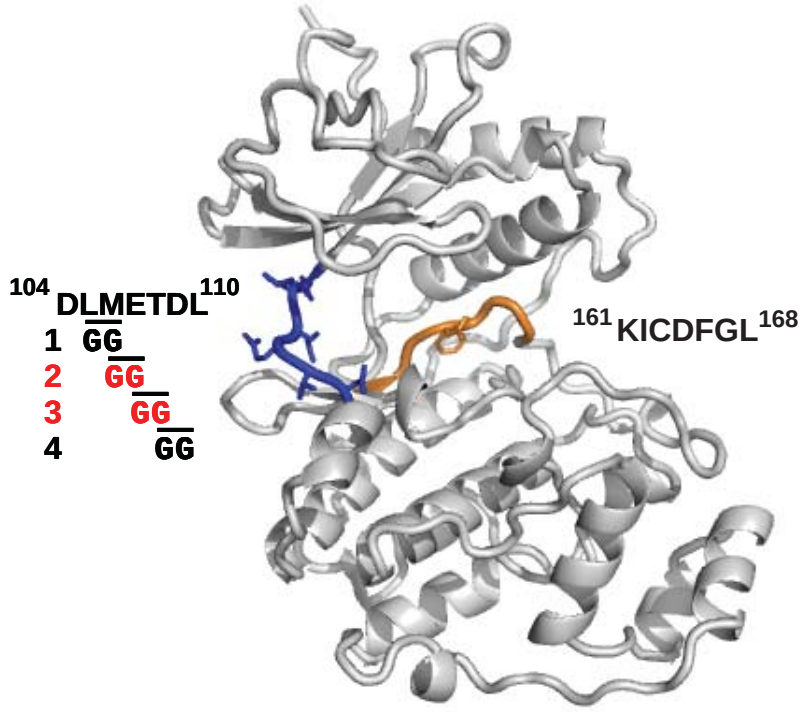

Figure 1: Outline of an experimental strategy to test the effects of increased hinge flexibility on domain closure as measured by protection from hydrogen exchange in the C-terminal domain. Four Gly-Gly mutations (labeled on the left) were engineered in the hinge region (shown in blue) in order to increase backbone flexibility. Previous studies (Lee et al., 2005) established that domain closure can be monitored by increased HX protection in the conserved DFG region of the C-terminal domain (shown in orange, sequence indicated on the right).

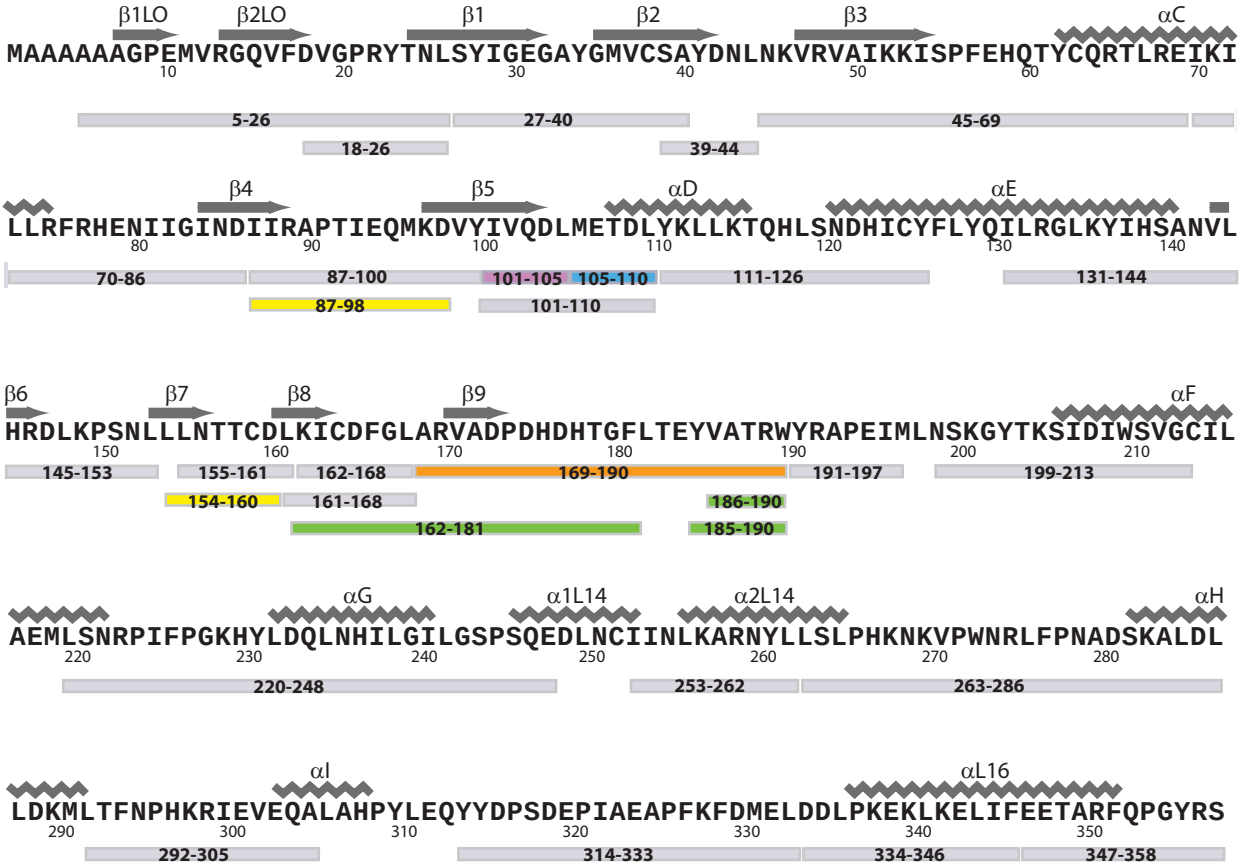

Figure 2: Summary of peptides monitored in our HX-MS analyses of ERK2. Sequence coverage map of ERK2, indicating residue numbers and secondary structures as reported (Zhang et al, 1994). Observed peptides are shown as bars below the sequence and are named according to residue number. Peptides colored grey were found in all six proteins and were analyzed as described in Materials and Methods. Peptides that are unique to certain kinase forms, and produced by differential proteolysis are colored as follows: Orange: unique to phosphorylated (2P); Green: unique to unphosphorylated (0P). Peptides showing differential proteolysis between wild type and mutant kinases within the hinge region are colored as follows: Pink: Unique to wild type and mutant TD/GG; Cyan: Unique to wild type, ME/GG, and TD/GG; Yellow: Unique to 0P- and 2P-ERK2 (WT).

Table 3: Observed monoisotopic masses in the HX-MS experiment for 0P / 2P-ERK2 & the hinge mutants.

					Observed mass for analyzed ERK2 peptides						
Residue #	**Peptide**	**# E.A.**	**Calc. Mass**	**Calc. Mass for Analyzed m/z**	**2P**	**0P**	**LM**	**ME**	**ET**	**TD**	**Elution Time**
5.26	AAAGPEMVRGQVFDVGPRYTNL	19	2347.17	783.39	783.44	783.40	783.42	783.41	783.42	783.47	9.6
18.26	DVGPRYTNL	7	1033.52	517.76	517.79	517.81	517.82		517.81	517.80	7.5
27.40	SYIGEGAYGMVCSA	13	1406.58	704.29	704.29	704.31	704.35	704.33	704.35	704.37	9.5
39.44	SAYDNL	5	681.30	682.30	682.32	682.33	682.34	682.31	682.34	682.37	6.7
45.69	NKVRVAIKKISPFEHQTYCQRTLRE	23	3043.65	1015.55	1015.55	1015.62	1015.54	1015.57	1015.62	1015.64	8.2
70.86	IKILLRFRHENIIGIND	16	2063.20	688.73	688.74	688.77	788.74	788.75	688.78	688.80	9.3
87.98	IIRAPTIEQMKD	10	1413.76	707.88	707.87	707.88					7.9
87.100	IIRAPTIEQMKDVY	12	1675.90	838.95	838.94	838.99	839.00	839.00	839.00	839.01	9.2
101.105	IVQDL	4	586.33	587.33	587.32	587.35				587.38	5.8
101.110	IVQDLMETDL	9	1175.57	1176.57	1176.56	1176.56					9.0
101.110	IVQDGGETDL	9	1045.49	1046.49			1046.54				6.0
101.110	IVQDLGGTDL	9	1029.53	515.77				515.81			7.7
101.110	IVQDLMGGDL	9	1059.53	1060.53					1060.67		9.0
101.110	IVQDLMEGGL	9	1073.54	1074.54						1074.66	6.0
105.110	LMEGGL	5	618.30	619.30						619.39	7.0
106.110	METDL	4	607.25	608.25	608.25	608.28					6.4
106.110	GGTDL	4	461.21	462.21				462.22			7.0
111.126	YKLLKTQHLSNDHICY	15	1975.00	659.33	659.35	659.39	659.35	659.36	659.39	659.41	8.2
131.144	ILRGLKYIHSANVL	13	1595.95	532.98	532.99	532.97	532.97	532.99	532.97	533.00	8.7
145.153	HRDLKPSNL	7	1078.59	540.29	540.30	540.33	540.30	540.31	540.32	540.35	5.6
154.160	LLNTTCD	6	778.35	779.35	779.36	779.37	779.36	779.38	779.43	779.43	5.0
155.161	LNTTCDL	6	778.35	779.35	779.36	779.39					7.1
161.168	LKICDFGL	7	907.48	454.74	454.76	454.78	454.76	454.76	454.76	454.77	10.0
162.168	KICDFGL	6	794.40	795.40	795.42	795.43	795.42	795.43	795.44	795.49	9.0
162.181	KICDFGLARVADPDHDHTGF	18	2213.03	1107.52		1107.56	1107.56	1107.56	1107.61	1107.62	9.1
169.190	ARVADPDHDHTGFLpTEpYVATRW	20	2716.15	680.04	680.07						10.0
185.190	YVATRW	5	794.41	795.41		795.44	795.44	795.43	795.44	795.49	8.1
186.190	VATRW	4	631.34	632.34		632.41					6.8
191.197	YRAPEIM	5	878.43	440.23	440.21	440.23	440.24	440.25	440.25	440.25	7.7
199.213	NSKGYTKSIDIWSVG	14	1653.84	827.92	827.92	827.94	827.92	827.94	827.99	828.00	9.4
220.248	LSNRPIFPGKHYLDQLNHILGILGSPSQE	25	3242.72	1081.91	1081.97	1082.90	1081.96	1081.95	1081.95	1081.98	10.8
253.262	IINLKARNYL	9	1216.73	609.36	609.38	609.40	609.38	609.40	609.39	609.44	8.3
263.286	LSLPHKNKVPWNRLFPNADSKALDL	21	2872.57	958.52	958.6	958.50	958.53	958.57	958.58	958.58	9.9
292.305	LTFNPHKRIEVEQA	12	1680.89	841.45	841.47	841.42	841.47	841.49	841.52	841.54	7.9
314.333	YYDPSDEPIAEAPFKFDMEL	16	2376.05	1189.03	1189.01	1189.06	1189.01	1189.07	1189.08	1189.11	11.0
334.346	DDLPKEKLKELIF	11	1586.89	529.96	529.99	530.01	529.99	529.99	530.01	530.00	9.4
347.358	EETARFQPGYRS	10	1439.68	720.84	720.84	720.89	720.87	720.89	720.91	720.89	6.8

Footnotes:

(1) Information for each peptide includes Residue number, Amino acid sequence, Number of exchangable amides (#EA), Calculated mass, Observed mass/charge, and Elution Time.

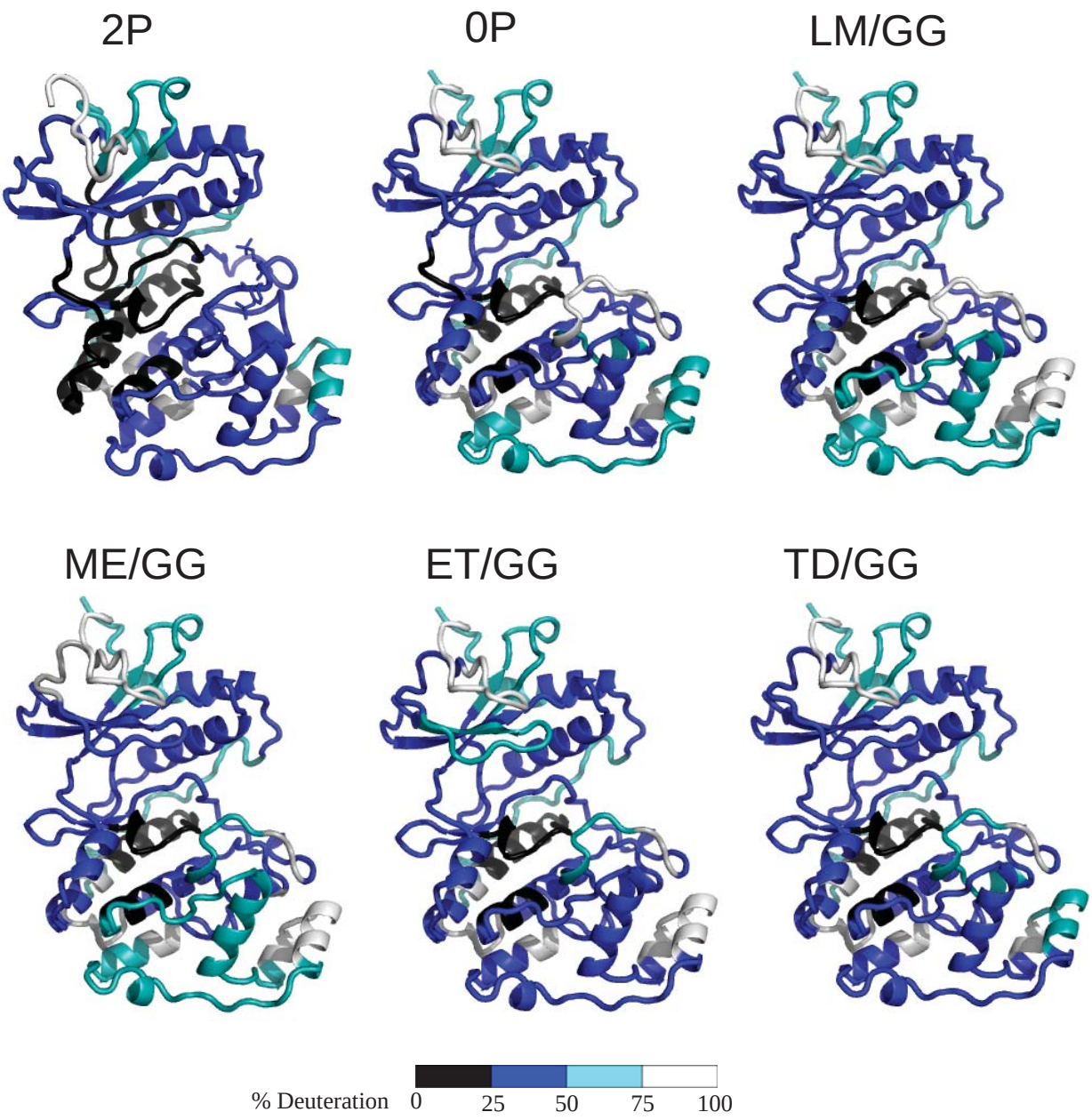

Figure 3: Hydrogen exchange in different forms of ERK2. Colors reflect the extent of deuteration at 4 hours, normalized for each peptide by the number of exchangeable amides and multiplied by 100. X-ray structures were PDB:1ERK, for 0P-ERK2, LM/GG, ME/GG, ET/GG, and TD/GG (Zhang et al.1994), and PDB:2ERK for 2P-ERK2 (Canagarajah et al.1997). The color coding is Black: 0-25%, Blue: 26-50%, Teal: 51-75%, and White: 76-100%. Similar HX patterns are observed between wild type and mutant kinases, indicating comparable solution structure and folding.

structures of ERK2 (Zhang et al., 1994; Canagarajah et al., 1997). The 0P and 2P forms of wild-type ERK2 showed similar patterns of deuteration which was low in core regions of N- and C-terminal domains and higher in peripheral regions and loops (Figure 3). These repeated the patterns reported previously by Hoofnagle et al. (2001). Similar patterns were also observed in each of the hinge mutants (Figure 3). Thus, the extent of deuteration reached only 7% in the solvent protected αE-β6 core region of the C-terminal domain, which is known to be stabilized by extensive hydrogen bonding interactions, whereas deuteration reached 91% within β1LO-β2LO in the N-terminal domain which is highly solvent exposed. The similar extent of hydrogen exchange between all six proteins suggested comparable solvent accessibility for each, and argued against extensive unfolding introduced by mutagenesis. Likewise, evidence for bimodal HX patterns, which occur when proteins are partially unfolded, was absent in all datasets.

Differential effects of AMP-PNP binding on HX patterns in mutant forms of ERK2

We next asked whether the Gly-Gly mutations at the hinge region altered interdomain interactions in ERK2. Upon AMP-PNP binding, steric protection from solvent leads to reduced HX in regions of 0P-ERK2 and 2P-ERK2 containing the Gly-rich loop, the conserved Lys-Glu ion pair within β3-αC-β4, the hinge region, and the catalytic base; all of which are known to form close interactions with nucleotide. In addition, 2P-ERK2 shows greater protection from HX than 0P-ERK2 within the conserved DFG motif, part of the C-terminal domain which forms metal coordination interactions with Mg^{+2}-ATP. Thus, AMP-PNP-dependent protection from HX in the DFG

motif provides an indirect assay for interdomain closure. We applied this assay to measure domain closure in ERK2 mutants containing Gly-Gly substitutions at the hinge.

Figure 4 summarizes different forms of ERK2, indicating regions where altered HX were observed upon AMP-PNP binding. Regions in green showed reduced HX upon nucleotide binding, regions in red showed increased HX upon binding, and regions in grey showed no change. Overall, most regions showed little difference in HX rates between bound and unbound states, as shown by time courses for representative peptides in each protein (Figure 5). However, every wild type and mutant protein showed protection from HX within regions known to form the ATP binding site, including the Gly-rich loop, hinge, β3-αC-β4, and the DFG motif, as noted previously for 0P- and 2P-ERK2 (Lee et al., 2005) (Figures 6-8). The exception was the mutant ERK2-LM/GG, which showed no protection at all in any region, suggesting that the mutations disrupted nucleotide binding without grossly altering the protein solution structure. Figure 6 showed decreased in-exchange in the Gly-rich loop (^{27}SYIGEGAYGMVCSA^{40}) with maximal HX protection by nucleotide binding of ~1 Da in every protein. Figure 7 shows protection in a peptide spanning β3 and the N-terminus of helix αC (^{45}NKVRVAIKKISPFEHQTYCQRTLRE^{69}) which contains the conserved ^{52}Lys and ^{69}Glu residues known to coordinate the α and β phosphoryl groups in ATP, and an adjacent peptide spanning the C-terminus of helix αC and β4 (^{70}IKILLRFRHENIIGIND^{83}). Peptide 45-69 previously was reported to show a minor decrease in HX (0.5 Da upon AMP-PNP binding) with little change in peptide 70-83. However, in my hands, decreased HX in peptide 45-69 was seen only in the mutants ERK2-ME/GG and ET/GG, and not in the wild-type proteins, while peptide 70-83

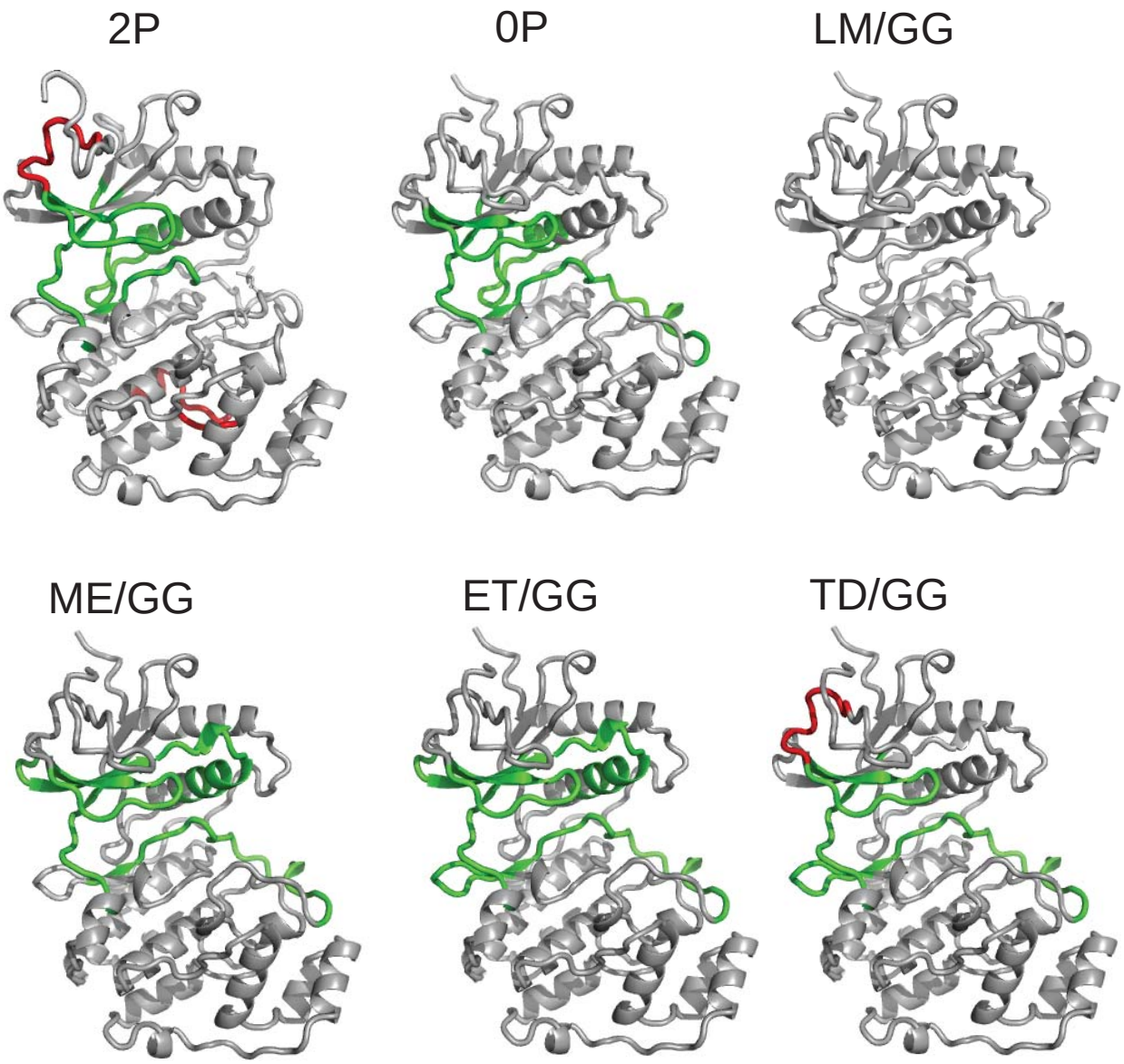

Figure 4: Changes in hydrogen exchange upon AMP-PNP binding in different forms of ERK2. Regions corresponding to peptides showing reduced deuteration upon AMP-PNP binding (1 mM) are colored green. Regions corresponding to peptides showing increased HX upon AMP-PNP binding are colored red. Mutant LM/GG shows little HX protection at all, reflecting low nucleotide binding affinity. The changes due to AMP-PNP binding are mostly localized around the active site, where nucleotide binding would be expected to provide steric protection from hydrogen exchange. PDB structures used were as described in Figure 3.

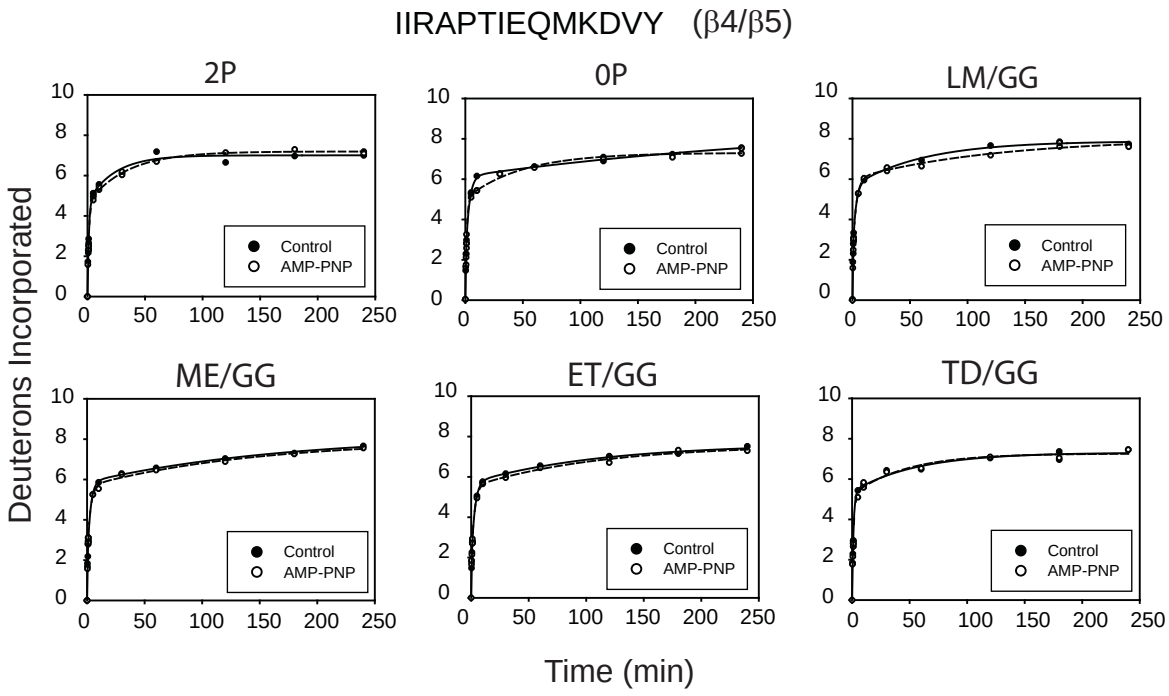

Figure 5: Effect of AMP-PNP binding on HX in a region of ERK2 outside the nucleotide binding interface. Deuteration time courses for the peptide, IIRAP-TIEQMKDVY, located in strands β4-β5 in the N-terminal domain and not predicted to be directly involved in nucleotide binding. As expected, time courses of deuterium incorporation were comparable between experiments in the presence and absence of 1 mM AMP-PNP. This indicates that AMP-PNP binding does not introduce nonspecific global effects on structure, and that the hinge mutations do not perturb hydrogen exchange behavior in this region.

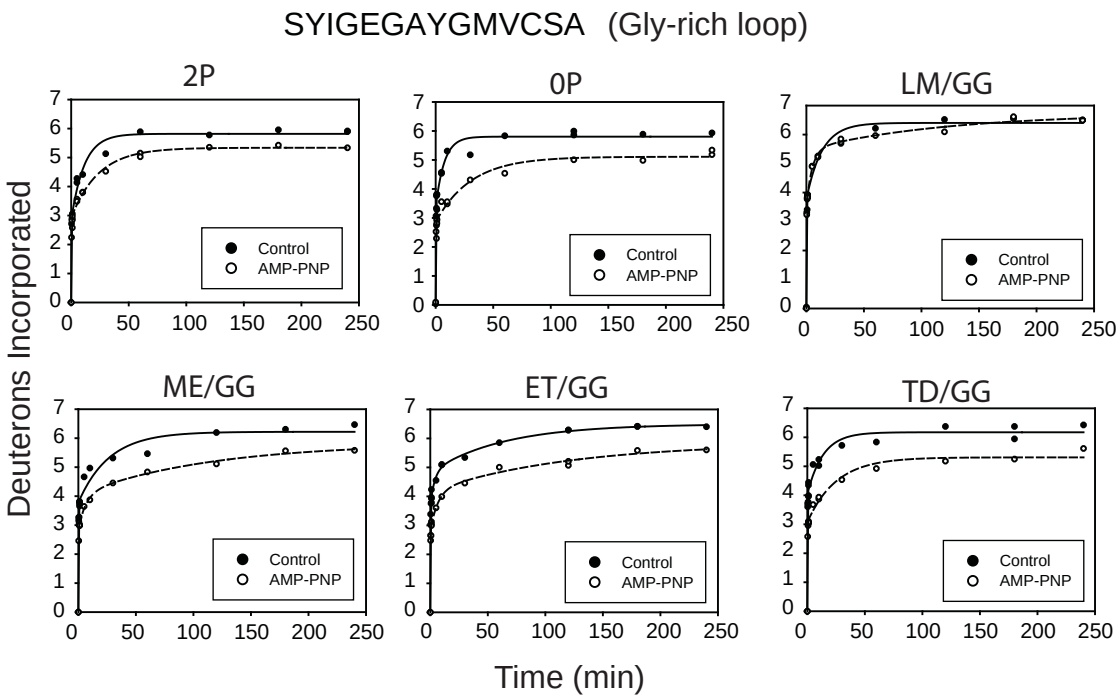

Figure 6: Effect of AMP-PNP binding on HX in the Gly-rich loop region. Deuteration time courses for the peptide, SYIGEGAYGMVCSA, located in the Gly-rich loop, which in protein kinases forms backbone atom contacts with bound ATP. As expected, partial HX protection upon AMP-PNP binding is found in all wild type and mutant ERK2 proteins. The exception is mutant LM/GG, which shows little HX protection upon AMP-PNP binding in this and other regions, consistent with low nucleotide binding affinity.

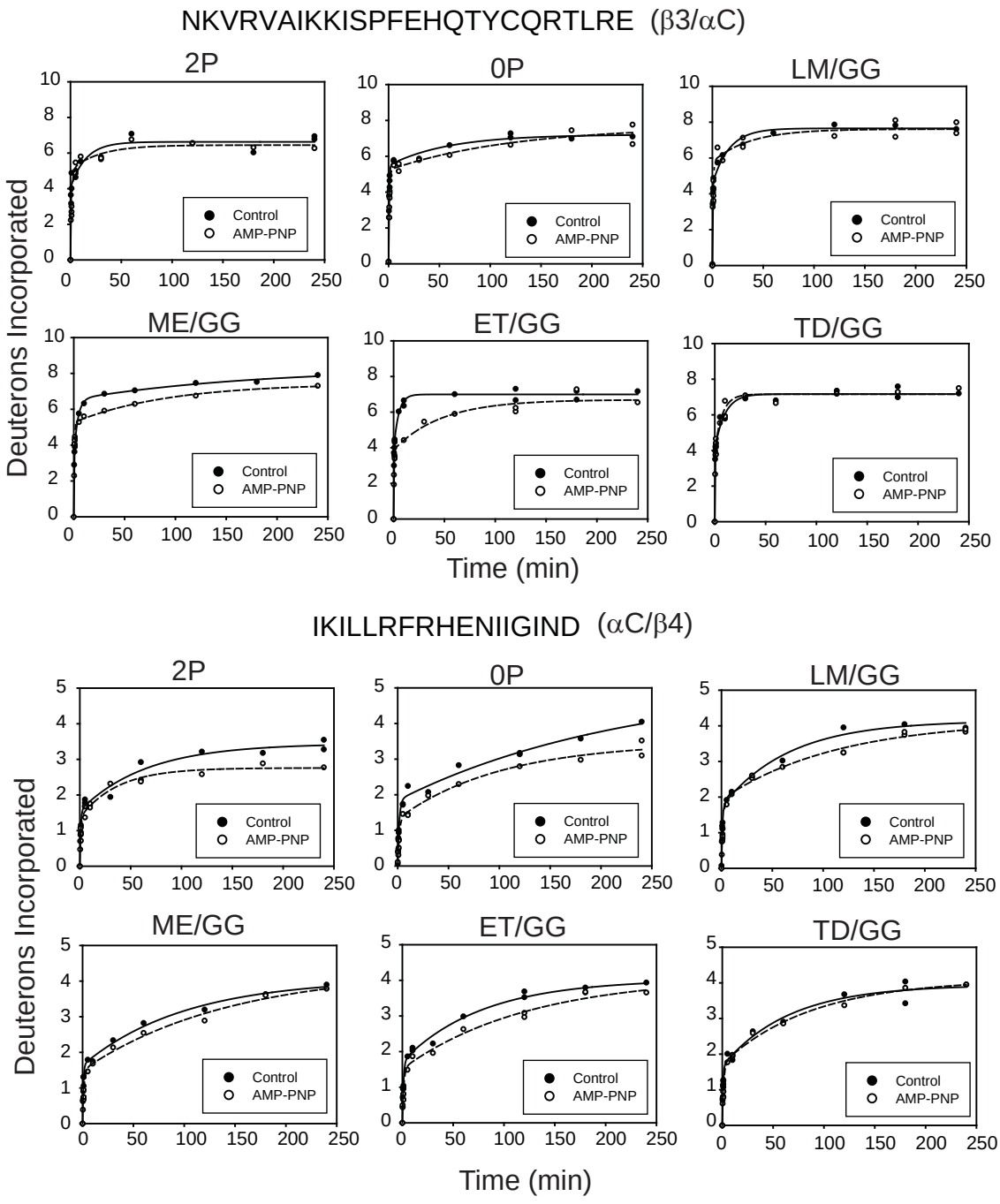

Figure 7: Effect of AMP-PNP binding on HX of peptides representing β3-αC-β4. Deuteration time courses of peptide ^{45}NKVRVAIKKISPFEHQTYCQRTLRE^{69} residing in N-terminal strand β3 and helix αC, which contains a conserved glutamic acid residue (E^{69}) and is involved in coordinating ATP. Peptide ^{70}IKILLRFRHENIIGIND^{86} resides in helix αC and strand β4, immediately following the conserved glutamic acid. ME/GG and ET/GG mutants show protection in β3/αC while 0P- and 2P-ERK2 show protection in αC/β4 suggesting finite but weak interactions with AMP-PNP throughout the β3/αC/β4 region.

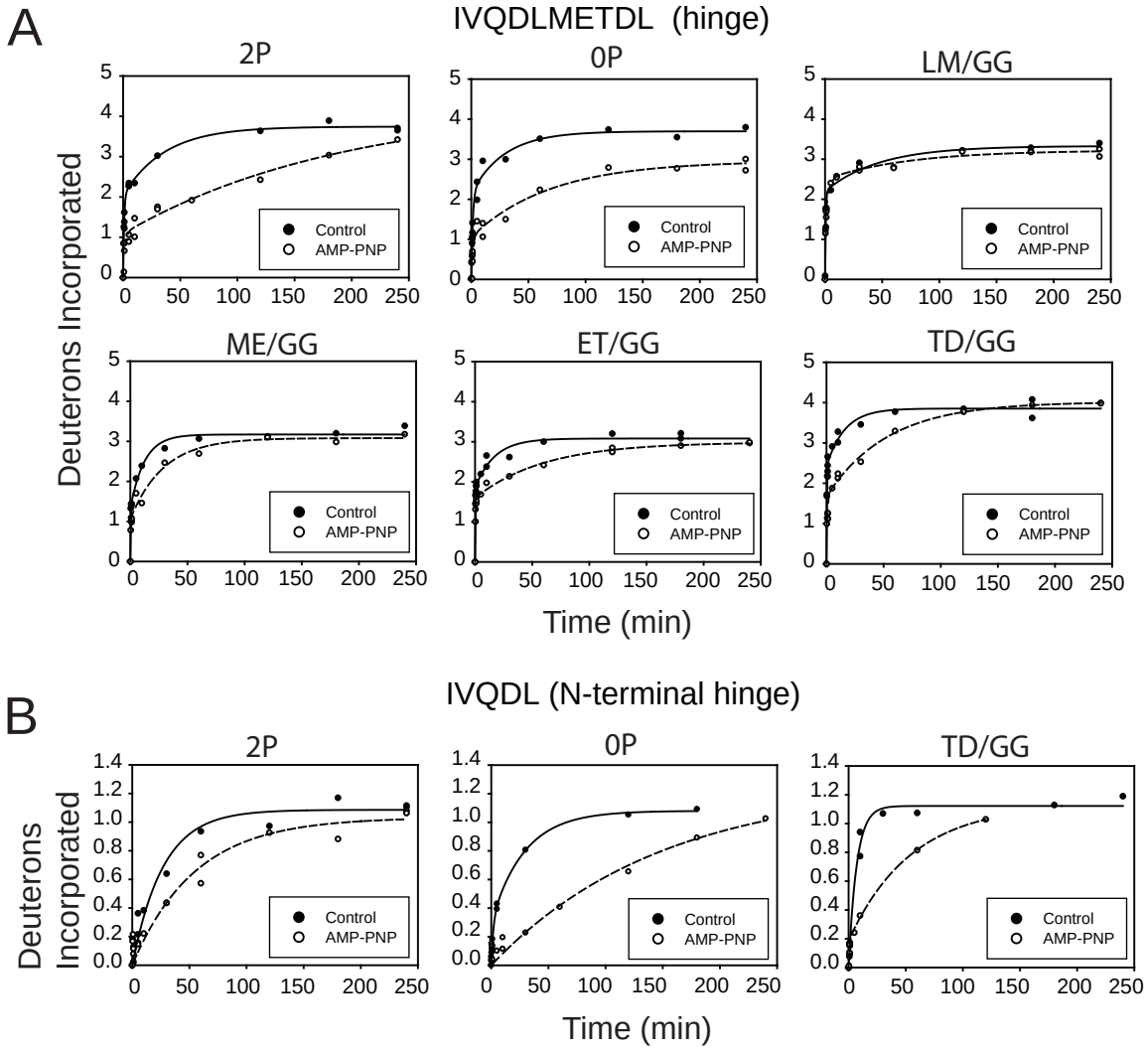
A
IVQDLMETDL (hinge)
2P
0P
LM/GG
ME/GG
ET/GG
TD/GG
Deuterons Incorporated
Time (min)
Control
AMP-PNP
B
IVQDL (N-terminal hinge)
2P
0P
TD/GG
Deuterons Incorporated
Time (min)
Control
AMP-PNP

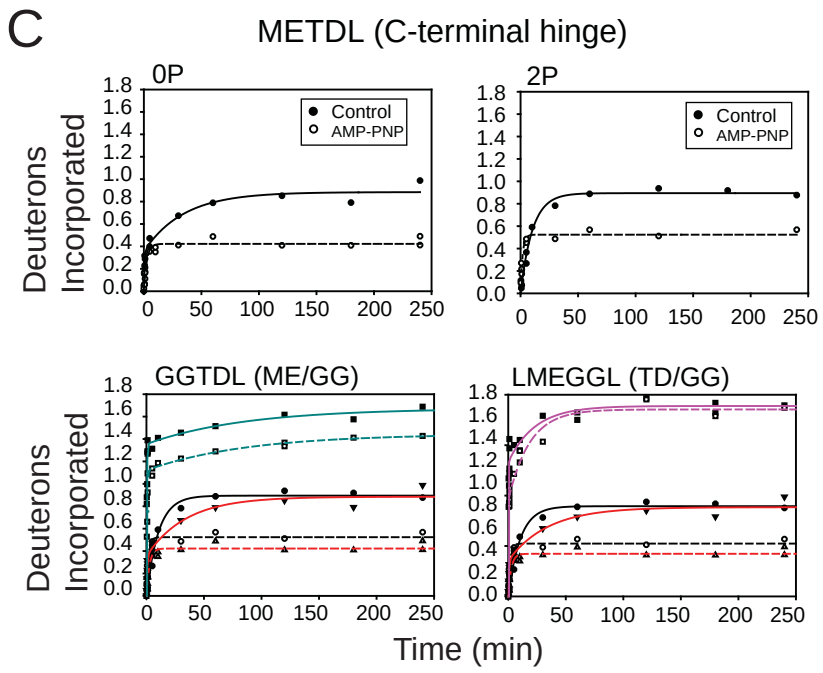

Figure 8: Effect of AMP-PNP binding on HX of peptides corresponding to the hinge region. A. Deuteration time courses of peptides corresponding to positions 101-110 in the hinge between β5-αD (^{101}IVQDLMETDL^{110} in WT) are present and show HX protection by AMP-PNP binding in all ERK2 proteins except mutant LM/GG. **B.** Peptides corresponding to positions 101-105 (^{101}IVQDL^{105} in WT) are observed in 0P- and 2P-ERK2 and mutant TD/GG. **C.** Peptides corresponding to positions 106-110 (^{106}METDL^{110} in WT) are observed in 0P- and 2P-ERK2 (top graphs) and mutant ME/GG (bottom left). Mutant TD/GG shows a different cleavage product corresponding to positions 105-110 (^{105}LMETDL^{110} in WT). The ME/GG and TD/GG graphs show 2P in black, 0P in red and the hinge mutant colored, ME/GG: teal and TD/GG: purple.

showed minor protection in all forms except mutant TD/GG. This suggests that AMP-PNP coordinates this N-terminal region and provides some steric protection from HX, but felt throughout αC and with some variation in amide localization.

In addition, two proteins showed evidence for increased HX. One region was located N-terminal to the Gly-rich loop outside the kinase consensus core (^{18}DVGPYTNL^{26}), as observed in 2P-ERK2 and the TD/GG mutant. The other region was localized to a loop (^{292}LTFNPHKRIEVEQA^{305}) between helices αH and αI in the C-terminal domain in 2P-ERK2. These increases were unexpected, because they were not observed previously for 2P-ERK2, and will require further investigation to fully understand. However, we conclude that the results for the most part revealed reduced HX in regions that were consistent with binding of AMP-PNP to the ATP binding site in wild type and mutant forms of ERK2.

Evidence for nucleotide binding and HX protection in the hinge region

The Gly-Gly mutations introduced altered proteolysis in the hinge region, resulting in variable peptides from those observed in wild type forms of ERK2, and in some cases, failure to observe related peptides. For example, while all forms generated cleavage products corresponding to hinge peptide ^{101}IVQDLMETDL^{110} (wild-type sequence), only the wild-type proteins and the TD/GG mutant generated the N-terminal hinge peptide, ^{101}IVQDL^{105}, while ME/GG generated the C-terminal hinge peptide, ^{106}GGTDL^{110}, and mutant TD/GG generated an alternative proteolytic product, ^{105}LMEGGL^{110} (see Tables 2 and 3).

Figure 8 details time courses observed in the hinge region for wild type and mutant proteins. For the peptide containing the entire hinge (corresponding to ^{101}IVQDLMETDL^{110} in the wild-type sequence), each mutant protein showed similar levels of overall deuteration (3.0-3.7 Da), comparable to those in wild type ERK2 (Figure 8A). Protection from HX upon AMP-PNP binding was observed in all mutants except LM/GG, although the magnitude of protection was lower than that of 0P-ERK2 or 2P-ERK2. The HX behavior suggested that each mutant bound AMP-PNP in the hinge region, but allowed higher accessibility to solvent penetration in the bound states, consistent with greater flexibility introduced by the Gly-Gly mutations.

In the shorter N- and C-terminal hinge peptides (^{101}IVQDL^{105}, corresponding to ^{106}METDL^{110} in the wild-type sequence), HX behavior in 0P- and 2P-ERK2 showed similar behavior to that observed previously in our lab (Hoofnagle et al., 2001; Lee et al., 2005). Peptide ^{101}IVQDL^{105} in mutant TD/GG provides the only direct comparison with the mutant forms, and shows faster HX than wild-type proteins, with comparable HX-protection upon nucleotide binding.

Evidence for domain closure in hinge mutants

Previous studies suggested that interdomain closure could be reflected by enhanced HX protection in 2P-ERK2 compared to 0P-ERK2, of a peptide containing the conserved DFG motif within the C-terminal domain (^{162}KICDFGL^{168}) (Lee et al., 2005). It is this metric that I used to assay for domain closure in the hinge mutants. Figure 9 shows the same peptide, found in all six proteins compared in this HX-MS study. HX behavior in 2P and 0P recapitulated the result from Lee et al. (2005), with increased HX

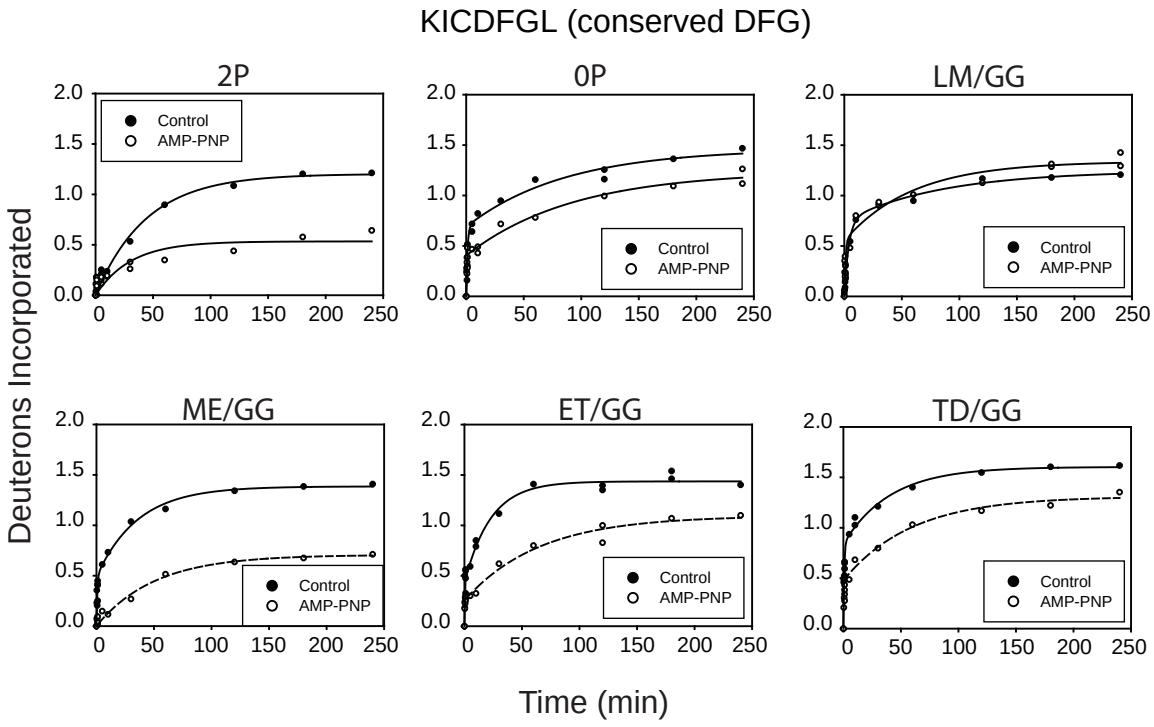

Figure 9: Effect of AMP-PNP binding on HX in the conserved DFG region. Deuteration time courses of peptide ^{162}KICDFGL^{168} containing the conserved DFG sequence. All ERK2 proteins show similar deuteration in this region in absence of AMP-PNP, but vary in HX protection in the presence of AMP-PNP. 0P-ERK2 and mutant TD/GG show less protection when bound to AMP-PNP, while ME/GG and ET/GG show greater HX protection, similar to that observed in 2P-ERK2. LM/GG shows no HX protection, consistent with low nucleotide binding affinity.

protection in 2P-ERK2 bound to AMP-PNP compared to 0P-ERK2. In addition, 2P-ERK2 showed a slower rate of overall deuteration in the unbound state, as previously observed, hinting that this form may be less solvent accessible due to partial closure in absence of nucleotide. My results were consistent with previous conclusions suggesting that 2P-ERK2 adopts a more closed conformation in solution compared to 0P–ERK2, and suggesting that phosphorylation overcomes a constraint to domain closure.

All ERK2 mutants showed overall deuteration into ^{162}KICDFGL^{168} (1.4-1.5 Da) comparable to that of the wild-type proteins. HX protection upon AMP-PNP binding was observed in ME/GG, ET/GG and TD/GG mutants. Importantly, mutant ME/GG showed maximal HX reaching 0.6 Da in the bound state, which was comparable to that of 2P-ERK2. In contrast, mutants ET/GG and TD/GG showed maximal HX reaching 1.3 Da in the bound state, comparable to that of 0P-ERK2. Furthermore, HX rates in the bound state were slower in ET/GG than TD/GG. Taken together, my results indicate that introduction of Gly-Gly mutations in the hinge region can recapitulate behavior seen upon phosphorylation and activation of ERK2, and suggest that ME/GG adopts a bound conformation consistent with domain closure in 2P-ERK2, while TD/GG is constrained from closure as in 0P-ERK2, and ET/GG adopts a partially closed state intermediate between ME/GG and TD/GG. The results argue that mutations which would be expected to enhance flexibility in the hinge appear to enhance interdomain interactions in ERK2.

IC_{50} concentrations report similar binding affinity among ERK2 proteins

The time courses shown above showed that all mutants, except LM/GG, bound AMP-PNP with similar degree of protection from HX to that of 0P-ERK2 and 2P-ERK2

(Figures 6 & 7), suggesting that the binding affinities are comparable between mutant and wild-type proteins. However, direct measurements of the mutations on binding affinity have not been tested directly. In order to address this, I have tested two approaches, one comparing inhibition of initial rate measurements by AMP-PNP, and the other using isothermal titration calorimetry (ITC) to measure equilibrium dissociation constants for AMP-PNP binding.

I first measured initial rates for phosphorylation of myelin basic protein (MBP) by phosphoryl transfer from [γ-^{32}P]ATP, catalyzed by wild-type or mutant forms of ERK2. Initial rates normalized to total enzyme are plotted vs [AMP-PNP] in Figure 10, indicating the best fit IC_{50} values for each protein. IC_{50} reports the concentration of an inhibitor that will produce 50% inhibition of the enzyme activity, which is related to inhibitor dissociation constant (K_i) by the following relationship:

$$IC_{50} = K_i (1 + S / K_m) \qquad (2)$$

where S is the substrate concentration and K_m is the Michaelis constant (Cheng & Prusoff, 1973). In my experiments, [MBP] and [ATP] were held constant at 25 μM and 200 μM, respectively, with rate measurements carried out at 30 ºC. Therefore, the IC_{50} measurements are not necessarily proportional to K_i in all cases unless K_m is also constant between different protein forms. But it was reasonable to begin with this approximation, in carrying out the initial experiments.

IC_{50} values measured for wild-type ERK2 were 194 ± 25 μM for 0P-ERK2 and 366 ± 47 μM for 2P-ERK2, while IC_{50} values for mutants LM/GG, ME/GG, ET/GG and TD/GG were respectively 176 ± 21 μM, 356 ± 30 μM, 280 ± 31, and 298 ± 20 μM (Figure 10). On the surface, the results suggest that all of the mutants showed comparable

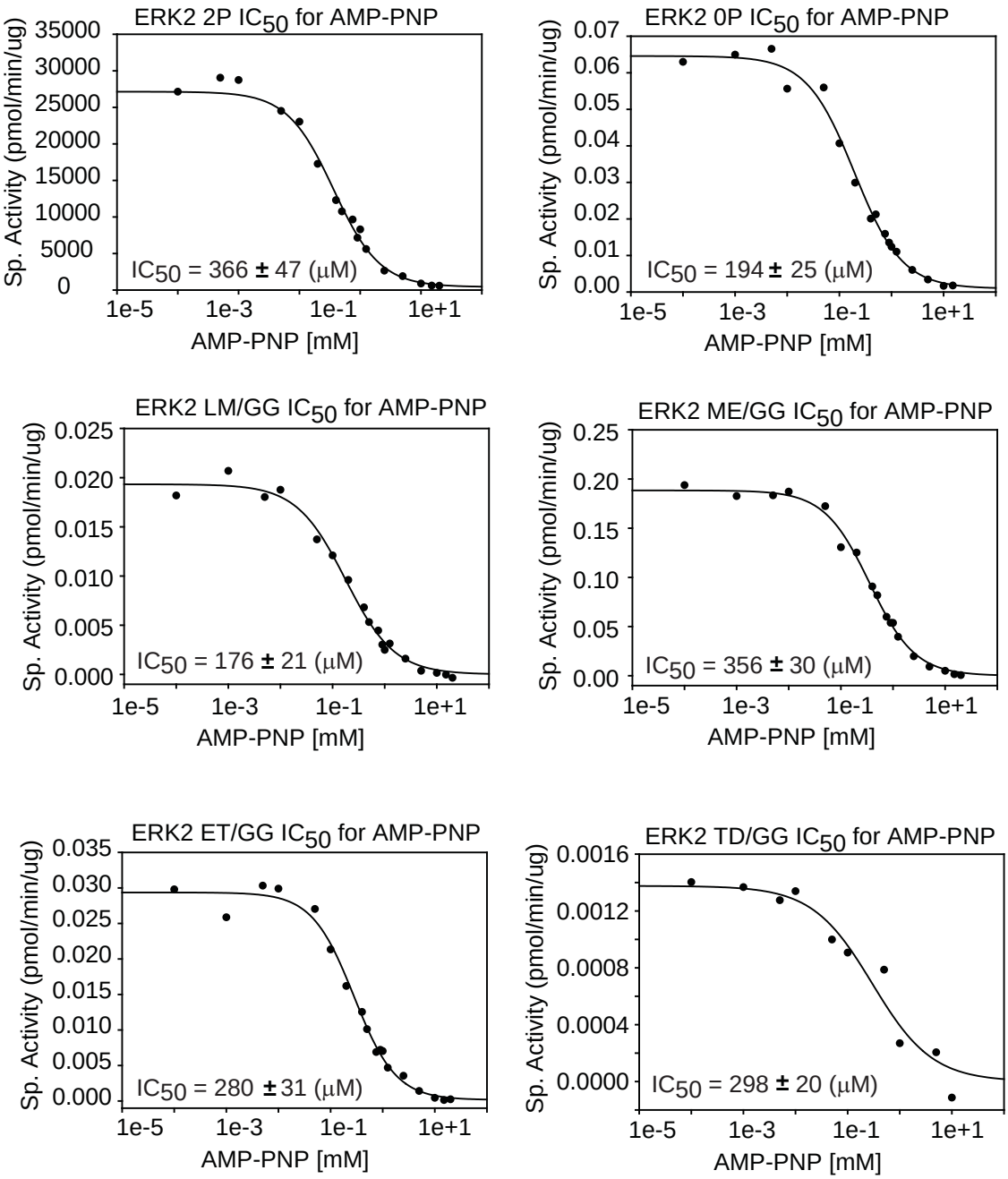

Figure 10: Specific activity and IC50 measurements for wild type and mutant forms of ERK2. Specific activity (pmol/min/mg) was measured in the presence of varying AMP-PNP concentrations as described in Materials and Methods. Curves were fit by non-linear least squares to equation (1). Fitted IC_{50} values and standard deviations are indicated for each protein.

affinity for AMP-PNP under the reaction conditions. However, the IC_{50} was comparable even for mutant LM/GG, which was surprising, given the absence of HX protection by AMP-PNP for this protein form (Figure 4). This suggested the potential for misinterpretation of the IC_{50} measurements.

I can explain these apparently contradictory results in the following way. Phosphorylated ERK2 shows a 60,000 fold rate enhancement over unphosphorylated ERK2 (Prowse & Lew, 2001), and previous studies from our lab have shown that diphosphorylated mutant LM/GG still maintains ~15-20% activity compared to 2P-ERK2 (Emrick et al., 2006). A trace amount of 2P-ERK2-LM/GG could have an activity which exceeds that of 0P-ERK2-LM/GG, so that the IC_{50} primarily reflects inhibition of the diphosphorylated enzyme. The HX and IC_{50} data would be consistent, if the binding affinity of AMP-PNP for unphosphorylated LM/GG protein were very low, but the affinity of AMP-PNP for diphosphorylated LM/GG were similar to that of wild-type ERK2. This is what is observed in p38α MAP kinase, where the K_d for ATP is 360 μM in 2P-p38α but 13.0 mM in 0P-p38α (Zhang et al. 2005). Taken together the IC_{50} results indicate similar affinity of AMP-PNP for all six ERK2 proteins, but I cannot be sure that the affinity measurements reflect unphosphorylated forms of each protein.

ITC experiments should provide more accurate measurements of AMP-PNP binding affinity, and confirm that my hypothesis regarding LM/GG is correct. These experiments are ongoing; to date I have successfully measured $K_d = 97 \pm 33$ μM for wild-type 0P-ERK2, in three experiments performed at 10 °C (Figure 11), which is comparable to IC_{50} estimates. Although the affinity is fairly weak and the C value is low, because the goal is to measure equilibrium binding constants without requiring

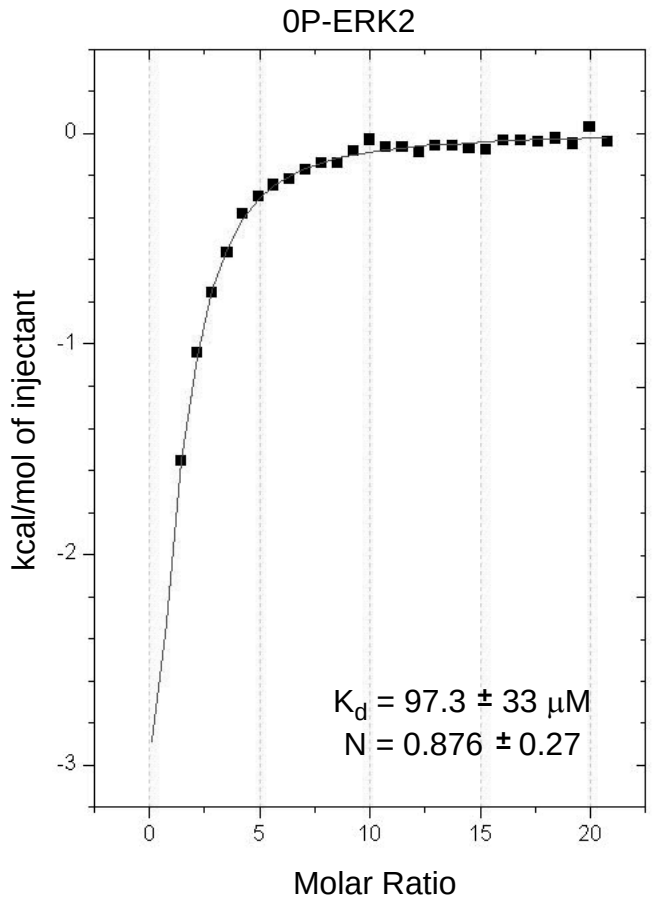

Figure 11: Equilibrium binding of AMP-PNP to 0P-ERK2. ITC was used to measure K_d and number of binding sites (N) for AMP-PNP binding to 0P-ERK2. Average values and standard deviations measured from n = 3 experiments.

characterization of thermodynamic parameters, the experimental conditions are adequate (Turnbull & Daranas, 2003). I plan to repeat these experiments for each mutant, in order to confirm that LM/GG shows reduced AMP-PNP binding affinity in its unphosphorylated form, while ME/GG, ET/GG, and TD/GG show AMP-PNP binding comparable to 0P-ERK2.

Does hinge flexibility control enzyme rate?

Lastly, I asked whether mutations which increased hinge flexibility and domain closure could promote catalytic activity. In other protein kinases, such as MAP kinase kinase 1 or protein kinase C, substituting phosphorylatable residues at the activation lip with negatively charged amino acids (Glu or Asp) often leads to partial activation by mimicking the effect of phosphorylation (e.g., Mansour et al., 1994; Orr & Newton, 1994). However, this has been unsuccessful for ERK2 (Zhang et al., 1995), where substituting Thr^{183} and/or Tyr^{185} to Asp or Glu had minimal effects on enzyme activation (Robbins et al., 1993; Zhang et al., 1995). However, I was curious to test whether acidic mutations at the activation lip would generate active enzyme when combined with mutations that enhanced hinge flexibility. Such a result might be observed if flexibility at the hinge and ion pairing interactions at the activation lip are both important for enzyme activation.

I engineered single or double mutations at Thr^{183} and Tyr^{185} to Asp, Glu, or Phe, producing the following sequences in place of TEY: EEY, DEY, TEE, TED, DED, EEE, EEF, and DEF. These eight activation lip mutations were then combined with wild-type and each of the four hinge mutations, to generate 43 different ERK2 mutants. In addition,

each activation lip mutant was generated in its diphosphorylated form by mutagenesis of a dual expression plasmid expressing ERK2 and constitutively active MAP kinase kinase 1 (Khokhlatchev et al., 1997). Each form was tested for specific activity, measured by the initial rate of phosphoryl transfer from [γ-^{32}P]ATP to MBP. Figure 12 shows the results of the kinase assays for all ERK2 proteins. The most active enzymes were the four single activation lip mutants which were generated from the dual expression plasmid, creating monophosphorylated forms of each enzyme; interestingly each showed significantly different activity. The combination hinge and activation lip mutations did not produce enzymes with exceedingly higher activity over wild-type unphosphorylated enzyme, however, both the ME/GG and ET/GG mutants showed specific activities 2-7 fold higher than unphosphorylated wild-type. Most hinge mutants showed specific activity similar to that of wild-type when combined with activation lip mutations (e.g., 0P-EEE *versus* ME-EEE). Only one combinatorial mutant, ME-DED, showed a 30-fold increase in specific activity compared to 0P-DED. This example suggests that in at least one case, increased flexibility at the hinge combined with negative charge substitutions at the lip augments specific activity. However, the effect is rather small, indicating that other events are needed for complete activation.

Multiple experiments show reproducible differences upon binding AMP-PNP

Multiple analyses were performed in order to accurately judge variability and determine the threshold for significance within and across datasets. In order to judge the level of variability within a dataset, multiple measurements were performed each at 0 seconds and 1 minute (Table 2). These measurements provide an assessment of

A

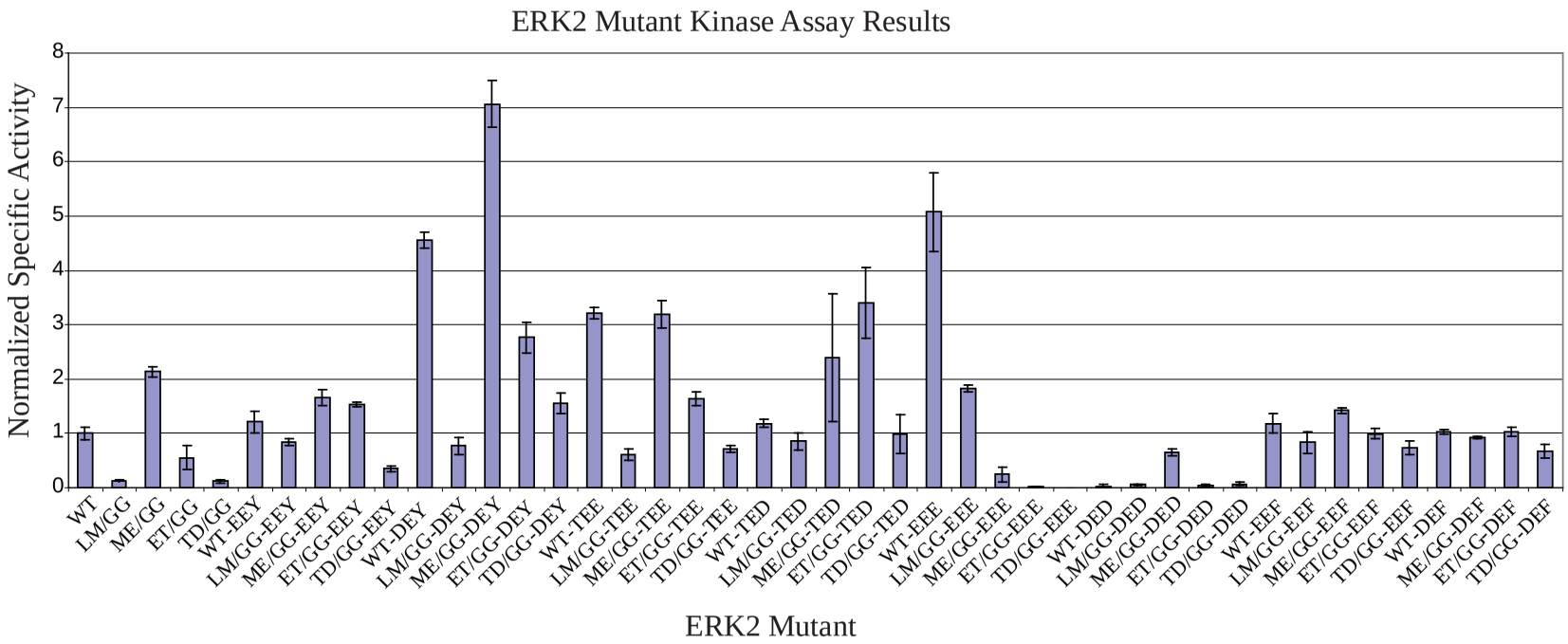
ERK2 Mutant Kinase Assay Results
Normalized Specific Activity
0
1
2
3
4
5
6
7
8
WT
LM/GG
ME/GG
ET/GG
TD/GG
WT-EEY
LM/GG-EEY
ME/GG-EEY
ET/GG-EEY
TD/GG-EEY
WT-DEY
LM/GG-DEY
ME/GG-DEY
ET/GG-DEY
TD/GG-DEY
WT-TEE
LM/GG-TEE
ME/GG-TEE
ET/GG-TEE
TD/GG-TEE
WT-TED
LM/GG-TED
ME/GG-TED
ET/GG-TED
TD/GG-TED
WT-EEE
LM/GG-EEE
ME/GG-EEE
ET/GG-EEE
TD/GG-EEE
WT-DED
LM/GG-DED
ME/GG-DED
ET/GG-DED
TD/GG-DED
WT-EEF
LM/GG-EEF
ME/GG-EEF
ET/GG-EEF
TD/GG-EEF
WT-DEF
ME/GG-DEF
ET/GG-DEF
TD/GG-DEF
ERK2 Mutant

B

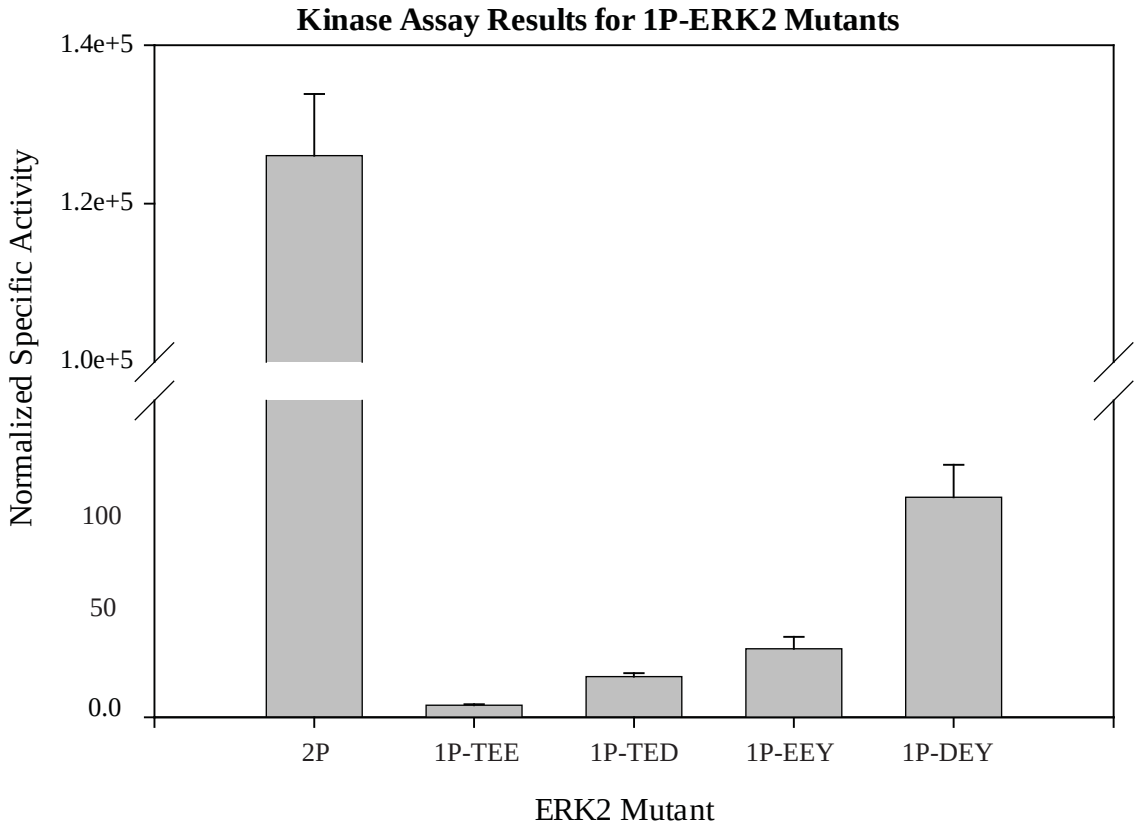

Figure 12: Activity measurements for ERK2 mutants. ERK2 mutants were prepared by combining various hinge mutations with substitutions of activation lip phosphorylation sites with Glu/Asp/Phe. **A.** Specific activities were measured for each mutant as described in Materials and Methods, and normalized by the specific activity of 0P-ERK2-WT. Each bar represents a different ERK2 mutant, labeled first by the hinge residues which were mutated to Gly-Gly, and second by change in activation lip sequence TEY to E, D, or F. The combined hinge and activation lip mutants show a modest increase in specific activity. **B.** Activation lip mutations (e.g.: EEY) were engineered into plasmids for dual expression of ERK2 and active mutant MKK1, in order to produce proteins phosphorylated at the activation lip (designated "1P"). The mutants with highest activity were those mono-phosphorylated at T^{183}.

variability in artifactual in-exchange as well as an early time point subject to highest error. Table 2 shows the average standard deviation of deuteration at 1 minute (0.12 Da) for every peptide from all six ERK2 proteins. This value has remained consistent over recent HX-MS experiments that have utilized the current instrumentation (Lee et al. 2005, Sours et al. 2008), and helped to determine the threshold of significance (0.5 Da) for these and previous studies.

It is well understood that experimental conditions such as pH, salt concentration, and temperature significantly alter the rate of exchange, thus, great care is given to minimize these factors. The results discussed in the hinge mutant study involve ERK2 proteins from six different preparations performed in parallel. To minimize variation due to buffer conditions, proteins are dialyzed into the identical buffer before being frozen in aliquots. The pH is also tested with and without AMP-PNP to verify that the presence of ligand does not alter the buffer conditions. Such controls improve confidence that the average standard deviation of 0.12 Da measures experimental variability and not systematic bias. This provides increased confidence in our significance threshold for HX changes responsive to AMP-PNP binding.

I also examined reproducibility and significance by comparing the results from three different HX-MS studies involving ERK2 binding to AMP-PNP, which were performed over the past decade by two different experimenters, with different HPLC systems and different ERK2 preps. The buffer conditions, concentrations, mass spectrometer parameters, and pH were matched as best as time and technology allow, but variations in column packing (e.g. theoretical plates, back pressure), amount of ice, temperature at quenching, temperature of buffer, etc… were undoubtedly present. I found

that the HX time courses were qualitatively similar but quantitatively different (Figure 13). The peptides where no differences were observed upon AMP-PNP binding showed comparable overall exchange with similar time courses between three experiments (Fig 13C). This showed that regions of ERK2 where HX was unaffected by AMP-PNP binding were reproducible between conditions and protein preps.

When I examined peptides where HX protection by nucleotide was observed, the time courses were qualitatively similar, and in all but one case (Fig 13B, Exp 2, C-terminal hinge) showed a similar level of protection upon AMP-PNP binding (Fig 13A and 13B). The Gly-rich loop showed good reproducibility, with approximately 1 Da HX protection between all three experiments and similar overall exchange. The C-terminal hinge showed similar protection (~0.5 Da) and similar overall exchange in two of three experiments. The DFG peptide, which is my metric for domain closure, showed similar protection in 2P-ERK2 between all three experiments with slight differences in overall exchange, while 0P-ERK2 showed a similar lack of protection and a slight variability in overall exchange between two experiments (the third could not be easily interpreted). The comparable protection between experiments which we observed between each binding study showed that AMP-PNP altered exchange consistently and reproducibly. The differences in overall exchange were likely the result of altered back-exchange between experimenters and experimental setup. Unfortunately the variability in overall exchange and other slight differences due to unavoidable changes made it difficult to directly compare fitted rate constants.

Overall the reproducibility analysis supports the models developed in my thesis, namely that AMP-PNP binding conveys protection from exchange in the N-terminal

A

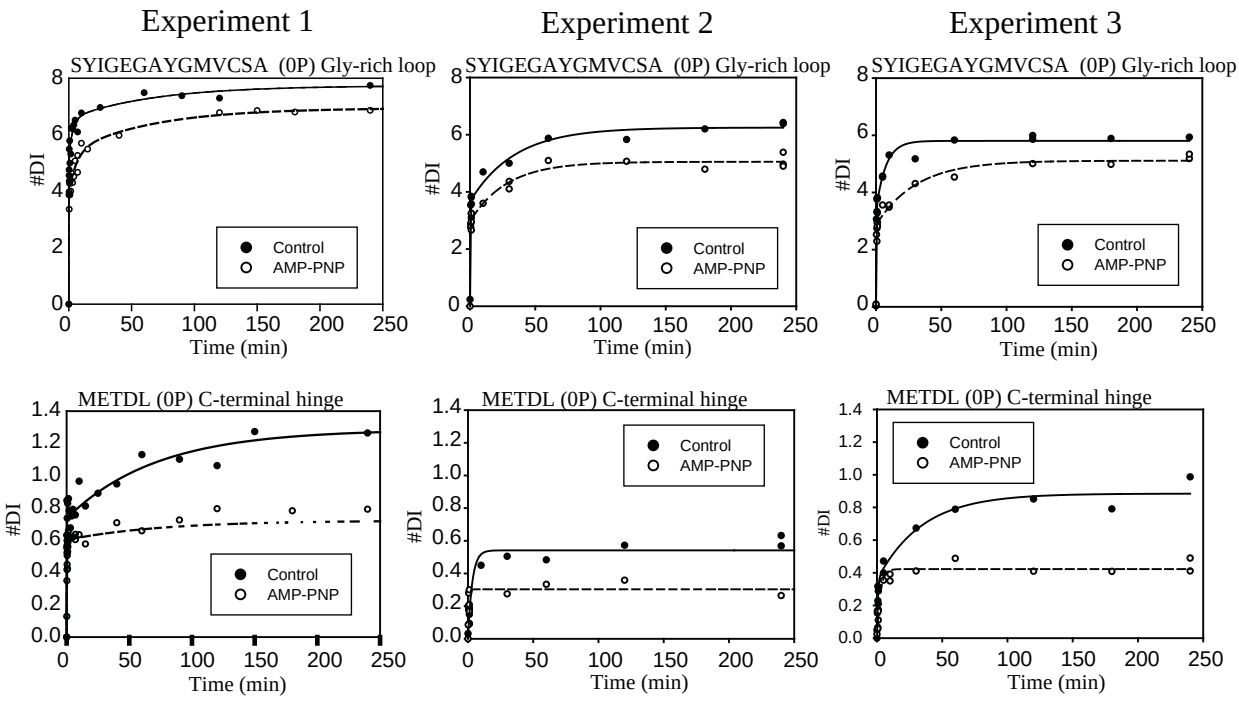
Experiment 1
Experiment 2
Experiment 3
SYIGEGAYGMVCSA (0P) Gly-rich loop
METDL (0P) C-terminal hinge
#DI
Time (min)
Control
AMP-PNP

B

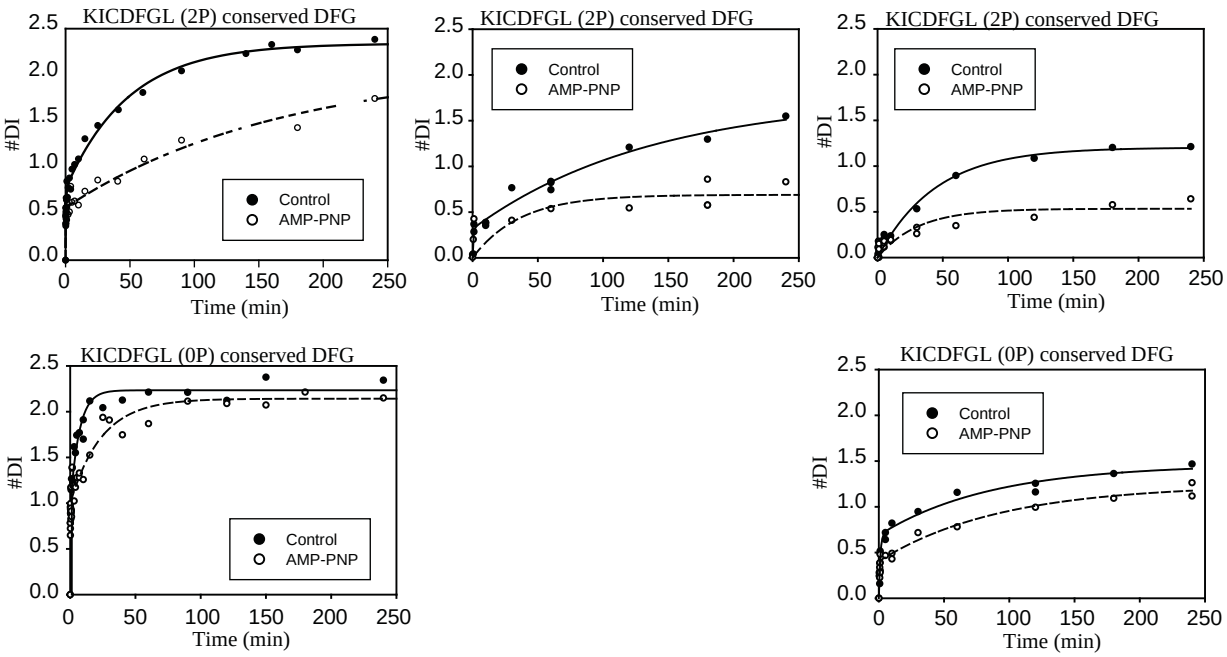
KICDFGL (2P) conserved DFG
KICDFGL (0P) conserved DFG
#DI
Time (min)
Control
AMP-PNP

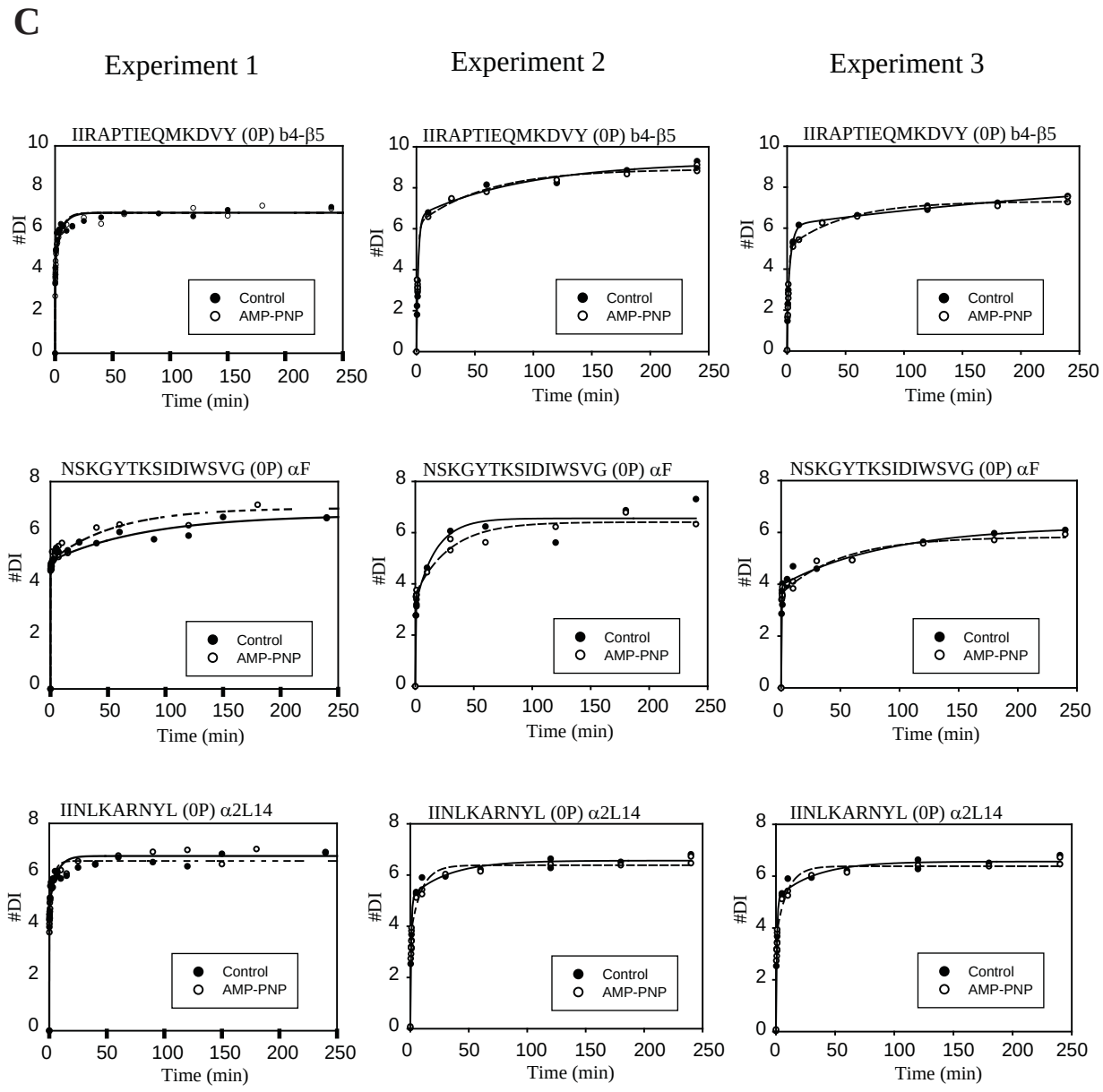

Figure 13: Peptide reproducibility between three different experiments involving ERK2 binding AMP-PNP. Three experiments were performed over 8 years (2002, 2008, 2010) with Experiment 1 performed by a different experimenter with different instrumentation (Lee et al. 2005) compared to Experiments 2 and 3. The Experiments are aligned vertically with each graph labeled with peptide sequence, 0P- or 2P-ERK2, and the region of the protein. **A.** Time courses for two peptides showing changes in exchange upon binding AMP-PNP. The time courses detail the Gly-rich loop region and the C-terminal hinge. **B.** Time courses for the conserved DFG peptide comparing 2P-ERK2 for all three experiments and 0P-ERK2 for Experiments 1 and 3. A clear pattern of protection in seen in the 2P time courses. **C.** Three peptides where no change in exchange was observed upon binding AMP-PNP.

domain and the hinge in both 0P- and 2P-ERK2, but conveys increased protection from exchange in the C-terminal domain of 2P-ERK2 consistent with changes in solution conformation equilibrium which allow 2P-ERK2 to adopt a closed conformation. A newly purchased Waters Synapt G2 mass spectrometer with 2D nanoacquity UPLC and an HDX module for refrigerated proteolysis and reversed phase chromatography should help to further minimize variabilities in buffer temperatures, columns, and back-exchange, and improve reproducibility between experiments.

DISCUSSION

Structural analysis has proven very informative in our understanding of kinase function and activation, and in the case of ERK2 it has been beneficial that proteins in both the inactive and active states have been crystallized. However, the observed structural differences may not completely explain the 60,000-fold rate enhancement upon activation by phosphorylation (Prowse & Lew, 2001). There is much evidence for interdomain closure as a necessary step in catalysis by protein kinases, such as PKA (Knighton et al., 1993; Karlsson et al., 1993; Zheng et al., 1993; Bossemeyer, 1994; Cox et al., 1994; Li et al., 2002; Akamine et al., 2003; Heller et al., 2004; Taylor et al., 2004; Taylor et al., 2005; Kim et al., 2005; Kim et al., 2006; Vigil et al., 2006; Cheng et al., 2009). However, such effects have not been obvious in ERK2, where both the active and inactive enzymes are in an “open” conformation. This may in part reflect distortions in the conformation of 2P-ERK2 by crystal packing interactions, where the C-terminus of one monomer forms an interface with the active site of another monomer (Canagarajah et

al., 1997; Zhang et al., 1995), which makes it difficult to determine whether the open conformation represents the solution structure or an artifact of crystallization.

HX-MS is able to monitor solution conformational mobility, which is more difficult to observe in crystal structures, and this is precisely why I used it in this study. To date, HX-MS studies from the Ahn lab have provided the only evidence for differences in solution conformation between 0P- and 2P-ERK2 (Lee et al., 2005). However, causality is not proven by the studies of Lee et al. (2005), so these experiments could be interpreted in more than one way. On one hand, our laboratory proposes that increased HX within the METDL sequence at the hinge upon phosphorylation reflects increased backbone flexibility, which in turn allows the kinase to bypass the constraint to interdomain interactions, allowing domain closure. On the other hand, it is conceivable that phosphorylation instead leads to interdomain closure, which in turn causes the observed enhancement of HX at the hinge. The results of my study now demonstrate that Gly-Gly mutations at the hinge, which should increase backbone flexibility, do appear to bypass the constraints to domain closure in 0P-ERK2, as measured by enhanced protection from HX at the DFG motif.

My HX results together with structural examinations argue that the substitution of Gly-Gly for ^{106}Met-Glu^{107} increases backbone flexibility at the hinge, as expected. Previous measurements of HX in peptides comprising the hinge region (^{101}IVQDL^{105}, ^{106}METDL^{110}, ^{101}IVQDLME^{110}) suggested that within peptide ^{101}IVQDL^{105}, HX occurs primarily at amide hydrogens corresponding to Asp^{104} and Leu105, with estimated k_{obs} ~ 0.03 min^{-1} and ~ 0.2 min^{-1}, respectively, and that within peptide ^{106}METDL^{110}, HX occurs at Glu^{107} and Leu^{110} with estimated k_{obs} ~ 1.7 min^{-1} and ~ 0.007 min^{-1}, respectively

(Resing et al., 1999). In addition, peptide ^{101}IVQDLME^{110} showed maximal deuteration that was 2 Da higher than in ^{101}IVQDL^{105}, consistent with fast exchange at Met^{106} and Glu^{107}, with estimated k_{obs} >20 min^{-1} and ~1.7 min^{-1}, respectively (Resing et al., 1999). My current results are consistent with previous findings. In 0P-ERK2, I observed maximal deuteration of 3.7 Da in ^{101}IVQDLMETDL^{110}, and maximal deuteration of 1.1 Da and 1.0 Da in ^{101}IVQDL^{105} and ^{106}METDL^{110}, respectively (Figure 8, Table 2). In mutant protein TD/GG, I observed maximal deuteration of 1.9 Da in peptide ^{105}LMEGGL^{110}, suggesting that the mutation yielded no further HX over that seen in wild-type ERK2. In contrast, in mutant protein ME/GG, the maximal deuteration was ~1.7 Da for ^{106}GGTDL^{110}, indicating that the mutation enhanced HX by nearly 1 Da over wild-type ERK2 in this region. Thus, the higher rate of hydrogen exchange in the ME/GG mutant is consistent with higher solvent accessibility and/or flexibility at this position.

The crystal structures show little difference in the hinge region between 0P- and 2P-ERK2, with respect to hydrogen bonding or distance to surface of amide hydrogens. The exception is Glu^{107}, whose amide hydrogen is partially occluded from solvent in 0P-ERK2, due to a rotation of the Glu^{107} side chain to form hydrogen bonding interactions between the side chain carboxyl group and the amide hydrogen (Figure 14A, Table 4). This leads to an increase in distance of the amide hydrogen to the surface of 1 Å (Table 5). However, in solution, the side chain of Glu^{107} should be able to rotate freely, and I would not expect there to be a variation in HX protection between 0P- and 2P-ERK2 due to this difference between the structures. Inspection of a surface representation comparing 0P-ERK2 to mutants where individual side chains had been removed and

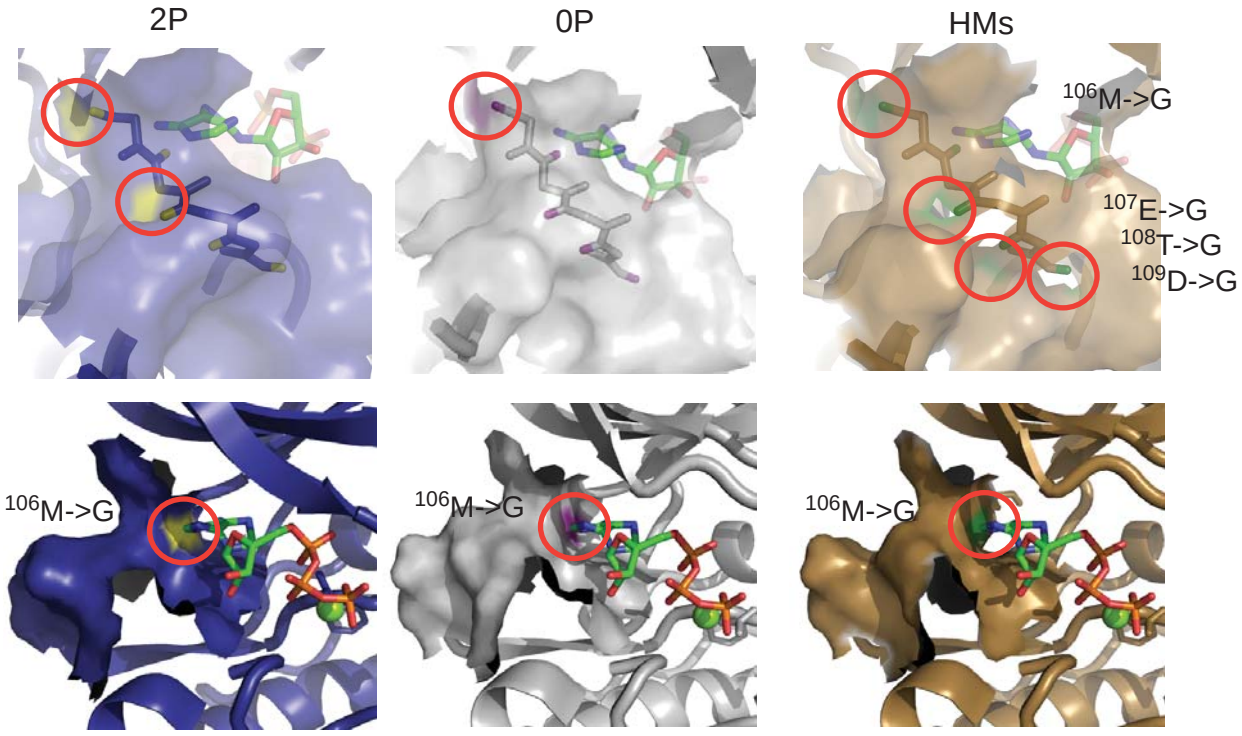

Figure 14: Removal of hinge side chains predict increased amide solvent accessibility. ERK2 structures showing residues at the hinge region. ATP is modeled in the active site and colored by atom [green (C), red (O), blue (N), orange (P), Mg (sphere)]. **A.** Top left: 2P-ERK2, showing the backbone in blue, solvent accessible amides in yellow. Top middle: 0P-ERK2, showing the backbone in grey, solvent accessible amides in purple. Top right: 0P-ERK2, showing hinge residue side chains removed upon mutation to Gly. Backbone is gold, solvent accessible amides are green. The mutated residues are highlighted in circles. Bottom left, middle and right: Structures are as indicated in top panels, but compared from a different angle. Residues in and surrounding the hinge (including αD residues ^{110}LYKL^{113} and β7 residues ^{154}LLNT^{157}) pack tightly as shown by the surface representation. 2P-ERK2 was drawn from PDB:2ERK (Canagarajah et al., 1997), 0P-ERK2 was drawn from PDB:1ERK (Zhang et al., 1994), and ATP coordinates were adapted from the ERK2 K52R structure (PDB:1GOL, Robinson et al., 1996). Images were created using PyMol v.0.99.

Table 4: Hydrogen bonds predicted for the C-terminal hinge peptide of ERK2

0P Hydrogen bonds predicted for hinge residues

Donor Atom #	Donor Atom	Donor Residue	Acceptor Atom #	Acceptor Atom	Acceptor Residue	Distance	Angle
107	GLU	H	107	GLU	OE2	2	132.6
108	THR	H	155	LEU	O	2.36	145.7
108	THR	HG1	109	ASP	O	2.85	161.01
109	ASP	H	108	THR	OG1	1.96	125.5
110	LEU	H	153	LEU	O	1.92	153.5
112	LYS	H	109	ASP	OD1	1.95	163.16
112	LYS	HO	109	ASP	OD1	1.95	157.92
113	LEU	H	109	ASP	O	2.15	176.4
114	LEU	H	110	LEU	O	1.83	154.8
114	LEU	H	110	LEU	O	1.77	159.9
155	LEU	H	108	THR	O	1.91	161.28
157	THR	H	107	GLU	OE2	3.05	124.9

2P Hydrogen bonds predicted for hinge residues

Donor Atom #	Donor Atom	Donor Residue	Acceptor Atom #	Acceptor Atom	Acceptor Residue	Distance	Angle
108	THR	H	155	LEU	O	1.92	173.7
109	ASP	H	108	THR	OG1	2.01	123.2
110	LEU	H	150	PRO	O	2.76	124.1
110	LEU	H	153	LEU	O	2.12	140.9
111	TYR	H	109	ASP	OD1	2.46	121.1
112	LYS	H	109	ASP	OD1	1.94	162
113	LEU	H	109	ASP	O	2.1	148.5
114	LEU	H	110	LEU	O	1.98	178
155	LEU	H	108	THR	O	1.74	161.6

Notes

Predicted hydrogen bonds for residues ^{106}METDL^{110} of 0P- & 2P-ERK2 based on crystal structures.
PDB numbering, atom designation, and residue are listed for H-bond donor & acceptor
H-bond distance and angle were calculated with maximum distance 3.0 Å and angle range 120-180°.

Table 5: Amide distance to surface measurements for the hinge and DFG regions of 0P- & 2P-ERK2

Hinge Peptide

Residue	Residue #	2P	0P
Ile	101	5.09	5.44
Val	102	5.65	7.89
Gln	103	3.63	5.77
Asp	104	3.33	4.49
Leu	105	1.20	2.42
Met	106	1.20	3.74
Glu	107	1.20	2.61
Thr	108	3.08	2.69
Asp	109	2.80	2.98
Leu	110	4.93	6.30

DFG Peptide

Residue	Residue #	2P	0P
Lys	162	4.47	3.33
Ile	163	5.55	2.78
Cys	164	4.88	4.82
Asp	165	2.47	4.26
Phe	166	2.82	4.53
Gly	167	1.20	4.90
Leu	168	1.20	4.07

Notes

Table lists Residue, Residue Number and the estimated Distance to Surface (Å) for 0P- & 2P-ERK2

residues changed to glycine showed full exposure of the Glu^{107} amide hydrogen, and partial exposure of amide hydrogens corresponding to Thr^{108} and Asp^{109} (Figure 14A). To the extent that the amide hydrogen for both Glu^{107} in wild-type ERK2 and Gly^{107} in mutant ME/GG are solvent exposed, I would conclude that the increase in HX by ~1 Da observed in the mutant is best explained by enhanced backbone flexibility upon Gly-Gly substitutions at positions 106 and 107. On the other hand, because mutant TD/GG shows little change in total in-exchange compared to wild-type ERK2, there is no evidence that Gly-Gly substitutions at positions 108 and 109 affect backbone conformational mobility.

The focus of my study was the conserved DFG motif within the C-terminal domain (^{162}KICDFGL^{168}), where HX protection observed upon AMP-PNP binding reflects interdomain closure. The environment around the KICDFGL sequence is very similar between the 0P- and 2P-ERK2 structures (Figure 15), with the exception of Asp^{165}, which between the two states is rotated around the Cα-Cβ bond. The 0P-ERK2 structure shows a hydrogen bond formed between the carboxyl side chain of Asp^{165} and the backbone amide of Gly^{165}, which is absent in the 2P-ERK2 structure (Table 6). Asp^{165} is known to coordinate with two Mg^{2+} ions at the active site, which in turn coordinate with ATP phosphoryl groups, and the Asp^{165} in 2P-ERK2 is closer to Mg^{2+} and the phosphoryl groups than in 0P-ERK2. However, I believe that this rotamer is not fixed in 0P-ERK2, given that modeling shows it free to rotate. This is supported by measurements of HX in this region, which in 0P-ERK2 is higher than that seen in 2P-ERK2, in the absence of AMP-PNP (Figure 9).

As previously observed by Lee et al. (2005), I found that AMP-PNP binding to 0P-ERK2 showed less protection from HX within the KICDFGL sequence than 2P-

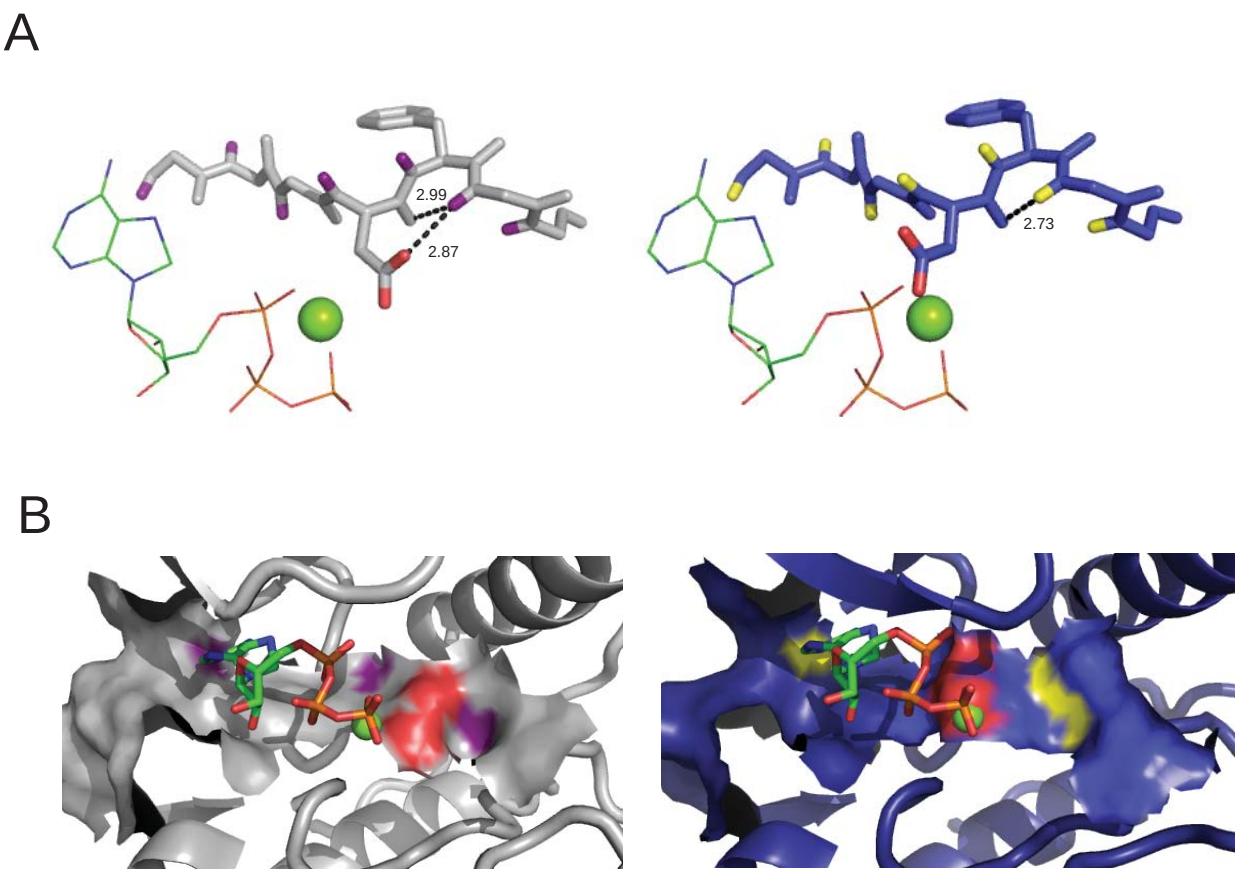

Figure 15: Structural models of the DFG region. A. Structural models of peptide ^{162}KICDFGL^{168} containing the DFG region in (left, grey) 0P- and (right, blue) 2P-ERK2, showing hydrogen bonding associated with Asp^{165}. 0P- and 2P-ERK2 show rotamers corresponding to Asp^{165} which different in proximity to ATP and Mg^{2+}, but we believe these are probably not fixed in solution. **B.** Structures of the active site showing the surfaces of the hinge (^{105}METDL^{110}) and DFG (^{162}KICDFGL^{168}) regions. PDB coordinates and colors are as described in Figure 13.

Table 6: Hydrogen bonds predicted for the DFG peptide residues

0P Hydrogen bonds predicted for DFG peptide residues

Donor Atom #	Donor Atom	Donor Residue	Acceptor Atom #	Acceptor Atom	Acceptor Residue	Distance	Angle
82	ILE	H	163	ILE	O	1.94	147.6
154	LEU	H	162	LYS	O	1.91	157.2
162	LYS	H	154	LEU	O	2.05	144.8
163	ILE	H	80	ASN	O	1.85	159.4
164	CYS	H	152	ASN	O	2.06	160.7
166	PHE	H	69	GLU	OE2	2.34	166.6
167	GLY	H	165	ASP	O	2.99	124.7
167	GLY	H	165	ASP	OD1	2.89	159.4
169	ALA	H	166	PHE	O	2.5	150.1

2P Hydrogen bonds predicted for DFG peptide residues

Donor Atom #	Donor Atom	Donor Residue	Acceptor Atom #	Acceptor Atom	Acceptor Residue	Distance	Angle
82	ILE	H	163	ILE	O	1.86	162.7
154	LEU	H	162	LYS	O	2	140.6
162	LYS	H	154	LEU	O	2	145.7
163	ILE	H	80	ASN	O	1.9	170.2
164	CYS	H	152	ASN	O	2.16	169.4
166	PHE	H	69	GLU	OE2	2.19	142.1
167	GLY	H	165	ASP	O	2.72	126.4
169	ALA	H	166	PHE	O	2.18	152.4

Notes

Predicted hydrogen bonds for residues ^{162}KICDFGL^{168} of 0P- & 2P-ERK2 based on crystal structures.
PDB numbering, atom designation, & residue are listed for H-bond donor & acceptor
H-bond distance and angle were calculated with maximum distance 3.0 Å and angle range 120-180°.

ERK2 (Figure 9). Because the KICDFGL peptide appeared in all mutant forms of ERK2, its extent of HX in 2P-ERK2 and 0P-ERK2 can be used to mark the upper and lower range of HX protection upon nucleotide binding. In mutant ME/GG, the extent of HX in this peptide resembles that of 2P-ERK2. In mutant TD/GG, its extent of HX resembles that of 0P-ERK2. In mutant ET/GG, its extent of HX is intermediate between these extremes. Thus, the mutation ME/GG, which appears to enhance backbone flexibility at the hinge to the greatest extent, is the mutation which yields the highest HX protection in the DFG region and evidence for interdomain closure. The HX protection patterns observed in wild-type and mutant ERK2 are summarized in Figure 16A.

I conclude that increased hinge flexibility underlies the mechanism allowing domain closure upon ERK2 phosphorylation, consistent with a role for regulated conformational mobility in controlling kinase activation. Figure 16B illustrates this model, presenting the hypotheses that hinge flexibility is needed for domain closure, and that the increase in conformational mobility in the hinge region upon diphosphorylation of ERK2 might be part of the mechanism for bypassing the constraint to closure in 0P-ERK2.

Further experiments are needed to corroborate this mechanism. A key assumption I have made thus far is that AMP-PNP binding is comparable between wild-type and mutant ERK2 forms. Lee et al. (2005) showed comparable K_d for AMP-PNP binding between 0P-ERK2 and 2P-ERK2, using isothermal titration calorimetry (ITC). However, my attempts to perform similar measurements on mutant ERK2 have failed, due to obstacles in maintaining a constant baseline and problems due to spurious heat gain and loss. An important difference between my experiments and those of Lee et al. (2005)

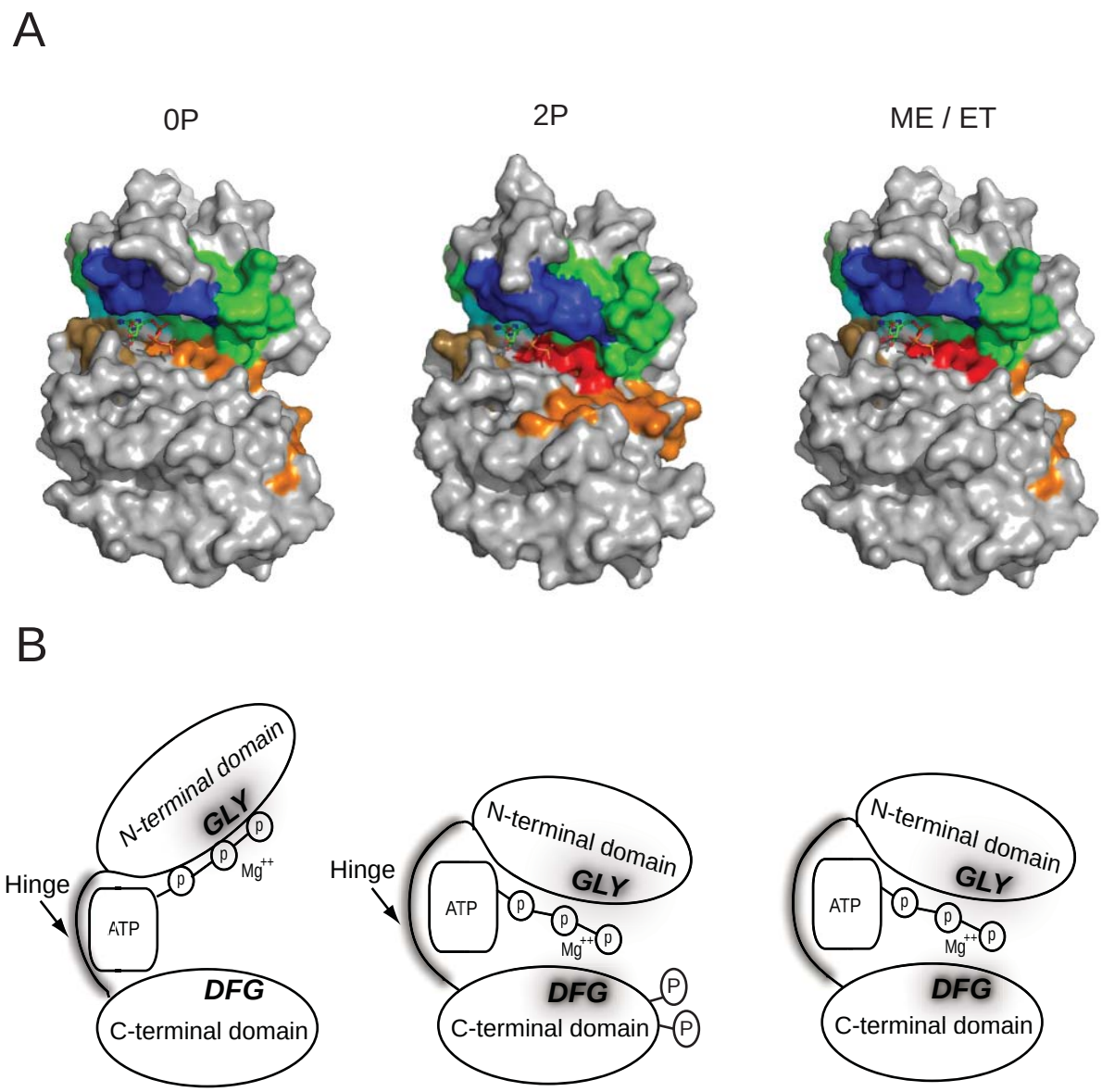

Figure 16: A model to explain the importance of hinge flexibility in domain closure. **A.** Surface representations of 0P-ERK2, 2P-ERK2, and mutants ME/GG and ET/GG. Shown are peptides that reveal HX protection upon AMP-PNP binding, colored as follows: blue - Gly-rich loop; green - αC; cyan - β5/hinge; brown - hinge/αD; red - DFG region; orange - activation lip. The increased protection in the DFG region of the mutants ME/GG and ET/GG compared to 0P-ERK2 is similar to that seen in 2P-ERK2, indicating that mutations which increase hinge flexibility promote domain closure. **B.** Cartoon schematics summarizing open and closed states predicted for each ERK2 form upon AMP-PNP binding.

was our use of different ITC instruments, where the older instrument used in previous studies had a sample cell which was 7 times larger than the current newer instrument. Thus, while the newer instrument is more sensitive, this advantage may be offset by the higher signal to noise measurements allowed by the larger cell in prior experiments. I am currently conducting purification strategies to scale up production of ERK2 proteins, in order to repeat the experiments at higher concentrations in order to obtain higher signal to noise with the new ITC instrument.

Finally, I considered the potential effects of hinge flexibility on kinase activity. Ideally, the role of hinge flexibility on activation must be tested directly, by asking whether changes in flexibility impact kinase activity or activation. While negative charge substitutions at the activation lip sometimes convey higher activity over basal, as in PKC (Orr & Newton 1994), the same experiment in ERK2 produced little activation (Zhang et al., 1995). Mutations at ^{183}T to Glu/Asp conveyed no increase in activity but led to a slight increase in crystallographic B-factors for the activation lip. The mutation of ^{185}Y to Glu/Asp also failed to activate, but led to a significant loss of electron density and an increase in B-factors to >50 Å^2, reflecting significant disorder. Lastly, the double mutant, ^{183}T / ^{185}Y to Glu-Xxx-Glu, had the highest degree of disorder, and resulted in no increased activity. This was interpreted as the mutations were unable to stabilize the low activity 0P form, due to high conformational flexibility of the activation lip, but were also unable to promote catalysis because the mutations were unable to form the ion pair interactions predicted from homology modeling. While no enzymatic variables were measured, other than specific activity, one might predict these mutations would decrease V_{max}, increase K_m for substrate, and have little effect or slightly increase K_m for ATP.

Nonetheless, I engineered hinge mutations together with mutations which incorporated negative charge at the activation lip into the same ERK2 proteins, in order to ask whether these mutations could in combination elevate activity. The results were inconclusive, in that specific activities were higher in some combinations, but only by 2-3 fold, which was insignificant compared to the >1,000 fold increase in rate upon diphosphorylation. If the combined mutants had synergized in elevating activity, it would have indicated that hinge flexibility and interdomain closure indeed contribute to activation. An experiment I have yet to perform is to combine hinge mutations with single phosphorylation events at the activation lip. This can be tested by substituting the wild type TEY lip sequence with TEF or AEY sequences, combining these with hinge mutations, and phosphorylating the combinatorial mutants with active MAP kinase kinase 1. Conceivably, negative charge mutations replacing TEY may not be able to stabilize the conformation of the lip enough to enhance catalysis under conditions where domain closure is favored by the hinge mutations. This remains an important goal for the future.

CHAPTER 4

Future Directions

My HX-MS experiments on p38α MAP kinase and ERK2 highlight the regulation of conformational mobility in protein kinases and changes occurring between inactive, unphosphorylated, and active, phosphorylated forms. My study on p38α MAP kinase demonstrated key differences in activation-dependent alterations in HX between p38α MAP kinases and ERK2, despite their similarities in overall deuteration. This suggests that, although MAP kinases are closely related with respect to primary sequence and tertiary structure, they have distinct mechanisms for dynamical control of enzyme function. My findings on ERK2 indicated that activation-dependent alterations in HX provide meaningful contributions to the mechanism of catalytic activation, by controlling hinge flexibility and interdomain closure. A third study, carried out under my supervision by undergraduate honors student, Adam Ring, and included as Appendix 2, showed that ERK1, a MAP kinase which shares 90% sequence identity with ERK2, also shares similarities in overall deuteration, consistent with their similar tertiary structures (Ring et al., 2011). However, the alterations seen in HX at the hinge region in ERK2 were not observed in ERK1, suggesting that the two enzymes differ with respect to their

regulation of hinge mobility and interdomain closure. Upon AMP-PNP binding, HX-MS measurements in the DFG region revealed domain closure in both inactive and active forms of ERK1. The results suggest that like p38α MAPK, ERK1 which is even more closely related to ERK2 in primary sequence and tertiary structure, utilizes distinct mechanisms for controlling enzyme function through interdomain interactions.

Future work will require further studies aimed at understanding how regulated interdomain closure can be linked to hinge flexibility. Further studies are needed to validate domain closure using alternative approaches. While the method of monitoring protection from HX in the DFG region is so far consistent with my model, I still lack direct evidence that the closed conformation is truly achieved. Some approaches that could be used to document the closed conformation in 2P-ERK2 and hinge mutants include measurements of domain movements by small angle X-ray scattering (SAXS), residual dipolar couplings measured by NMR, and X-ray crystallography.

Use of small angle X-ray scattering (SAXS) to document interdomain closure has been previously done on cAMP-dependent protein kinase (PKA). Olah et al. (1993) examined the PKA catalytic subunit in the presence and absence of PKI inhibitor peptide, and documented interdomain movement by a decrease in radius of gyration (Rg) of 2 Å and 11 Å decrease in d_{max} in the bound form. This fit an overall contraction of the enzyme with inhibitor bound, upon modeling hinge movement between the two domains of the kinase. We note that in PKA, the hinge residue sequence Gly-Gly is that which aligns with ^{106}ME^{107} in ERK2. Thus, PKA contains residues that would promote flexibility at the pivot point between the two domains, and our ERK2 ME/GG mutant

mimics this sequence. Thus, it may not be surprising that PKA is able to adopt a closed conformation without activation lip phosphorylation.

Advanced NMR methods can provide distance and angle information from ^{1}H-^{15}N and ^{1}H-^{13}C residual dipolar couplings (RDC) (Mittermaier & Kay, 2009; Neudecker et al., 2009; Ruschak & Kay, 2010). RDCs complement distance information from NOE, because the couplings have both a distance and *angle* dependence for the two involved nuclei. Thus, measurement of RDC for two nuclei at a known fixed distance (e.g. covalently bonded ^{1}H-^{15}N and ^{1}H-^{13}C) gives information about the angle of the internuclear vector relative to the applied magnetic field. Therefore RDCs can give angular information on ^{1}H-^{15}N and ^{1}H-^{13}C bonds in the molecule, and protein solution structures can be generated from information about RDC constraints. Our lab in collaboration with Arthur Pardi's lab are comparing 0P- and 2P- forms of U-[^{2}H,^{15}N], ILV ^{1}H-^{13}C methyl-labeled ERK2 using NMR relaxation experiments (mainly Carr–Purcell–Meiboom–Gill (CPMG) T_2 and/or $T_{1\rho}$) to monitor Ile, Leu and Val side chain motions that correspond to conformational exchange processes with μs-ms timescales. I am not involved in these studies, but conceivably RDC measurements might be used to probe changes in interdomain orientation as a future goal.

A final approach might involve crystallization of the ERK2 hinge mutants in the presence or absence of nucleotide, and examination of whether certain mutants are able to adopt a closed conformation. This would provide a readout of the conformational state corresponding to the hinge and DFG with atomic resolution, and resolve the ambiguity in interpreting the HX protection. These experiments should be feasible, given that crystallization conditions have been found for several wild-type and mutant forms of

ERK2, and in my opinion this may be the most feasible of all the possibilities listed above for proving that hinge flexibility allows ERK2 to adopt the closed conformation.

Future studies are also needed to understand how the hinge backbone responds to phosphorylation at the activation lip. The hinge is far from the closest region at which conformational differences can be observed upon phosphorylation, therefore, somehow information about conformational mobility must be transmitted over long distances in the enzyme. Here, further comparisons of ERK1 and ERK2 may provide an answer. The two enzymes are 90% identical by sequence and greatly overlapping in structure, but ERK1 appears to have a more flexible hinge which allows domain closure, even in its unphosphorylated, inactive state. Therefore, the mechanism that constrains domain closure in 0P-ERK2 might be found in the sequence and structural variations between these enzymes. One way to approach this problem is to align the sequences and create chimeras that swap the 37 amino acids which differ between the enzymes. For example, by substituting residues in ERK2 with those unique to ERK1, we might be able to bypass the constraint to closure in 0P-ERK2. Residues may be swapped one by one, or multiple residues may be swapped in various combinations by designing full length cDNAs that can be synthesized by contract. In addition, residues in ERK1 can be substituted for those in ERK2, in order to see whether these mutations now confer constraints to closure in ERK1. Effects on hinge flexiblity can be monitored by HX rate measurements, and interdomain closure can be monitored by HX protection in the DFG region. Other assays for domain closure, found in studies outlined above, may be used to monitor the closed conformation.

I expect that differences in structure and sequence will account for differences in regulated conformational mobility observed between ERK1 and ERK2, measured by HXMS. The regions in ERK1/2 that are most relevant to domain closure are probably localized near the hinge, and this will be the region to initially prioritize. For example, comparisons between ERK1 and 2 suggest different packing interactions in the hinge region due to the substitution of Leu^{155} in ERK2 by Ile^{174} in ERK1. Leu has helical propensity, while Ile favors β-sheets due to steric constraints in the side chain (Steven Mayo, personal communication), therefore the residue difference may alter flexibility in a manner that depends on the backbone torsion angles. Even minor changes in packing interactions by Leu *vs* Ile might account for the constrained flexibility in ERK2 not seen in ERK1. Other critical residues may be ERK2-N85 in place of ERK1-R104, which disrupts a salt bridge with D104/D123 near the hinge, or ERK1-P35 in place of ERK2-V16 which may disrupt H-bonds that prevent closure of the ATP loop in ERK2. By systematically testing these and other mutants, and assaying each for interdomain closure using methods described in my thesis, we may be able to understand what aspects of protein architecture constrain domain closure in ERK2, and ultimately trace the relevant pathway in ERK2 that allows activation lip phosphorylation to enhance hinge flexibility and releases the constraint to domain closure.

REFERENCES

Akamine, P., Madhusudan, Wu, J., Xuong, N., Ten Eyck, L. F. & Taylor, S. S. (2003) Dynamic features of cAMP-dependent protein kinase revealed by apoenzyme crystal structure *J. Mol. Biol.* 327: 159–171.

Alverdi, V., Mazon, H., Versluis, C., Hemrika, W., Esposito, G., van den Heuvel., R., Scholten, A. & Heck, A.J. (2007) cGMP binding prepares PKG for substrate binding by disclosing the C-terminal domain. *J. Mol. Biol.* 375: 1380-1393.

Arrington, C. B., Teesch, L. M. & Robertson, A. D. (1999) Defining protein ensembles with native-state NH exchange: kinetics of interconversion and cooperative units from combined NMR and MS analysis. *J. Mol. Biol.* 285: 1265-1275.

Arrington, C. B. & Robertson, A. D. (2000a) Microsecond to minute dynamics revealed by EX1-type hydrogen exchange at nearly every backbone hydrogen bond in a native protein. *J. Mol. Biol.* 296: 1307-1317.

Arrington, C. B. & Robertson, A. D. (2000b) Correlated motions in native proteins from MS analysis of NH exchange: evidence for a manifold of unfolding reactions in ovomucoid third domain. *J. Mol. Biol.* 300: 221-232.

Avitzour, M., Diskin, R., Raboy, B., Askari, N., Engelberg, D. & Livnah, O. (2007) Intrinsically active variants of all human p38 isoforms. *FEBS Journal* 274: 963-975.

Bellon, S., Fitzgibbon, M. J., Fox, T., Hsiao, H. M. & Wilson, K. P. (1999) The structure of phosphorylated p38 gamma is monomeric and reveals a conserved activation-loop conformation. *Structure* 7: 1057-1065.

Bossemeyer, D. (1994) the glycine-rich sequences of protein kinases: a multifunctional element. *Trends in Biochem. Sci.* 19: 201-205.

Briggs, M. S. & Roder, H. (1992) Early hydrogen-bonding events in the folding reaction of ubiquitin. *Proc. Natl. Acad. Sci. USA.* 89: 2017-2021.

Busenlehner, L.S. & Armstrong, R.N. (2005) Insights into enzyme structure and dynamics elucidated by amide H/D exchange mass spectrometry. *Arch. Biochem. Biophys.* 433: 34-46.

Canagarajah, B. J., Khokhlatchev, A., Cobb, M. H. & Goldsmith, E. J. (1997) Activation mechanism of the MAP kinase ERK2 by dual phosphorylation. *Cell* 90: 859-869.

Chang, C. I., Xu, B. E., Akella, R., Cobb, M. H. & Goldsmith, E. J. (2002) Crystal structure of MAP kinase p38 complexed to the docking sites on its nuclear substrate MEF2A and activator MKK3b. *Mol. Cell* 9: 1241-124.

Chen, S., Brier, S., Smithgall, T. E. & Engen, J. R. (2007) The Abl SH2-kinase linker naturally adopts a conformation competent for SH3 domain binding. *Protein Sci.* 16: 572-581.

Chen, S., Dumitrescu, T. P., Smithgall, T. E. & Engen, J. R. (2008a) Abl N-terminal Cap stabilization of SH3 domain dynamics. *Biochemistry* 47: 5795–5803.

Chen, S., O'Reilly, L. P., Smithgall, T. E. & Engen, J. R. (2008b) Tyrosine Phosphorylation in the SH3 Domain Disrupts Negative Regulatory Interactions within the c-Abl Kinase Core. *J. Mol. Biol*. 383: 414–423.

Cheng, Y. and Prusoff, W. H. (1973) Relationship between the inhibition constant (K_i) and the concentration of inhibitor which causes 50 per cent inhibition (I_{50}) of an enzymatic reaction. *Biochem. Pharmacol.* 22: 3099-3108.

Cheng, C. Y., Yang, J., Taylor, S. S. & Blumenthal, D. K. (2009) Sensing domain dynamics in protein kinase A-I{alpha} complexes by solution X-ray scattering. *J. Biol. Chem.* 284: 35916-35925.

Cox, S., Radio-Andzelm, E. & Taylor, S. S. (1994) Domain movements in protein kinases. *Curr. Opin. Struc. Biol.* 4: 893-901.

Cravello, L., Lascoux, D. & Forest, E. (2003) Use of different proteases working in acidic conditions to improve sequence coverage and resolution in hydrogen/deuterium exchange of large proteins. *Rapid Commun. Mass Spectrom.* 17: 2387-2393.

Dharmasiri, K. & Smith, D. L. (1996) Mass spectrometric determination of isotopic exchange rates of amide hydrogens located on the surfaces of proteins. *Anal. Chem.* 68: 2340-2344.

Diskin, R. Askari, N., Capone, R., Engelberg, D. & Livnah, O. (2004) Active mutants of the human p38a mitogen-activated protein kinase. *J. Biol. Chem*. 279: 47040-47049.

Diskin, R., Lebendiker, M., Engelberg, D. & Livnah, O. (2007) Structures of p38alpha active mutants reveal conformational changes in the L16 loop that induce autophosphorylation and activation. *J. Mol. Biol.* 365: 66-76.

Doza, Y. N., Cuenda, A., Thomas, G. M., Cohen, P. & Nebreda, A. R. (1995) Activation of the MAP kinase homologue RK requires the phosphorylation of Thr-180 and Tyr-182 and both residues are phosphorylated in chemically stresses KB cells. *FEBS Lett.* 364: 223-228.

Englander, S. W. (2006) Hydrogen exchange and mass spectrometry: A historical perspective. *J Am. Soc. Mass Spectrom.* 17: 1481-1489.

Englander, S.W. & Mayne, L. (1992) Protein folding studied using hydrogen-exchange labeling and two-dimensional NMR. *Annu. Rev. Biophys. Biomol. Struct.* 21:243-65.

Engel, K., Kotlyarov, A. & Gaestel, M. (1998) Leptomycin B-sensitive nuclear export of MAPKAP kinase 2 is regulated by phosphorylation. *EMBO J.* 17: 3363-3371.

Emrick, M. A., Lee, T. Starkey, P. J., Mumby, M. C., Resing, K. A., & Ahn, N. G. (2006) The gatekeeper residue controls autoactivation of ERK2 via a pathway of intramolecular connectivity. *Proc. Natl. Acad. Sci. USA.* 103(48): 18101-18106.

Ferraro, D. M., Lazo, N. D., & Robertson, A. D. (2004) EX1 hydrogen exchange and protein folding. *Biochemistry* 43: 587-594.

Ferguson, P.L. & Konermann, L. (2008) Nonuniform isotope patterns produced by collision-induced dissociation of homogeneously labeled ubiquitin: implications for spatially resolved hydrogen/deuterium exchange ESI-MS studies. *Anal. Chem.* 80: 4078-4086.

Fox, T., Fitzgibbon, M.J., Fleming, M.A., Hsiao, H.M., Brummel, C.L. & Su, M. S. (1999) Kinetic mechanism and ATP binding site reactivity of p38γ MAP kinase. *FEBS Letters* 461: 323-328.

Frantz, B., Klatt, T., Pang, M., Parsons, J., Rolando, A., Williams, H., Tocci, M.J., O'Keefe, S.J. & O'Neill, E.A. (1998) The activation state of p38 mitogen-activated protein kinase

determines the efficiency of ATP competition for pyridinylimidazole inhibitor binding. *Biochemistry* 37: 13846-13853.

Ge, B., Gram, H., DiPadova, F., Huang, B., New, L., Ulevitch, R. J., Luo, Y. & Han, J. (2002) MAPKK-independent activation of p38alpha mediated by TAB1-dependent autophosphorylation pf p38alpha. *Science* 295: 1291-1294.

Goldsmith, E. J., Cobb, M. H. & Chang, C. I. (2004) Structure of MAPKs. *Methods Mol. Biol.* 250: 127-144.

Haystead, T.A., Dent, P., Wu, J., Haystead, C.M. & Sturgill, T.W. (1992) Ordered phosphorylation of p42mapk by MAP kinase kinase. *FEBS Lett.* 306: 17-22.

Hamuro, Y., Wong, L., Shaffer, J., Kim, J. S., Stranz, D. D., Jennings, P. A., Woods Jr., V. L. & Adams, J. A. (2002) Phosphorylation driven motions in the COOH-terminal Src kinase, Csk, revealed through enhanced hydrogen–deuterium exchange and mass spectrometry (DXMS) *J. Mol. Biol.* 323: 871–881.

Hamuro, Y., Zawadzki, K.M., Kim, J.S., Stranz, D.D., Taylor, S.S. & Woods, V.L. (2003) Dynamics of cAPK type II beta activation revealed by enhanced amide H/2H exchange mass spectrometry (DXMS). *J. Mol. Biol.* 327: 1065-1076.

Heller, W. T., Vigil, D., Brown, S., Blumenthal, D. K., Taylor, S. S. & Trewhella, J. (2004) C subunits binding to the protein kinase A RIα dimer induce a large conformational change. *J. Biol. Chem.* 279: 19084-19090.

Hoofnagle, A. N., Resing, K. A., Goldsmith, E. J. & Ahn, N. G. (2001) Changes in protein conformational mobility upon activation of extracellular regulated protein kinase-2 as detected by hydrogen exchange. *Proc. Natl. Acad. Sci. USA* 98: 956-961.

Hoofnagle, A. H., Resing, K. A. & Ahn, N. G. (2003) Protein analysis by hydrogen exchange mass spectrometry. *Annu. Rev. Biophys. Biomol. Struct.* 32: 1-25.

Hoofnagle, A. H., Stoner, J. W., Lee, T., Eaton, S. S. & Ahn, N. G. (2004a) Phosphorylation-dependent changes in structure and dynamics in ERK2 detected by SDSL and EPR. *Biophys. J.* 86: 395-403.

Hoofnagle, A.N., Resing, K.A. & Ahn, N.G. (2004b) Practical methods for deuterium exchange/mass spectrometry. *Methods Mol. Biol.* 250: 283–298.

Iacob, R. E., Dumitrescub, T. P., Zhang, J., Gray, N. S., Smithgall, T. E. & Engen, J. R. (2009) Conformational disturbance in Abl kinase upon mutation and deregulation. *Proc. Natl. Acad. Sci. USA* 106: 1386–1391.

Johnson, M. L., Correia, J. J., Yphantis, D. A. & Halvorson, H. R. (1981) Analysis of data from the analytical ultracentrifuge by nonlinear least-squares techniques. *Biophys. J.* 36: 575-588.

Johnson, R. S. and Walsh, K. A. (1994) Mass-spectrometric measurement of protein amide hydrogen-exchange rates of apo-myoglobin and holo-myoglobin. *Protein Sci.* 3: 2411-2418.

Johnson, D. A., Akamine P., Radzio-Andzelm, E., Madhusudan, M. & Taylor, S. S. (2001) Dynamics of cAMP-dependent protein kinase. *Chem. Rev.* 101: 2243-2270.

Karlsson, R., Zheng, J., Ten Eyck, L. F., Xuong, N., Taylor, S. S. & Sowadski, J. M. (1993) Structure of the mammalian catalytic subunit of cAMP-dependent protein kinase and an inhibitor peptide displays an open conformation. *Acta Cryst.* 49: 381-388.

Khokhlatchev, A., Xu, S., English, J., Wu, P., Schaefer, E. & Cobb, M. H. (1997) Reconstitution of mitogen-activated protein kinase phosphorylation cascades in bacteria. *J. Biol. Chem.* 272: 11057-11062.

Kim, C., Nguyen-Huu Xuong, N. & Taylor, S. S. (2005) Crystal structure of a complex between the catalytic and regulatory (RIα) subunits of PKA. *Science* 307: 690- 696.

Kim, C., Vigil, D., Anand, G. & Taylor, S. S. (2006) Structure and dynamics of PKA signaling proteins. *Eur. J. Cell Biol.* 85: 651-654.

Knighton, D. R., Bell, S. M., Zheng, J., Ten Eyck, L. F., Xuong, N., Taylor, S. S. & Sowadski, J. M. (1993) 2.0 Å refined crystal structure of the catalytic subunit of cAMP-dependent protein kinase complexed with a peptide inhibitor and detergent. *Acta Cryst.* 49: 357-361.

Lee, J. C., Kumar, S., Griswold, D. E., Underwood, D. C., Votta B. J. & Adams, J. L. (2000) Inhibition of p38 MAP kinase as a therapeutic strategy. *Immunopharmacology* 47: 185-201.

Lee, T., Hoofnagle, A. N., Kabuyama, Y., Stroud, J., Min, X., Goldsmith, E. J., Chen, L., Resing, K. A. & Ahn, N. G. (2004) Docking motif interactions in MAP kinases revealed by hydrogen exchange mass spectrometry. *Mol. Cell.* 14: 43-55.

Lee, T., Hoofnagle, A. N., Resing, K. A. & Ahn, N. G. (2005) Hydrogen exchange solvent protection by an ATP analogue reveals conformation change in ERK2 upon activation *J. Mol. Biol.* 353: 600-612.

Lee, T., Hoofnagle, A.N., Resing, K.A. & Ahn, N.G. (2006) Protein hydrogen exchange measured by electrospray ionization mass spectrometry. in "Cell Biology: A Laboratory Handbook", Third Edition, J.E. Celis, Ed., Elsevier Science. 4: 443-449.

Li, F., Gangal. M., Juliano, C., Gorfain, E., Taylor, S. S. & Johnson, D. A. (2002) Evidence for an internal entropy contribution to phosphoryl transfer: A study of domain closure, backbone flexibility, and the catalytic cycle of cAMP-dependent protein kinase. *J. Mol. Biol.* 315: 459-469.

Mansour, S. J., Matten, W. T., Hermann, A. S., Candia, J. M., Rong, S., Fukasawa, K., Vande Woude, G. F. & Ahn, N. G. (1994) Transformation of mammalian cells by constitutively active MAP kinase kinase. *Science* 265: 966-970.

Marmorino, J. L., Auld, D., Betz, S. F., Doyle, D. E., Young, G. B. & Pielak, G. J. (1993) Amide proton exchange rates of oxidized and reduced *Saccharomyces cerevisiae* iso-1-cytochrome c. *Protein Sci.* 2: 1966-1974.

Mayne L, Paterson Y, Cerasoli D. & Englander S.W. (1992) Effect of antibody binding on protein motions studied by hydrogen-exchange labeling and two-dimensional NMR. *Biochemistry.* 31:10678-10685.

Milne, J. S., Mayne, L., Roder, H., Wand, A. J. & Englander, S. W. (1998) Determinants of protein hydrogen exchange studied in equine cytochrome c. *Protein Sci.* 7: 739-745.

Mittermaier, A. K. & Kay, L. E. (2009) Observing biological dynamics at atomic resolution using NMR. *Trends Biochem. Sci.* 34: 601-611.

Neudecker, P., Lundstrom, P. & Kay, L. E. (2009) Relaxation dispersion NMR spectroscopy as a tool for detailed studies of protein folding. *Biophys. J.* 96: 2045-2054.

Olah, G. A., Mitchell, R. D., Sosnick,, T. D., Walsh, D. A. & Trewhella, J. (1993) Solution structure of the cAMP-dependent protein kinase catalytic subunit and its contraction upon binding the protein kinase inhibitor peptide. *Biochemistry* 32: 3649-3657.

Orr, J. W. & Newton, A. C. (1994) Requirement for negative charge on "activation loop" of protein kinase C. *J. Biol. Chem.* 269: 27715-27718.

Paterson, Y., Englander, S. W. & Roder, H. (1990) An antibody binding site on cytochrome c defined by hydrogen exchange and two-dimensional NMR. *Science.* 249:755-759.

Perkins, D. N., Pappin, J. C., Creasy, D. M. & Cottrell, J. S. (1999) Probability-based protein identification by searching sequence databases using mass spectrometry data. *Electrophoresis* 20: 3551-3567.

Prowse, N. C. & Lew, J. (2001) Mechanism of ERK2 activation by dual phosphorylation. *J. Biol. Chem.* 276: 99-103.

Raingeaud, J., Gupta, S., Rogers, J. S., Dickens, M., Han, J., Ulevitch, R. J. & Davis, R. J. (1995) Pro-inflammatory cytokines and environmental stress cause p38 mitogen activated

protein kinase activation by dual phosphorylation on tyrosine and threonine. *J. Biol. Chem.* 270: 7420-7426.

Rand, K. D., Zehl, Jensen, O. N. & Jørgensen, T.J.D. (2009) Protein hydrogen exchange measured at single-residue resolution by electron transfer dissociation mass spectrometry. *Anal. Chem.* 81: 5577–5584.

Rand, K. D., Zehl, M., Jensen, O. N. & Jørgensen, T. J. (2010) Loss of ammonia during electron-transfer dissociation of deuterated peptides as an inherent gauge of gas-phase hydrogen scrambling. *Anal Chem.* 82: 9755-9762.

Resing, K. & Ahn, N.G. (1998) Deuterium exchange mass spectrometry as a probe of protein kinase activation. Analysis of wild-type and constitutively active mutants of MAP kinase kinase-1. *Biochemistry* 37: 463-475.

Resing, K. A., Hoofnagle, A. N. & Ahn, N. G. (1999) Modeling deuterium exchange behavior of ERK2 using pepsin mapping to probe secondary structure. *J Am. Soc. Mass. Spectrom.* 10: 685-702.

Ring, A. Y., Sours, K. M., Lee, T. & Ahn. N. G. (2010) Distinct patterns of activation-dependent changes in conformational mobility between ERK1 and ERK2. *Internat. J. Mass. Spec.* 302: 101-109.

Robbins, D., Zhen, E., Owaki, H., Vanderbilt, C. A., Ebert, D., Geppert, T. & Cobb, M. H. (1993) Regulation and properties of extracellular signal regulated-protein kinases 1 & 2 *in vitro*. *J Biol. Chem.* 268: 5097-5106.

Robinson, M. J., Harkins, P C., Zhang, J., Baer, R., Haycock, J. W., Cobb, M. H. & Goldsmith, E. J. (1996) Mutation of position 52 in ERK2 creates a nonproductive binding mode for adenosine 5'-triphosphate. *Biochemistry* 35: 5641-5646.

Roder, H., Elöve, G. A. & Englander, S. W. (1988) Structural characterization of folding intermediates in cytochrome c by H-exchange labeling and proton NMR. *Nature* 335: 700-704.

Ruschalk, A. M. & Kay, L. E. (2010) Methyl groups as probes of supra-molecular structure, dynamics and function. *J. Biomol. NMR.* 46: 75-87

Sivaraman, T., Arrington, C. B., & Robertson, A. D. (2001) Kinetics of unfolding and folding from amide hydrogen exchange in native ubiquitin. *Nat. Struct. Biol.* 8: 331-333.

Smith, D. L., Deng, Y. & Zhang, Z. (1997) Probing the non-covalent structure of proteins by amide hydrogen exchange and mass spectrometry. *J. Mass. Spectrom.* 32: 135-146.

Sours, K. M., Kwok, S. C., Rachidi, T., Lee, T., Ring, A., Hoofnagle, A. N., Resing, K. A. & Ahn, N. G. (2008) Hydrogen-exchange mass spectrometry reveals activation-induced

changes in the conformational mobility of p38alpha MAP kinase. *J. Mol Biol.* 379: 1075-1093.

Sours, K. M. & Ahn, N. G. (2010) Analysis of MAP kinases by hydrogen exchange mass spectrometry. *Methods Mol. Biol.* 661: 239-255.

Sun, S., Meyer-Arendt, K., Eichelberger, B., Brown, B., Yen, C. Y., Old, W., Pierce, K., Cios, K. J., Ahn, N. G. & Resing, K. A. (2006) Improved validation of peptides MS/MS assignments using spectral intensity prediction. *Mol. Cell Proteomics.* 6: 1-17.

Taylor, S. S., Yang, J., Wu, J., Haste, N. M., Radzio-Andzelm, E. & Anand, G. (2004) PKA: a portrait of protein kinase dynamics. *Biochim. Biophys. Acta* 1697: 259–269.

Taylor, S. S., Kim, C., Vigil, D., Haste, N. M., Yang, J., Wu, J. & Anand, G. S. (2005) Dynamics of signaling by PKA. *Biochim. Biophys. Acta* 1754: 25–37.

Tanoue, T., Adachi, M., Moriguchi, T. & Nishida, E. (2000) A conserved docking motif in MAP kinases common to substrates, activators and regulators. *Nat. Cell Biol.* 2: 110-116.

ter Haar, E., Prabhakar, P., Liu, X. & Lepre, C. (2007) Crystal structure of the p38 alpha-MAPKAP kinase 2 heterodimer. *J. Biol. Chem.* 282: 9733-9739.

Turnbull, W. B. and Daranas, A. H. (2003) On the value of C: Can low affinity systems be studied by isothermal titration calorimetry? *J. Am. Chem. Soc.* 125: 14859-14866.

Vigil, D., Blumenthal, D. K., Taylor, S. S. & Trewhella, J. (2006) Solution scattering reveals large differences in the global structures of type II protein kinase A isoforms. *J. Mol Biol.* 357: 880-889.

Wang , Z., Harkins, P. C., Ulevitch, R. J., Han, J., Cobb, M. H. & Goldsmith, E. J. (1997) The structure of mitogen-activated protein kinase p38 at 2.1 Å resolution. *Proc. Natl. Acad. Sci. USA* 94: 2327-2332.

Wang, Z., Canagarajah, B.J., Boehm, J.C., Kassisà, S., Cobb, M.H., Young, P.R., Abdel-Meguid, S., Adams, J.L. & Goldsmith, E.J. (1998) Structural basis of inhibitor selectivity in MAP kinases. *Structure* 6: 1117-1128.

Wales, T. E., Fadgen, K.E., Gerhardt, G.C. & Engen, J.R. (2008) High-speed and high-resolution UPLC separation at zero degrees celsius. *Anal. Chem.* 80: 6815-6820.

Wilsbacher J. L. & Cobb, M. H. (2001) Bacterial expression of activated mitogen-activated protein kinases. *Methods Enzymol.* 332: 387-400.

White, A., Pargellis, C.A., Studts, J.M., Werneburg, B.G. & Farmer, B.T. (2007) Molecular basis of MAPK-activated protein kinase 2:p38 assembly. *Proc. Natl. Acad. Sci. USA* 104: 6353-6358.

Wilson, K.P., Fitzgibbon, M.J., Caron, P.R., Griffith, J.P., Chen, W., McCaffrey, P.G., Chambers, S.P. & Su, M.S. (1996). Crystal structure of p38 mitogen-activated protein kinase. *J. Biol. Chem.* 271: 27696-27700.

Wong, L., Lieser, S., Chie-Leon, B., Miyashita, O., Aubol, B., Shaffer, J., Onuchic, J.N., Jennings, P.A. & Adams, J.A. (2004) Dynamic coupling between the SH2 domain and active site of the COOH terminal Src kinase, Csk. *J. Mol. Biol.* 341: 93-106.

Xie, X., Gu, Y., Fox, T., Coll, J. T., Fleming, M. A., Markland, W., Caron, P.R., Wilson, K.P. & Su, M.S. (1998) Crystal structure of JNK3: a kinase implicated in neuronal apoptosis. *Structure* 6: 983-991.

Zhang, Z. and Smith, D. L. (1993) Determination of amide hydrogen exchange by mass spectrometry: a new tool for protein structure elucidation. *Protein Sci.* 2: 522-531.

Zhang, F., Strand, A., Robbins, D., Cobb, M.H. & Goldsmith, E.J. (1994) Atomic structure of the MAP kinase ERK2 at 2.3 A resolution. *Nature* 367: 704-711.

Zhang, J., Zhang, F., Ebert, D., Cobb, M.H. & Goldsmith, E.J. (1995) Activity of the MAP kinase ERK2 is controlled by a flexible surface loop. *Structure* 3: 299-307.

Zhang, Z. (2004) Prediction of low-energy collision-induced dissociation spectra of peptides. *Anal. Chem.* 76: 3908-3922.

Zhang, Z. (2005) Prediction of low-energy collision-induced dissociation spectra of peptides with three or more charges. *Anal. Chem.* 77: 6364-6373.

Zhang, W. X., Wang, R., Wisniewski, D., Marcy, A. I., LoGrasso, P., Lisnock, J., Cummings, R. T. & Thompson, J. E. (2005) Time-resolved Forester resonance energy transfer assays for the binding of nucleotide and protein substrates to p38α protein kinase. Anal. Biochem. 343: 76-83.

Zhang, J., Adria´n, F. J., Jahnke, W., Cowan-Jacob, S. W., Li, A. G., Iacob, R. E., Sim, T., Powers, J., Dierks, C., Sun, F., Guo G., Ding, Q., Okram, B., Choi, Y., Wojciechowski, A., Deng, X., Liu, G., Fendrich, G., Strauss, A., Vajpai, N., Grzesiek, S., Tuntland, T., Liu, Y., Bursulaya, B., Azam, M., Manley, P. W., Engen, J. R., Daley, G. Q., Warmuth, M. & Gray, N. S. (2010) Targeting Bcr–Abl by combining allosteric with ATP-binding-site inhibitors. *Nature* 463: 501-508.

Zehl, M., Rand, K. D., Jensen, O. N. & Jørgensen, T. J. (2008) Electron transfer dissociation facilitates the measurement of deuterium incorporation into selectively labeled peptides with single residue resolution. *J. Am. Chem. Soc.* 130: 17453-17459.

Zheng, J., Knighton, D. K., Ten Eyck, L. F., Karlsson, R., Xuong, N., Taylor, S. S. & Sowadski, J. M. (1993) Crystal structure of the catalytic subunit of CAMP-dependent protein kinase complexed with MgATP and peptide inhibitor. *Biochemistry* 32: 2154-2161.

Zhou, H., Zheng, M., Chen, J., Changchuan, X, Kolatkar, A. R., Zarubin, T., Ye, Z., Akella, R., Lin, S., Goldsmith, E. J. & Han, J. (2006a) Determinants that control the specific interactions between TAB1 and p38α. *Mol. Cell. Biol.* 26: 3824-3834.

Zhou, B., Zhang, J., Liu, S., Reddy, S., Wang, F. & Zhang, Z. (2006b) Mapping ERK2-MKP3 binding interfaces by hydrogen/deuterium exchange mass spectrometry. *J. Biol. Chem.* 281: 38834-38844.

APPENDIX A

This appendix lists the primers used to generate the activation lip / hinge double mutants.

P1 T183E
CATACAGGGTTCTTGGAGGAGTATGTAGCCACGCG

P2 T183E RevComp
CGCGTGGCTACATACTCCTCCAAGAACCCTGTATG

P3 T183D
CATACAGGGTTCTTGGACGAGTATGTAGCCACGCG

P4 T183D RevComp
CGCGTGGCTACATACTCGTCCAAGAACCCTGTATG

P5 T183E/Y185E
ACAGGGTTCTTGGAGGAGGAGGTAGCCACGCGTTGG

P6 T183E/Y185E RevComp
CCAACGCGTGGCTACCTCCTCCTCCAAGAACCCTGT

P7 Y185E
ACAGGGTTCTTGACAGAGGAGGTAGCCACGCGTTGG

P8 Y185E RevComp
CCAACGCGTGGCTACCTCCTCTGTCAAGAACCCTGT

P9 Y185D
ACAGGGTTCTTGACAGAGGACGTAGCCACGCGTTGG

P10 Y185D RevComp
CCAACGCGTGGCTACGTCCTCTGTCAAGAACCCTGT

P11 T183D/Y185D
ACAGGGTTCTTGGACGAGGACGTAGCCACGCGTTGG

P12 T183D/Y185D RevComp
CCAACGCGTGGCTACGTCCTCGTCCAAGAACCCTGT

P13 T183E/Y185F
ACAGGGTTCTTGGAGGAGTTTGTAGCCACGCGTTGG

P14 T183E/Y185F RevComp
CCAACGCGTGGCTACAAACTCCTCCAAGAACCCTGT

P15 T183D/Y185F
ACAGGGTTCTTGGACGAGTTTGTAGCCACGCGTTGG

P16 T183D/Y185F RevComp
CCAACGCGTGGCTACAAACTCGTCCAAGAACCCTGT

International Journal of Mass Spectrometry 302 (2011) 101–109

Contents lists available at ScienceDirect

International Journal of Mass Spectrometry

journal homepage: www.elsevier.com/locate/ijms

Distinct patterns of activation-dependent changes in conformational mobility between ERK1 and ERK2

Adam Y. Ring[a], Kevin M. Sours[a], Thomas Lee[a,b], Natalie G. Ahn[a,b,*]

[a] Department of Chemistry and Biochemistry, University of Colorado, Boulder, CO 80309, United States
[b] Howard Hughes Medical Institute, University of Colorado, Boulder, CO 80309, United States

ARTICLE INFO

Article history:
Received 1 June 2010
Received in revised form 17 August 2010
Accepted 19 August 2010
Available online 15 September 2010

Keywords:
Hydrogen exchange
Mass spectrometry
ERK1
MAP kinase
Interdomain interactions

ABSTRACT

Hydrogen/deuterium exchange measurements by mass spectrometry (HX-MS) can be used to report localized conformational mobility within folded proteins, where exchange predominantly occurs through low energy fluctuations in structure, allowing transient solvent exposure. Changes in conformational mobility may impact protein function, even in cases where structural changes are unobservable. Previous studies of the MAP kinase, ERK2, revealed increases in HX upon activation occurred at the hinge between conserved N- and C-terminal domains, which could be ascribed to enhanced backbone flexibility. This implied that kinase activation modulates interdomain closure, and was supported by evidence for two modes of nucleotide binding that were consistent with closed *vs* open conformations in active *vs* inactive forms of ERK2, respectively. Thus, phosphorylation of ERK2 releases constraints to interdomain closure, by modulating hinge flexibility. In this study, we examined ERK1, which shares 90% sequence identity with ERK2. HX-MS measurements of ERK1 showed similarities with ERK2 in overall deuteration, consistent with their similar tertiary structures. However, the patterns of HX that were altered upon activation of ERK1 differed from those in ERK2. In particular, alterations in HX at the hinge region upon activation of ERK2 did not occur in ERK1, suggesting that the two enzymes differ with respect to their regulation of hinge mobility and interdomain closure. In agreement, HX-MS measurements of nucleotide binding suggested revealed domain closure in both inactive and active forms of ERK1. We conclude that although ERK1 and ERK2 are closely related with respect to primary sequence and tertiary structure, they utilize distinct mechanisms for controlling enzyme function through interdomain interactions.

1. Introduction

Extracellular signal-regulated protein kinases, ERK1 and ERK2, are mitogen-activated protein (MAP) kinases which control diverse cellular responses, including cell proliferation, differentiation, transformation, and survival. ERK activation is frequently dysregulated in human cancers, due to oncogenic mutations in upstream pathway components, including Ras, Raf, and MAP kinase kinase (MKK), as well as receptor tyrosine kinases, EGFR, Her2/Neu, and Met [1,2], all which are attractive targets for drug intervention. Although ERK1 and ERK2 are functionally redundant in many cell types, each shows a distinct mouse knockout phenotype, where deletion of ERK2 leads to embryonic lethality while deletion of ERK1 yields viable animals with defects in thymocyte maturation and immunodeficiency [3,4]. Thus, at least some functions of ERK1 and ERK2 are non-redundant. On the other hand, relatively little is known about how regulatory mechanisms controlling ERK1 and ERK2 differ, which might impact the development of different strategies for specifically targeting each form.

Crystallographic studies of ERK1 and ERK2 show a conserved tertiary structure shared with all protein kinases, consisting of an N-terminal ATP binding and C-terminal substrate binding domains surrounding the catalytic site [5–8]. Both ERK1 and ERK2 are activated by dual phosphorylation at a conserved pThr-Glu-pTyr sequence located within the activation lip region, which is catalyzed by the upstream MAP kinase kinases, MKK1 and MKK2. Structural remodeling events which accompany ERK activation have been revealed by X-ray structures of inactive, unphosphorylated (0P) and active, diphosphorylated (2P) forms of ERK2 [6–8]. Diphosphorylation triggers new phosphate-side chain ion pair interactions which lead to dramatic conformational changes within the activation lip, reorganizing the substrate binding site to enable recognition of the proline-directed phosphorylation motif (pSer/pThr-Pro), and reorienting active site residues involved in catalysis.

* Corresponding author at: Department of Chemistry and Biochemistry, University of Colorado, Boulder, CO 80309-0215, United States.
Tel.: +1 303 492 4799; fax: +1 303 492 2439.
E-mail address: natalie.ahn@colorado.edu (N.G. Ahn).

1387-3806/$ – see front matter © 2010 Elsevier B.V. All rights reserved.
doi:10.1016/j.ijms.2010.08.020

Hydrogen-exchange mass spectrometry (HX-MS) studies have shown that protein kinases are regulated not only through changes in conformation, but also through changes in conformational mobility. In previous studies of ERK2, comparisons between the active and inactive states of this kinase revealed increased HX in the hinge region upon activation, consistent with enhanced flexibility and conformer interconversions, which were not observable by X-ray crystallography [9]. Electron paramagnetic resonance (EPR) analysis of backbone residues in ERK2 that were individually coupled to a MTSL nitroxide spin label probe demonstrated that changes in side chain correlation rates occurred upon phosphorylation and activation [10]. Taken together, the results suggested a model in which the changes in HX could be explained by regulated protein motions, such as underlying backbone flexibility. Further measurements of steric protection from HX by the ATP analogue, AMP-PNP, suggested a function for this control of hinge flexibility. On one hand, HX within the N-terminal domain was comparable between 0P-ERK2 and 2P-ERK2, in regions containing the Gly loop, the conserved Lys-Glu ion pair within β3 and αC, the hinge region, and the catalytic base, all of which are known to form close interactions with nucleotide [11]. On the other hand, 2P-ERK2 showed 10-fold greater protection from HX than 0P-ERK2 within the conserved DFG motif, part of the C-terminal domain which forms metal coordination interactions with Mg^{+2}–ATP. Thus, AMP–PNP binding sterically protected both N- and C-terminal domains of 2P-ERK2 from solvent, but mainly protected only the N-terminal domain of 0P-ERK2. Because the two kinase forms shared similar binding affinities for AMP-PNP, the results suggested that distinct modes of nucleotide binding occur in solution. The protection patterns are consistent with a model in which 2P-ERK2 adopts a closed conformation, whereas 0P-ERK2 is somehow constrained to interfere with interdomain closure. Thus, HX protection by Mg^{+2}–AMP–PNP binding provides a useful way to monitor domain closure, an event needed to form a competent catalytic site. These results, together with the observed changes in hinge flexibility upon activation, led us to propose that activation of ERK2 releases constraints to domain closure by increasing backbone flexibility at the hinge [11].

Given their sequence and structural conservation, different MAP kinases might be expected to show similar regulatory mechanisms. In agreement, p38α MAP kinase appears to undergo conformational rearrangements following phosphorylation which parallel those seen in ERK2. For example, structural comparisons between p38α MAP kinase in its inactive, unphosphorylated form and the related p38γ MAP kinase in its active, diphosphorylated form show large conformational changes within the activation lip following phosphorylation by MKK3/6 [12–14]. Thus, although the activation lip conformation of 0P-p38α MAP kinase differs from that of 0P-ERK2, the lip conformation of 2P-p38γ MAP kinase is similar to that of 2P-ERK2, revealing that diverse activation lip conformers in MAP kinases converge towards a uniform structure in the active state, which allows catalytic rate enhancement. In contrast, HX-MS studies show that p38α MAP kinase differs significantly from ERK2 with respect to the patterns of regional HX which change in response to kinase activation [15]. This suggests that the effect of kinase activation on conformational mobility diverges between related protein kinases, leading to the hypothesis that different MAP kinases may have distinct mechanisms for regulating enzyme activity through their control of internal protein motions.

In this study, we wished to understand whether differences in patterns of regulated conformational mobility upon activation might also be observed between enzymes that are even more closely related. Here, we analyzed ERK1, which shares 90% sequence identity with ERK2. We found that ERK1 showed significant differences in how the HX behavior changes in response to kinase activation within conserved regions of the core structure. Notably, ERK1 did not display altered HX within hinge residues as previously observed in ERK2. This suggests that ERK1 might lack constraints to interdomain closure which are present in the inactive form of ERK2. In order to test this hypothesis, we measured changes in protection from HX upon AMP–PNP binding in ERK1, and compared these to prior studies of ERK2 [11]. The results showed significant protection from HX within the C-terminal domain of both 0P-ERK1 and 2P-ERK1, indicating that both inactive and active forms appear capable of interdomain closure in solution. Thus, the occurrence and functional effects of regulated protein motions differ in substantive ways between ERK1 and ERK2.

2. Materials and methods

2.1. Protein purification

Active, diphosphorylated (2P) ERK1 was produced from plasmid pET-His-ERK1-R4F, containing wild-type human His_6-ERK1 expressed in tandem with constitutively active mutant MKK1 (R4F: ΔN3/S218E/S222D) [16]. Inactive, unphosphorylated (0P) human His_6-ERK1 was produced using plasmid NpT7-ERK1 [17]. Each kinase form was expressed in *E. coli* strain BL21(DE3)-pLysS, and purified using Ni-NTA agarose (Qiagen) chromatography, desalted by gel filtration (PD10, GE Healthcare), and further purified by MonoQ FPLC. Proteins were dialyzed overnight into 50 mM KPO_4 (pH 7.4), 100 mM KCl and 5 mM dithiothreitol, and stored in aliquots at −80 °C. The 0P-ERK1 protein was found to be mono-phosphorylated to 0.13 mol/mol, and was therefore dephosphorylated using λ phosphatase (New England Biolabs, 100 U/μg, 3 h, 30 °C) before Mono Q separation. The activation lip phosphorylation stoichiometries of the final kinase preparations showed 0% phosphorylation in 0P-ERK1 at the regulatory Thr and Tyr residues in the activation lip, and 95% diphosphorylation in 2P-ERK1. Intact ESI-MS of 0P-ERK1 and 2P-ERK1 showed full length masses expected of the recombinant ERK1 sequences, in unphosphorylated and diphosphorylated forms (Supplementary Fig. S1).

2.2. HX-MS measurements

Data were collected on a QStar Pulsar QqTOF mass spectrometer (ABI) interfaced with an Agilent Cap1100 HPLC (0.5 mm i.d. × 10 cm column, packed with POROS R1 20 resin), and measurements of weighted average mass were performed as described [18,19]. Proteins (4 μg) were incubated in 90% D_2O (Sigma) at 10 °C, allowing in-exchange reactions to take place between 8 s and 4 h. Reactions were quenched with 90 μL 25 mM succinic acid, 25 mM citric acid (pH 2.4), and cooled rapidly to 0 °C. Proteins were digested by adding 10 μL pepsin (4 μg) and analyzed immediately by LC–MS. Time-zero measurements were performed by quenching the reaction before adding D_2O.

Peptides in pepsin digests of ERK1 were identified by LC–MS/MS, analyzing replicate digests on two instruments in order to maximize the probability that a peptide would be selected for MS/MS. Aliquots (4 μg) of proteolyzed ERK1 were analyzed on the QStar mass spectrometer, with *m*/*z* window 400–1600 Da, duty cycle 15.5 s, and three MS/MS per cycle. Aliquots (60 ng) of ERK1 were analyzed on an LTQ-Orbitrap mass spectrometer interfaced with an Eksigent 2DLC HPLC (75 μm i.d. × 150 mm column, Zorbax C18 resin), with *m*/*z* window 300–2000 Da, duty cycle 4–6 s (10–14 cycles/min), and five MS/MS per cycle. MS/MS were converted to .mgf files and searched against the human ERK1 sequence using MASCOT (v. 1.9), with no enzyme specified. Mass tolerances were 2.5 Da (parent) and 1.2 Da (fragment) for QStar datasets, and 1.2 Da (parent) and 0.6 Da (fragment) for LTQ-Orbitrap datasets. Peptides with MOWSE score greater than 20 were validated by manual analysis of MS/MS spectra. LC–MS of ERK1 was then carried

out in water on the QStar, and only peptides with validated MS/MS that were also observed in the LC–MS run were reported.

HX-MS measurements of protection by Mg^{+2}–AMP–PNP were carried out as above, with the following modifications. Prior to the HX reaction, 8 μL (5 μg) of 0P-ERK1 or 2P-ERK1 was incubated on ice for 10 min with either 7 μL of 21 mM $MgCl_2$ + 2.1 mM AMP–PNP or 7 μL of 21 mM $MgCl_2$. At $t = 0$, exchange was initiated by adding 85 μL of a D_2O/solute mixture to the kinase solution to reach a final buffer composition of 85% (v/v) D_2O, 25 mM KPO_4 (pH 7.4), 50 mM KCl, and 0.25 mM DTT, 10 mM $MgCl_2$, and ±1 mM AMP–PNP. Samples were incubated between 8 s and 110 min at 10 °C to allow in-exchange, then quenched by acidification with 90 μL 25 mM sodium succinate, 25 mM sodium citrate (pH 2.4), and cooled to 0 °C. Proteins were digested by addition of pepsin, and peptides were analyzed on the QStar mass spectrometer. Time-zero controls were performed by quenching the sample prior to addition of the D_2O/solute mixture. To avoid systematic variations, time points and the order of sample analysis ±AMP–PNP were randomized.

Weighted average mass measurements were facilitated by using in-house HX-Analyzer software [15]. Samples were randomized to control for systematic variations, and replicate runs were performed at 0 and 60 s in order to quantify the average standard deviation of weighted average mass (0.05 Da) and maximum standard deviation (0.13 Da). Estimates of artifactual in-exchange and back-exchange were obtained as described [18,19]. Back-exchange was estimated in two ways. First, back-exchange was calculated for each peptide using an empirical formula which assumes 1% back-exchange per minute after quenching [Eq. (4) in Ref. [18]]. Second, back-exchange was estimated by desalting and then lyophilizing peptides generated from pepsin digestion of 2P-ERK1, incubating with 90% D_2O for 90 min at 90 °C to allow complete in-exchange, and measuring peptide mass by LC–MS under HX experimental conditions [18,20]. When counting the number of exchangeable amides for a given peptide, we included the first amide proton and did not assume rapid back-exchange on the timescale of the experiment. The two methods for estimating back-exchange were in reasonable agreement, where the measured values yielded an average of 28 ± 7% back-exchange for 21 observable peptides, while the empirical calculation yielded an average of 22 ± 2% back-exchange for the same peptides. Therefore we applied the second method involving back-exchange calculations to all peptides.

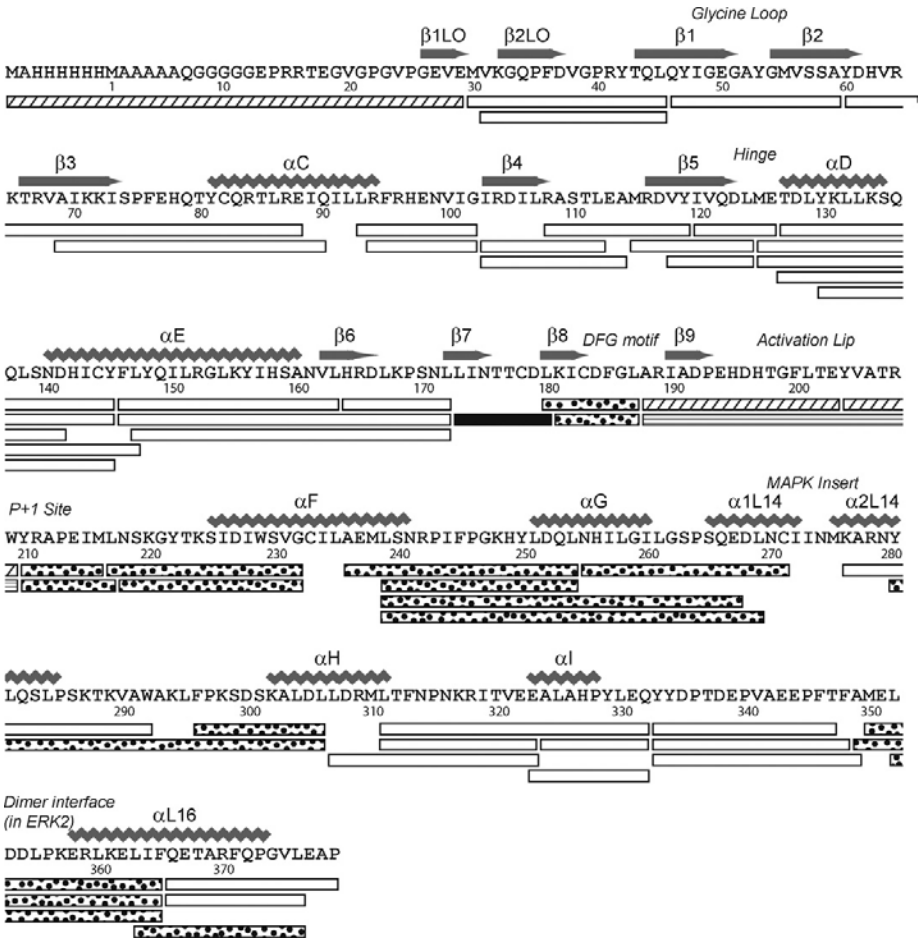

Fig. 1. Pepsin cleavage map of human ERK1. Shown is the sequence of His_6-ERK1, indicating residue numbers and secondary structure as reported by Kinoshita et al. [5]. All peptides indicated were present in LC–MS/MS datasets of ERK1 in water, as well as HX datasets in D_2O. Peptides indicated by stippled bars (−8–29, 188–203, and 204–209) were observed only in 0P-ERK1 datasets, and the peptide indicated with horizontal stripes (188–209) was observed only in 2P-ERK1 datasets, reflecting differences in proteolysis in the activation lip. One peptide indicated by a solid bar (173–179) showed increased in-exchange following phosphorylation and activation, and peptides indicated by dotted fill showed decreased in-exchange following phosphorylation and activation (see time courses in Supplementary Fig. S2).

After correcting weighted average masses for artifactual in-exchange and back-exchange, deuteration time courses were fitted by nonlinear least squares to the equation $Y = N - Ae^{-k1t} - Be^{-k2t} - Ce^{-k3t}$, where Y is the number of deuterons exchanged at time t; A, B, and C are the numbers of backbone amides exchanging at rates k_1, k_2, and k_3, respectively; and N is the maximal deuteration over the experimental time period ($N = A + B + C$). Subtracting N from the total number of exchangeable backbone amides yields NE, the number of amides that are non-exchanging over the experimental time period. Nonlinear least squares calculations and graphics of time courses were generated using Sigmaplot v9.0 (SPSS Inc.).

3. Results

3.1. Hydrogen exchange measurements

Hydrogen–deuterium in-exchange measurements of ERK1 were obtained by LC–MS as described Section 2. Fifty-five peptides were identified after pepsin proteolysis, ranging in length between 6 and 36 residues (Table S1). These accounted for 98% coverage of the primary sequence (370 of 379 residues), and 94% coverage of exchangeable amides (334 of 356 amides). The peptides are annotated onto the primary sequence of His_6-ERK1 in Fig. 1.

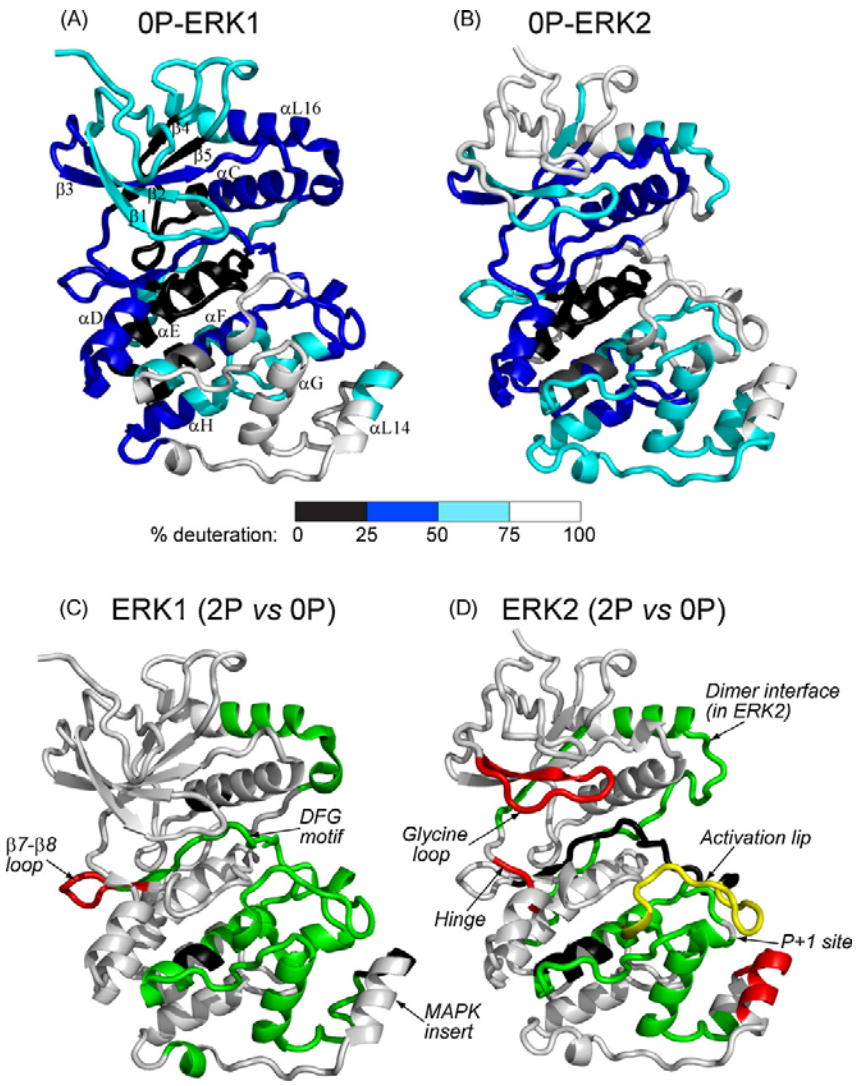

Fig. 2. Hydrogen exchange patterns in ERK1. (A and B) Extent of deuteration into (A) 0P-ERK1 and (B) 0P-ERK2 after 4 h, normalized by the number of exchangeable amides in each region. For reach region, the extent of deuteration was measured as the sum of $A + B + C$ (Supplementary Table S2), and mapped as colors corresponding to 0–25% (black), 25–50% (blue), 50–75% (cyan) and >75% (white) of exchangeable amides. Overall, ERK1 and ERK2 showed similar patterns of regional hydrogen exchange, with differences that could be attributed to variations in sequence or structure. (C and D) Changes in HX induced upon phosphorylation and activation of (C) ERK1 and (D) ERK2. Peptides that showed increased (red) or decreased (green) HX following activation by phosphorylation were colored against the X-ray structures of 1P-ERK1 (2ZOQ) and 0P-ERK2 (1ERK). Peptides found in only one form of ERK1 or ERK2 (black) precluded comparison between inactive and active kinases. Yellow denotes a peptide in ERK2 which showed both increased and decreased HX rates upon activation. Of particular interest was the hinge region, which in ERK2 underwent enhanced HX surrounding the pivot point for interdomain closure, but in ERK1 was unaltered by kinase activation (see Supplementary Fig. S3). Data on ERK2 were from Lee et al. [11].

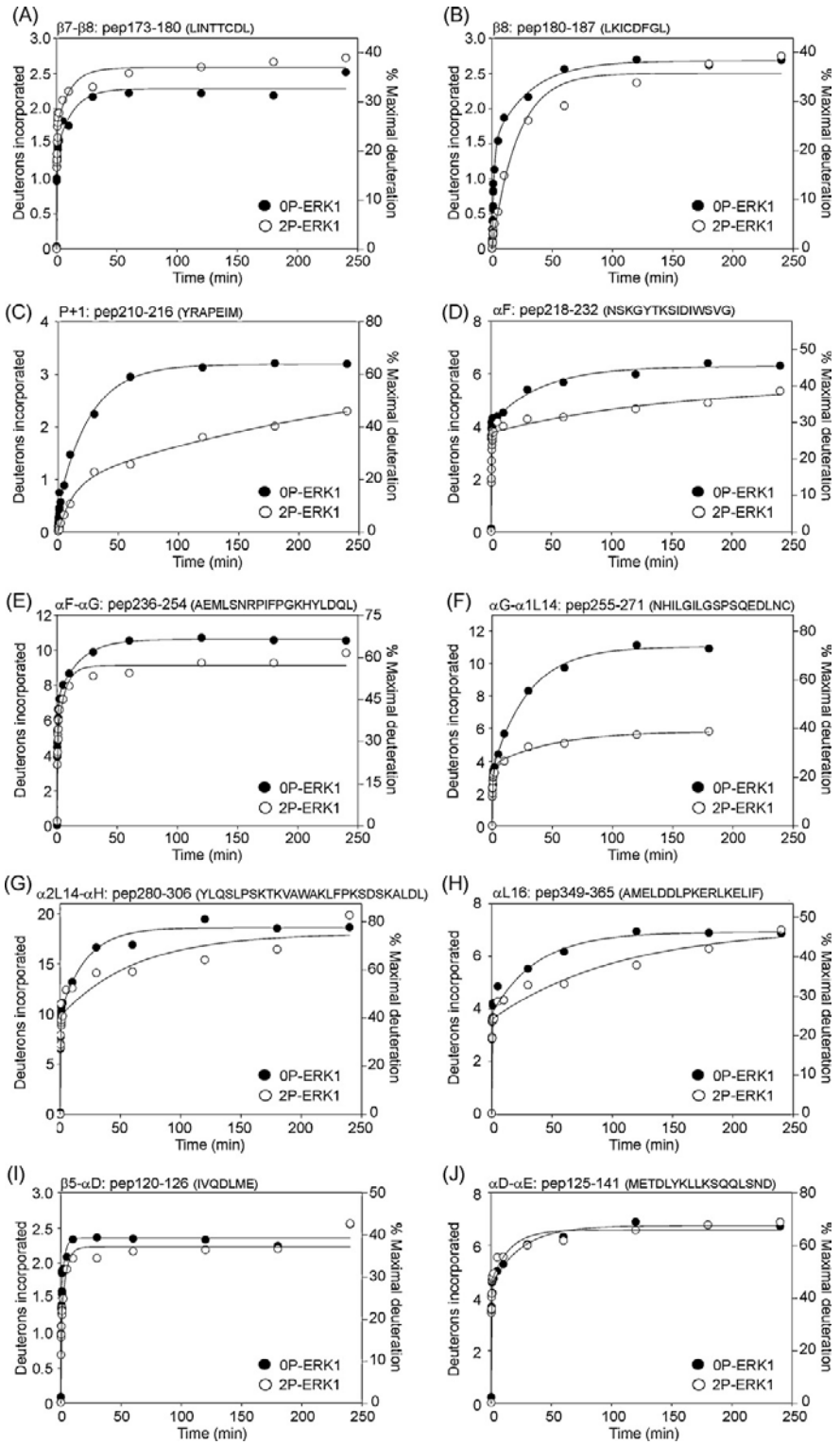

Fig. 3. HX time courses for peptides in ERK1 altered upon kinase activation. (A–J) Peptides are labeled by residue numbers as in Table S1, followed by the corresponding amino acid sequence. HX data on 0P-ERK1 are indicated by closed circles (●), and data on 2P-ERK1 are indicated by open circles (○). (I and J) Peptides 120–126 and 125–141 include the hinge region which in ERK1 showed no change upon activation, although HX within the sequence METDL was increased upon activation, in ERK2 [9,11].

Information about the degree of HX occurring within localized regions of 0P-ERK1 was assessed by measuring the extent of deuteration into different peptides over the 4 h timescale of the experiment, and mapping these against an X-ray structure determined for ERK1 [5] (Fig. 2A, Table S2). Slow exchange, leading to deuteration of <25% of exchangeable amides, was observed within core regions of the kinase corresponding to helix αE and strand β6 within the C-terminal lobe, the latter which contains the catalytic base within the active site. Slow exchange was also observed in the loop between helix αC and β4 as well as in strand β5, which contain residues that create a hydrophobic core within the N-terminal lobe. In ERK2, these residues form intramolecular connectivities with distal residues that in turn prevent autophosphorylation and autoactivation of the enzyme by constraining flexibility at the activation lip [21]. Fast exchange, leading to >75% deuteration of exchangeable amides, was observed within loop regions, including part of the activation lip and loops connecting the MAP kinase insert with C-terminal helices αG and αH. Deuteration exceeding

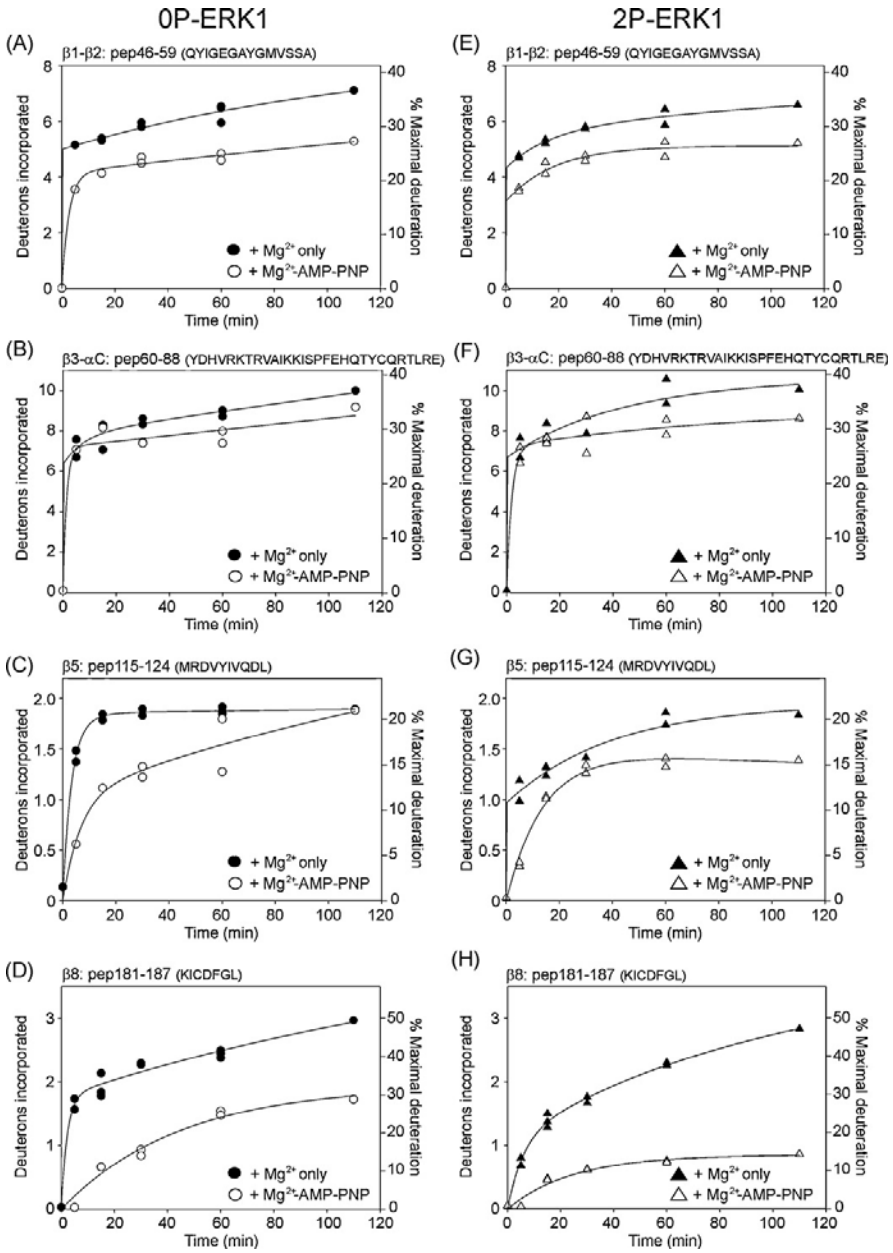

Fig. 4. HX time courses for peptides showing protection of ERK1 upon nucleotide binding. (A–H) Peptides from 0P-ERK1 (left panels) and 2P-ERK1 (right panels) show effects of AMP–PNP binding to ERK1. HX data on apoenzyme were indicated by closed symbols, and data collected with AMP–PNP were indicated by open symbols. Both 0P-ERK1 and 2P-ERK1 showed significant protection of HX upon binding AMP–PNP, suggesting interdomain closure in both inactive and active forms.

50% of exchangeable amides was also observed within N-terminal loop regions, the P+1 substrate binding loop, and the MAP kinase insert.

The extent of deuteration in ERK1 revealed many similarities with previous HX measurements of ERK2 [9,11] (Fig. 2A and B). Both enzymes showed low levels of exchange within the core regions of the N- and C-terminal domains, including the active site, helices αE and αF in the C-terminal domain, and the N-terminal core containing β3–αC–β4–β5. In both enzymes, high levels of exchange occurred within loops and peripheral secondary structure including the N-terminal strands β1LO-β2LO and β1–β2, intervening loop regions between β4–β5 and αF–αG, and the MAPK insert. Interestingly, some dissimilarities in HX behavior were observed between ERK1 and ERK2. Several prominent regions that underwent nearly complete in-exchange in ERK2 showed only partial exchange in ERK1; these included the activation lip and C-terminal helix αL16, which showed <50% exchange in ERK1, but greater than 90% exchange in ERK2. These differences in HX suggested lower conformational mobility in ERK1 compared to ERK2 within regions of the molecule linked to catalytic function.

3.2. Regulation of HX by ERK1 activation

Time courses comparing 0P-ERK1 to 2P-ERK1 (Supplementary. Fig. S2) revealed significant changes in hydrogen exchange behavior following activation of ERK1 by dual phosphorylation. Sites of proteolytic cleavage were nearly identical between the 0P and 2P forms, with the exception of the activation lip, where cleavage between residues Glu203 and Tyr204 (numbered as in Fig. 1) was observed only in the unphosphorylated form of ERK1. In total, eight peptides exhibited altered in-exchange behavior between 0P-ERK1 and 2P-ERK1 (Figs. 1 and 3A–H). In 7 of 8 cases, kinase activation led to decreased HX rates; these included peptide 180–187 (LKICDFGL), containing the conserved DFG motif; peptide 210–216 (YRAPEIM), containing the P+1 substrate binding loop; peptides 218–232 (NSKGYTKSIDIWSVG) and 236–254 (AEMLSNRPIFPGKHYLDQL), containing αF-αG; peptides 255–271 (NHILGILGSPSQEDLNC) and 280–306 (YLQSLPSKTKVAWAKLFPKSDSKALDL), containing the αL14 MAP kinase insert and αH; and peptide 349–365 (AMELDDLPKERLKIELIF), containing the C-terminal helix αL16. These could either reflect structural changes leading to solvent inaccessibility, or else decreased flexibility and internal motions, following activation lip phosphorylation. Only one peptide exhibited increased HX upon activation; this region corresponded to the β7–β8 loop (peptide 173–180, LINTTCDL), which forms part of a docking motif binding site (Fig. 3A), and might reflect increased backbone flexibility within a binding pocket for high affinity interactions with substrates, MKKs, and other effectors.

The localized regions which showed HX alterations upon kinase activation were mapped against the backbone structure of ERK1, and compared to those previously reported for ERK2 (Figs. 2C and D). ERK1 and ERK2 showed some similarities in the patterns of HX that were correlated with activity. Both enzymes showed activation-induced changes in HX within the activation lip, a region which undergoes significant conformational remodeling in ERK2, which would also be expected to occur in ERK1. Decreased HX was observed in both enzymes at the C-terminal αL16 helix and surrounding regions, which in ERK2 has been shown to form an interface for dimerization. Similarly, decreased HX was observed in both enzymes within the P+1 substrate interaction loop, as well as helices αF and αG, which comprise the likely interface for extended substrate binding interactions. ERK2 showed few structural changes within this region that might account for

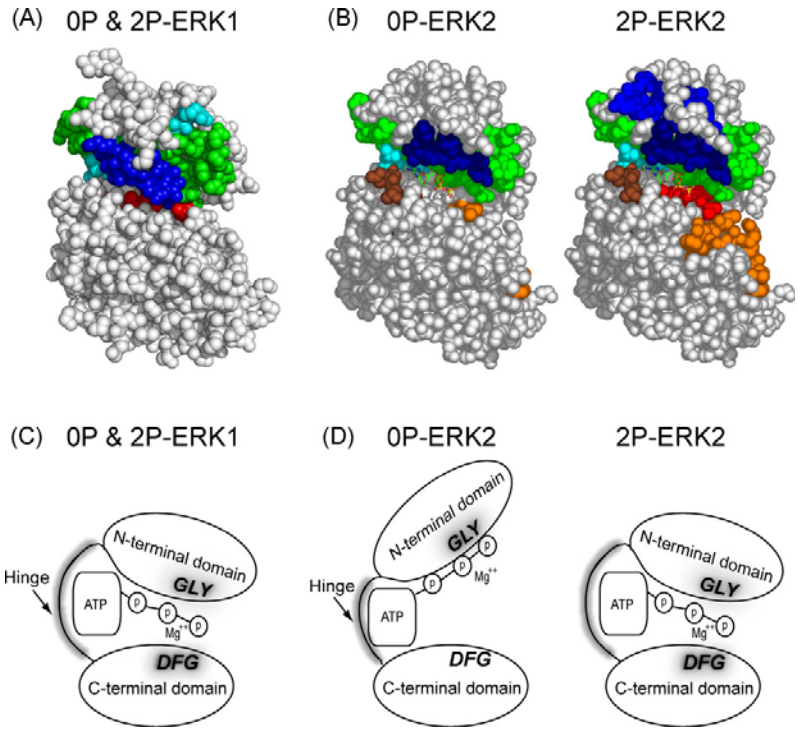

Fig. 5. Summary of results and conceptual model. (A and B) Peptides protected from HX by Mg^{+2}–AMP–PNP binding are shown in color. (C) Model of results, showing interdomain interactions leading to domain closure in both 0P- and 2P-ERK1, based on HX protection in the C-terminal domain. (D) Model indicating that in solution, interdomain interactions leading to domain closure are enhanced in ERK2 by phosphorylation and activation.

the observed changes in HX, suggesting that reduced hydrogen exchange rates reflected decreased conformational mobility following kinase activation. Decreased HX had also been observed in this region following activation of p38α MAP kinase [15], suggesting that decreased flexibility in the substrate binding interface is a feature common to several MAP kinases.

ERK1 and ERK2 also showed key differences in their patterns of HX regulated by activation. For example, ERK1 showed no increased HX in the MAP kinase insert, which had previously been observed in ERK2 and ascribed to disrupted hydrogen bonding with activation lip residues upon kinase activation [9]. Likewise, ERK1 did not recapitulate the increased HX observed in the glycine-rich loop upon activation of ERK2, a region implicated in nucleotide binding. Importantly, differences were noted between the two enzymes in the hinge region localized between the N- and C-terminal domains, which in cAMP-dependent protein kinase corresponds to the pivot point for rigid body rotation and interdomain closure needed for formation of the catalytic site. In ERK2, this region of the hinge (METDL, Supplementary. Fig. S3) showed significant enhancement of HX upon activation, which correlated with altered internal motions, allowing the kinase to switch from an open to closed solution conformation [9–11]. In contrast, peptide 125–141 (METDLYKLLKSQQLSND), peptide 125–145 (METDLYKLLKSQQLSNDHICY), and the overlapping peptide 130–145 (YKLLKSQQLSNDHICY) exhibited no change in HX behavior between active and inactive states in ERK1, from which we conclude that no change in HX occurs within the corresponding METDL hinge sequence in ERK1 (Fig. 3I and J, Supplementary Fig. S3). This suggested that hinge flexibility is not regulated by activation of ERK1 as it is in ERK2, and that the two enzymes differ with respect to the regulation of interdomain closure.

3.3. Domain closure in ERK1 can be monitored by HX-MS

The results above suggested that unlike ERK2, the hinge flexibility of ERK1 might not be controlled by activity state, and thus might allow interdomain closure in both inactive and active forms. In order to test this hypothesis, we conducted an HX-MS experiment which measured the steric protection from HX upon AMP–PNP binding to ERK1. Prior studies with ERK2 have shown that AMP–PNP protects N-terminal and hinge regions in the inactive and the active kinase, as expected from the known interactions between kinases and ATP, and that active ERK2 shows additional protection of the conserved DFG motif in the C-terminal domain. Thus, steric protection of the DFG motif reflects interdomain closure between N- and C-terminal lobes in solution. If our hypothesis were correct, we would expect to see protection of the DFG motif comparable in both forms of ERK1.

We measured HX time courses in the presence or absence of 1 mM Mg^{2+}–AMP–PNP, comparing inactive *vs* active ERK1 (Supplementary Fig. S4). Only 20 of the 54 peptides were observed in these experiments between each of the four conditions, which nevertheless included most of the ERK1 sequence. Of these, four peptides showed significant reduction in HX rates upon AMP–PNP binding (Fig. 4A–D). Three of these corresponded to regions which are known to form contacts with nucleotide within the N-terminal domain. These included peptide 46–69 (QYIGEGAYGMVSSA), containing the glycine loop which forms hydrogen bond interactions with β and γ-phosphate groups of ATP and forms a flexible gate for nucleotide binding; peptide 60–88 (YDHVRKTRVAIKKISPFEHQTYCQRTLRE), containing conserved Lys and Glu residues in strand β3 and helix αC, respectively, which form ion-pair interactions with ATP α and β-phosphate groups; and peptide 115–124 (MRDVYIVQDL), containing residues in strand β5 which form hydrogen bonding interactions with nucleotide (Fig. 4A–C). The fourth peptide, peptide 181–187 (KICDFGL), contains the conserved DFG motif (Fig. 4D). Here, we observed comparable protection upon AMP–PNP binding to both inactive and active kinase forms. This was in contrast to the corresponding DFG region in ERK2, where previous measurements revealed 10-fold greater nucleotide protection from HX in the active kinase compared to the inactive form (Supplementary Fig. S5) [11]. Our measurements of ERK1 indicate that that nucleotide interacts productively with both the N-and C-terminal domains in 0P- and 2P-ERK1, and more productively with the C-terminal domain in 0P-ERK1 than 0P-ERK2. Taken together, the findings suggest that both inactive and active forms of ERK1 are able to adopt interdomain interactions leading to a closed conformation in solution.

4. Discussion

This study reveals novel insight into the manner in which internal motions in ERK1 are regulated by enzyme activation, as revealed by HX-MS. We demonstrate that ERK1 and ERK2, which are 90% identical in primary sequence, show differences in HX behavior that suggest differences in conformational mobility between closely related kinases.

Interpretation of HX results can be greatly aided by the availability of information on atomic structure. Numerous X-ray structures of ERK2 have been solved in varying forms, including unphosphorylated, diphosphorylated, peptide-bound, inhibitor-bound, or harboring mutations within the phosphorylation lip and active site. In contrast, only one X-ray structure of ERK1 has been published to date, representing a form which is mono-phosphorylated at its regulatory Tyr residue (1P-ERK1, Ref. [5]), and whose activity is approximately 10% of the fully active, diphosphorylated enzyme [17]. The tertiary structure of ERK1 shows a consensus kinase core structure containing two insertions unique to MAP kinases (αLO, αL14). The backbone conformation is very similar to the structure of ERK2 [6–8], consistent with the extensive sequence identity between these enzymes. In its configuration of the activation lip, the 1P-ERK1 structure appears most consistent with what would be expected for an inactive conformation of the enzyme, resembling the inactive, unphosphorylated form of ERK2 (0P-ERK2) more than the active diphosphorylated form (2P-ERK2).

While the overall extent of HX was generally similar between 0P-ERK1 and 0P-ERK2 and consistent with the conserved tertiary structures, certain dissimilarities were observed. For example, the extent of HX was lower in ERK1 than ERK2 within the β1LO–β2LO and β1 strands of the N-terminal lobe, and higher in regions surrounding the MAP kinase insertion. Both of these regions showed significant differences in primary sequence as well as structure (Supplementary Fig. S6 sequence alignment). Likewise, HX was lower in ERK1 within the β7–β8 loop and the C-terminal αL16 helix, suggesting lower flexibility. Both regions showed similar sequences, but higher structural order in ERK1 than ERK2, reflected by closer beta-sheet hydrogen bonding distances in the β7–β8 loop of ERK1, as well as an additional helical turn proximal to αL16 in ERK1 which was absent in ERK2. Lower HX was also observed around the activation lip of ERK1, compared to ERK2. Although primary sequences and conformations were similar between these regions of ERK1 and ERK2, residues immediately adjacent to pTyr as well as within helix αC in ERK1 were distorted relative to 0P-ERK2 in a manner suggesting greater similarity to corresponding regions in 2P-ERK2, which might account for the partial activity of 1P-ERK1. Thus, for the most part, differences in extent of HX between ERK1 and ERK2 could be attributed to variations in sequence and/or structure.

Intriguing differences were observed between ERK1 and ERK2, when we assessed the effects of phosphorylation and activation

on conformational mobility. Our previous studies on ERK2 showed that enzyme activation led to significant changes in HX within localized regions of the protein. These could be attributed to changes in protein flexibility and internal motions, especially when HX changes occurred in a manner inconsistent with structural differences between 0P-ERK2 and 2P-ERK2. In particular, regions of ERK2 that showed regulated HX ascribed to changes in flexibility were those implicated in substrate binding or catalysis, which could conceivably contribute to enzyme activation. This was further examined in the hinge region, where increased flexibility upon kinase activation correlated with release of constraints to interdomain closure. In the case of ERK1, the limited X-ray information was insufficient to draw dependable conclusions about how well the changes in HX could be explained by changes in structure *vs* internal motions. Nevertheless, to the extent that ERK1 behaves similarly to ERK2, whose conformational changes were largely restricted to the activation lip and active site, our HX measurements on ERK1 could conceivably reflect effects of activation on protein dynamics. As in ERK2, the regions showing regulated HX in ERK1 are associated with kinase function. Increased HX in ERK1 upon activation may reflect increased mobility of the β7–β8 loop which is involved in substrate docking motif recognition. Likewise, reduced mobility upon activation might also occur in the DFG motif which is involved in ATP binding, in the C-terminal helix αL16, which is involved in kinase dimerization, and in the P + 1 loop and helices αF–αG, which form the interface for substrate binding and recognition.

Notably, differences were observed between the two enzymes in the hinge region, which in ERK2 showed increased backbone flexibility upon activation, but in ERK1 showed little change between active and inactive states (Supplementary Fig. S3). Further evidence showing that AMP–PNP interacts productively with N- and C-terminal domains in both 0P-ERK1 and 2P-ERK1 suggests a model in which both the active and inactive states of ERK1 allow interdomain closure and formation of a closed active site (Fig. 5). This behavior differs substantively from ERK2, where constraints to domain closure consistent with an open solution conformation were observed in the inactive, unphosphorylated form, and were released upon activation by diphosphorylation, enabling the formation of a closed solution conformation that would be needed for catalysis. We conclude that ERK1 and ERK2, while closely related in sequence and structure, nevertheless differ significantly in their constraints to kinase activation, and the mechanisms by which they overcome these barriers through activation-induced regulation of conformational mobility.

Acknowledgements

We are indebted to Stephane Houel, Shuji Kato, Kutralanathan Renganathan, and William Old for assistance with LC–MS/MS and peptide search programs, to Rebecca West for help with data analysis, and to Melanie Cobb for her gift of ERK1 expression plasmids. This work was supported by NIH grant GM074134 (NGA) and a fellowship for undergraduate independent research from the Undergraduate Research Opportunities Program (UROP) at the University of Colorado, Boulder (AYR).

Appendix A. Supplementary data

Supplementary data associated with this article can be found, in the online version, at doi:10.1016/j.ijms.2010.08.020.

References

[1] J. Baselga, Targeting tyrosine kinases in cancer: the second wave, Science 312 (2006) (2006) 1175–1178.
[2] C.J. Montagut, J. Settleman, Targeting the RAF–MEK–ERK pathway in cancer therapy, Cancer Lett. 283 (2009) 125–134.
[3] G. Pagès, S. Guérin, D. Grall, F. Bonino, A. Smith, F. Anjuere, P. Auberger, J. Pouysségur, Defective thymocyte maturation in p44 MAP kinase (Erk1) knockout mice, Science 286 (1999) 1374–1377.
[4] Y. Yao, W. Li, J. Wu, U.A. Germann, M.S. Su, K. Kuida, D.M. Boucher, Extracellular signal-regulated kinase 2 is necessary for mesoderm differentiation, Proc. Natl. Acad. Sci. U.S.A. 100 (2003) 12759–12764.
[5] T. Kinoshita, I. Yoshida, S. Nakae, K. Okita, M. Gouda, M. Matsubara, K. Yokota, H. Ishiguro, T. Tada, Crystal structure of human mono-phosphorylated ERK1 at Tyr204, Biochem. Biophys. Res. Commun. 377 (2008) 1123–1127.
[6] F. Zhang, A. Strand, D. Robbins, M.H. Cobb, E.J. Goldsmith, Atomic structure of the MAP kinase ERK2 at 2.3 A resolution, Nature 367 (1994) 704–711.
[7] B.J. Canagarajah, A. Khokhlatchev, M.H. Cobb, E.J. Goldsmith, Activation mechanism of the MAP kinase ERK2 by dual phosphorylation, Cell 90 (1997) 859–869.
[8] T. Fox, J.T. Coll, X. Xie, P.J. Ford, U.A. Germann, M.D. Porter, S. Pazhanisamy, M.A. Fleming, V. Galullo, M.S. Su, K.P. Wilson, A single amino acid substitution makes ERK2 susceptible to pyridinyl imidazole inhibitors of p38 MAP kinase, Protein Sci. 7 (1998) 2249–2255.
[9] A.N. Hoofnagle, K.A. Resing, E.J. Goldsmith, N.G. Ahn, Changes in protein conformational mobility upon activation of ERK2, as detected by hydrogen exchange, Proc. Natl. Acad. Sci. U.S.A. 98 (2001) 956–961.
[10] A.N. Hoofnagle, J.W. Stoner, T. Lee, S.S. Eaton, N.G. Ahn, Phosphorylation-dependent changes in structure and dynamics in ERK2 detected by site directed spin labelling and electron paramagnetic resonance, Biophys. J. 86 (2004) 395–403.
[11] T. Lee, A.N. Hoofnagle, K.A. Resing, N.G. Ahn, Hydrogen exchange solvent protection by an ATP analogue reveals conformational changes in ERK2 upon activation, J. Mol. Biol. 353 (2005) 600–612.
[12] Z. Wang, P.D. Harkins, R.J. Ulevitch, J. Han, M.H. Cobb, E.J. Goldsmith, The structure of mitogen-activated protein kinase p38 at 2.1 Á resolution, Proc. Natl. Acad. Sci. U.S.A. 94 (1997) 2327–2332.
[13] K.P. Wilson, M.J. Fitzgibbon, P.R. Caron, J.P. Griffith, W. Chen, P.G. McCaffrey, S.P. Chambers, M.S. Su, Crystal structure of p38 mitogen-activated protein kinase, J. Biol. Chem. 271 (1996) 27696–27700.
[14] S. Bellon, M.J. Fitzgibbon, T. Fox, H.M. Hsiao, K.P. Wilson, The structure of phosphorylated p38 gamma is monomeric and reveals a conserved activation-loop conformation, Structure 7 (1999) 1057–1065.
[15] K.M. Sours, S.C. Kwok, T. Rachidi, T. Lee, A. Ring, A.N. Hoofnagle, K.A. Resing, N.G. Ahn, Hydrogen exchange mass spectrometry reveals activation-induced changes in conformational mobility of p38α MAP kinase, J. Mol. Biol. 379 (5) (2008) 1075–1093.
[16] J.L. Wilsbacher, M.H. Cobb, Bacterial expression of activated mitogen-activated protein kinases, Methods Enzymol. 332 (2001) 387–400.
[17] D.J. Robbins, E. Zhen, H. Owaki, C.A. Vanderbilt, D. Ebert, T.D. Geppert, M.H. Cobb, Regulation and properties of extracellular signal-regulated protein kinases 1 and 2 in vitro, J. Biol. Chem. 268 (1993) 5097–5106.
[18] K.A. Resing, A.N. Hoofnagle, N.G. Ahn, Modeling deuterium exchange behavior of ERK2 using pepsin mapping to probe secondary structure, J. Am. Soc. Mass Spectrom. 10 (1999) 685–702.
[19] T. Lee, A.N. Hoofnagle, K.A. Resing, N.G. Ahn, Protein hydrogen exchange measured by electrospray ionization mass spectrometry, in: J.E. Celis (Ed.), Cell Biology: A Laboratory Handbook, vol. 4, 3rd ed., Elsevier Science, 2006, pp. 443–449.
[20] K.A. Resing, N.G. Ahn, Deuterium exchange mass spectrometry as a probe of protein kinase activation. Analysis of wild-type and constitutively active mutants of MAP kinase kinase, Biochemistry 37 (1998) 463–475.
[21] M.A. Emrick, T. Lee, P. Starkey, M.C. Mumby, K.A. Resing, N.G. Ahn, The gatekeeper residue in ERK2 controls autoactivation via a pathway of intramolecular connectivity, Proc. Natl. Acad. Sci. U.S.A. 103 (2006) 18101–18106.